The Utilization of τ Pairs in Determining the Tracking Efficiency at the BaBar Experiment

by

Ian Michael Nugent

B.Sc., University of Victoria, 2002.

A Dissertation Submitted in Partial Fulfillment of the
Requirements for the Degree of

MASTERS OF SCIENCE

in the Department of Physics and Astronomy.

Supervisor: Dr. J. M. Roney

Abstract

This thesis presents the detailed measurements of the tracking efficiency of the BaBar detector using τ pair events. These efficiency measurements are critical for many physics analyses at BaBar. The tracking efficiency is determined both as a global value for the detector and in terms of the parameters on which the BaBar tracking reconstruction software depends. In addition, the charge asymmetry of the tracking efficiency as well as a detailed analysis of the systematic uncertainties related to this method are also presented. It was discovered that the sample of data conventionally used by BaBar for measuring the efficiency is contaminated by background and a new protocol for measuring the efficiencies is presented. Under this new protocol, the global tracking efficiency correction factor and the global tracking efficiency charge asymmetry are determined to be consistent with zero. A new method for determining the efficiency as a function of the reconstruction parameters, was also successfully demonstrated.

Contents

List of Tables

List of Figures

This thesis is dedicated to
my parents

Acknowledgments

I would like to thank all the professors and students from the University of Victoria in Particle Physics who have made this analysis possible. Special thanks goes to my supervisor, Dr. J. M. Roney. I would also like to thank the members of the BaBar community who have assisted with this study: Dr. Robert Kowalewski, Dr. Swagato Banerjee, Dr. Bipul Bhuyan, Dr. Askok Agarwal, Chris Brown, Kenji Hamano and Dr. Thomas Allmendinger.

Chapter 1

Introduction

This work determines the detection efficiency of charged particles in the BaBar Detector. The BaBar Detector, located at the Stanford Linear Accelerator Center, is a device designed to identify and measure the energy, momentum and velocity of subatomic particles produced in electron and positron[1] collisions. The electrons and positrons are supplied by PEP II storage rings, an asymmetric collider which has a centre-of-mass energy at the $\Upsilon(4s)$ resonance, 10.58GeV. The purpose of this experiment is to probe the Standard Model of Particle Physics, mainly in CP violation from B meson decays. In addition to the CP violation research conducted with BaBar, the BaBar detector has also recorded over 170 million τ pairs which are used to probe a wide variety of fundamental questions.

It is the unique topology of the τ pairs that enables a subset of the events to be identified with a possible missing track[2]. This enables an efficiency to be determined in terms of the parameters upon which the reconstruction depends. Furthermore, this study presents a detailed analysis of the systematic uncertainties associated with this method. From these efficiencies, correction factors for the deviation between the Monte Carlo Simulated Data (MC) and data are obtained. In addition, tracking efficiency charge asymmetries are deter-

[1] A positron is the antiparticle of an electron. Thus, a positron has the opposite quantum numbers and charge of an electron.

[2] A track is defined as the reconstructed trajectory of a charged subatomic particle transversing the detector.

mined for the detector. The specific results of this study will be employed to correct the data-MC difference in BaBar physics analyses utilizing data collected by BaBar from 2000 to 2003. This will be achieved by using the results of this study directly, and by combining the results of this study with an alternative analysis for which the relative tracking efficiency can be determined in events with a higher number of tracks. The principles developed for this study will also be useful for analyses of data yet to be collected.

A brief introduction to the Standard Model of Particle Physics, in Chapter 2, describes the model of the fundamental particles and the forces which the BaBar experiment is probing and how these measurements depend on the tracking efficiency. This discussion includes a description of CP violation and a basic introduction to the τ particle. Chapter 3 provides an overview of the BaBar detector. Special emphasis is given to the two tracking chambers, the Drift Chamber and the Silicon Vertex Tracker, necessary for the in depth description of the tracking reconstruction method employed in BaBar (Chapter 4). The analysis of tracking reconstruction is separated into two components: the general methods for track identification and fitting, and the application of these methods to the BaBar detector reconstruction software. The methods for determining the efficiency, tracking efficiency, charge asymmetry and the associated complications are discussed in Chapter 5. The method is introduced by discussing the general philosophy behind using physics events, such as τ decay, to determine the tracking efficiency of a detector. The specific methods for employing τ pairs to ascertain the global efficiency and efficiency for the reconstruction dependent parameters will then be described. The parameters upon which the reconstruction depends are: the momentum orthogonal to the initial electron beam direction called the transverse momentum (P_t) and the polar angles θ and ϕ which are defined for the detector coordinate system. The results of this study are presented in Chapter 6. In Chapter 7 the effect of background contamination and reconstruction parameters P_t, θ and ϕ on the efficiency study are quantified in a study of systematic uncertainties. Chapters 8 and 9 contain the

summary of the results and the associated conclusions. For completeness, a comprehensive set of the tracking efficiency results may be found in the appendices.

Chapter 2

Motivation: The Standard Model

In this section, the Standard Model of Particle Physics [6] is introduced as is the crucial role of tracking efficiency to techniques employed at BaBar to probe the Standard Model.

2.1 Introduction to the Standard Model of Particle Physics

The Standard Model of Particle Physics is the theoretical model which encompasses all of the current experimental measurements in particle physics. It describes the interaction between the elementary particles and the forces that bind them. The two main classifications of particles in the Standard Model are bosons, integer spin particles, and fermions, half spin particles, where spin may be defined as the intrinsic quantized angular momentum of a particle. The forces are mediated by bosons, while the particles, which matter is composed of, are the leptons and quarks. Below is a table of the boson and fermion particles in the Standard Model.

Mediators of the Interactions (Bosons)				
Force	Particle	Charge	Mass (GeV)	Couples With
Strong	Gluon (g)	0	0	Quarks, g
Electro-magnetic	Photon (γ)	0	0	Charged Particles
Weak	$W^{\pm}$	± 1	(80.423 $\pm$ 0.039)	Fermions, Z^0, γ
	Z^0	0	(91.1876 $\pm$ 0.0021)	Fermions, $W^{\pm}$

Fundamental Fermions				
Family	Particle	Charge	Mass (GeV)	Couples With
Leptons	Electron (e)	-1	$(5.10998902 \pm 0.00000021) 10^{-4}$	γ, $W^{\pm}$, Z^0
	e Neutrino (ν_e)	0	m$<3\times10^{-6}$	$W^{\pm}$, Z^0
	Muon (μ)	-1	$(0.105658357 \pm 0.000000005)$	γ, $W^{\pm}$, Z^0
	μ Neutrino (ν_μ)	0	m$<0.19\times10^{-3}$,CL=90%	$W^{\pm}$, Z^0
	Tau (τ)	-1	$(1.77699^{+0.00029}_{-0.00026})$	γ, $W^{\pm}$, Z^0
	τ Neutrino (ν_τ)	0	m$<18.2\times10^{-3}$,CL=95%	$W^{\pm}$, Z^0
Quarks	Up (u)	2/3	$(1.5 \text{ to } 4.5) 10^{-3}$	γ, $W^{\pm}$, Z^0, g
	Down (d)	-1/3	$(5.0 \text{ to } 8.5) 10^{-3}$	γ, $W^{\pm}$, Z^0, g
	Charm (c)	2/3	1.0 to 1.4	γ, $W^{\pm}$, Z^0, g
	Strange (s)	-1/3	0.080 to 0.155	γ, $W^{\pm}$, Z^0, g
	Top (t)	2/3	174.3$\pm$5.1	γ, $W^{\pm}$, Z^0, g
	Bottom (b)	-1/3	4.0 to 4.5	γ, $W^{\pm}$, Z^0, g

Table 2.1: The Fundamental Forces and Particles in the Standard Model [1, 010001-25].

The masses of these particles is modeled through their interactions with a neutral boson called the Higgs particle. In addition to these particles, the Standard Model also includes antiparticles. Antiparticles have both opposite charge and quantum numbers to that of their corresponding particle.

2.1.1 Introduction to Electroweak Theory

The Electroweak Interactions in the Standard Model are described by combining Quantum Electrodynamics (QED), the theory of electromagnetic on a quantum scale, and the Weak Theory, the theory of the weak interaction. These are quantized field theories that utilize Lorentz invariance, Charge-Parity-Time invariance and local gauge invariance [3, pg. 311]. The electromagnetic force is described by the abelian local gauge group U(1) where electrical

charge is the conserved current. Moreover, electromagnetism has one carrier of force, the photon, corresponding to the one symmetry in the gauge group U(1). Similarly, the weak force is described by the non-abelian gauge group $SU_L(2)$ where the subscript L denotes that the force carriers can only couple to left handed fermions. The weak interaction has three particles, one neutral and two charged, corresponding to the three symmetries, with hypercharge being the conserved current. The gauge groups $SU_l(2)$ and U(1) have the property that they can be combined to form a composite group, $SU_L(2)\times U(1)$. When this is done, the force carriers mix producing the four force carriers which were introduced in table 2.1, the photon (γ), Z^0, W^+ and W^- bosons. It is the properties of the resulting particles that define the nature of the forces. The photon, being a massless particle, has an infinite range and a coupling strength of $\alpha_{EM} = \frac{1}{137} \sim 10^{-2}$ in natural units[1]. In contrast, the $W^{\pm}$ and the Z^0 bosons have a short range of approximately $\frac{1}{100}\text{GeV}^{-1}$ and a weak coupling strength of $\alpha_W \sim 10^{-6}$, in natural units, due to their large mass. Furthermore, the non-commutative nature of non-abelian groups allows the weak force carriers to self couple, thus allowing the $W^{\pm}$ and the Z^0 bosons to interact with each other.

In the Standard Model, the interactions Hamiltonian[2] for the weak and electromagnetic forces can be calculated using perturbation theory[3]. Utilizing the interaction Hamiltonian, useful quantities such as the cross section[4] or the decay rate[5] for a particular interaction can be calculated. Employing the former method, Feynman invented a tool for calculating the cross section called "Feynman Diagrams". The Feynman diagrams have a one to one correspondence with the perturbative series of the interaction Hamiltonian. Feynman diagrams,

[1]Natural units are a set of measurement units in which $c = \hbar = 1$.

[2]The Hamiltonian for a given system, is the energy in that system.

[3]Perturbation theory is a method in which measurable parameters of the interactions are decomposed into a series that converges rapidly.

[4]The cross section, for a particular interaction, is the rate at which the interaction occurs normalized to a unit of incident flux.

[5]The decay rate is the mean rate of decay for a given particle.

which represent how the interaction occurs in the corresponding perturbative series, consist of a final and an initial state with a number of intermediate states, depending on the order of the corresponding term in the perturbative series. The intermediate states in a Feynman diagram may be on shell, a real particle, or off shell, a "virtual particle". A particle which is off shell is virtual because the particle the does not have the mass properties of the real particle. For massive particles, this occurs when the kinematic constraint of the interaction yields a mass which is below threshold for the real particle to condense out. For massless particles, the intermediate particle is off shell when the kinematic constraints require that the particle has mass. When a particle is off shell, its contribution to the Hamiltonian is suppressed relative to an on shell particle. An example of a Feynman diagram's one to one correspondence with an element in the perturbative expansion of the expected Hamiltonian is the $e^+e^- \rightarrow \tau^+\tau^-$ interaction which is the primary production mechanism for τ particles in the BaBar Detector. The interaction Hamiltonian of this interaction, $\langle \tau^+\tau^- | H_{Int} | e^+e^- \rangle$, when expanded in a perturbation series yields $\langle \tau^+\tau^- | H_{Int} | \gamma \rangle^\nu \langle \gamma | H_{Int} | e^+e^- \rangle_\nu$ as the lowest order term. Where $\langle \tau^+\tau^- |$ represents the final state with two τ's, $| e^+e^- \rangle$ represents the initial state with an electron and a positron, $| \gamma \rangle$ represents the intermediate state, and ν is the Lorentz index. The corresponding diagram to the lowest order term in the perturbation series can be seen in figure 2.1.

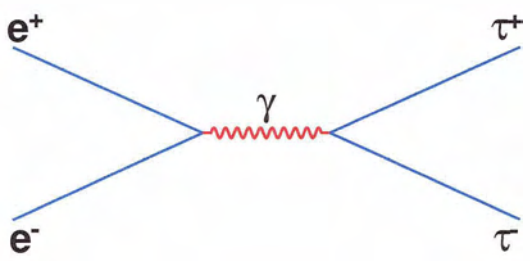

Figure 2.1: The dominant Feynman diagram for the $e^+e^- \rightarrow \tau^+\tau^-$ interaction.

The above diagram is the dominant Feynman diagram for the $e^+e^- \rightarrow \tau^+\tau^-$ interaction. This is because the coupling constants for the electromagnetic force is small, thus in all electromagnetic interactions, where the terms of nth order are proportional to α_{EM}^n, the higher order terms will be suppressed relative to the lower order terms resulting in the perturbative series converging rapidly. Similarly, the weak force has a small coupling constant causing all the perturbative series for weak interactions to also converge rapidly.

2.1.2 Introduction to Quantum Chromodynamics

In the Standard Model the strong interaction is described by the non-abelian local gauge invariant group SU(3) in a theory called Quantum Chromodynamics (QCD). The gauge group SU(3) has eight symmetries, and thus there are eight types of force carriers known as gluons. These gluons, although massless and electrically neutral, carry a form of charge called colour. Colour charge is the conserved charge of the SU(3) group. Gluons have one colour charge and one anti-colour charge, while quarks carry either one colour or one anti-colour. There are three charges of colour, red (R), blue (B) and green (G) and three complimentary colours, anti-red ($\bar{R}$), anti-blue ($\bar{B}$) and anti-green ($\bar{G}$). Because the quarks and anti-quarks can have three colour configurations and the gluons can have 8 colour configurations they correspond to multiplets, "irreducible representations of SU(3)" [4, pg. 66], of dimension 3, 3* and 8 respectively. When particles represented by the multiplets are bound together, they are represented by the product of their associated multiplets. Particular products of the previously mentioned multiplets contain the dimension 1 multiplet, or colour singlet state. This construction of colour singlets is important in QCD because only colourless objects have been observed in nature. This confinement is believed to be a result of the non-abelian and massless nature of the gluon. More specifically, in QCD when two quarks contained in a colour singlet are separated, the gluon fields form flux tubes between them. Because the gluons belong to a non-abelian group with a strong coupling constant, $\alpha_S \sim 1$ in natural units, and they are massless, the force between the two quarks grows with

the distance. Eventually, there is enough energy that a quark and anti-quark pair with the appropriate charge and colour can be created from the quantum vacuum resulting in two colour singlets. This is called "quark confinement". These composite particles of quarks and gluons are called hadrons.

2.1.3 Introduction to the Leptons Sector

The Lepton family consists of 3 generations, the electron and electron neutrino, the muon and muon neutrino, and the tau and tau neutrino. Because leptons do not interact through the strong force, they are found as isolated particles. The electron is the lightest and the only stable charged lepton while the τ and μ's are unstable particles and decay weakly. The τ particle is the only lepton heavy enough to decay into hadrons.

The Standard Models description of the leptons is based on "the premise that the only physical difference among the charge leptons is that of mass" [5, pg. 145]. This premise is called Lepton Universality. Stated another way, Lepton Universality means that the coupling amplitude (or weak charge) between leptons of different flavours and $W^{\pm}$ bosons are equal [6, pg. 195-196]. This universality can be exploited experimentally, when comparing the ratio of lepton interaction rates since the mass independent terms cancel reducing the theoretical uncertainty. Moreover, the lepton type, or the generation, is a conserved quantity in the Standard Model. This conservation principle is the result of imperical evidence.

2.1.4 Introduction to the Quark Sector

In contrast to leptons, the quarks and anti-quarks are contained in composite particles called hadrons. The particles in hadrons consist of valence quarks, sea-quarks and gluons. There are two main types of hadrons which have been observed, mesons which consist of a valence quark anti-quark pair and baryons which consist of three valence quarks. Both the quarks and the gluon fields that bind them form colour singlets. The gluon field also produces

quark anti-quark pairs called "sea-quarks". These quarks are radiated and absorbed by the gluon field [3, pg. 198]. In addition to the strong force, the quarks inside the hadrons also interact with the electromagnetic and weak force. The quarks state with which the weak force interacts, the weak quark eigenstates, are not the same as the mass eigenstates mentioned in table 2.1. Instead, the weak eigenstates are a linear combination of the mass eigenstates. The unitary transform matrix which transforms from the mass eigenstates to the weak eigenstates is called the Cabibbo-Kobayashi-Maskawa Matrix (CKM Matrix).

$$|q_{Weak}\rangle = \begin{bmatrix} V_{ud} & V_{us} & V_{ub} \\ V_{cd} & V_{cs} & V_{cb} \\ V_{td} & V_{ts} & V_{tb} \end{bmatrix} |q_{Mass}\rangle \tag{2.1}$$

This matrix consists of nine linearly dependent complex parameters. It is the complex phase in the CKM Matrix that is responsible for the violation of the charge parity symmetry (CP violation) in the Standard Model. The violation of the CP symmetry is the source of the asymmetry between particles and their anti-particles. The charge parity symmetry may be decomposed into two simpler symmetries: charge conjugation and parity. Charge conjugation is a symmetry which connects particles to their antiparticle. While parity is a discrete symmetry about the spatial origin which "flips" the sign of the spatial coordinates, and hence the helicity[6] of a particle.

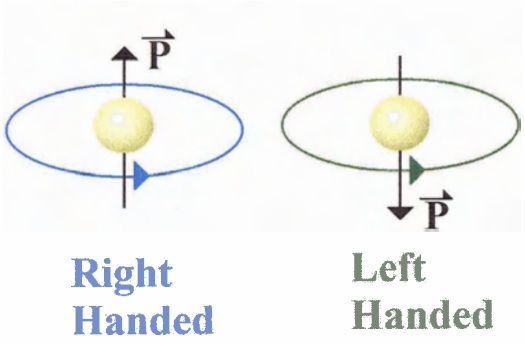

Figure 2.2: Diagram of helicity being flipped due to a parity transformation.

[6]Helicity is the alignment of the spin of a particle relative to the particles momentum.

The CP violation is a result of the complex phase of the matrix elements because the strength of the weak interaction, for a particular quark mass eigenstate, depends on the corresponding transform element in the CKM Matrix. However, the CP of that particular reaction depends on the complex conjugate of that transform element. Clearly these are not, in general, equal, resulting in CP violation when two or more amplitudes interfere [30].

2.2 Measurements of Interactions in the Standard Model

Experimentally, the Standard Model is probed through measuring the statistical probability for the interactions as a function of the fundamental parameters of those interactions and comparing them to the corresponding theoretical predictions.

2.2.1 Branching Ratio Measurements

Branching Ratio Measurements and CP Violation

CP Violation is manifested in three ways in the Standard Model: CP violation in the decay of a subatomic particle, CP asymmetry resulting from the mixing of CP eigenstates and interference terms at the decay vertex resulting in an asymmetry of the decay [29, pg. 5]. The latter two criteria are satisfied by three systems, the $K^0 - \bar{K}^0$ system, the $D^0 - \bar{D}^0$ system and the $B^0 - \bar{B}^0$ system. Each system is composed of two mesons, neither of which are eigenstates of CP. However, a linear combination of these two mesons form two eigenstates of CP. CP Violation is then exhibited as an asymmetry in the branching ratio[7] of the decay products as a function of time.

Branching Ratio Measurements and τ Events

Being the most massive of the leptons, the τ particle is a unique probe for precision measurement in the Standard Model. The branching ratios of the $\tau \rightarrow hhh\nu_\tau$ decays, where h signifies a $K^\pm$ or $\pi^\pm$ meson, are directly correlated, through QCD, to the fundamental

[7]The probability of a specific decay occurring is called the branching ratio.

parameters V_{us} and the strange quark mass. In addition, the premise in the Standard Model that the lepton type is a conserved quantity is tested by searching for the branching ratio in rare decays that is significantly higher than allowed by models, such as the Standard Model, that require this conservation. The current searches for lepton violation at BaBar include: $\tau \rightarrow \mu\gamma$, $\tau \rightarrow e\gamma$, $\tau \rightarrow lll$ and $\tau \rightarrow lhh$. In contrast, the branching ratio of the $\tau^- \rightarrow (\mathrm{K}\pi)^-\nu_\tau$ decay allows precision measurements of the weak current, while the branching ratio of multi-hadron events allow QCD to be studied.

Branching Ratio Measurements and Tracking Efficiency

Experimentally, the measurement of the probability of a particular decay is dependent upon the probability of identifying the decay and not merely the branching ratio. Thus, the branching ratio is

$$\beta(X \rightarrow Y) = P(X \rightarrow Y) = \frac{P^{meas}(X \rightarrow Y)}{\epsilon_{(X \rightarrow Y)}} \tag{2.2}$$

where $\beta(X \rightarrow Y) = P(X \rightarrow Y)$ is the branching ratio for the event $X \rightarrow Y$, $P^{meas}(X \rightarrow Y)$ is the probability of measuring the event $X \rightarrow Y$ with the efficiency $\epsilon_{(X \rightarrow Y)}$ and $\epsilon_{(X \rightarrow Y)}$ is the efficiency of measuring the event $X \rightarrow Y$ when it has occurred. The efficiency of measuring an event, when it has occurred, is dependent upon the efficiency of selecting an event from events that have been reconstructed correctly and the efficiency of reconstructing an event correctly. The latter efficiency may be decomposed further to the set of efficiencies for reconstructing the elements within the event. The particular element with which this paper is concerned is the track.

The tracking efficiency is defined as the efficiency of reconstructing the trajectory of a final state particle that was produced inside the detector. Thus, the inefficiencies of the track reconstruction may be categorized in two groups: particles that failed to produce a signal in the detector and signals created by a particle that pattern recognition software was unsuccessful in identifying as a track pattern. The former group includes cases where

particles are absorbed by material before entering the tracking region of the detector and particles that were not within the geometric acceptance of the detector. The latter group consists of signals with insufficient information to be correlated with a known pattern and particle trajectories. For example, those cases where the trajectory is altered by the detector material, which degrades the pattern recognition. The tracking efficiency of a detector is not necessarily independent of the charge of the subatomic particle. This charge dependence can be a result of detector geometry and detector components utilized to measure the path of a particle. As a result, determining the tracking efficiency charge asymmetry is required for any measurement sensitive to the charge of the track, such as CP asymmetry measurements.

Chapter 3

The PEP-II Accelerator and the BaBar Detector

3.1 The PEP-II Accelerator

The PEP-II Ring is an upgrade of the original PEP Ring to enable CP Violation to be studied in the B^0 and $\bar{B}^0$ meson. The PEP-II Accelerator, seen in figure 3.1, is an asymmetrical electron and positron collider. It consists of two rings, a high energy storage ring (9.0GeV) for the electrons and a low energy ring (3.1GeV) for the positrons. The former ring is an upgrade of the existing PEP ring to accommodate the high currents while the latter ring is a new addition thus enabling asymmetric beam energies. Since many of the interactions which are expected to have CP Violation in the B^0 and $\bar{B}^0$ meson have a small branching ratio, approximately 10^{-5} or smaller, the PEP-II upgrade required an "unprecedented" nominal luminosity[1], or rate of collisions per area, of $3 \times 10^{-33}\text{cm}^{-2}\text{s}^{-1}$. The PEP-II ring utilizes the linac to inject the electron and positron into the PEP-II ring at colliding energies. In the centre-of-mass frame, the collision energy corresponds to the mass of the $\Upsilon(4s)$ particle, a resonant state that is composed of a b and anti-b quark with a mass of $10.58 GeV/c^2$. The $\Upsilon(4s)$ particle is slightly above the threshold energy of B^0 and $\bar{B}^0$ production, resulting in a decay rate greater than 96% into B^0, $\bar{B}^0$, B^- and B^+ particles.

[1]Luminosity is defined as the number of incident particles per unit area per unit time.

If the centre-of-mass energy of the collisions were higher, there would be both an increase in the background and a reduced cross section for B^0 and $\bar{B}^0$ production. The boost[2] between the centre-of-mass frame and the laboratory frame enables time dependent CP Violation to be studied. This is because a time delay between B^0 and $\bar{B}^0$ decays, which are nearly at rest in the centre-of-mass frame, translates into a measurable displacement along the beam axis.

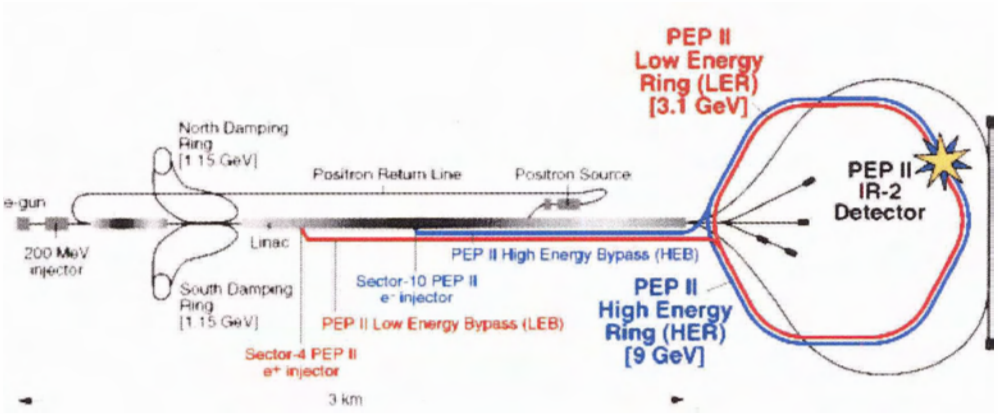

Figure 3.1: The diagram of the PEP-II Accelerator. [8, BaBar Detector Image Gallery].

The high luminosity of the PEP-II accelerator coupled with the relatively large cross section for τ pairs at the centre-of-mass energy 10.58GeV results in the BaBar facilities doubling as a τ factory. Below is a table of the relative cross sections at a centre-of-mass energy 10.58GeV [9].

[2]In special relativity, the transformation between two reference frames, which differ only by a relative velocity, is referred to as a boost.

Interaction	σ (nb)
Leptonic Interactions	
$e^+e^- \rightarrow e^+e-$ $(17 < \theta < 160)$	21.2
$e^+e^- \rightarrow e^+e-$ $(20 < \theta < 120)$	14.4
$e^+e^- \rightarrow \mu^+\mu-$	1.16
$e^+e^- \rightarrow \tau^+\tau-$	0.94
Semi-Hadronic Interactions	
$e^+e^- \rightarrow u\bar{u}$	0.35
$e^+e^- \rightarrow d\bar{d}$	1.39
$e^+e^- \rightarrow s\bar{s}$	0.35
$e^+e^- \rightarrow u\bar{u}/d\bar{d}/s\bar{s}$	2.09
$e^+e^- \rightarrow c\bar{c}$	1.30
$e^+e^- \rightarrow b\bar{b}$	1.05

Table 3.1: The relative cross sections for a e^+e^- collider at 10.58GeV [9]

3.2 The Interaction Region

The PEP-II ring has one detector, the BaBar Detector, located at the second interaction region on the ring. The electron and positron beams are manipulated through bending, by dipole magnets, and focused, by quadrapole magnets so that they collide approximately along the central axis of the BaBar Detector at the "interaction point" or IP. CsI(Tl) crystals, a scintillating material, which are positioned beside the beam pipe are utilized to monitor the focusing of the beams. This interaction region is incapsulated inside a "low mass beryllium cylinder". The low z of beryllium minimizes the interactions of the subatomic particles with the detector support tube to a radiation length[3] of $0.005X_0$.

Since the PEP-II ring is a high current machine, the interaction region produces several significant sources of background. The quadrapole and dipole magnets, which are located close to the interaction region to maximize the focusing of the beam, produce sychrotron radiation[4] as the trajectory of the beams is altered. Production of a e^+e^- pairs, referred to

[3]Radiation length of a material is defined as the distance in which energy of a particle is reduced by e^{-1} through electromagnetic interactions with that material.

[4]Sychrotron radiation is the radiation that is emitted by a relativistic charged particle in a circular path

as Bhabha scattering, cause electrons and positions to enter the detector. Beam particles are "lost" through Bremsstrahlung[5] and Coulomb scattering[6] with residual gas molecules in the beam. The beam particles not at the correct momentum for stable storage in the ring also interact with the magnets and the beam pipe to produce additional upstream background. The accumulation of dose, which causes a high occupancy and radiation damage inside the active components of the detector, is monitored with pin diodes located around the detector. To reduce the accumulation of unnecessary dose to the detector, potential high radiation regions are suppressed by the addition of extra material [9].

3.3 The BaBar Detector

The BaBar Detector is composed of five main Detector components. An illustration of the BaBar Detector and its components can be seen in figure 3.2. They are the Silicon Vertex Tracker (Vertex Detector), the Drift Chamber (Tracking Chamber), the DIRC (Cherenkov Detector), Electromagnetic Calorimeter (Electron/Photon Detector) and the Instrumented Flux Return (Muon/Hadron Detector). The NbTi 1.5 Tesla superconducting solenoid magnet produces a magnetic field parallel to the detector axis in the tracking region which bends the trajectory of the charged subatomic particle through the Lorentz Force. The uncertainty in the BaBar Detector for determining the transverse momentum P_t, the momentum orthogonal to the initial electron beam direction, with this method is

$$\frac{\sigma_{P_t}}{P_t} = (0.13 \pm 0.01)\% \cdot P_t \oplus (0.45 \pm 0.03)\%. \tag{3.1}$$

The z axis is defined as the central axis of the detector which is within 100mrad of the direction of the high energy electron beam. The y axis is in the vertical direction toward the zenith, while the x axis is in the horizontal direction pointing away from the centre of the

due to the acceleration.

[5]Bremsstrahlung scattering is the scattering of an electron through the emission of a photon.

[6]Coulomb scattering is the scattering of an electron by a photon.

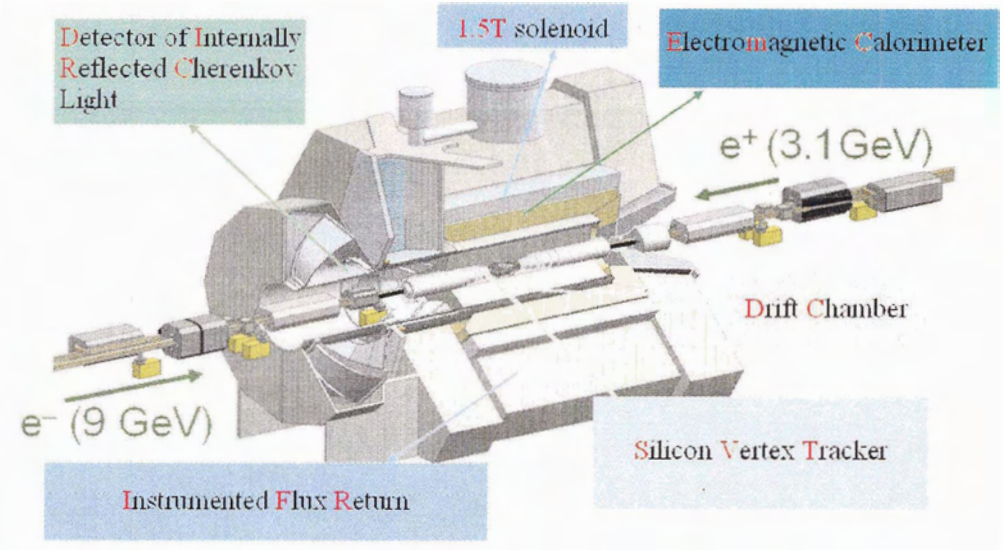

Figure 3.2: The BaBar Detector [8, BaBar Detector Image Gallery].

PEP-II ring. The interaction point is the origin of the BaBar coordinate system [9]. From these cartesian coordinates, the spherical angles θ and ϕ are derived. θ is the polar angle defined relative to the z axis, while ϕ is the angle relative to the x axis in the xy plane.

3.3.1 The Silicon Vertex Tracker

The Silicon Vertex Tracker (SVT) is one of the two tracking sub-detectors in the BaBar Detector. As seen in figure 3.2, it is the innermost detector positioned around the beam pipe. The purpose of the SVT is to "reconstruct the decay vertices of two primary B mesons in order to determine the time between the two decays" [9, pg. 81]. This allows for time-dependent CP asymmetries to be studied. Moreover, the SVT is capable of reconstructing low momentum tracks that do not enter the Drift Chamber.

The SVT is constructed from 52 "double-sided" silicon modules. These modules are positioned in a 5 layer configuration as seen in figures 3.3 and 3.4. The detector consists of readout strips to give information in z and ϕ. The inner two layers are primarily designed to determine the z location of the vertex, while the outer two layers are designed to merge

the reconstructed tracks with the Drift Chamber. The third or middle layer enables the reconstruction of trajectories using only SVT tracks, such as low momentum tracks that do not reach the Drift Chamber. The intrinsic resolution of the silicon detectors in the three inner most layers is 10μm in the ϕ direction and 12μm in the z direction. In the two outer layers, the intrinsic resolution in ϕ is 10-12μm and in the z direction 25μm.

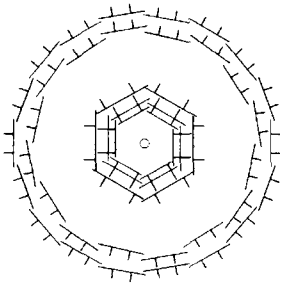

Figure 3.3: A cross section view of the SVT in the plane orthogonal to the beam pipe [10, Figure 4-3].

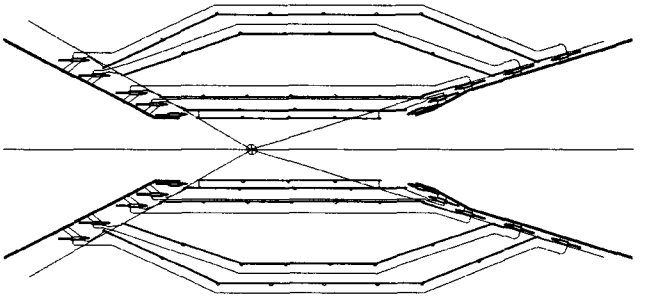

Figure 3.4: A cross section view of the SVT in the beam pipe plane [10, Figure 4-2].

The above geometry has a solid angle coverage designed to maximize the geometric acceptance. However, this is constrained by the location of the bending magnets. As a result, the solid angle coverage is constrained to be between the polar angles 20.1 degrees and 150.2 degrees. This corresponds to 29.5 degrees and 161.8 degrees in the centre-of-mass frame. The exterior two layers of the SVT, which are kinked in z to minimize the incident angles, are arranged in an overlapping geometry, while the interior layers are in a pin-wheel arrangement. This ensures that an incident particle crosses through a module at each layer it transverses.

The modules consist of a composite fiber frame upon which the silicon detector and kevlar support ribs are mounted. The frame is constructed of carbon fiber to minimize the radiation length. The silicon detectors are connected with wire bonds into two "half modules". These half modules are composed of two to four silicon detectors and separate the modules into electrically isolated forward and backward sections. The outward pointing

side of the silicon detectors have strips parallel to the z direction for measurements in the ϕ direction. On the inward side of the silicon detectors, the strips are orthogonal to the z direction for measurements in the z direction. The data is read out through high density interconnect electronic hybrid devices mounted at each end of the modules [9] and [10].

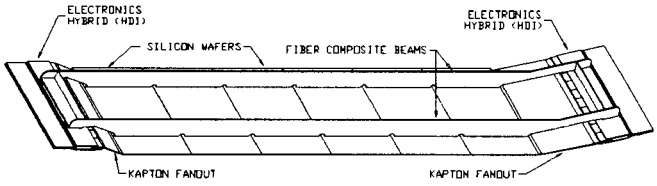

Figure 3.5: A diagram of a Module in the SVT [10, Figure 4-15].

3.3.2 The Drift Chamber

Exterior to the SVT is the second tracking detector, the Drift Chamber (DCH). The DCH is the primary tracking detector in the BaBar Detector. The chamber is composed of two end plates made of carbon fiber and an inner and outer support tube. The forward and backward end plates are 1.2-2.4cm and 2.4cm respectively. The forward end plate has a reduced thickness, near the outer radius, to minimize the radiation length a particle must travel before entering the calorimeter system. The outer support tube, which is composed of two carbon fiber layers around a Nomex core, is the structural support that carries the load of the internal wire. The inner support tube is made of beryllium, again, to minimize the radiation length. The chamber, which is filled with 80% helium and 20% ISO-butane, contains an array of sense and field wires. A diagram of the DCH can be seen in figure 3.6. The charged sense wires, which detect the signal, are 20μm gold plated tungsten-rhenium wires. Although the sense wires were maintained at a potential of 1900V and 1960V at the beginning of the experiment, the majority of the data was recorded with a potential of 1930V on the sense wires. The wires employed to produce the electric field pattern, the

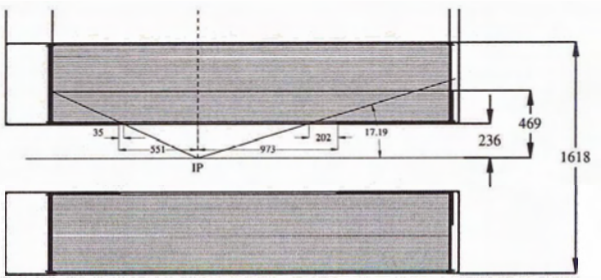

Figure 3.6: A cross sectional view of the of DCH [9, Figure 3-7].

field wires, are 120μm and 80μm gold plated aluminum. The field wires surrounding the sense wires are grounded while the other field wires have a potential of 340V. The array of sense and field wires consists of 40 stereo (U and V) and axial (A) layers, with the charged sense wires positioned between the super-layers. In the axial layers the field wires and sense wires are parallel to the z axis, yielding a position measurement in the axial or xy plane. In contrast, the stereo wires have an angle relative to the z axis. In addition to this, the stereo angle varies with the radial distance of the wires from the beam axis to maintain the shape of the cells. These layers are arranged in sets of four, where each layer has an unique stereo angle and twist that increases in magnitude with the radial distance from the interaction region. Figure 3.7 illustrates the stereo axial pattern employed in the Drift Chamber. The U stereo layers correspond to the wire arrangements with both a positive stereo angle and a positive twist angle, while the V stereo layers correspond to a negative stereo angle and a negative twist angle. This difference in stereo angle between the U, V and A layers set up a non-orthogonal basis for the solid angle that allows the particles path to be reconstructed in terms of θ in addition to ϕ and the radius r.

The field wires within the layers form hexagonal cells around the sense wires, and, thus the potential difference between the field and sense wires produces an electric field. When a subatomic particle travels through a cell, it ionizes the gas. The free electrons, attracted by the positive charge, drift with a mean velocity of v_{drift} towards the sense wire.

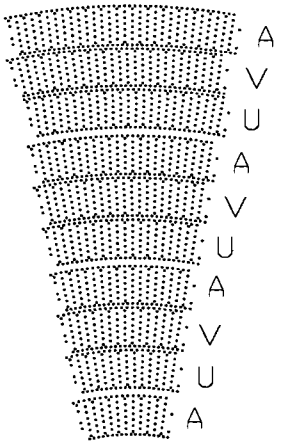

Figure 3.7: A diagram of the axial and stereo arrangement [9, Figure 3-8].

The length of the path that the electrons travel, L_{path}, is dependent upon the position where the ionization took place and the electric and magnetic field in that cell. Due to the strong electric field, the electrons in the gas undergo amplification when within a distance of several wire radii from the sense wire. Positive ions are produced in the avalanche close to the sense wire, and their movement away from the wire creates a measurable signal on the sense wire. This signal is proportional to the ionization created by the subatomic particle travelling through the gas. Hence, the $\frac{dE}{dx}$ [7] information is obtained from summing the total charge deposited on the wire and correcting for the incident angle of the charged particle. In order to obtain a precise measurement of the trajectory, the drift time is measured and converted to a drift distance from prior knowledge of the drift velocity. To use the "time-to-distance relationship" the time that the particle transversed the cell, t_0, is required. The t_0 time is obtained from a knowledge of the collision times of the beams and the distance that the particle travelled from the interaction point to the location of inonization in the cell. The time-to-distance relations can be depicted graphically in terms of "isochrones", or surfaces of equal drift time. The maximum time for the electrons to drift to the sense wire

[7] $\frac{dE}{dx}$ is the average energy loss per unit length.

is approximately 600ns. Below is a diagram of a typical cell with lines of equal isochrone superimposed [9] and [10]. The intrinsic resolution of a DCH cell is $\sim 100\mu$m.

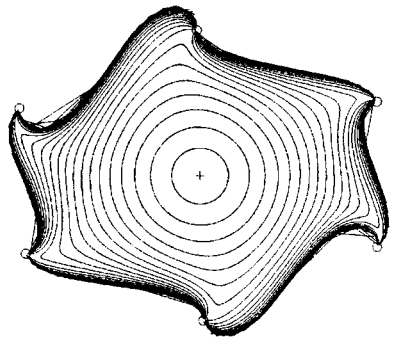

Figure 3.8: A diagram of the isochrones in a typical DCH cell. The isochrones are spaced by 50ns [9, Figure 3-9].

The Drift Chamber was constructed at TRIUMF in Vancouver, Canada as the Canadian contribution to the experiment.

3.3.3 The DIRC

The DIRC, the third detector from the centre in figure 3.2, is a "new kind" of ring Cherenkov detector and is intended for particle identification. The DIRC was designed to distinguish between kaons and pions which have a momentum of 1.7GeV to 4.2GeV, and to tag the flavour of a B meson decay through a $b \rightarrow c \rightarrow s$ cascade [42, Section 8.1]. The DIRC has a geometric acceptance of 25.5 degrees to 147 degrees in the laboratory frame. A schematic of the DIRC can be seen in figure 3.9 [10, Chapter 6].

The DIRC has two major components that measure the Cherenkov Cone: the Standoff Box and the set of twelve Bar Boxes. The Standoff Box, which is composed of stainless steel, is a toroidal structure with 12 cone shaped sectors. Each sector has 896 Photo Multiplier Tubes at a radial distance of $\approx 1.17m$ from the end of the Fused Silica Bars. The Standoff Box is filled with $6000L$ of purified water, a substance with an index of refraction similar to that of fused silica, to minimize the total internal reflection at the Fused Silica/water

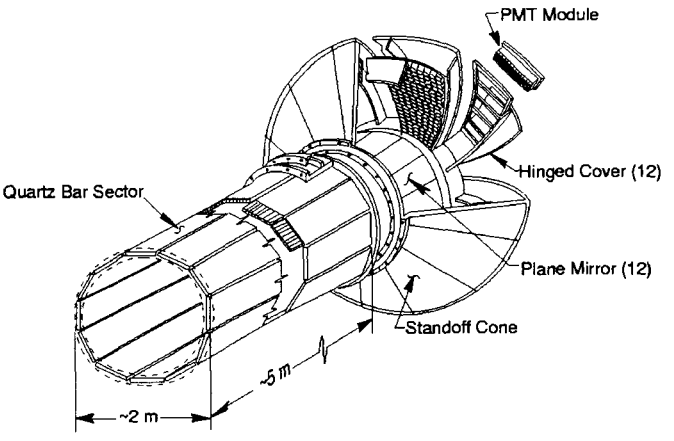

Figure 3.9: A diagram of the components in the DIRC [10, Figure 6-10].

surface. Each of the Bar Boxes, composed of thin aluminium-hexel panels, are connected to an individual sector of the Standoff Box with a 10mm thick Fused Silica window. Inside the Bar Box, the Fused Silica window is glued to a Fused Silica wedge, which, in turn, is glued to twelve optically isolated Fused Silica Bars with mirrors attached on the opposing end. It is in these 144 optically isolated Fused Silica Bars that the Cherenkov light[8] is produced. The 144 Fused Silica Bars are composed of four 1.225m bars of spectrosil, a fused silica [42, Chapter 8].

When a charged particle travelling above $0.679c$, the speed of light in fused silica, enters one of the 144 Fused Silica Bars, it emits an electromagnetic radiation wave front, called a Cherenkov Cone. The angle of this Cherenkov Cone is

$$\theta_C = arccos\left(\frac{1}{\beta\sqrt{\epsilon(\omega)}}\right), \tag{3.2}$$

where the β is the ratio of the particles velocity to the speed of light in the vacuum, and $\epsilon(\omega)$ is the frequency dependent dielectric constant of the medium through which the particle is travelling [43, eq.13.50]. Part or all of the cone will be transmitted through total internal

[8]Cherenkov light is the resulting light produced by a particle travelling faster than the speed of light in a medium.

reflection or specular reflection at the bar's end down the bar and into the Standoff Box. The geometry of the bar and wedge are such that the angle of the light is preserved. The light then travels to the detector surface where the incident number of photons is counted by the Photo Multiplier Tubes. An illustration of this can be seen in Figure 3.10.

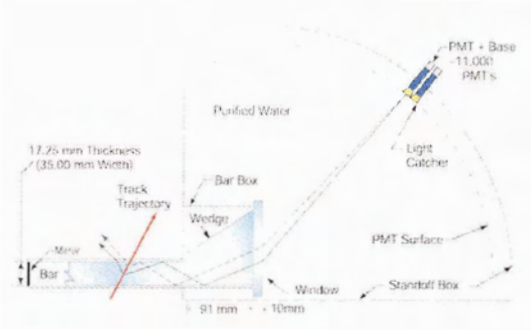

Figure 3.10: An illustration of the operation of the DIRC [8, DIRC Detector Image Collection].

3.3.4 The Electromagnetic Calorimeter

The Electromagnetic Calorimeter (EMC) is the fourth sub-detector in the BaBar Detector. The EMC is designed to measure the energy and momentum of photons and electrons. It is therefore useful for the measurement of photons that may have come from $\pi^0 \rightarrow \gamma\gamma$ and to assist in distinguishing electrons from muons as well as electrons from charged pions. To achieve this, the EMC has both a high angular and energy resolution. The angular resolution of the EMC is

$$\sigma_\theta = \frac{3mr}{\sqrt{E}} \oplus 2mr, \tag{3.3}$$

where E is the energy in units of GeV. The angular resolution in equation 3.3 is a result of the "transverse crystal size and (the) average distance to the interaction point" [10, pg. 248]. The energy resolution, which is defined for a photon with an angle of $\theta = \pi/2$, is

$$\frac{\sigma_E}{E} = \frac{1\%}{E^{\frac{1}{4}}} \oplus 1.2\%. \tag{3.4}$$

Again, the energy E is in units of GeV. The systematic error is a result of internal calibration errors, inhomogeneous light collection and leakage in the front and rear components.

The EMC is composed of a barrel section and conical endcap. The barrel and endcap have a combined geometric acceptance region from 15.8 degrees to 140.8 degrees in the laboratory frame. This corresponds to a geometric acceptance of 26.5 degrees to 156.3 degrees in the centre-of-mass frame. The barrel section contains 5880 trapezoidal CsI(Tl) crystals in 49 rows of 120 crystals. Each row has a specific size and shape such that the face of the crystal, in the row, points toward the interaction point. This is to minimize both the leakage due to the gaps between the crystals and the material through which the particle must transverse to enter the crystals. The CsI(Tl) crystals also vary in radiation length from $16.0X_0$ in the backward direction to $17.5X_0$ in the forward direction by $0.5X_0$ increments. In contrast, the endcap is composed of 900 CsI(Tl) crystals with a radiation length of $17.5X_0$. These crystals are also trapezoidal in shape. These crystals are arranged into nine rows so that the crystal dimensions are approximately uniform. The three outermost rows have 120 crystals, while the middle three rows and inner three rows have 100 and 80 crystals respectively. Figure 3.11 is a schematic of the crystal arrangement in the EMC.

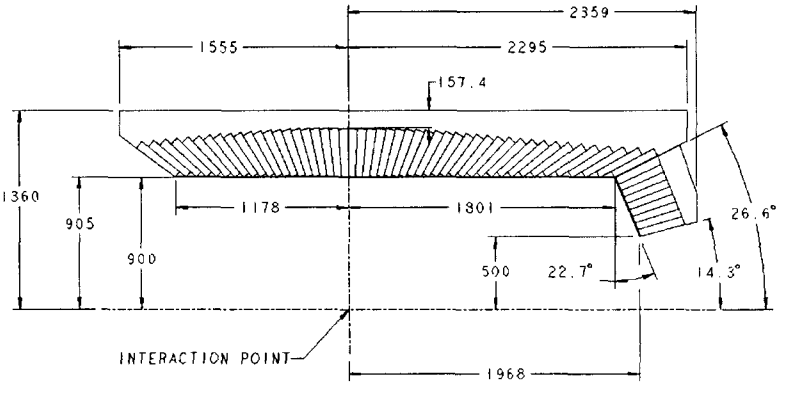

Figure 3.11: A schematic of the EMC [10, Figure 7-4].

CsI(Tl) crystals are scintillators, that floresce when valence electrons, which are excited

into the band gap by subatomic particles, decay into the valence band. Each crystal is connected to a wavelength shifter that shifts the florescent radiation scintillated from the CsI(Tl) crystal, a peak wavelength of 565nm, to 960nm. This is within the absorption wavelength range of the photo diodes, which have a quantum efficiency of 75%. The two photo diodes, which are not affected by the 1.5 Tesla magnetic field, are redundant as a result of reliability issues. The crystals are covered with Aluminum Mylar on the front, and Teflon AF, Diffused Reflector and Aluminum Mylar on the sides to ensure all the light is directed onto the photo diodes. The CsI(Tl) crystals are then mounted inside modules that house the signal cables and the cooling system. These modules are attached to a carbon fiber support cylinder with an aluminum frame [9] and [10].

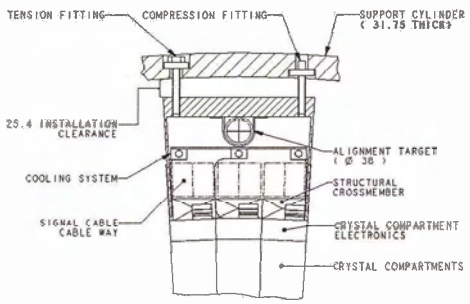

Figure 3.12: A schematic of the barrel module in the EMC [10, Figure 7-5].

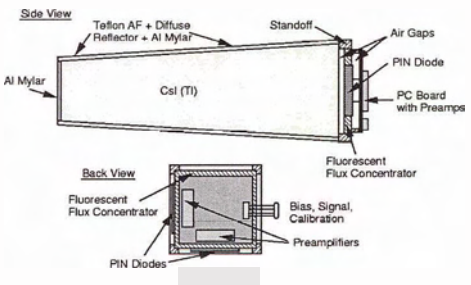

Figure 3.13: A schematic of A CsI(Tl) crystal and photo diodes [10, Figure 7-19].

3.3.5 The Instrumented Flux Return

The Instrumented Flux Return (IFR) facilitates a dual purpose as the magnetic flux return for the 1.5 Tesla super conduction magnet, and as a neutral hadron and muon detector. The IFR is composed of three components, the barrel and two endcaps. The barrel consists of six sextants each 3.75m in length and between 1.88m and 3.23m width while the endcaps are hexagonal plates. The IFR barrel is constructed with 18 layers of iron plates where the first nine interior plates are 2cm in thickness, the next four plates are 3cm thick, followed by two 5cm thick iron plates and the two exterior plates are 10 cm thick. The endcaps have

a similar arrangement of iron plates except there are three 5cm thick plates and only one 10cm thick exterior plate. The variation in the plate sizes with the radius is to allow low momentum muons to be detected, while insuring that hadrons are completely absorbed. An illustration of the IFR iron structure can be seen in figure 3.14.

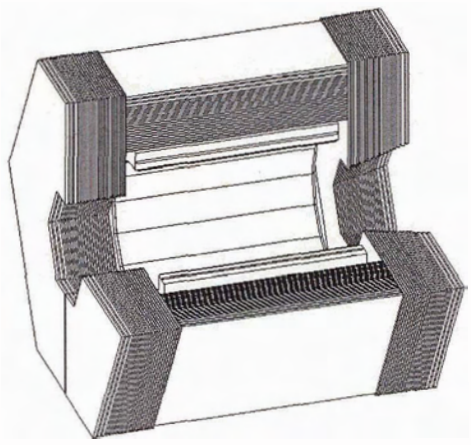

Figure 3.14: A schematic of the IFR [10, Figure 8-9].

The IFR also has 21 layers of Resistive Plate Counters (RPC). These layers are located in the 17 gaps between the plates, on the outside of the detector, between the solenoid magnet and IFR iron plates and in a double layer around the outside of the EMC. The RPC are segmented along the z and ϕ directions in the barrel section, and along the x and y direction in the end plates. Therefore, with the layer in which the hit occurred identified, the position can be reconstructed. Moreover, the hits are matched with the SVT and DCH tracks during reconstruction. RPC are a type of capacitor, a device in which two conducting plates with different potentials are separated by a dielectric material. In the RPC, the dielectric material is composed of a two layer of Bakelite along the conductors with a gas mixture, 134A ($C_2H_2F_6$), Freon ($C_xCl_yF_z$) [28], Argon and a small amount of ISO-butane in the central layer. When a particle travels through the gas filled layer, the gas becomes ionized, breaking down the dielectric resulting in a signal. [10].

Chapter 4

Track Reconstruction

The purpose of track reconstruction is to identify the passage of a charged particle through the detector and determine the parameters that quantify the trajectory of that particle. This is achieved in two main steps. First, the tracks must be identified from the hits in the detectors. Then, the identified tracks are reconstructed with a fit, thus enabling the parameters defining the track to be quantified.

4.1 Finding Tracks

In BaBar, there are two independent and distinct tracking detectors. Because of this, there are three separate methods of identifying tracks, two for the SVT and one for the DCH. Details of the preliminary fit which are used to determine these methods may be found in the next section.

4.1.1 Finding Tracks in the SVT

In the SVT, output from the SVT strips or ganged strips, called digis, contain the time stamp, the time corresponding to the time of ionization, and the period in which the strips had an ionization above the threshold. The time stamp is corrected for the latency in the readout of the channels. The amount of charge, caused by the ionization of the silicon strip, is determined from the period that the charge of the strip remains above a predefined threshold by utilizing the theoretical curve for the silicon detector strips. The collections of

signals from adjacent strips form clusters. The position, total pulse height and average times are calculated for each of the clusters. This information is then utilized by two independent track identification methods [21].

The first method uses three dimensional points constructed from the clusters, called space points. Clusters on the ϕ strips and the z strips, from the same silicon panel that satisfy a minimum cluster pulse height as well as a consistent time and pulse height, are correlated to form three dimensional space points from the ϕ, z and panel position. Triplets of space points that have the SVT layer orders (1,3,5), (2,4,5) or (1,3,4) are then considered. Each triplet of points for a given SVT layer order, neglecting one z coordinate, is employed to determine a corresponding helix. If the neglected z coordinate is within a predetermined distance of the helix, the track is analyzed further. All space points that have a distance of closest approach to the helix that is consistent with coming from the track are added. Tracks that have four or more space points and satisfy a minimum $\frac{dE}{dx}$ are accepted if all the space points in the track are unique to that track or if the track is determined to be more consistent with the space points than the other candidate tracks. The consistency of a track to a set of space points is determined from the number of space points unique to the track, the $\frac{dE}{dx}$ χ^2 and the kinematic χ^2 for each space point corresponding to the track helix. The space points corresponding to tracks in one SVT layer order, are not employed in the track identification in other two layer orders [24] [18].

The second method employs a pattern recognition of circular paths in the xy plane to identify tracks. A preliminary circle is constructed from a cluster in the outer two SVT layers, the track origin[1] and a cluster in the middle layer. The circle parameters are recalculated without the origin when clusters from three layers have been correlated to a circle. The cluster in the middle layer, the third or fourth SVT layer, is identified as any ϕ cluster that is on a predetermined set of possible SVT modules. This constrains the

[1]The origin of a SVT is estimated as the normal beam interaction point.

identification to tracks with a momentum of 36MeV or greater. Again, a predetermined set of possible SVT modules are used to determine those modules that contain candidate clusters. The candidate clusters, which satisfy a transverse momentum dependent distance of closest approach cut, are added to the preliminary track forming a tree[2] of possible circles. Branches from the trees that deviate by hits in one layer are merged. The most probable circle for each tree is then determined from the chisquare of each branch,

$$\chi^2 = \sum_i \frac{\Delta^2_{(i)}}{\sigma_{res_{(i)}}} \tag{4.1}$$

where i is the cluster number, $\Delta_{(i)}$ is the deviation between the cluster and the circle and $\sigma_{res_{(i)}}$ is the resolution in the layer of the cluster. The circle is then transformed into a helix by applying the clusters from the z strips. The z clusters are mapped into a line in a similar procedure to that of the ϕ clusters. The z cluster, in the outermost layer that may correspond to a ϕ cluster on a given circle, is used to construct a line with the origin. This is propagated down to the inner layers forming a tree. Again, the line is recalculated without the origin once two z clusters have been identified. The χ^2 of each branch is utilized to determine the most probable z component from each tree. The track circles and z dependence are then merged to form a helix [25].

4.1.2 Finding Tracks in the DCH

The DCH is divided into 10 superlayers each with 32 supercells, seen in figure 4.1. It is within these supercells that the segments of tracks are identified.

[2]A tree is algorithm for data manipulation.

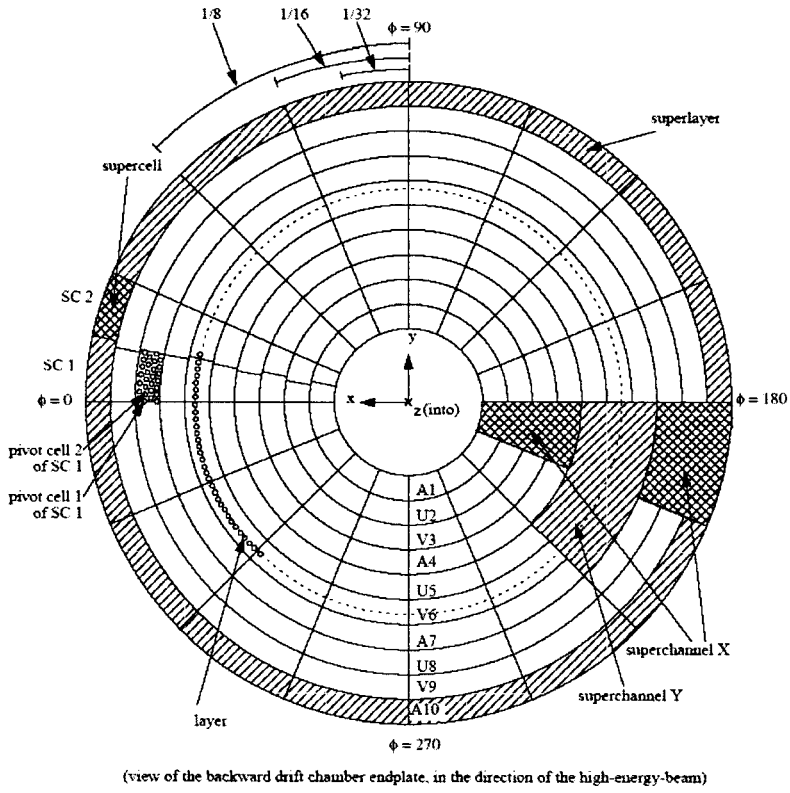

Figure 4.1: A diagram of the DCH decomposed into the regions required for track identification [22, Figure G1].

The third layer in every supercell is designated as the pivot layer. Each pivot cell in the pivot layer has an association with a pivot group, figure 4.2.

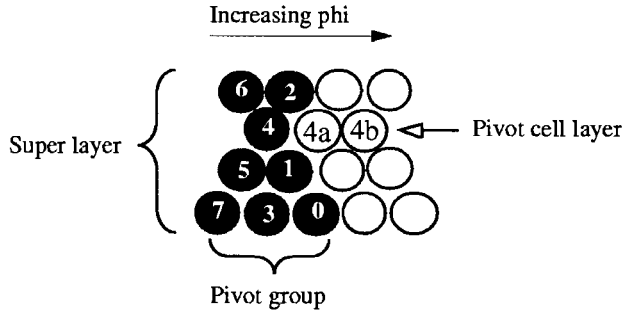

Figure 4.2: A diagram of a pivot group in the DCH [22, Figure 3].

Each pivot group is analyzed separately for track segments. The hit pattern is compared to valid hit patterns, which usually consist of a hit in 3 or 4 of the layers in the pivot group.

Each superlayer is divided into a map of the 10 superlayers and 120 cells in ϕ from which track segments from cells in adjacent superlayers are matched to form possible track patterns. These possible track patterns are then compared with precomputed track patterns with known parameters. These parameters can now be employed as seeds for a fitting procedure [22].

4.2 Fitting Tracks

4.2.1 Least Square Fit

The least square fit is a global fit in which the deviation between a Probability Density Function (PDF) and a distribution is minimized. The deviation between the PDF, $f(x_1, x_2, ..., x_n)$, and the distribution, g, is quantified by the chisquare,

$$\chi^2 = \sum_{i,j} \left(f_{(i)}(x_1, x_2, ..., x_n) - g_{(i)} \right) S_{ij} \left(f_{(j)}(x_1, x_2, ..., x_n) - g_{(j)} \right) \tag{4.2}$$

where i and j correspond to the bin number, $g_{(k)}$ the value in the kth bin of the distribution, $f_{(k)}(x_1, x_2, ..., x_n)$ is the value of the kth bin of the PDF, which depends on the parameters x_1 to x_n, and S_{ij} is the covariance matrix for the PDF bins.

The chisquare of the distribution g and PDF $f(x_1, x_2, ..., x_n)$, has a local minimum when $\frac{\partial \chi^2}{\partial x_k} = 0$ and $\frac{\partial^2 \chi^2}{\partial^2 x_k} < 0$. Thus, the global minimum of the chisquare is the point in parameter space that has the maximum probability of describing the distribution for a given PDF [12].

4.2.2 Kalman Filter

General Theory of Kalman Fitting

The Kalman Technique for fitting tracks (in contrast to the least square fit) is causal, enabling random stochastic [3] processes such as scattering, energy loss and inhomogeneity of the magnetic field, to be incorporated into the fit. The fit parameters are represented by a state vector $\mathbf{V}$, and the corresponding covariance matrix C. From this, the trajectory is expressed by a parametric equation, $\mathbf{T}(\mathbf{V}, x)$, parameterized in terms of x. Since the Kalman fit is causal, a set of initial parameters or reference parameters are used to seed the process. Then, the consequence of adding a hit to the reference trajectory, $\mathbf{R}$, and parameters is evaluated through the difference between the location of the hit and the reference trajectory at the distance of closest approach often called the residual, $\mathbf{r}$. The transformation rules to the weight space, where the addition of the hit to the reference trajectory is computed, are:

$$\beta \equiv \gamma\mathbf{V} \equiv \mathrm{C}^{-1}\mathbf{V} \tag{4.3}$$

$$\gamma_H \equiv \mathrm{L}^T\omega^2\mathrm{L} \tag{4.4}$$

$$\beta_\mathbf{H} \equiv \mathrm{L}^T\omega(\mathbf{LR}-\mathbf{r}) \tag{4.5}$$

where β is the state vector in weighted space, γ is the inverse of the covariance matrix, β_H is the residual vector in weighted space, γ_H is the inverse of the residual covariance matrix, $\omega = \frac{1}{\sigma^2}$ is the weight of the residual, σ is the uncertianty of the residual and $\mathrm{L} = \frac{\delta\mathbf{r}}{\delta\mathbf{V}}\Big|_R$ is Jacobian of the residual in parameter space for the reference trajectory at the closest point to the hit coordinates. In weighted space, the state vector and covariance matrix become

$$\beta' = \beta + \beta_\mathbf{H} \tag{4.6}$$

$$\gamma' = \gamma + \gamma_H \tag{4.7}$$

when the reference parameters are updated with a hit. This process is repeated until the state vector has been updated with all the hits identified with the given track. From least

[3] A stochastic process is defined as a process in which the conditions are not reproducible.

squares, it can be shown that

$$\beta_{\mathbf{opt}}(x) = \beta_{out}(x) + \beta_{in}(x) \quad (4.8)$$
$$\gamma_{opt}(x) = \gamma_{out}(x) + \gamma_{in}(x) \quad (4.9)$$

where β_{opt} and γ_{opt} are the optimized values for a given point x, $\beta_{out}(x)$ and $\gamma_{out}(x)$ are the values obtained by starting from the innermost hit and working outward, and $\beta_{in}(x)$ and $\gamma_{in}(x)$ are the values obtained by starting from the outer most hit and working inwards [20] [14].

Kalman Fitting in the BaBar Experiment

The trajectory of a charged track in a unidirectional magnetic field, such as the magnetic field in the inner tracking region of the BaBar detector, is a helix. A common parameterization of a trajectory along a helix in cartesian coordinates is:

$$\mathbf{T}(\mathbf{V},x) = \begin{bmatrix} \frac{\sin(\phi_0+\kappa x)-1}{\kappa} + d_0\sin(\phi_0) \\ \frac{1-\cos(\phi_0+\kappa x)}{\kappa} + d_0\cos(\phi_0) \\ z_0 + x\tan(\lambda) \end{bmatrix} \quad (4.10)$$

where x is the transverse distance of the particle with which the trajectory is parameterized. The state vector parameters are d_0 the distance of closest approach to the interaction point in the xy plane; ϕ_0, the ϕ angle at the distance of closest approach; κ, the curvature of the trajectory in the xy plane where the sign represents the charge of the track; z_0, the distance of closest approach along the z axis and λ, the dip angle, the complimentary angle to θ. The corresponding momentum may be written

$$\mathbf{P}(\mathbf{V},x) = \frac{qcB_z}{\kappa}\begin{bmatrix} \sin(\phi_0+\kappa x) \\ \cos(\phi_0+\kappa x) \\ \tan(\lambda) \end{bmatrix} \quad (4.11)$$

in cgs units. q is the charge of the particle, B_z is the z component of the magnetic field and c is the speed of light.

Energy loss and scattering interactions in the detector are incorporated into the Kalman fit as discrete changes to the state vector and covariant matrix. Therefore, as the trajectory

of the track is traversed during the addition of hits, the state vector and covariant matrix in parameter space are corrected at discrete intervals as shown below:

$$\begin{aligned} \mathbf{V}' &= \mathbf{V} \pm \Delta\mathbf{V} \\ &= \mathbf{V} \pm \frac{\sqrt{\mathrm{P}^2+\mathrm{m}^2}}{\mathrm{P}^2}\frac{\delta\mathbf{V}}{\delta\Psi}\frac{dE}{dx}\Delta s \qquad (4.12) \\ \mathrm{C}' &= \mathrm{C} \pm \Delta\mathrm{C} \\ &= \mathrm{C} \pm \left[\frac{\delta\mathbf{V}^T}{\delta\Phi}\frac{\delta\mathbf{V}}{\delta\Phi} + \frac{\delta\mathbf{V}^T}{\delta\Theta}\frac{\delta\mathbf{V}}{\delta\Theta}\right]\sigma_S^2 + \frac{\delta\mathbf{V}^T}{\delta\Psi}\frac{\delta\mathbf{V}}{\delta\Psi}\frac{\mathrm{P}^4}{\mathrm{P}^2+\mathrm{m}^2}\sigma_{\Delta E}^2 \qquad (4.13) \end{aligned}$$

where Θ and Φ are the two independent scattering angles, σ_S^2 is the variance for the scattering angles, Ψ is the fractional change in momentum, $\frac{dE}{dx}$ is the average energy loss, $\sigma_{\Delta E}$ is the variance for the change in energy, Δs is the path length, P is the momentum and m is the mass for the given hypothesis. The $+/-$ signs refer to the direction of the fitting process outward/inward. Since the correction for energy loss and scattering are dependent on the mass, the Kalman fit must be computed for all five mass hypothesis[4].

Similarly, the inhomogeneity of the magnetic field is treated as a set of discrete changes to the state vector and covariant matrix. The change in the momentum vector, $\Delta\mathbf{P} = \int_A^B [\mathbf{B}(\mathbf{T}(\mathbf{V},x)) - \mathbf{B}_{avg}] \times \mathrm{ds}$, corrects the trajectory at the midpoint of each discrete interval. The correction to the covariance matrix is neglected because the errors on the magnetic map are negligible. The correction to the state vector is

$$\begin{aligned} \mathbf{V}' &= \mathbf{V} \pm \Delta\mathbf{V} \\ &= \mathbf{V} \pm \frac{\delta\mathbf{V}}{\delta\Theta}\frac{\Delta\mathbf{P}}{|\mathbf{P}|}\cdot\hat{\Theta} + \frac{\delta\mathbf{V}}{\delta\Phi}\frac{\Delta\mathbf{P}}{|\mathbf{P}|}\cdot\hat{\Phi} \qquad (4.14) \end{aligned}$$

[20].

4.3 Track Reconstruction at BaBar

The implementation of the Tracking Reconstruction framework at BaBar transverses the complete event reconstruction process and is specific to the software version. The following

[4]The five mass hypothesis in BaBar correspond to the ten stable/pseudo-stable charged particles that can be detected: $e^{\pm}$, $\mu^{\pm}$, $\pi^{\pm}$, $K^{\pm}$ and $p^{\pm}$.

section is a description of the software version that this study is concerned with, release version 12. A flow chart of the reconstruction process is shown in figure 4.3. Analysis of the physics events begins with the acquisition of data from the detector components into the Trigger. It is in the Trigger that preliminary events selection is completed and the DCH tracks are identified. This stage is called online reconstruction since it is completed while the detector is actively collecting data.

4.3.1 Trigger Selection

The selection of events of interest in the BaBar Detector has been decomposed into two stages: the hardware based level 1 Trigger (L1) and the software based Level 3 Trigger (L3). An additional trigger, Level 2 which was not implemented, was also included in the data-flow design in case the luminosity produced a higher background in the detector than expected. These triggers are designed to select events of interest while reducing the background and random noise [11].

Level 1 Trigger

The Level 1 Trigger accepts information from the DCH, EMC and IFR as input for the Drift Chamber Trigger (DCT), Electromagnetic Calorimeter (EMT) and the Instrumented Flux Return Trigger (IFT). The SVT and DIRC are neglected due to their large latency.

The DCT is updated every 269ns with a 1 bit signal from each of the 7104 cells in the DCH. This information is separated into pivot cell groups, which the Track Segment Finder (TSF) can then search for track segments. This is uploaded to the Binary Track Linker (BTL) and to eight P_t (Transverse Momentum) Discriminatory (PTD) modules in parallel. The BLT links the track segments to form complete tracks, while the PTD utilizes the track segments in the axial superlayers to identify tracks with a momentum higher than 0.8GeV. The BLT and PTD produce three maps in ϕ, called ϕ-maps.

In addition to the ϕ-maps from the DCT, ϕ-maps from the EMT and the IFT output

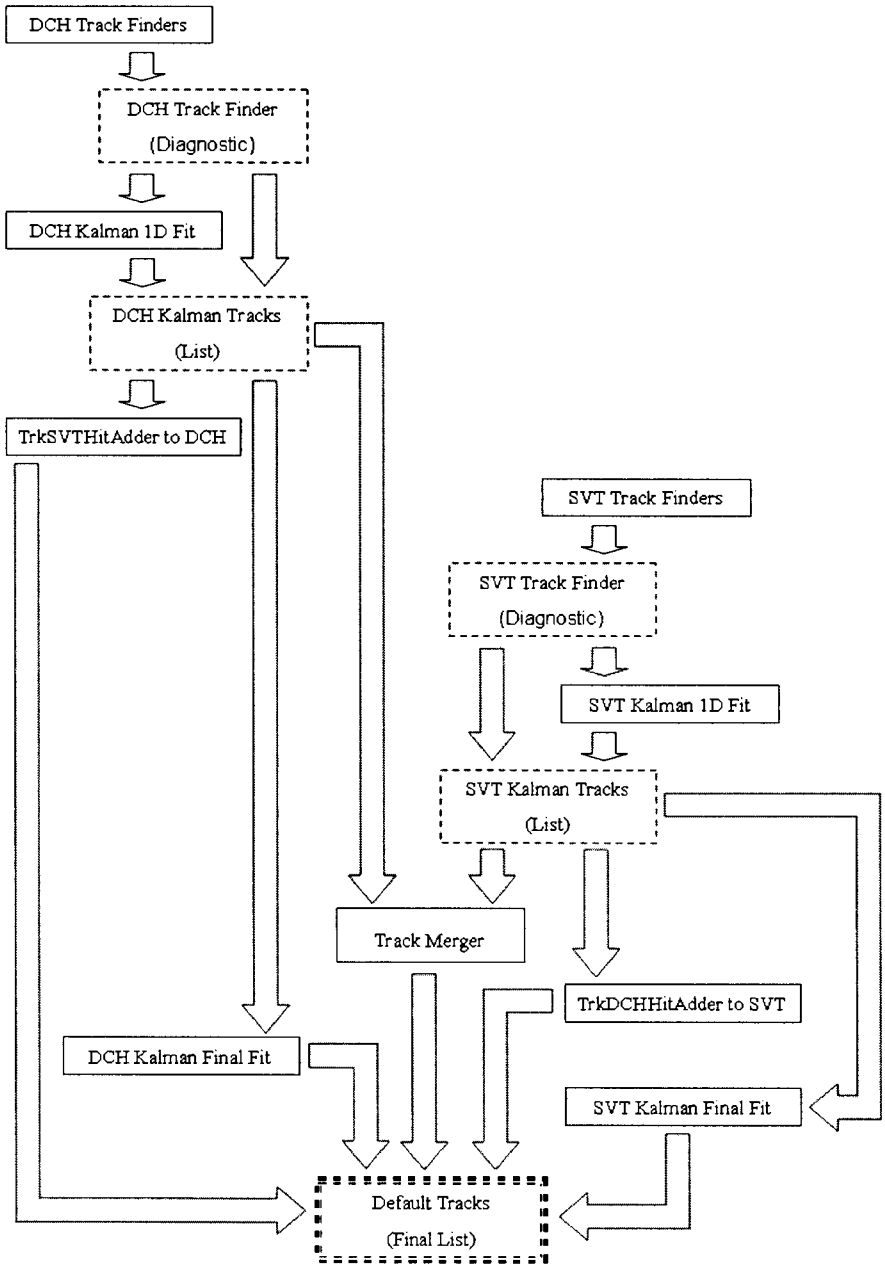

Figure 4.3: A Flow chart of the release version 12.x track reconstruction algorithms for the DCH and SVT. The execution order of the algorithms proceeds from the top to the bottom. [23, pg. 2]

are utilized by the Global Level Trigger (GLT) to determine if the signal contains a physics event. If the GLT yields an "accept", the detector and timing information is read out and forwarded to the Level 3 Trigger. The frequency at which the events are accepted by the GLT is approximately 1kHz, a result of the luminosity and the background rate of the detector [11].

Level 3 Trigger

The Level 3 Trigger, which runs on a farm of Linux machines, has a primary purpose of reducing the frequency of selected events from its maximum input rate, 2KHz, to less than 120Hz with a high efficiency in physics events of interest. The L3 Trigger also supports the online fast monitoring, and selects calibration samples. The L3 Trigger receives input from the L1 Trigger and two subdetectors, the DCH and the EMC.

The input from the DCH is used to find track patterns, to find the inital time of ionization in the cells, t_0, by the subatomic particle and then to fit the identified tracks. The track segments determined by the TSF is then utilized in the identification of tracks through the pattern recognition procedure. t_0, which enables the track to be associated with the correct event, is computed in a two step process from the measured time for the hit. First, an offset, determined from the average drift time, is removed from the time on all of the wires associated with a particluar track. Then, the drift time is improved through an iterative process in which the drift distances are converted to drift times with the "time-to-distance drift function" for each TSF segment until an acceptable convergence of t_0 is achieved, or the maximum of 5 iterations are completed. The tracks are fit with a least square fit to determine five track parameters. Again, due to time constraints, the fit is restricted to 5 iterations or less if an acceptable convergence has been reached.

The resulting track and calorimeter information is then evaluated to determine its significance to the physics. The "Physics Filters" are designed to select $\tau^+\tau^-$, two photon, $B\bar{B}$ and $c\bar{c}$ events with a high efficiency. In addition to the "Physics Filters", the "Bhabha

Filters" isolate the unique topology of electron-positron scattering and rejects them from the selected events. This selection reduces frequency to a rate in which the entire event from all of the subdetectors and the two triggers can be written to tape for storage and later, a complete reconstruction of the events [11].

4.3.2 Offline Track Reconstruction

The event reconstruction, which is completed after the events have been stored on tape, is called offline reconstruction. For a given event, each of the DCH tracks that were identified in the Trigger are fitted with a one-directional Kalman fit that is seeded from the preliminary least square fit. The direction of this Kalman fit proceeds from the outer wall of DCH to the inner support tube. Each of the DCH tracks is then processed in the TrkSVTHitAdder to determine if any of the hits, or space points, in the SVT correspond. Each track is extrapolated in SVT where all the clusters within a geometric path are associated with that track. The associated tracks form a tree which has the constraint that at each layer, as the tree is constructed by starting at the outermost layer, only the four branches with the lowest χ^2 are kept. The most probable track is selected from the tree based upon the χ^2 and geometrical cuts. When a match is determined, a bi-direction Kalman fit is completed and the track is added to the default track list, "Default Tracks". The remaining SVT clusters are utilized by the circle and the space point track identification methods. The resulting tracks are fitted with a helix by means of a global χ^2. The SVT tracks are then fit with a preliminary one directional Kalman fit in the opposite direction of the DCH tracks. The track parameters at the support tube of the fitted SVT and remaining DCH tracks are compared to determine if the χ^2 corresponding to their fitted parameters are consistent. Tracks that are deemed to be consistent are merged by a bi-direction Kalman fit and added to the "Default Tracks" list. In the TrkDCHHitAdder, the uncorrelated SVT tracks are projected into the DCH and associated with any independent hit, a hit that is not contained with a track, within a tolerance. The associated hits are utilized to form

a tree similar to those in the TrkSVTHitAdder. As the tree extends outwards, in each superchannel, defined in figure 4.1, the four branches with the lowest χ^2 are added. In parallel to the TrkSVTHitAdder, for a given SVT track the most probable track projection is selected from the tree based upon geometrical cuts and the χ^2. After a bi-directional Kalman fit is completed these tracks are also added to the "Default Tracks" list. The tracks that are specific to either the DCH or SVT, referred to as DCH only tracks and SVT only tracks, are fit with a bi-directional Kalman fit and added to the "Default Tracks" list, thus completing the track reconstruction process [16] [17] [18] [19].

The reconstructed events are then stored in three databases; the Mini database, the Micro database and the Nano database. The Mini database stores "pattern-recognition objects" [26, Data content of the mini], such as hits, clusters and tracks, and the reconstructed parameters of these objects. The primary purpose of this database is to enable the reconstruction database to be studied and for analyses that contain items that may not be reconstructed with the standard methods. The Micro database contains the physics parameters of objects in the associated events and is designed to be suitable for most physics analysis. In contrast to the former two databases, the Nano database is not for a complete physics analysis. Instead, it is designed for the rapid identification of physics events of interest through the use of tag variables [15].

4.3.3 Inefficiencies in the Track Reconstruction

The primary sources of inefficiencies at BaBar are caused by interactions between the material in the detector and the charged particles traversing the detector. Hard scattering of a charged particle by material in the detector may cause the trajectory of a charged particle to be severely altered. Thus, the signal pattern left by the particle will not conform to any of the known hit patterns preventing the track from being reconstructed. In addition to this, a particle may also be absorbed within the beam pipe or SVT before a signal pattern that can be reconstructed is produced. This primarily occurs for low energy particles.

Chapter 5

Tracking Efficiency Analysis

In Particle Physics, the primary means of comparing the theoretical predictions to experiment rely on comparisons between data and Monte Carlo simulations of the physics processes expected to describe the data. Therefore, it is important that the Monte Carlo simulator correctly models the behavior of the detector response. The response of the BaBar detector is simulated in great detail from first principles through the utilization of the GEANT4 package [32]. This is the state-of-the-art simulation tool in particle physics and its application to the BaBar has been exhaustively validated. The work of this thesis represents part of the validation process and quantifies the degree to which minor corrections to the MC need to be applied in order to have the MC completely consistent with the data.

One specific characteristic of a particle detector, which requires a correction, is the tracking efficiency. There are two main methods which can be employed to determine the correction factor between MC and data at BaBar: Detector dependent methods and physics dependent methods. The former method utilizes the relative independence of the SVT and DCH to determine the relative efficiency and the corresponding correction factor. The latter method, with which this work is concerned, uses a physical process to determine the efficiency and a correction factor for the detector. The results of these methods are then compared to determine the Monte Carlo Total Tracking Efficiency Correction Factor.

5.1 Method

5.1.1 General Method

One method to determine the tracking efficiency of a detector is to utilize events which are constrained to a specific multiplicity[1]. This can be utilized in a tracking efficiency study, when an event can be identified by selection criteria on $n-1$ of the particles in the event, to determine the probability of a nth track being reconstructed. Thus, the probability of reconstructing the track is

$$(\epsilon \mathrm{A}) = \frac{\mathrm{N}_{(n\ tracks)}}{\mathrm{N}_{(n-1\ tracks)} + \mathrm{N}_{(n\ tracks)}} \tag{5.1}$$

where ϵ is the efficiency of reconstructing a track, A is the geometric acceptance of the detector, $\mathrm{N}_{(n\ tracks)}$ is the number of events where n tracks were reconstructed and $\mathrm{N}_{(n-1\ tracks)}$ is the number of events where $n-1$ tracks were reconstructed. This pseudo-efficiency, which differs from the global efficiency of reconstructing a track only by the geometric acceptance, can be used to calculate the correction factor between data and MC. The correction factor is defined as:

$$\Delta = 1 - \frac{\epsilon_{Data}}{\epsilon_{MC}} = 1 - \frac{\epsilon_{Data} A}{\epsilon_{MC} A}. \tag{5.2}$$

From charge conservation, the nth track charge can be identified from the $n-1$ tracks, allowing the pseudo efficiency to be calculated for both positive and negative nth tracks. Therefore, the charge asymmetry of the tracking efficiency may be calculated as

$$a_{\pm} = \frac{\epsilon_+ - \epsilon_-}{\epsilon_+ + \epsilon_-} = \frac{\epsilon_+ A - \epsilon_- A}{\epsilon_+ A + \epsilon_- A}. \tag{5.3}$$

Understanding the charge asymmetry of the detector is important at BaBar because the experiment's primary focus is to study CP Violation in B mesons, which is detected through charge asymmetries.

Since the event selection is independent of the nth track, the nth track may be selected

[1]The multiplicity of an event is the number of tracks in the event.

with several different track criteria. This is advantageous because the BaBar collaboration has three definitions for identifying tracks produced by electrons, muons, pions ($\pi^{\pm}$), kaons ($K^{\pm}$) and protons, namely Charged Track (CT), Good Track Very Loose (GTVL) and Good Track Loose (GTL). A Charged Track is defined as any track which is reconstructed. A Good Track Very Loose is a Charged Track that satisfies two additional criteria: the particle has a physical momentum, P<10GeV and the particle is consistent with coming from the interaction region. The latter constraint is satisfied when the distance to the closest approach to the interaction region in the xy plane is less than 1.5cm and the distance to the closest approach in the z direction is less than 10cm. Good Track Loose is defined as any Good Track Very Loose that satisfies the Drift Chamber constraints: that there are 12 or more Drift Chamber hits and that the transverse momentum P_t >0.100GeV [1].

5.1.2 Application of Tau Decay to Tracking Efficiency: The τ Tracking Efficiency Method

The τ particle, when it decays, produces an odd number of charged tracks due to charge conservation; this constrains the final state to an odd multiplicity. As a result, τ decays are a prime candidate for the previously mentioned tracking efficiency method. The τ decay $\tau^{\pm} \rightarrow h^{\pm}h^{\pm}h^{\mp}\nu_{\tau}$, where h is a pion or a kaon, is the τ decay which has the largest branching fraction, $(10.01 \pm 0.09)\%$ and $n > 1$. The two specific decays used in this study are: $\tau^{\pm} \rightarrow \rho^0 h^{\pm}\nu_{\tau}$ and $\tau^{\pm} \rightarrow \pi^{\pm}\pi^{\pm}h^{\mp}\nu_{\tau}$. Because the τ particle, from which these tracks are produced, has a large momentum, all the final tracks have a similar direction. Clearly, the final products of the two τ decays are geometrically separated. The second τ is identified through a leptonic decay to an electron or a muon. The isolated lepton, produced in this decay, is called a lepton tag because it cleanly identifies the event as a τ pair event. Table 5.1 contains the four $\tau^{+}\tau-$ combinations which are employed in the τ Tracking Efficiency Study.

Channel	3-Track Side	1-Track Side
$e-\rho$	$\tau^- \to \rho^0 h^- \nu_\tau$	$\tau^+ \to e^+ \nu_e \bar{\nu}_\tau$
$\mu-\rho$	$\tau^- \to \rho^0 h^- \nu_\tau$	$\tau^+ \to \mu^+ \nu_\mu \bar{\nu}_\tau$
$e-\pi\pi$	$\tau^- \to \pi^-\pi^- h^+ \nu_\tau$	$\tau^+ \to e^+ \nu_e \bar{\nu}_\tau$
$\mu-\pi\pi$	$\tau^- \to \pi^-\pi^- h^+ \nu_\tau$	$\tau^+ \to \mu^+ \nu_\mu \bar{\nu}_\tau$

Table 5.1: The Channels employed in the τ Tracking Efficiency Method (charge conjugate decays are implied).

The electron and muon are referred to as the lepton tag, the identified pions are referred to as the $\pi 1$ and the $\pi 2$ track, while the hadron (h), used to measure the efficiency, is called the 4th track [1].

However, there are additional complications in this method when there is more than one missing track in higher track multiplicity τ decays, "Ghost Tracks" and "Loopers". Ghost Tracks are caused when the hits caused by a single particle are reconstructed as two tracks. Loopers are additional tracks, which are reconstructed, because a charged particle with a low momentum has formed multiple loops in the magnetic field. The deviation in the correction factor caused by these complications are quantified by calculating the correction factor and charge asymmetry with a second efficiency definition (ϵ'),

$$(\epsilon' \mathrm{A}) \quad = \quad \frac{\mathrm{N}_{(n\ tracks)}}{\mathrm{N}_{(n-1\ tracks)} + \mathrm{N}_{(n\ tracks)} + \mathrm{N}_{(n+1\ tracks)}} \tag{5.4}$$

where $\mathrm{N}_{(n+1\ tracks)}$ is the number of events with $n+1$ tracks. The correction factor and charge asymmetry which include Ghost Tracks and Loopers are:

$$\Delta' = 1 - \frac{\epsilon'_{Data}}{\epsilon'_{MC}} = 1 - \frac{\epsilon'_{Data} A}{\epsilon'_{MC} A} \tag{5.5}$$

and

$$a'_{\pm} = \frac{\epsilon'_{+} - \epsilon'_{-}}{\epsilon'_{+} + \epsilon'_{-}} = \frac{\epsilon'_{+} A - \epsilon'_{-} A}{\epsilon'_{+} A + \epsilon'_{-} A}. \tag{5.6}$$

The differences between the tracking efficiencies and charge asymmetry calculated with ϵ and ϵ' are treated as a systematic error.

5.1.3 Consideration of Tracking Efficiency as a Function of P_t, θ and ϕ

One disadvantage of the τ Tracking Efficiency Method is that the correction factor and the charge asymmetry can not be directly determined as a function of P_t, θ and ϕ, on which the detector reconstruction depends. This is a result of missing the P_t, θ and ϕ information when the 4th track is not reconstructed. Therefore, the P_t, θ and ϕ information for the 4th track must be estimated from kinematic constraints. However, these constraints are only an approximation because the kinematic information associated with the three neutrinos from the τ pair decay is lost. Moreover, the 4th track is required to be uniquely identified to enable a direct comparison between the P_t, θ and ϕ distributions of events with and without a reconstructed 4th track. This requirement is satisfied for the $\pi\pi$ channels since the charge of the 4th track is both unique to the 3-track side and equal to the charge of the lepton. The $\mu - \pi\pi$ channel is employed in this study because of contamination in the electron channels which is discussed in Chapter 7: Systematic Uncertainty Studies. The spherical angles, θ and ϕ, can be estimated from the averaged momentum of the measured tracks. This is a reasonable assumption because the lab frame momentum of a τ particle is much larger than the missing energy from the τ particle. Therefore, the angles of the missing track may be written:

$$\phi_{avg} = \frac{\mathrm{P}^{(lab)}_{y,\pi 1} + \mathrm{P}^{(lab)}_{y,\pi 2} + \hat{\mathcal{P}}\left(\mathrm{P}^{(lab)}_{y,Lep}\right)}{\left|\mathrm{P}^{(lab)}_{y,\pi 1} + \mathrm{P}^{(lab)}_{y,\pi 2} + \hat{\mathcal{P}}\left(\mathrm{P}^{(lab)}_{y,Lep}\right)\right|} \times arccos\left(\frac{\mathrm{P}^{(lab)}_{x,\pi 1} + \mathrm{P}^{(lab)}_{x,\pi 2} + \hat{\mathcal{P}}\left(\mathrm{P}^{(lab)}_{x,Lep}\right)}{\left|\mathbf{P}^{(lab)}_{t,\pi 1} + \mathbf{P}^{(lab)}_{t,\pi 2} + \hat{\mathcal{P}}\left(\mathbf{P}^{(lab)}_{t,Lep}\right)\right|}\right) \quad (5.7)$$

$$\theta_{avg} = \begin{cases} arcsin\left(\frac{\left|\mathbf{P}^{(lab)}_{t,\pi 1} + \mathbf{P}^{(lab)}_{t,\pi 2}\right|}{\left|\mathbf{P}^{(lab)}_{\pi 1} + \mathbf{P}^{(lab)}_{\pi 2}\right|}\right) & \text{if } 0 \leq \mathbf{P}^{(lab)}_{z,\pi 1} + \mathbf{P}^{(lab)}_{z,\pi 2} \\ \pi - arcsin\left(\frac{\left|\mathbf{P}^{(lab)}_{t,\pi 1} + \mathbf{P}^{(lab)}_{t,\pi 2}\right|}{\left|\mathbf{P}^{(lab)}_{\pi 1} + \mathbf{P}^{(lab)}_{\pi 2}\right|}\right) & \text{if } 0 > \mathbf{P}^{(lab)}_{z,\pi 1} + \mathbf{P}^{(lab)}_{z,\pi 2} \end{cases} \quad (5.8)$$

where $\hat{\mathcal{P}}$ is the parity operator and $\mathrm{P}^{(lab)}_{\mathrm{A,B}}$ is the momentum in the A direction for the B particle in the laboratory frame. The addition of the momenta is a pseudo-weighting system which reflects correlation between the particles momentum and the τ direction. The

momentum of the tag lepton is neglected in the estimate of θ because the boost between the centre-of-mass frame and laboratory frame biases the result independently of which frame the parity operator acts. Figure 5.1 and 5.3 show the correlation between the missing and 4th track angles in ϕ and θ respectively, while figures 5.2 and 5.4 show the resolution for the $\theta_{avg}^{(lab)}$ and $\phi_{avg}^{(lab)}$.

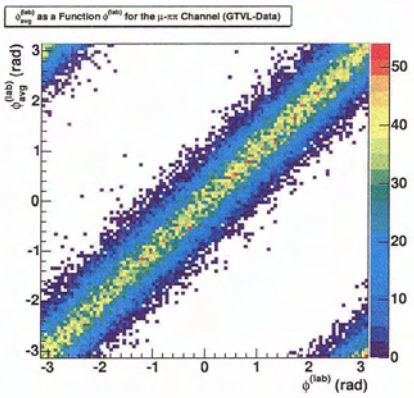

Figure 5.1: ϕ_{avg} as a function of $\phi_{4th\ Track}$ in the laboratory reference frame. This plot uses the data from the 1930V data that satisfies the GTVL definition.

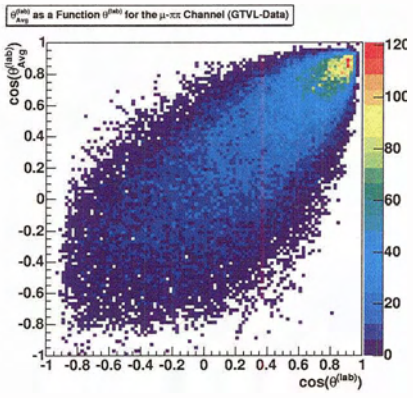

Figure 5.3: θ_{avg} as a function of $\theta_{4th\ Track}$ in the laboratory reference frame. This plot uses the data from the 1930V data that satisfies the GTVL definition.

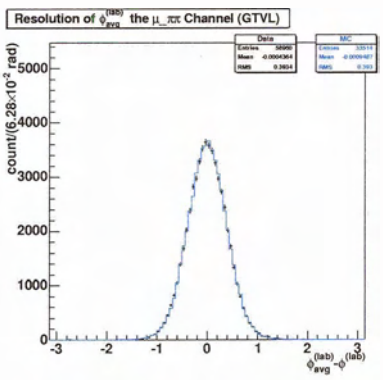

Figure 5.2: The resolution of ϕ_{avg} in the laboratory reference frame. This plot uses the data, represented by points, and MC, represented by the line, from the 1930V data that satisfies the GTVL definition.

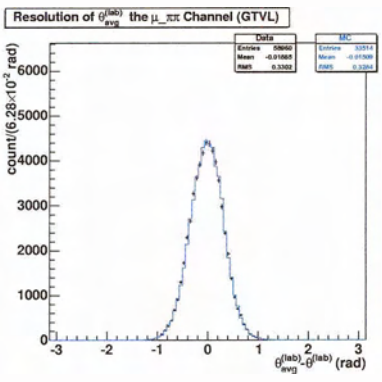

Figure 5.4: The resolution of θ_{avg} in the laboratory reference frame. This plot uses the data, represented by points, and MC, represented by the line, from the 1930V data that satisfies the GTVL definition.

The momentum distribution of the missing track can be estimated from the missing momentum distribution. This can be seen from the kinematic bound $E_{miss} = E_\tau - E_{\pi 1} - E_{\pi 2} > E_{4th\ Track}$ in the centre-of-mass frame. Since the masses are negligible compared to the momentum, the kinematic bound may be written as $P^{miss} = P_\tau - P_{\pi 1} - P_{\pi 2} > P_{4th\ Track}$. In the BaBar Detector, the transverse plane is nearly orthogonal to the boost, resulting in the bound holding true for the transverse momentum in the laboratory reference frame. Figure 5.5 illustrates the kinematic bound for the transverse momentum in the centre-of-mass frame while figure 5.6 is a correlation plot of the transverse momentum of the 4th track in the two reference frames.

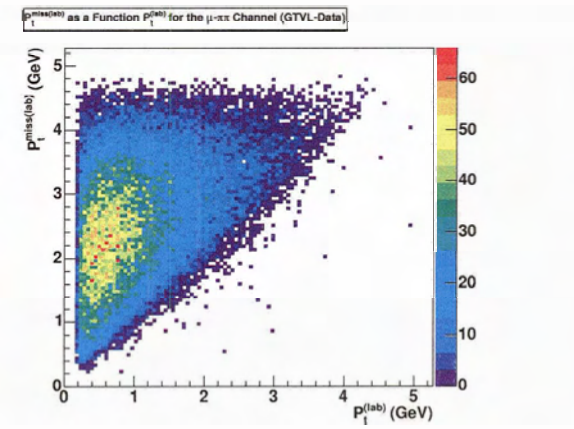

Figure 5.5: P_t^{miss} as a function of P_t of the 4th track in the centre-of-mass reference frame. This plot uses the data from the 1930V data that satisfies the GTVL definition.

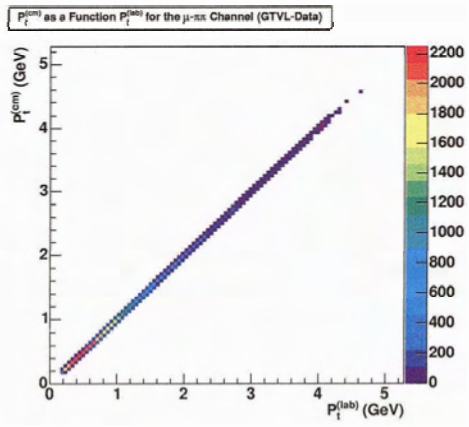

Figure 5.6: $P_t^{(cm)}$ as a function of $P_t^{(lab)}$ for the 4th track. This plot uses the data from the 1930V data that satisfies the GTVL definition.

Clearly, by selecting a region in $P_t^{miss} = (E_\tau - E_{\pi 1} - E_{\pi 2}) \times cos(\theta_{avg}^{(cm)})$, a corresponding region in $P_t^{(cm)} \simeq P_t^{(lab)}$, the transverse momentum of the 4th track in the centre-of-mass and laboratory frame, is made. Therefore, if the 4th track is measured, the probability distribution of the missing momentum can be determined. If the bin size of the transverse momentum is chosen such that the variation in the efficiency is small, the efficiency can be

treated as a constant resulting in a distribution which is independent of the efficiency. This allows for the probability matrix to be determined from events in which the 4th track is measured and then for it to be applied to the events in which the 4th track is missing, thus estimating the P_t distribution of the 4th track. The P_t for the events with three, four and five tracks can then be used to determine the efficiency. Figure 5.7 illustrates the separation in $P_t^{(lab)}$ by employing $P_t^{miss(lab)}$

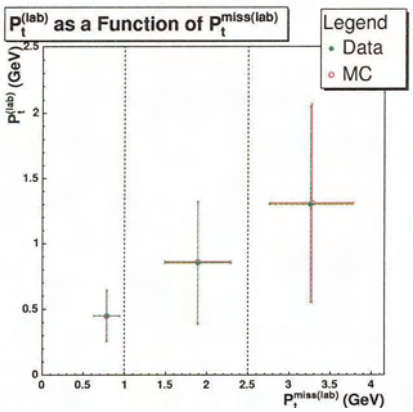

Figure 5.7: The mean value of $P_t^{(lab)}$ as a function of the mean value of $P_t^{miss(lab)}$ in the three bins: $P_t^{miss} < 1.0$GeV, $1.0\text{GeV} < P_t^{miss} < 2.5$GeV and $2.5\text{GeV} < P_t^{miss}$. The error bars represent the RMS in each bin. This plot uses the data from the 1930V data that satisfies the GTVL definition. The closed circles correspond to the data, while the open circles represent the MC.

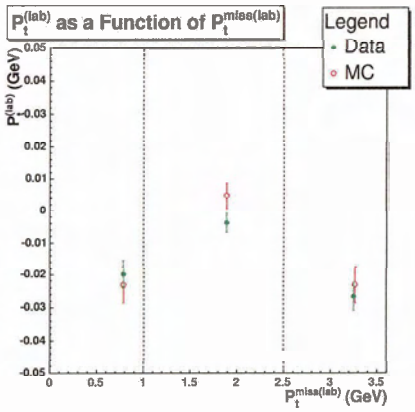

Figure 5.8: The mean deviation of $P_t^{(lab)}$ from a linear fit as a function of the mean value of $P_t^{miss(lab)}$ in the three bins: $P_t^{miss} < 1.0$GeV, $1.0\text{GeV} < P_t^{miss} < 2.5$GeV and $2.5\text{GeV} < P_t^{miss}$. The linear fit employed in this plot magnifies the error bars which represent the standard deviation on the average in each bin. This plot uses the data from the 1930V data set that satisfies the GTVL definition. The closed circles correspond to the data, while the open circles represent the MC.

Unfortunately, when these results are applied to the events with only three tracks, a bias, resulting from the loss of information in the low $P_t^{(lab)}$ region where the efficiency is zero, is introduced. This bias could be estimated by the MC Truth if the information about the track prior to reconstruction were avaliable. The next version of the code will have this

information. The statistical uncertainty in this method was estimated with "Toy MC"[2]. The measured number of events for the 3, 4 and 5 track events in each of the relevant bins was employed as the input for the Gaussian distribution. From this, the distributions for the matrix solutions, tracking efficiencies and therefore the corresponding statistical uncertainties were obtain. Details of the tables and matrices are given in Appendix K.

5.2 Event Selection Criteria in the τ Tracking Efficiency Study

In the τ Tracking Efficiency Study, only events with 3 to 5 tracks are analyzed; therefore, events are selected which contain 3 to 5 Charged Tracks. When two extra tracks are identified, the track with the highest mometum is defined as the 4th track. Events with a total charge of -1, 0 and +1 are selected, as a requirement of the τ Tracking Efficiency Study and to suppress beam gas. Contamination from photons that have interacted with the material in the detector to produce an electron positron pair (called photon conversions) and K_s^0 meson decays ($K_s^0 \rightarrow \pi^+\pi^-$) are then suppressed. Photon conversions are suppressed by rejecting events containing two tracks with an invariant mass $<$ 50MeV where one of these tracks passes the Very Loose Electron criteria, defined in table L.2. The K_s^0 are suppressed by vetoing events which contain two tracks with a vertex more than 2cm from the beam spot, a decay vertex with a χ^2 probability > 0.01 for being K_s^0 and an invariant mass within 10MeV of the K_s^0 mass.

The events that passed the base selection criteria are then required to pass the track selection criteria for the lepton and two pion tracks. The three tracks, which are considered as lepton or pion candidates, must satisfy the Good Track Loose definition, have a transverse momentum $P_t > 200MeV$ and have both a xy impact parameter less than 1mm and a z impact parameter less than 3cm. For kinematic reasons, the lepton tag is the most isolated track in the event. Therefore, the most isolated track in the event is required to be a

[2]Toy MC refers to an implementation of Monte Carlo simulation method to estimate a distribution of a known quantity, such as statistical fluxuations, for calculations that may contain unkown correlations.

minimum of 120^o in the centre-of-mass frame from the other tracks. In addition to this, the lepton tag is isolated from neutral particles by requiring that there are no energy clusters in the EMC that are independent of the charged tracks, with an energy 100MeV, within 90^o of the lepton in the laboratory frame. To remove background, the lepton momentum is constrained to be between $20 - 80\%$ of the of the beam energy in the centre-of-mass frame. Then, the lepton tag candidate is required to satisfy the particle selection criteria. The lepton tag is identified as an electron if it passes the Very Tight Electron criteria and a muon if it passes the Loose Muon Selection criteria. Again, the particle selection criteria are defined in tables L.3 and L.4. On the three track side, the two pions are identified by requiring that two of the 3-track tracks have a $\frac{dE}{dx}$ pull,

$$\left(\frac{dE}{dx}\right)_{\text{Pull}} = \left(\frac{\left(\frac{dE}{dx}\right)_{meas} - \left(\frac{dE}{dx}\right)_{theor}}{\sigma_{\left(\frac{dE}{dx}\right)}}\right), \tag{5.9}$$

less than the 3σ. $\left(\frac{dE}{dx}\right)_{meas}$ is the measured $\frac{dE}{dx}$ value, $\left(\frac{dE}{dx}\right)_{theor}$ is the theoretical value for a pion in the DCH, and $\sigma_{\left(\frac{dE}{dx}\right)}$ is the error on the measured $\frac{dE}{dx}$ value. If the two identified pions have opposite charge and an invariant mass within 100MeV of the ρ^0 mass, 770MeV, the pion pair is identified as a ρ^0 in the $l - \rho$ channel. If the pions both have the opposite charge of the lepton tag and an invariant mass $>$ 300MeV, they are identified as the pion pair in the $l - \pi\pi$ channel.

Potential sources of background are eliminated by constraining the total missing momentum and the total energy of the identified tracks. The total missing momentum of the three identified tracks is constrained by requiring the angular constraint $|cos(\theta_{miss})| < 0.80$ and that the transverse component is greater than 300MeV. The total energy of the identified tracks is less than 80% of the invariant mass of the colliding electron and positron [1].

5.3 Monte Carlo and Data Set

The τ Tracking Efficiency Study has been employed to calibrate the BaBar data set which was collected between October 1999 and June 2003 and reconstructed with the release version 12. During this period, the only known significant change to the tracking conditions was the change between the three DCH high voltage settings, 1900V, 1960V and 1930V, to maximize the DCH performance. The original voltage setting, 1900V, collected 10.68fb^{-1} of data, while the 1960V setting was used to collect 9.39fb^{-1}. However, the majority of the data set, 91.87fb^{-1}, was collected with the 1930V setting from 2001-2003 [27, pg. 5]. Therefore, the efficiency has been calculated for each of the voltage settings. In addition to this, the study was repeated for three one year periods, 2001, 2002 and 2003, to verify that the tracking efficiency was constant over time. In this study, twenty percent of the data classified as "Good Runs" by the Run Quality Manager was employed. For the Monte Carlo, ten percent of the corresponding "e+e-→ tau+ tau- (KK2F generator)" [33], "e+e- → mu+mu-gamma (KK2F)" [33], "B+B- Generic" [39], "B0B0bar Generic" [39], "e+e- → ccbar" [39] and "e+e- → uubar/ddbar/ssbar" [36] [37] [38] generators from the fifth simulated production (SP5) data sets were employed. These MC generators are known to accurately model the well understood physics utilized in this study. All the MC was normalized for the relative luminosity for the different run periods.

Chapter 6

Tracking Efficiency Results

6.1 Global Tracking Efficiency

The global tracking efficiency, evaluated on the full detector acceptance, was determined for the three voltage settings. Figures 6.1, 6.2 and 6.3 show the pseudo-efficiencies, $\epsilon \times A$ and $\epsilon' \times A$, with the corresponding statistical error for the 1900V, 1930V and 1960V settings respectively. The large difference between the CT track definition results and that of the GTVL and GTL track definitions is due to the requirement that the track is consistent with originating from the origin. The 1.5% decrease in the $\epsilon' \times A$ values relative to the $\epsilon \times A$ results indicate a significant presence of Ghost Tracks, Loopers and contamination from higher track multiplicity τ decays. There is a systematic deviation between the electron and muon channels in the efficiency results. A detailed analysis of this deviation, described in Chapter 7: Systematic Uncertainty Studies, indicates that this is the result of background contamination in the electron channels.

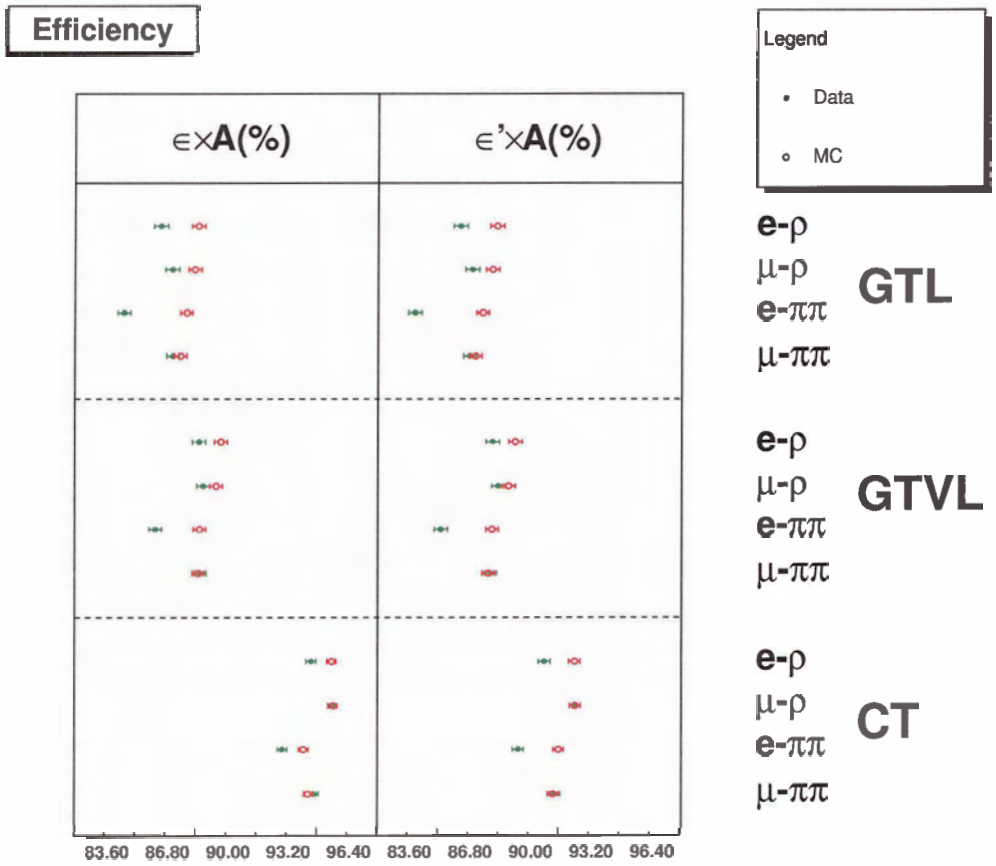

Figure 6.1: The pseudo-efficiencies, $\epsilon \times A$ and $\epsilon' \times A$, for the 1900V setting. Only the $\mu - \rho$ and $\mu - \pi\pi$ are used in the final results because the $e - \rho$ and $e - \pi\pi$ channels contain contamination. A complete discussion of the contamination in the electron channels can be found in Chapter 7: Systematic Uncertainty Studies. The closed circles correspond to the data, while the open circles represent the MC.

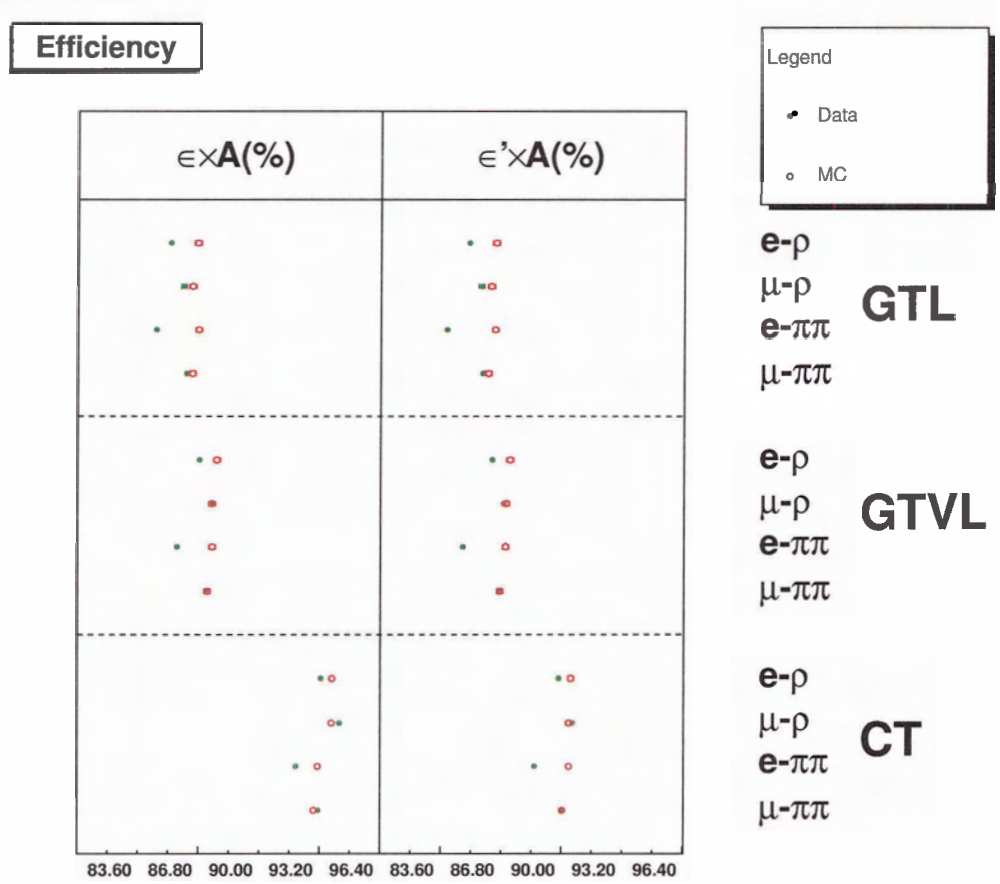

Figure 6.2: The pseudo-efficiencies, $\epsilon \times A$ and $\epsilon' \times A$, for the 1930V setting. Only the $\mu - \rho$ and $\mu - \pi\pi$ are used in the final results because the $e - \rho$ and $e - \pi\pi$ channels contain contamination. A complete discussion of the contamination in the electron channels can be found in Chapter 7: Systematic Uncertainty Studies. The closed circles correspond to the data, while the open circles represent the MC.

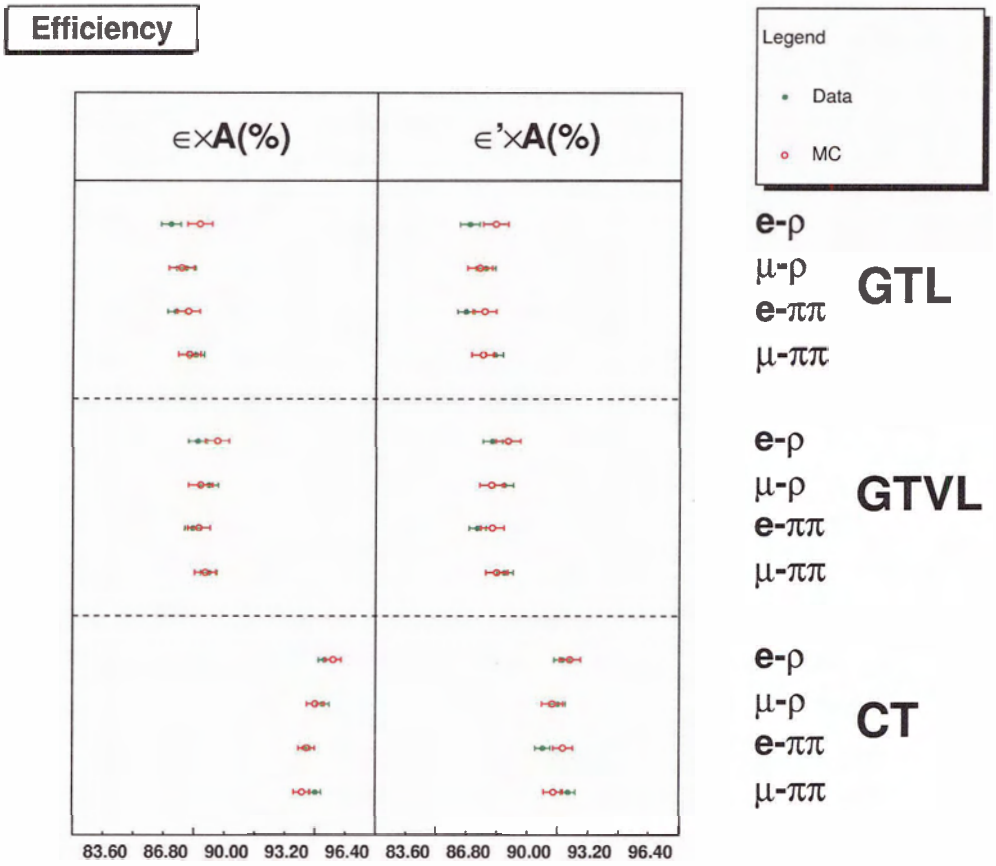

Figure 6.3: The pseudo-efficiencies, $\epsilon \times A$ and $\epsilon' \times A$, for the 1960V setting. Only the $\mu - \rho$ and $\mu - \pi\pi$ are used in the final results because the $e - \rho$ and $e - \pi\pi$ channels contain contamination. A complete discussion of the contamination in the electron channels can be found in Chapter 7: Systematic Uncertainty Studies. The closed circles correspond to the data, while the open circles represent the MC.

The correction factors corresponding to the global tracking efficiency are presented in figures 6.4, 6.5 and 6.6.

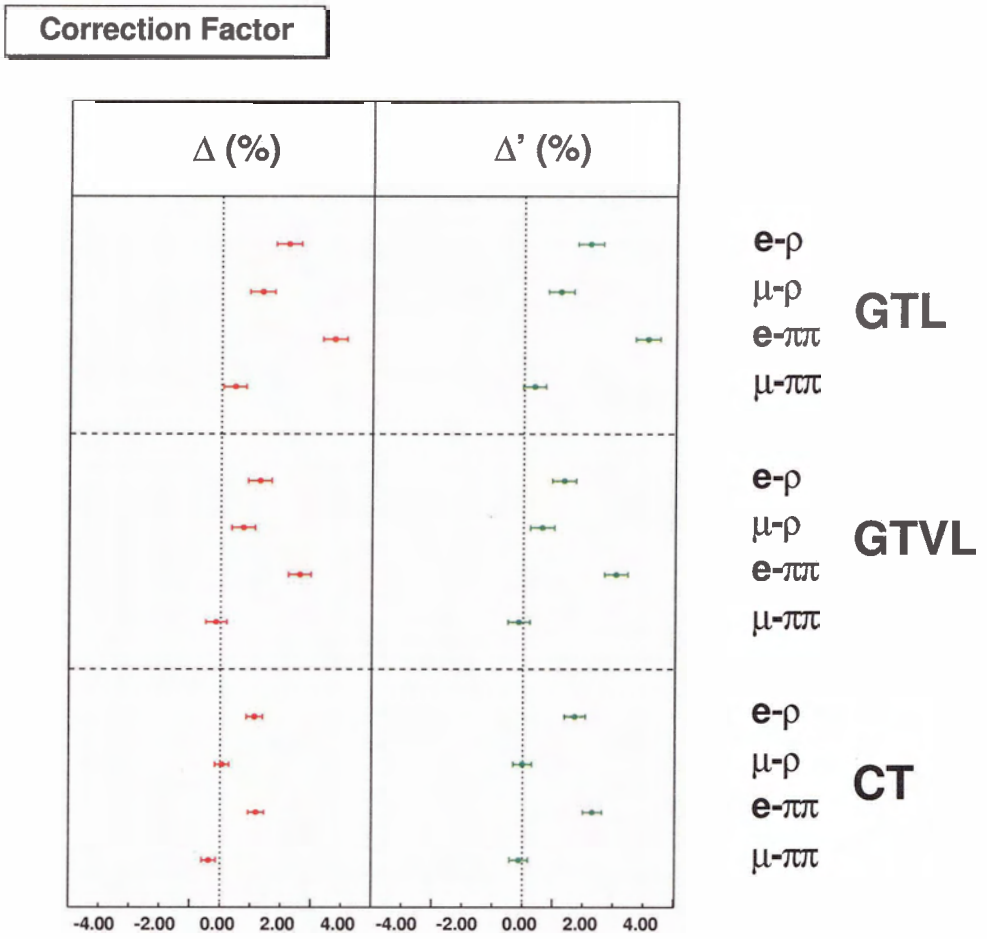

Figure 6.4: The correction factors, Δ and Δ', for the 1900V setting. Only the $\mu - \rho$ and $\mu - \pi\pi$ are used in the final results because the $e - \rho$ and $e - \pi\pi$ channels contain contamination. A complete discussion of the contamination in the electron channels can be found in Chapter 7: Systematic Uncertainty Studies. The closed circles correspond to the data, while the open circles represent the MC.

Neglecting the electron channels due to contamination, the correction factor is less than 1% for the three track definitions. The correction factor of the GTVL track definition is consistent with zero for all of the voltage settings. In contrast, the CT correction factor has

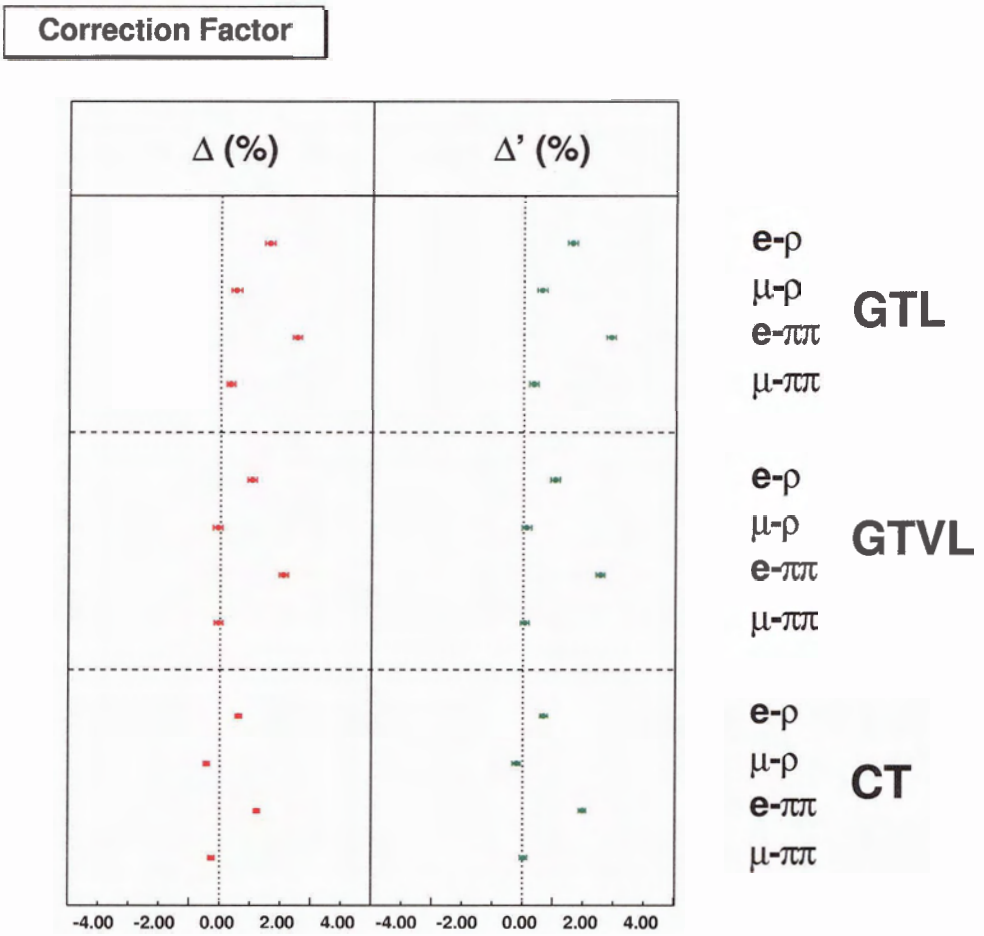

Figure 6.5: The correction factors, Δ and Δ', for the 1930V setting. Only the $\mu - \rho$ and $\mu - \pi\pi$ are used in the final results because the $e - \rho$ and $e - \pi\pi$ channels contain contamination. A complete discussion of the contamination in the electron channels can be found in Chapter 7: Systematic Uncertainty Studies. The closed circles correspond to the data, while the open circles represent the MC.

a slightly negative deviation from zero because scattering events and material interactions, which reduce the efficiency in pattern recognition, are modeled in the MC with less accuracy. Additional constraints such as those in the GTL and GTVL track definitions remove these events, thus improving the data-MC ratio. However, the GTL correction factor does not follow this pattern because of a known problem in the modeling of the number of DCH

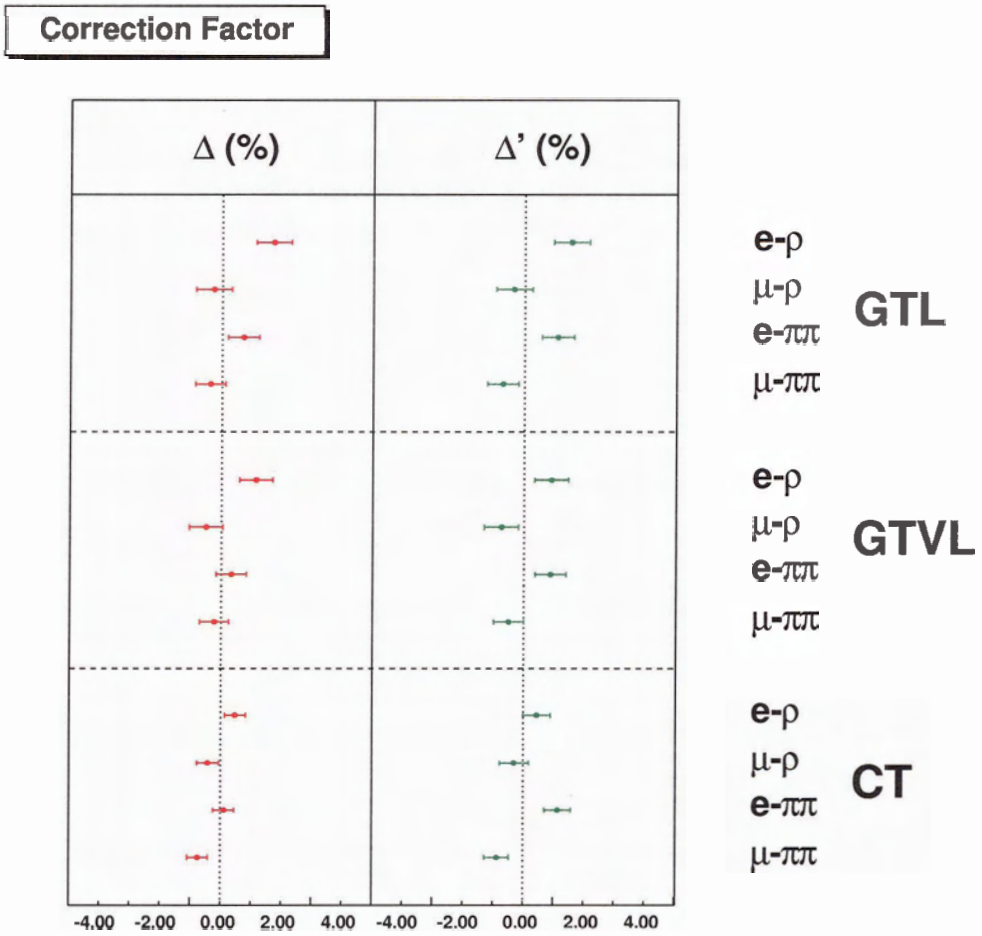

Figure 6.6: The correction factors, Δ and Δ', for the 1960V setting. Only the $\mu - \rho$ and $\mu - \pi\pi$ are used in the final results because the $e - \rho$ and $e - \pi\pi$ channels contain contamination. A complete discussion of the contamination in the electron channels can be found in Chapter 7: Systematic Uncertainty Studies. The closed circles correspond to the data, while the open circles represent the MC.

hits, a requirement unique to the GTL track definition. The Δ' values have a positive bias relative to the true correction factor, Δ. This indicates that the MC is not modeling the contamination from Ghost Track, Loopers and contamination from higher track multiplicity τ decays correctly at less than the 0.5% level.

The tracking efficiency charge asymmetry derived from the charge dependent global tracking efficiency can be seen in figures 6.7, 6.8 and 6.9.

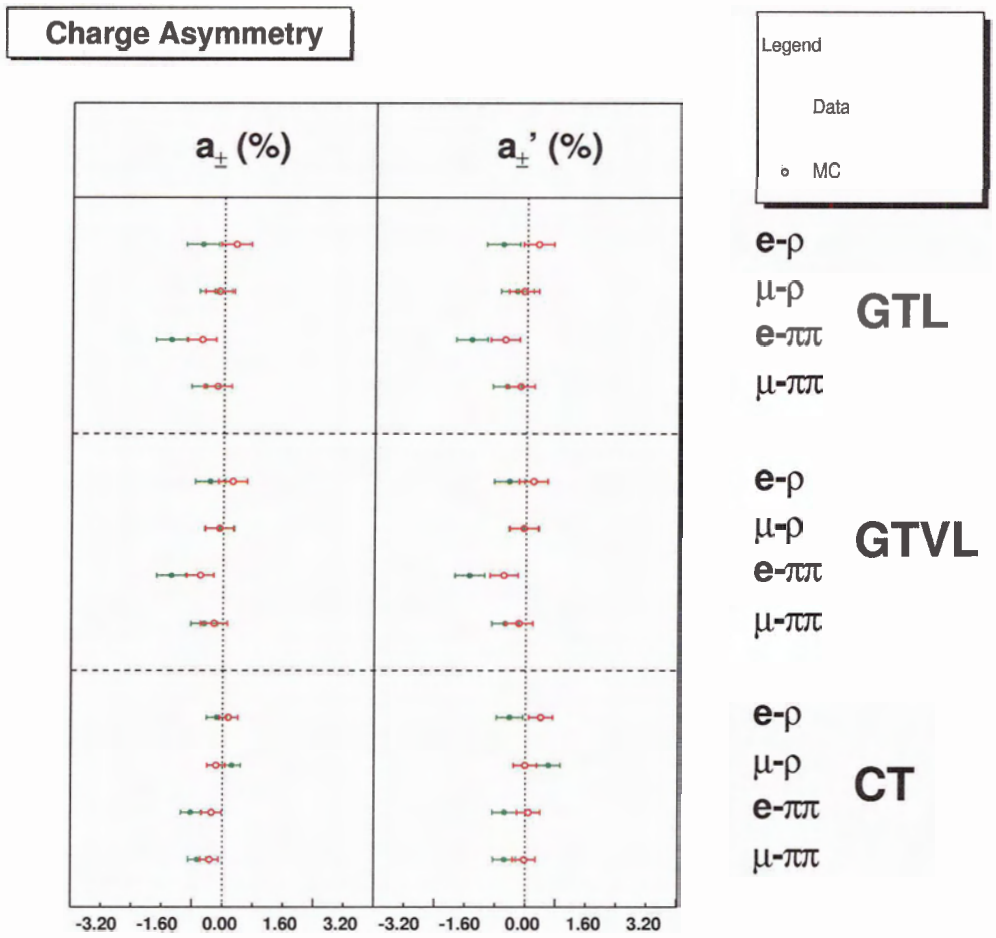

Figure 6.7: The charge asymmetry, $a_{\pm}$ and $a'_{\pm}$, for the 1900V setting. Only the $\mu - \rho$ and $\mu - \pi\pi$ are used in the final results because the $e - \rho$ and $e - \pi\pi$ channels contain contamination. A complete discussion of the contamination in the electron channels can be found in Chapter 7: Systematic Uncertainty Studies. The closed circles correspond to the data, while the open circles represent the MC.

The charge asymmetry, both for MC and data, are consistent with zero for the three track definitions for 1900V, 1930V and 1960V. The deviations resulting from Ghost Track, Loopers and contamination from higher track multiplicity τ decays are also consistent bewteen

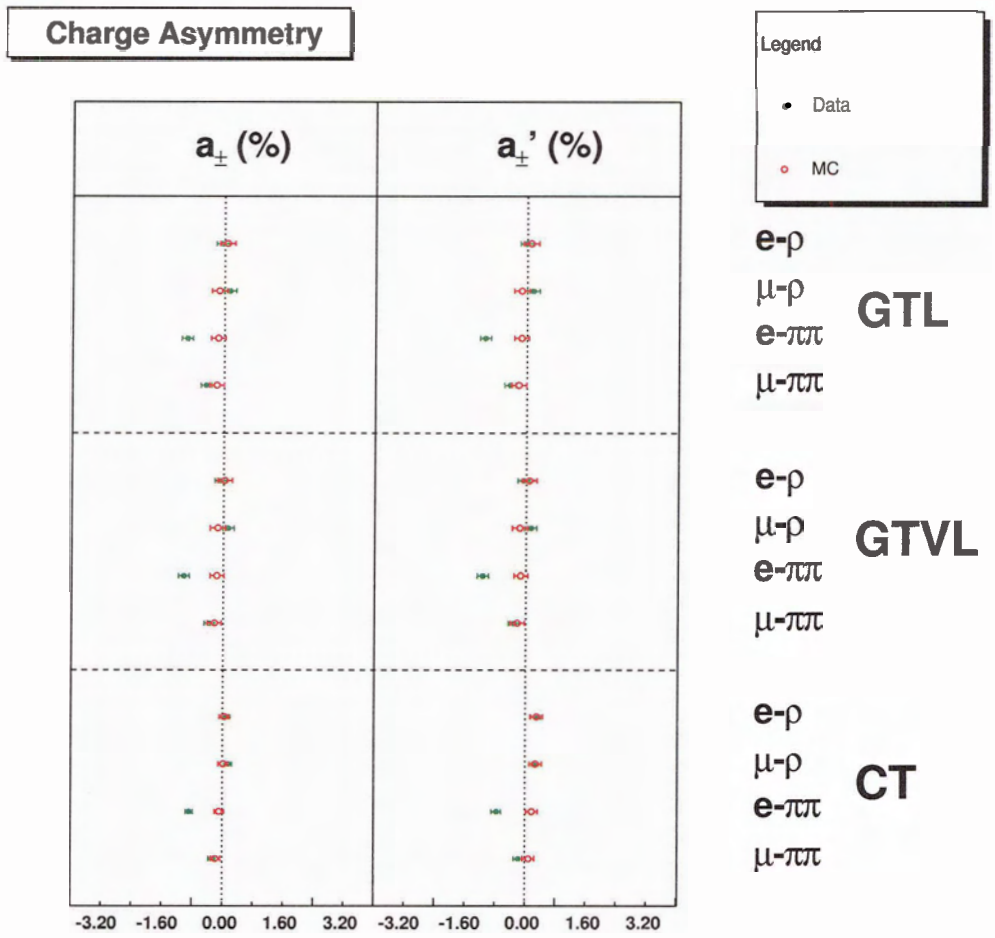

Figure 6.8: The charge asymmetry, $a_{\pm}$ and $a'_{\pm}$, for the 1930V setting. Only the $\mu - \rho$ and $\mu - \pi\pi$ are used in the final results because the $e - \rho$ and $e - \pi\pi$ channels contain contamination. A complete discussion of the contamination in the electron channels can be found in Chapter 7: Systematic Uncertainty Studies. The closed circles correspond to the data, while the open circles represent the MC.

data and MC.

A complete set of the global tracking efficiency, correction factor and charge asymmetry results in tabular form can be seen in Appendix A for the 1900V setting, Appendix B for the 1930V setting and Appendix C for the 1960V setting.

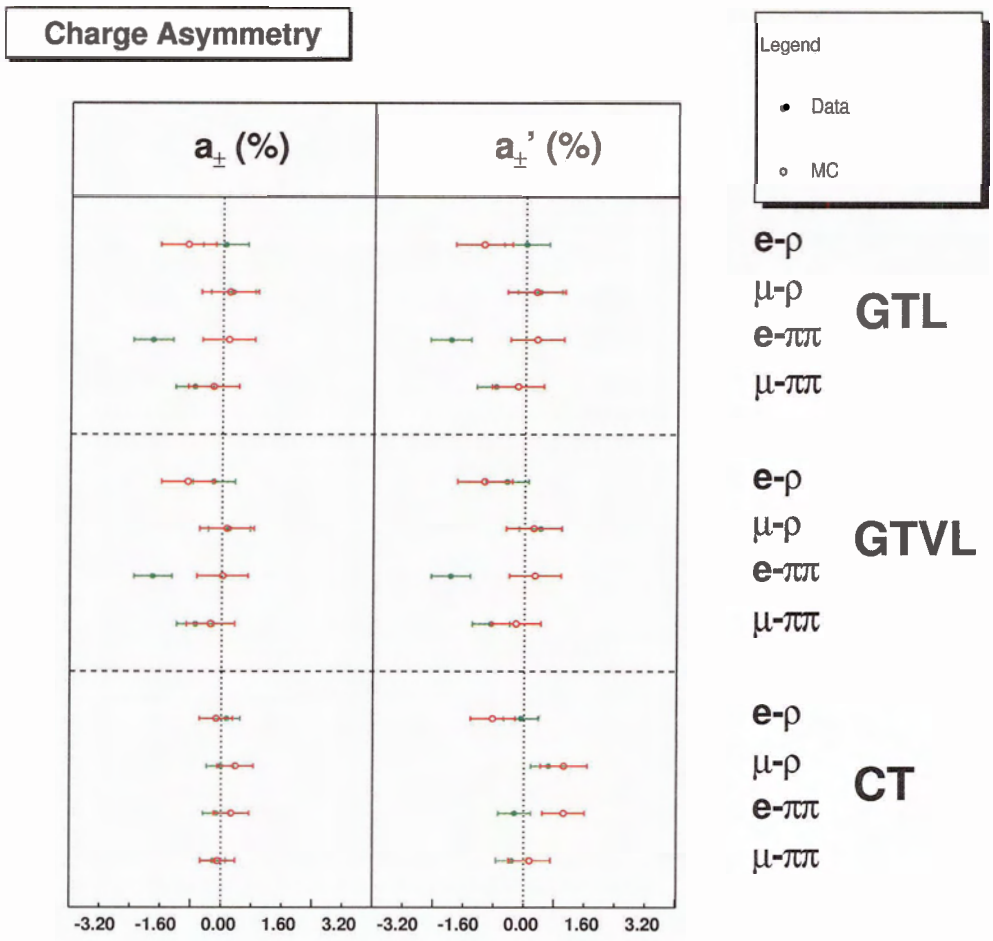

Figure 6.9: The charge asymmetry, $a_{\pm}$ and $a'_{\pm}$, for the 1960V setting. Only the $\mu - \rho$ and $\mu - \pi\pi$ are used in the final results because the $e - \rho$ and $e - \pi\pi$ channels contain contamination. A complete discussion of the contamination in the electron channels can be found in Chapter 7: Systematic Uncertainty Studies. The closed circles correspond to the data, while the open circles represent the MC.

6.2 Tracking Efficiency in P^t, θ, and ϕ

6.2.1 Tracking Efficiency Dependency in P_t

The results for the P_t tracking efficiency, using the 1930V setting, can be seen in figure 6.10. The statistical errors were estimated with Toy MC which was generated from the mean and variance of the measured values using a Gaussian distribution. The efficiency distribution is currently limited by a bias resulting from the missing information in the low P_t region. Therefore, these results are presented as a demonstration of this method only. To minimize the bias and maximize the statistics, the $P_t^{(lab)}$ and $P_t^{miss(lab)}$ cuts employed when the 4th track was identified are:

Matrix Component	Cut
row 1	$2.25\text{GeV} < P_t^{miss(lab)} < 5.28\text{GeV}$
row 2	$1.5\text{GeV} < P_t^{miss(lab)} < 2.25\text{GeV}$
row 3	$0.4\text{GeV} < P_t^{miss(lab)} < 1.5\text{GeV}$
column 1	$0.0\text{GeV} < P_t^{(lab)} < 0.4\text{GeV}$
column 2	$0.4\text{GeV} < P_t^{(lab)} < 2.0\text{GeV}$
column 3	$2.0\text{GeV} < P_t^{(lab)} < 5.28\text{GeV}$

Table 6.1: The cuts employed in the P_t probability matrix for determining the tracking efficiency as a function of $P_t^{(lab)}$.

Figure 6.10 demonstrates that the efficiency of the detector is at a minimum in the low momentum region, momentum less than 0.4GeV, and then saturates at higher momenta. This is expected because the lower momentum tracks tend to have larger scattering angles, and less penetration depth into the detector. The bin of high momentum, $2.0\text{GeV} < P_t^{(lab)} < 5.28\text{GeV}$, contain an efficiency central value greater than 100%, but this is still consistent with an efficiency of less than 100%. This is a result of both statistical fluctuation and the bias caused by the zero efficiency region.

The correction factor for the transverse momentum dependence can be seen in figure

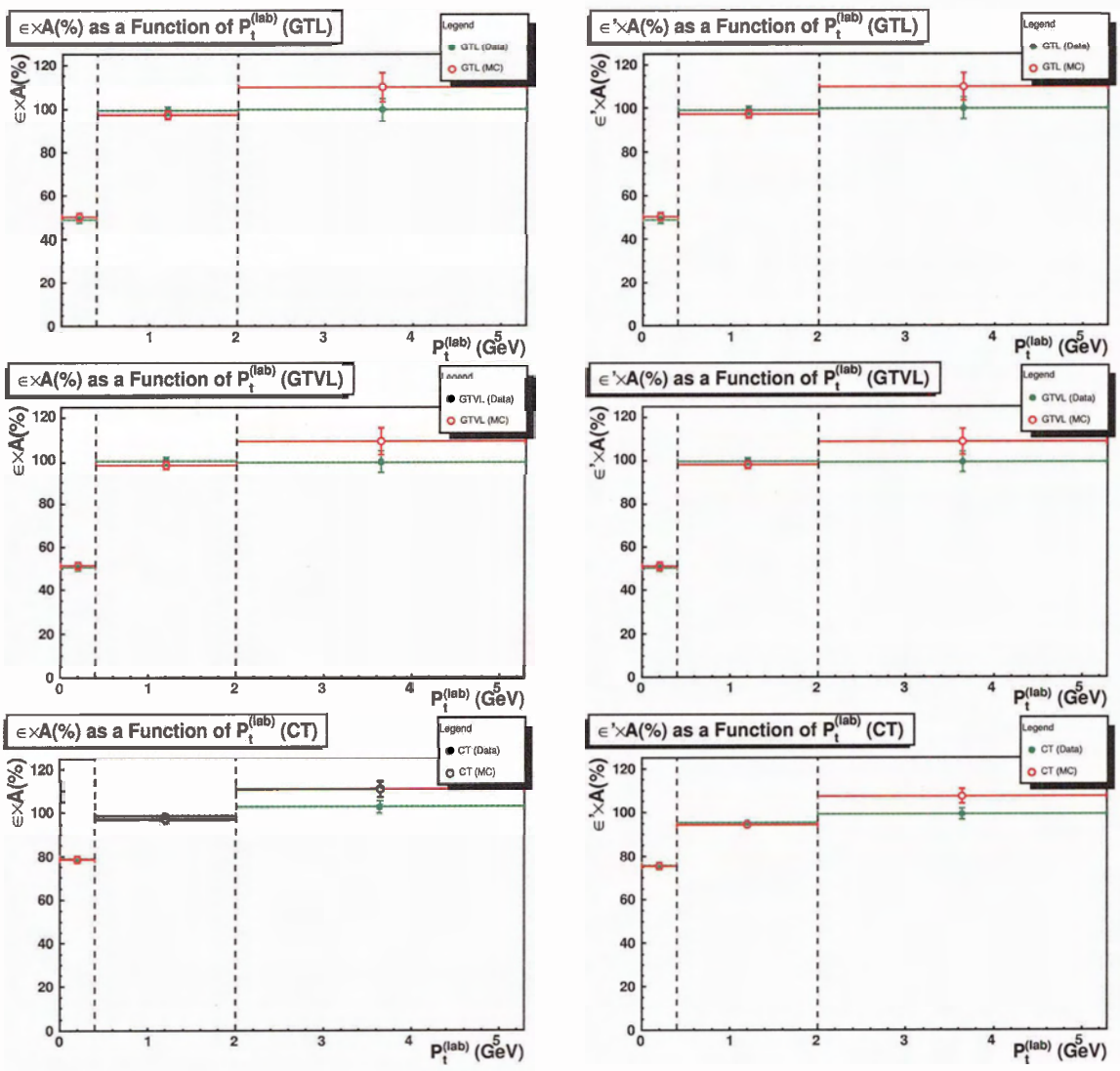

Figure 6.10: The pseudo-efficiencies, $\epsilon \times A$ and $\epsilon' \times A$, as a function of $P_t^{(lab)}$ in the $\mu - \pi\pi$ channel. The error bars display the statistical uncertainty estimated with Toy MC, while the horizontal error bars represent the bin size. The closed circles correspond to the data, while the open circles represent the MC.

6.11. The two lower momentum bins indicate that the correction factor is consistent with zero, while the correction factor in the high momentum bin is inconsistent with zero. Further development of this method is required to remove the bias before any conclusions can be

made.

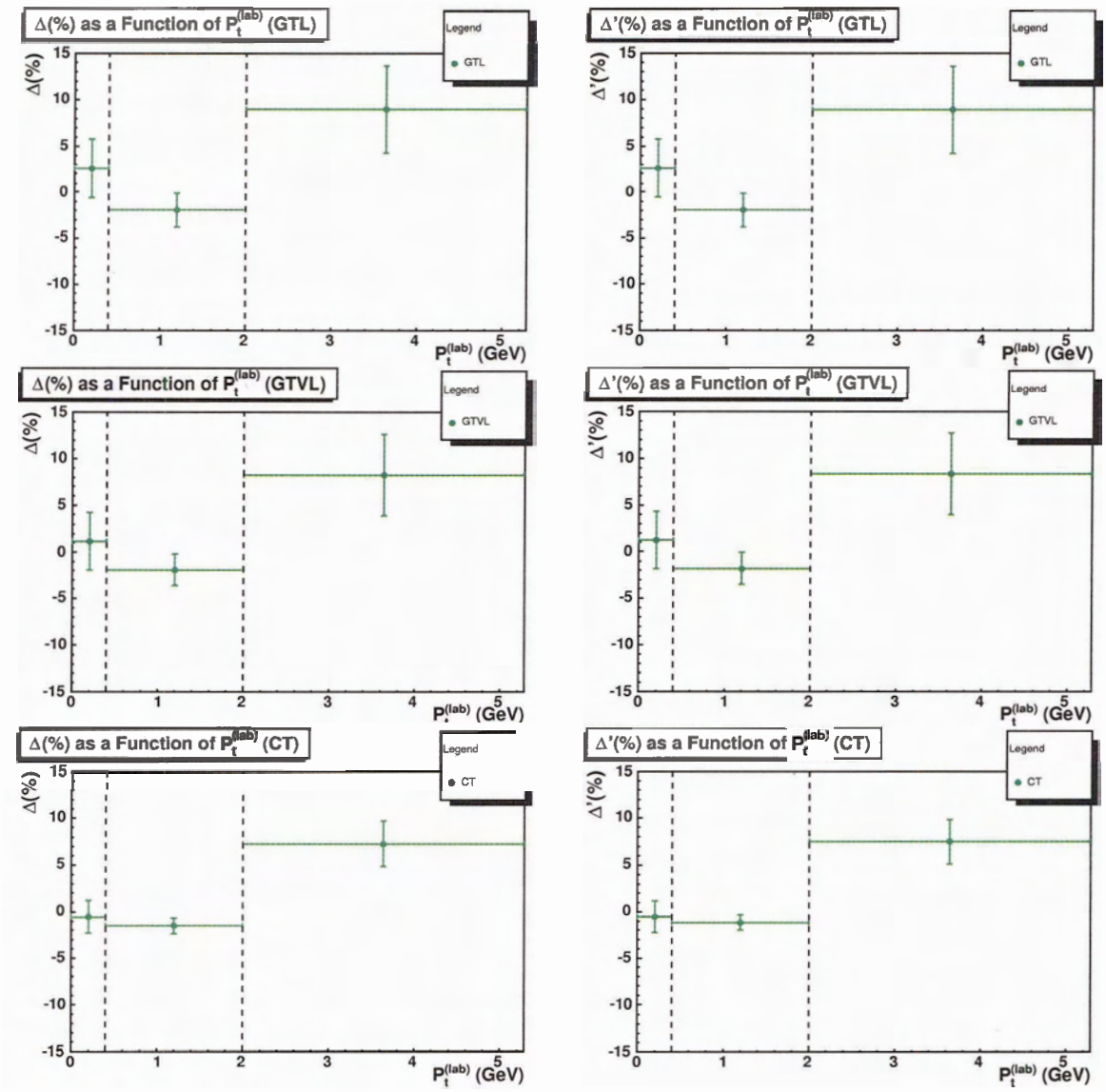

Figure 6.11: The tracking efficiency correction factors, Δ and Δ', as a function of $P_t^{(lab)}$ in the $\mu - \pi\pi$ channel. The vertical error bars display the statistical uncertainty estimated with Toy MC, while the horizontal error bars represent the bin size. The closed circles correspond to the data, while the open circles represent the MC.

The tabular results and probability matrix information for this study can be found in Appendix K.

6.2.2 Tracking Efficiency Dependency in $cos(\theta)$

The tracking efficiency $cos(\theta^{(lab)})$ dependence was analyzed for the 1930V setting in three bins of $cos(\theta^{(lab)}_{avg})$: $cos(\theta^{(lab)}_{avg}) < 0.2$, $0.2 < cos(\theta^{(lab)}_{avg}) < 0.6$ and $0.6 < cos(\theta^{(lab)}_{avg})$. The mean $cos(\theta^{(lab)}_{avg})$ and $cos(\theta^{(lab)})$ value in each of the bins, for events with 4 tracks, is represented by the position of the markers in figure 6.12. The error bar in this figure corresponds to RMS in each of the bins. The plots from which these values are derived are in Appendix F.

The $cos(\theta^{(lab)})$ dependent pseudo-efficiency, seen in figure 6.13, is dominated by the geometry acceptance of the detector. The position of the marker in $cos(\theta^{(lab)})$ corresponds to the mean $cos(\theta^{(lab)})$ position for the associated $cos(\theta^{(lab)}_{avg})$ bin. The efficiency in the central $cos(\theta^{(lab)})$ bin, $0.2 < cos(\theta^{(lab)}_{avg}) < 0.6$, has a geometric acceptance of 100%, thus it represents the true efficiency of the detector. Appendix G contains the efficiency of the detector in the central $cos(\theta^{(lab)})$ region for three slices in $P_t^{miss(lab)}$

The correction factor as a function of $cos(\theta^{(lab)})$ is shown in figure 6.14. The plot indicates that the correction factor contains a $cos(\theta^{(lab)})$ dependence.

Similarly, the tracking efficiency charge asymmetry, seen in figure 6.15, displays a dependency on $cos(\theta^{(lab)})$. Currently, there is no explanation for a dependency on $cos(\theta^{(lab)})$ in either the correction factor or the charge asymmetry. However, the momentum distribution of the tracks produced in an asymmetrical collider is dependent on $cos(\theta^{(lab)})$. Therefore, it is possible that this dependency on $cos(\theta^{(lab)})$ is a result of correlation between the momentum distribution and the $cos(\theta^{(lab)})$ distribution. Unfortunately, the tracking efficiency in $P_t^{(lab)}$ study must be must be completed with more statistics before these correlations can be analyzed.

A complete set of the $cos(\theta^{(lab)})$ dependency results, displayed in tabular form, and plots of the corresponding $cos(\theta^{(lab)})$ and $cos(\theta^{(lab)}_{avg})$ distributions can be found in Appendix F.

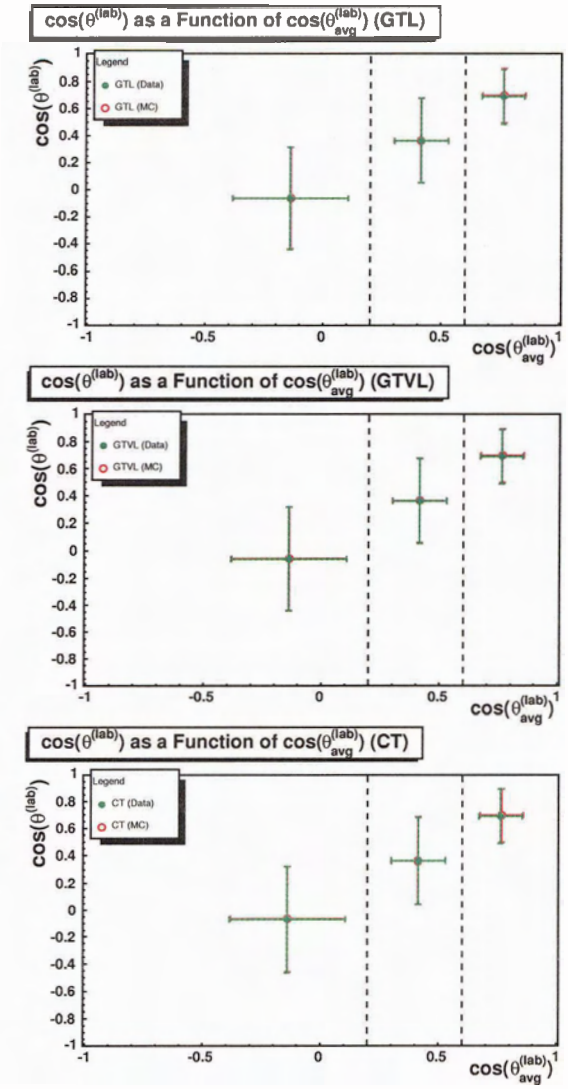

Figure 6.12: The $cos(\theta^{(lab)})$ as a function of $cos(\theta^{(lab)}_{avg})$ for the $\mu - \pi\pi$ channel. The three bins are $cos(\theta^{(lab)}_{avg}) < 0.2$, $0.2 < cos(\theta^{(lab)}_{avg}) < 0.6$ and $0.6 < cos(\theta^{(lab)}_{avg})$. The closed circles correspond to the data, while the open circles represent the MC.

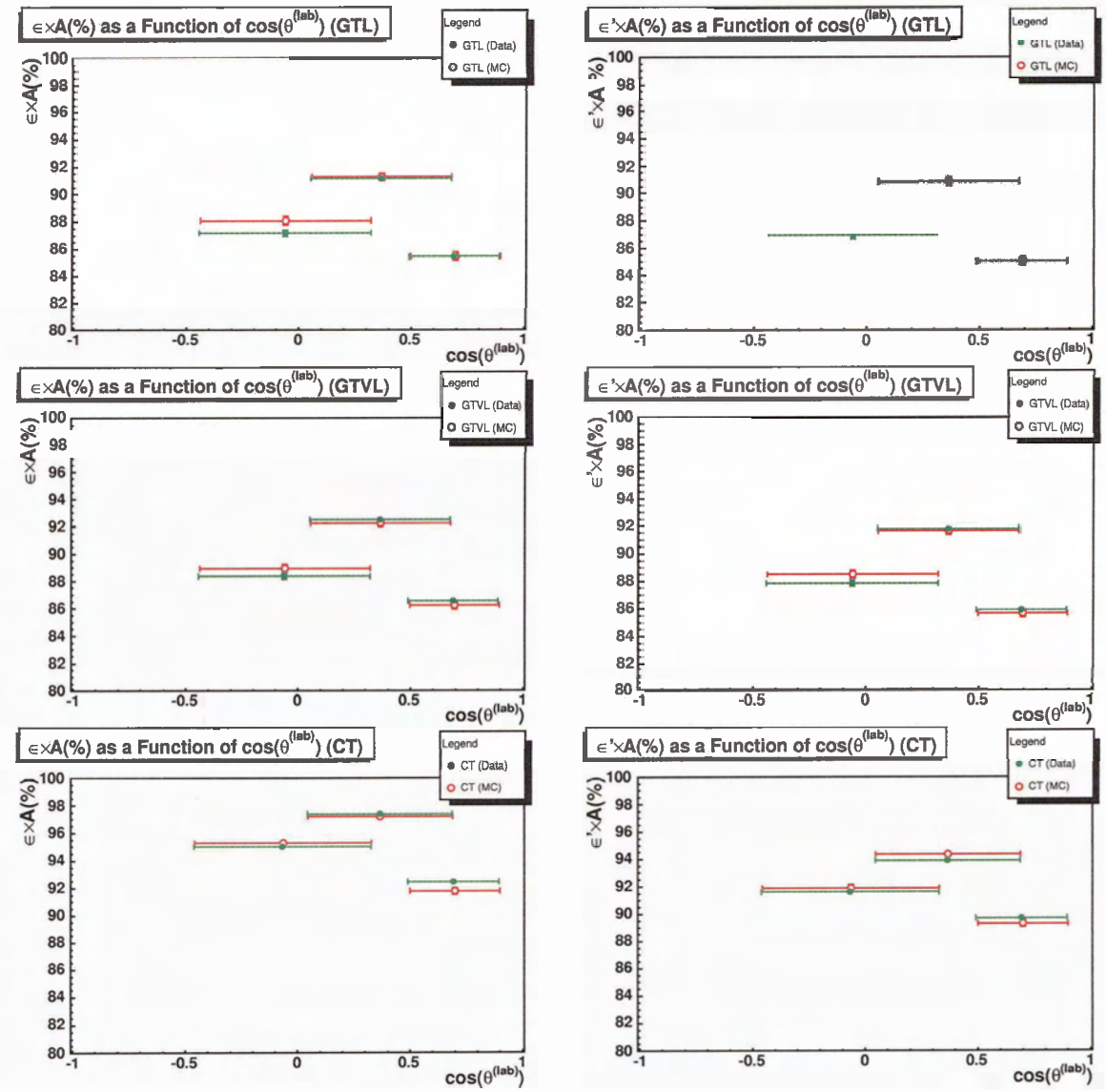

Figure 6.13: The pseudo-efficiencies, $\epsilon \times A$ and $\epsilon' \times A$, as a function of $cos(\theta^{(lab)})$ for Data in the $\mu - \pi\pi$ channel. $cos(\theta^{(lab)})$ is determined from the three bins $cos(\theta^{(lab)}_{avg}) < 0.2$, $0.2 < cos(\theta^{(lab)}_{avg}) < 0.6$ and $0.6 < cos(\theta^{(lab)}_{avg})$. The closed circles correspond to the data, while the open circles represent the MC.

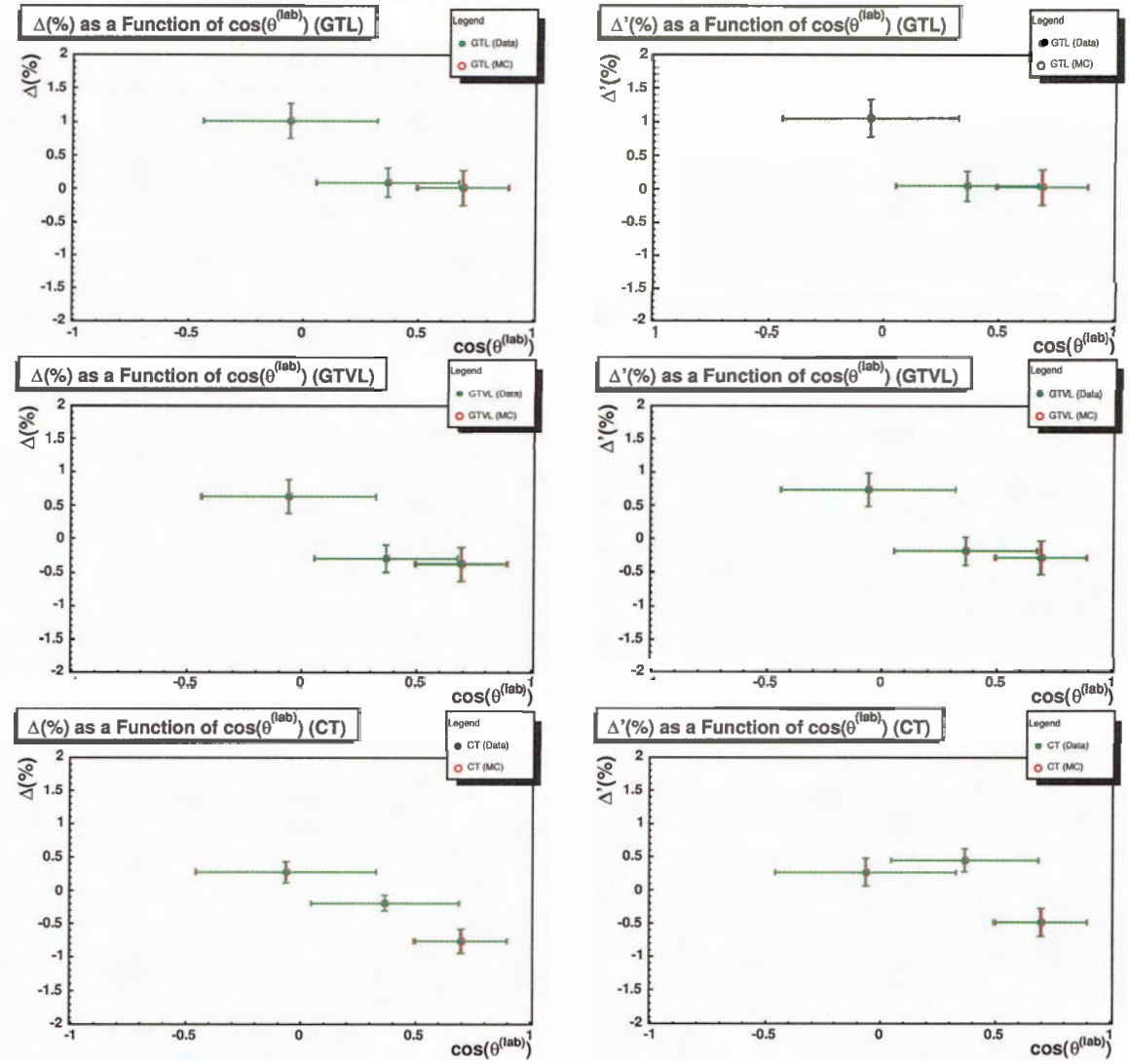

Figure 6.14: The correction factor, Δ and Δ', as a function of $cos(\theta^{(lab)})$ for the $\mu - \pi\pi$ channel. $cos(\theta^{(lab)})$ is determined from the three bins $cos(\theta^{(lab)}_{avg}) < 0.2$, $0.2 < cos(\theta^{(lab)}_{avg}) < 0.6$ and $0.6 < cos(\theta^{(lab)}_{avg})$. The closed circles correspond to the data, while the open circles represent the MC.

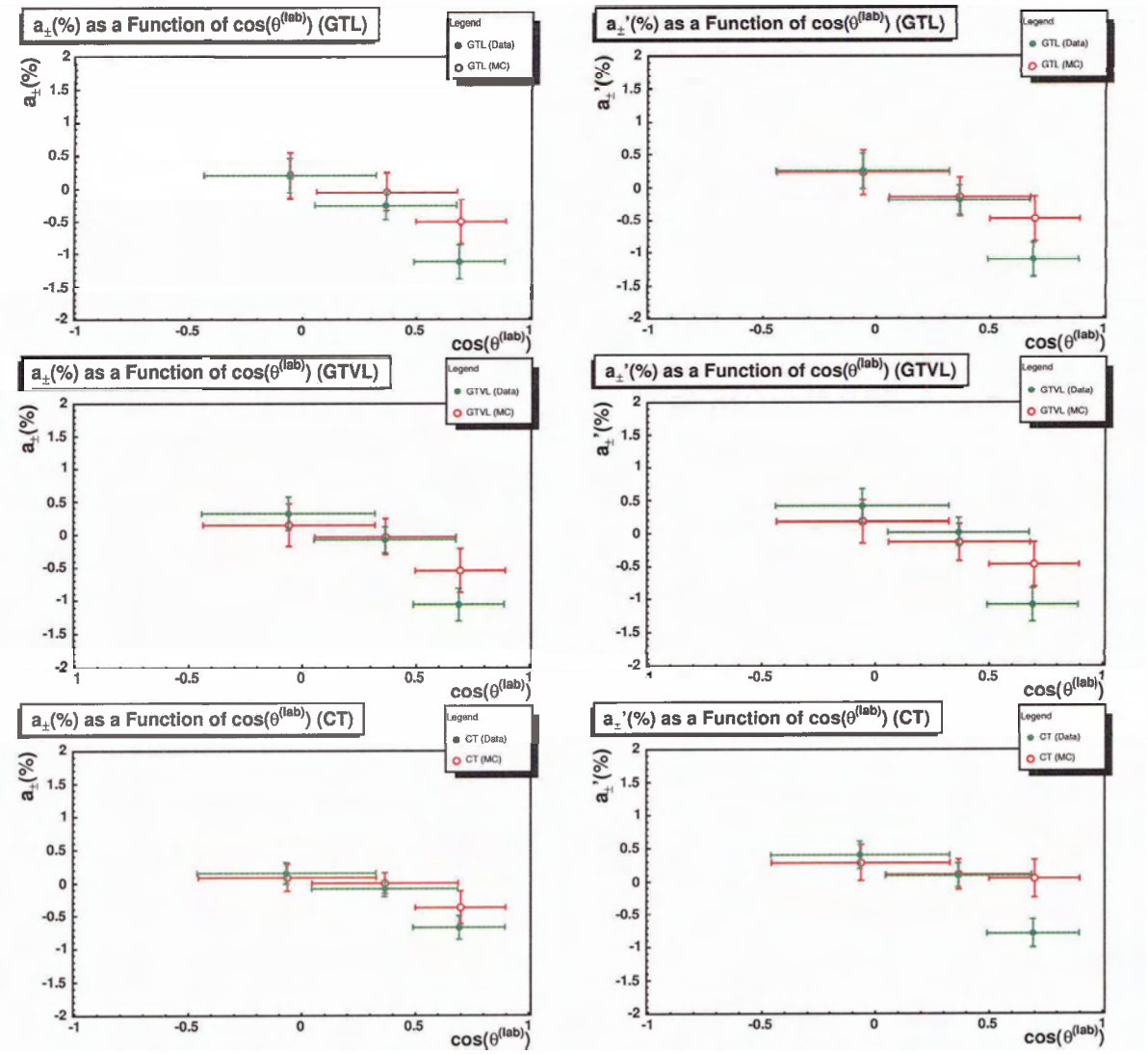

Figure 6.15: The charge asymmetry, $a_{\pm}$ and $a'_{\pm}$, as a function of $cos(\theta^{(lab)})$ for the $\mu - \pi\pi$ channel. $cos(\theta^{(lab)})$ is determined from the three bins $cos(\theta^{(lab)}_{avg}) < 0.2$, $0.2 < cos(\theta^{(lab)}_{avg}) < 0.6$ and $0.6 < cos(\theta^{(lab)}_{avg})$. The closed circles correspond to the data, while the open circles represent the MC.

6.2.3 Tracking Efficiency Dependency in ϕ

The $\phi^{(lab)}$ dependence of the tracking efficiency was analyzed in a similar method to that of the $cos(\theta^{(lab)})$ dependence. The bins utilized for determining the $\phi^{(lab)}$ dependence for the 1930V setting are:$\phi^{(lab)}_{avg} < -1.046$rad, $-1.046\text{rad} < \phi^{(lab)}_{avg} < 1.046$rad and $1.046\text{rad} < \phi^{(lab)}_{avg}$. The mean position of these bins in $\phi^{(lab)}_{avg}$ and $\phi^{(lab)}$ are represented by the points in figure 6.16, with the RMS of each position represented by the error bars. The RMS for the boundary bins in $\phi^{(lab)}$, $\phi^{(lab)}_{avg} < -1.046$rad and $1.046\text{rad} < \phi^{(lab)}_{avg}$, is greater than the RMS for the central bin because of the cyclic nature of the cylindrical angle ϕ. Appendix F contains the distribution plots in $\phi^{(lab)}$ and $\phi^{(lab)}_{avg}$ which demonstrate this effect.

Figure 6.17 indicates that the tracking efficiency is independent of ϕ in the laboratory frame. This is consistent with the symmetry in ϕ of the tracking detectors.

Similarly, the tracking efficiency correction factor, seen in figure 6.18, and the charge asymmetry, seen in figure 6.19, are consistent with being independent in $\phi^{(lab)}$.

A complete set of the results for the ϕ dependency study, in tabular form, and the corresponding $\phi^{(lab)}$ and $\phi^{(lab)}_{avg}$ distribution plots can be found in Appendix F.

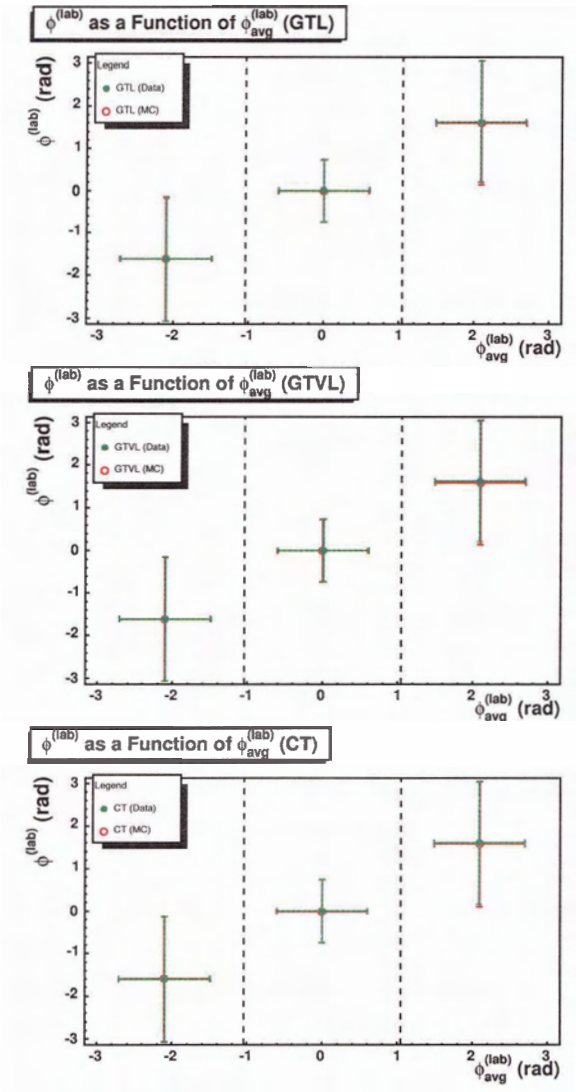

Figure 6.16: The $\phi^{(lab)}$ as a function of $\phi^{(lab)}_{avg}$ for the $\mu - \pi\pi$ channel. The three bins are $\phi^{(lab)}_{avg} < -1.046$rad, $-1.046\text{rad} < \phi^{(lab)}_{avg} < 1.046$rad and $1.046\text{rad} < \phi^{(lab)}_{avg}$. The closed circles correspond to the data, while the open circles represent the MC.

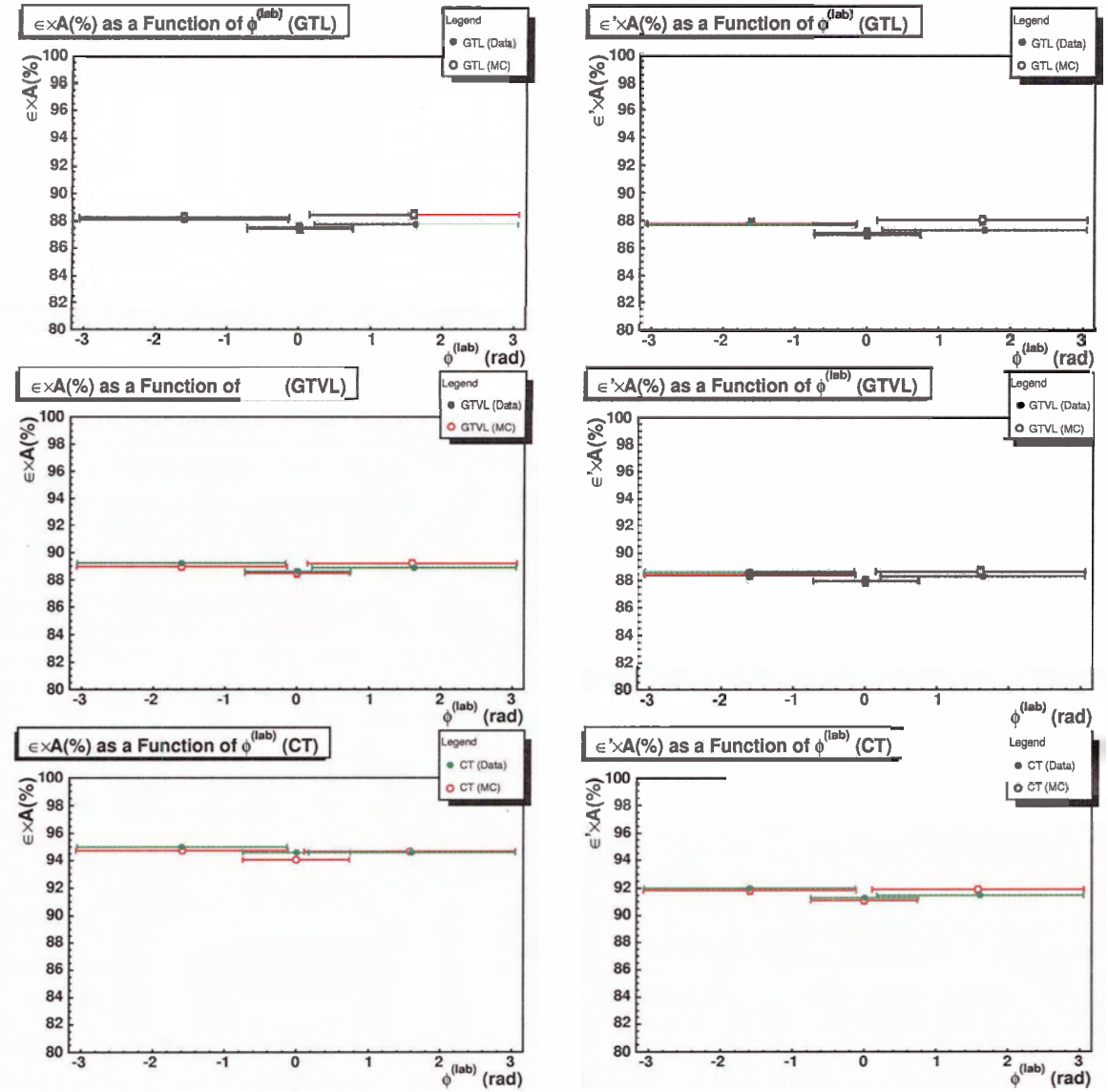

Figure 6.17: The pseudo-efficiencies, $\epsilon \times A$ and $\epsilon' \times A$, as a function of $\phi^{(lab)}$ for the CT $\mu - \pi\pi$ channel. $\phi^{(lab)}$ is determined from the three bins $\phi_{avg}^{(lab)} < -1.046$rad, -1.046rad $< \phi_{avg}^{(lab)} < 1.046$rad and 1.046rad $< \phi_{avg}^{(lab)}$. The closed circles correspond to the data, while the open circles represent the MC.

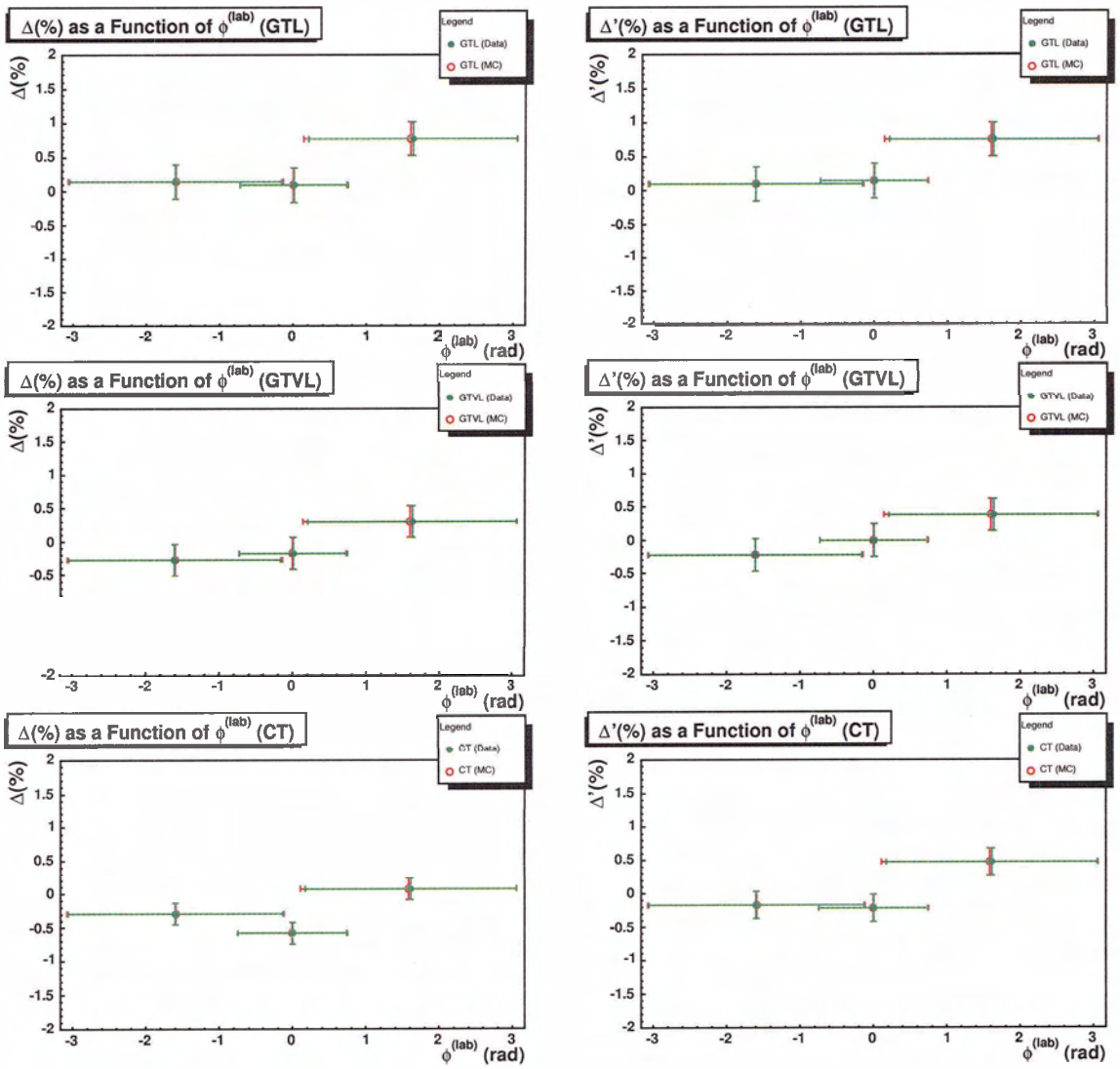

Figure 6.18: The correction factor, Δ and Δ', as a function of $\phi^{(lab)}$ for the $\mu - \pi\pi$ channel. $\phi^{(lab)}$ is determined from the three bins $\phi^{(lab)}_{avg} < -1.046$rad, $-1.046\text{rad} < \phi^{(lab)}_{avg} < 1.046$rad and $1.046\text{rad} < \phi^{(lab)}_{avg}$. The closed circles correspond to the data, while the open circles represent the MC.

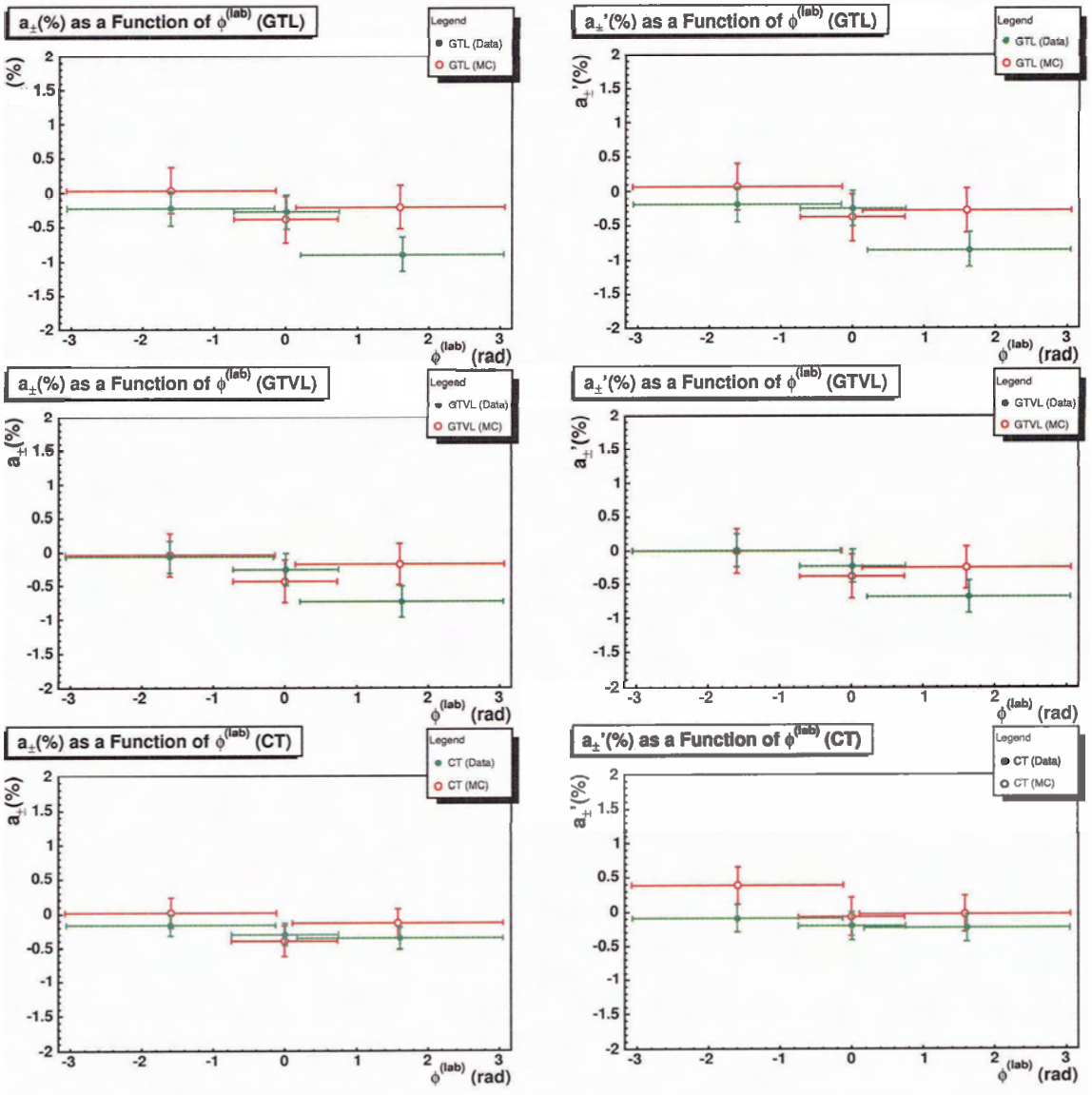

Figure 6.19: The charge asymmetry, $a_{\pm}$ and $a'_{\pm}$, as a function of $\phi^{(lab)}$ for the $\mu-\pi\pi$ channel. $\phi^{(lab)}$ is determined from the three bins $\phi^{(lab)}_{avg} < -1.046$rad, $-1.046\text{rad} < \phi^{(lab)}_{avg} < 1.046$rad and $1.046\text{rad} < \phi^{(lab)}_{avg}$. The closed circles correspond to the data, while the open circles represent the MC.

Chapter 7

Systematic Uncertainty Studies

7.1 Correction for Channel Variations

The deviation between the electron tag channels and the muon tag channels is potentially a limiting systematic uncertainty for the tracking correction in the Tau31 study. Thus, the potential sources of contamination for the electron channels were analyzed to determine the source of the deviation. One such potential source of contamination is background resulting from radiative Bhabhas[1], which are not included in the MC employed in this study. The detection of energy from electrons is more efficient than for muons and hadrons in BaBar. Therefore, the energy deposited in the EMC, E_{raw}, is approximately equal to the momentum in the laboratory frame, P^{lab}, only for electrons. In contrast, the momentum in the laboratory frame is greater than the energy deposited in the EMC for hadrons. This enables $\sum_{3\pi} E_{raw} - \sum_{3\pi} \mathrm{P}^{lab}$, for the 1 vs 3 prong case and $\sum_{2\pi} E_{raw} - \sum_{2\pi} \mathrm{P}^{lab}$, for both the 1 vs 3 prong case and 1 vs 2 prong case, to be employed as unique identifiers for electron contamination. Figures 7.1, 7.2 and 7.3 show the $\sum_{3\pi} E_{raw} - \sum_{\mathbf{3\pi}} \mathrm{P}^{lab}$ for the 1 vs 3 prong case, $\sum_{\mathbf{2\pi}} E_{raw} - \sum_{2\pi} \mathrm{P}^{lab}$ for the 1 vs 3 prong case and $\sum_{2\pi} E_{raw} - \sum_{2\pi} \mathrm{P}^{lab}$ for the 1 vs 2 prong case respectively. The latter figures are for the GTVL track criteria. Although there is a shift in the associated hadronic energy measured in the EMC between the data and MC,

[1]Radiative Bhabhas are the result a scattering process between electron and position, referred to as Bhabha scattering, in which a photon is radiated.

$\sum E_{raw} - \sum \mathrm{P}^{lab}$ still provides a means of identifying electrons at $\sum E_{raw} - \sum \mathrm{P}^{lab} = 0\mathrm{GeV}$.

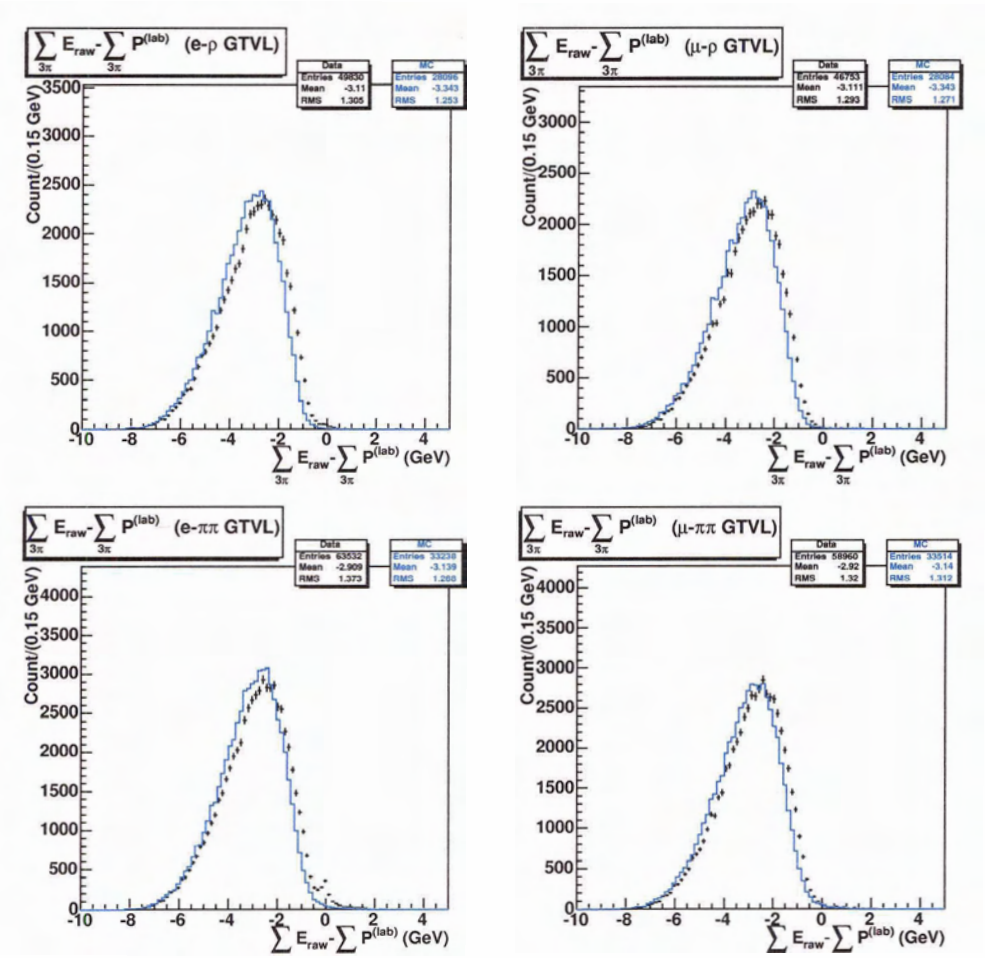

Figure 7.1: The $\sum_{3\pi} E_{raw} - \sum_{3\pi} \mathrm{P}^{lab}$ for the 1 vs 3 prong case and the GTVL section criteria from 2002-2003 (1930V). The MC types have a relative luminosity normalization that has been area normalized to the data. The data is represented by the points, while the MC is represented by the line.

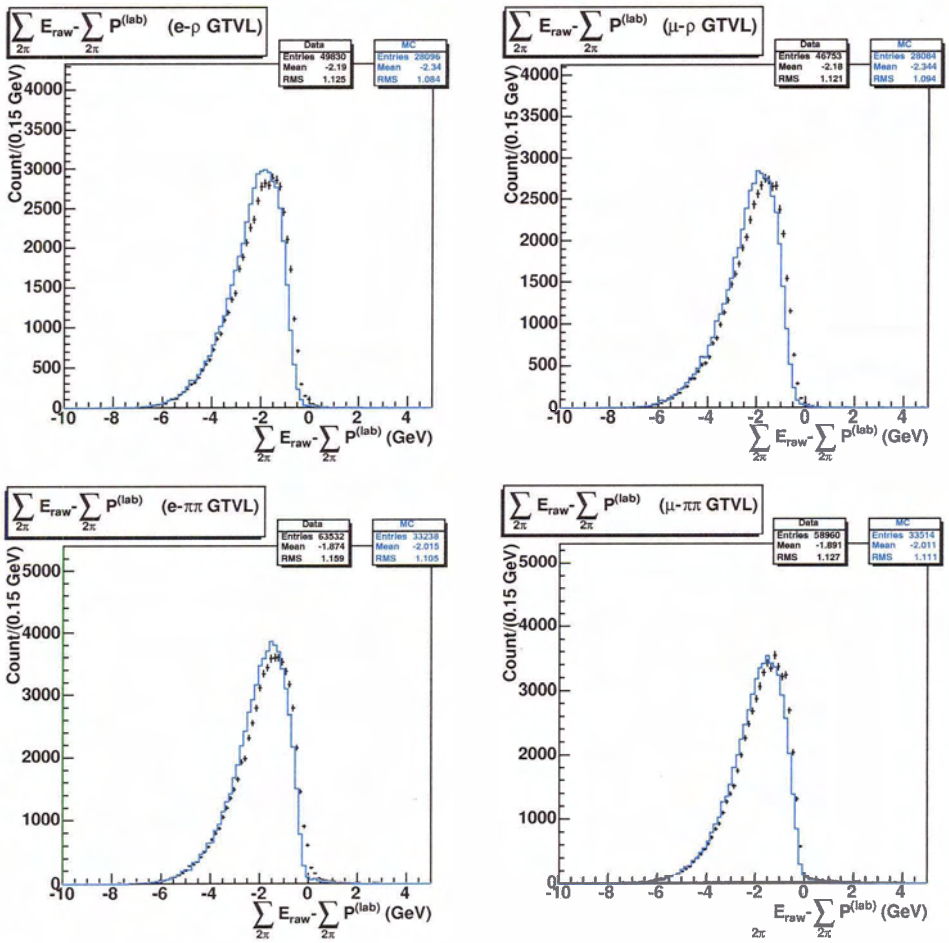

Figure 7.2: The $\sum_{2\pi} E_{raw} - \sum_{2\pi} \mathrm{P}^{lab}$ for the 1 vs 3 prong case and the GTVL section criteria from 2002-2003 (1930V). The MC types have a relative luminosity normalization that has been area normalized to the data. The data is represented by the points, while the MC is represented by the line.

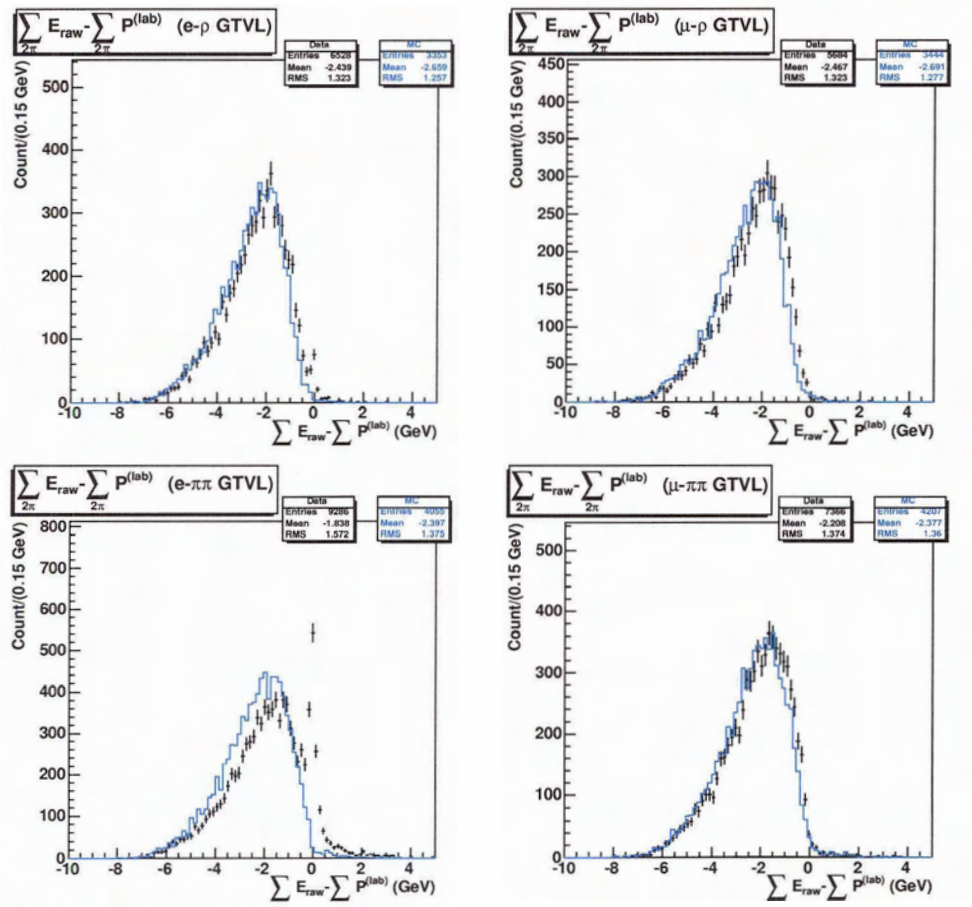

Figure 7.3: The $\sum_{2\pi} E_{raw} - \sum_{2\pi} P^{lab}$ for the 1 vs 2 prong case and the GTVL section criteria from 2002-2003 (1930V). The MC types have a relative luminosity normalization that has been area normalized to the data. The data is represented by the points, while the MC is represented by the line.

In figure 7.1 the $e - \pi\pi$ channel contains a significant peak in the data around 0GeV. The $e - \rho$ channel also contains a small peak in the data, but it is statistically insignificant. The muon channels, as expected, do not contain the 0GeV peaks that indicate the presence of electron contamination. In figure 7.2, none of the four channels contain a peak at 0GeV. Figure 7.3, which corresponds to events with a missing track, contains significant peaks at

0GeV in both the $e-\pi\pi$ and $e-\rho$ channels. This indicates that there is a background source consistant with being electrons which the MC does not describe. The region $\sum_{2\pi} E_{raw} - \sum_{2\pi} \mathrm{P}^{lab} > -0.5GeV$ is defined as the background region. Another unique identifier of radiative Bhabhas is the angular dependence of the cross section which is preferential to the beam line. The angular dependence of the tagged lepton for the 1 vs 3 prong, 1 vs 2 prong and 1 vs 2 prong background region can be seen in figures 7.4, 7.5, and 7.6. Although figure 7.4 contains no indication of a preference toward the beam line, the distributions illustrate the relative efficiency of electron and muon identification as a function of polar angle. The 1 vs 2 prong plots in figure 7.5 contain a small excess number of events near beam axis, thus indicating the presence of radiative Bhabhas in the $e-\rho$ and $e-\pi\pi$ channels. The number of excess events is enhanced in the background region shown in figure 7.6. The $e-\pi\pi$ channel contains a significant excess of events, especially along the backward beam line. The $e-\rho$ channel also contains a significant amount of excess events, which can be seen by comparing the area normalized distribution shapes of the data and MC. Again, the muon channels lack the identifiers which are unique to electron contamination.

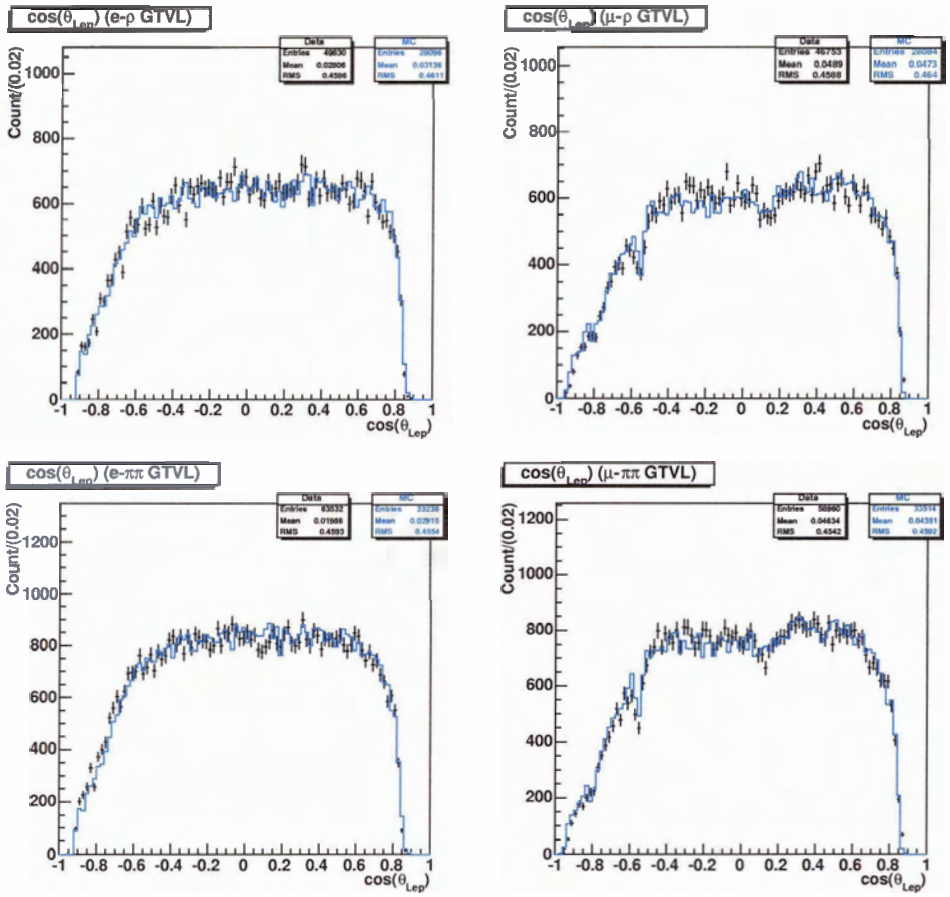

Figure 7.4: $cos(\theta_{\mathrm{Lep}})$ for the 1 vs 3 prong case and the GTVL section criteria from 2002-2003 (1930V). The MC types have a relative luminosity normalization that has been area normalized to the data. The data is represented by the points, while the MC is represented by the line.

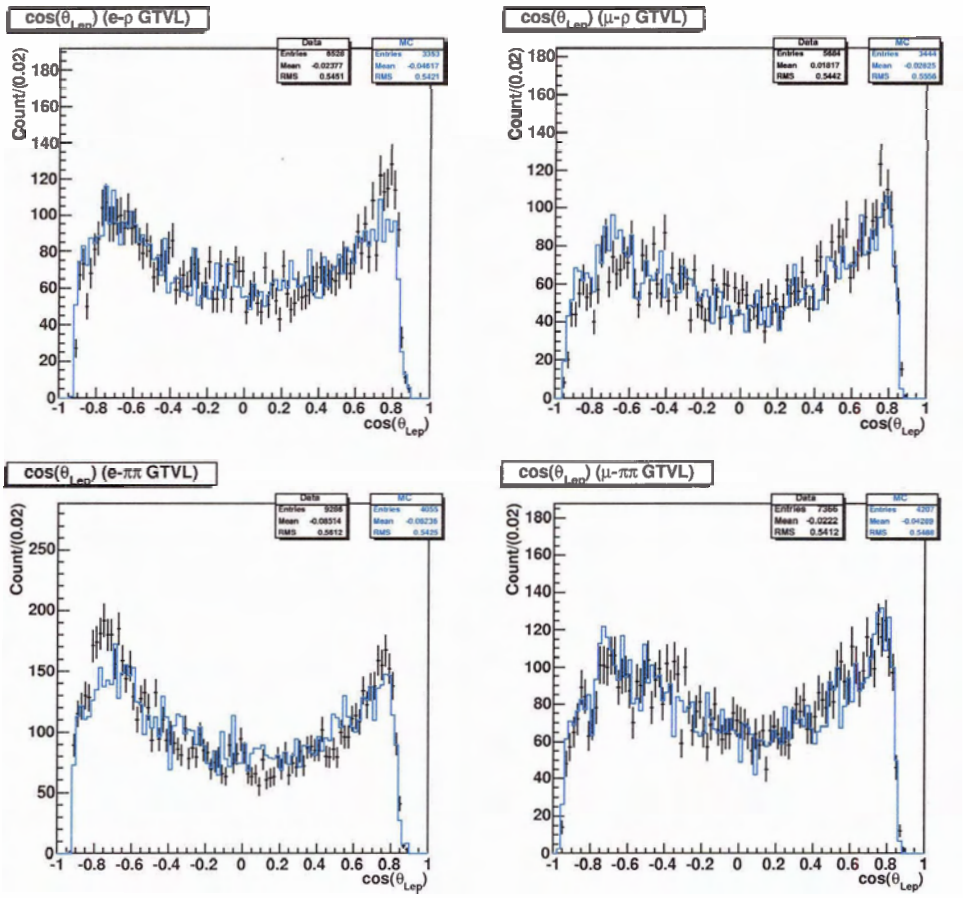

Figure 7.5: $cos(\theta_{\mathrm{Lep}})$ for the 1 vs 2 prong case and the GTVL section criteria from 2002-2003 (1930V). The MC types have a relative luminosity normalization that has been area normalized to the data. The data is represented by the points, while the MC is represented by the line.

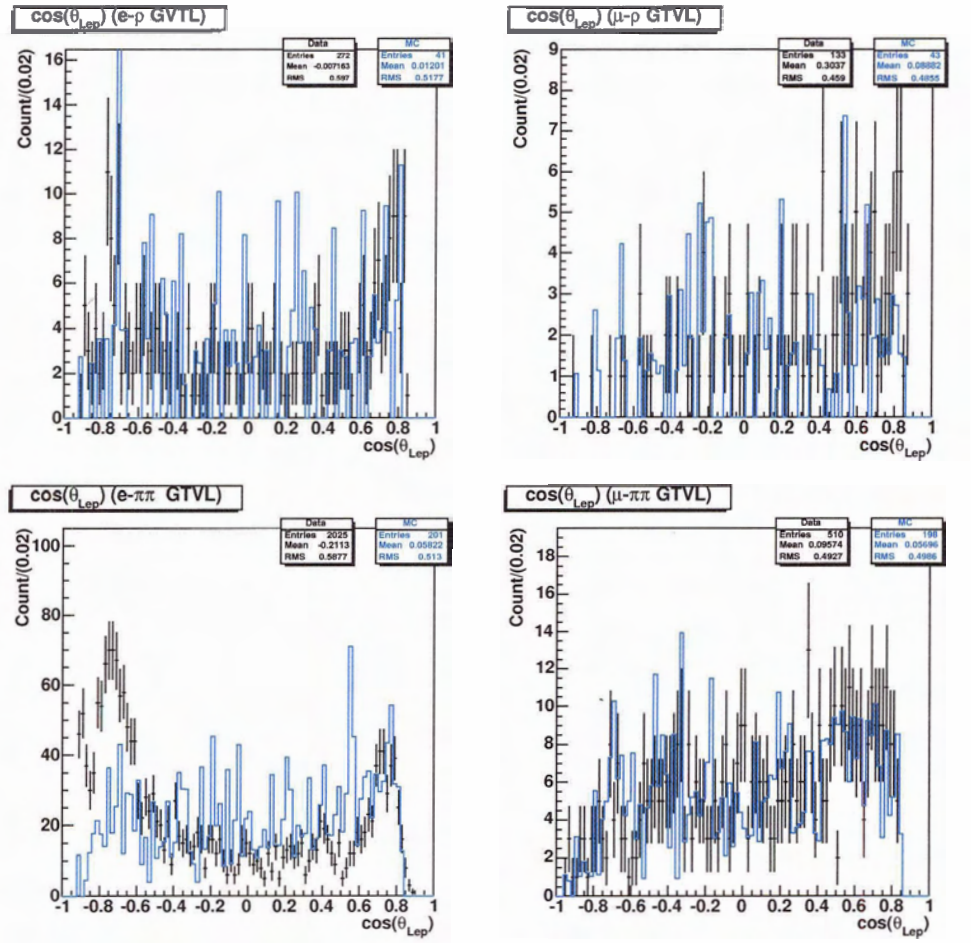

Figure 7.6: $cos(\theta_{\mathrm{Lep}})$ for the 1 vs 2 prong background region case and the GTVL section criteria from 2002-2003 (1930V). The MC types have a relative luminosity normalization that has been area normalized to the data. The data is represented by the points, while the MC is represented by the line.

The radiative Bhabha events also differ from the τ signal in that the invariant mass of radiative Bhabhas tend to be much smaller than invariant mass of $\tau \rightarrow hhh\nu_{\tau}$. This is result of the directional dependence of the radiated photon upon the direction of the primary electron or positron in a radiative Bhabha event. The invariant mass distribution of the pions in the 1 vs 3 prong and 1 vs 2 prong can be seen in figures 7.7, 7.8, 7.9, 7.10,

7.11 and 7.12. In the latter two figures, for the 1 vs 2 prong and 1 vs 2 prong background region, the $e-\pi\pi$ channel has an excess number of events in the low mass region illustrated by the discrepancy between the data and MC distribution shapes. This indicates that the background is a result of Bhabha contamination.

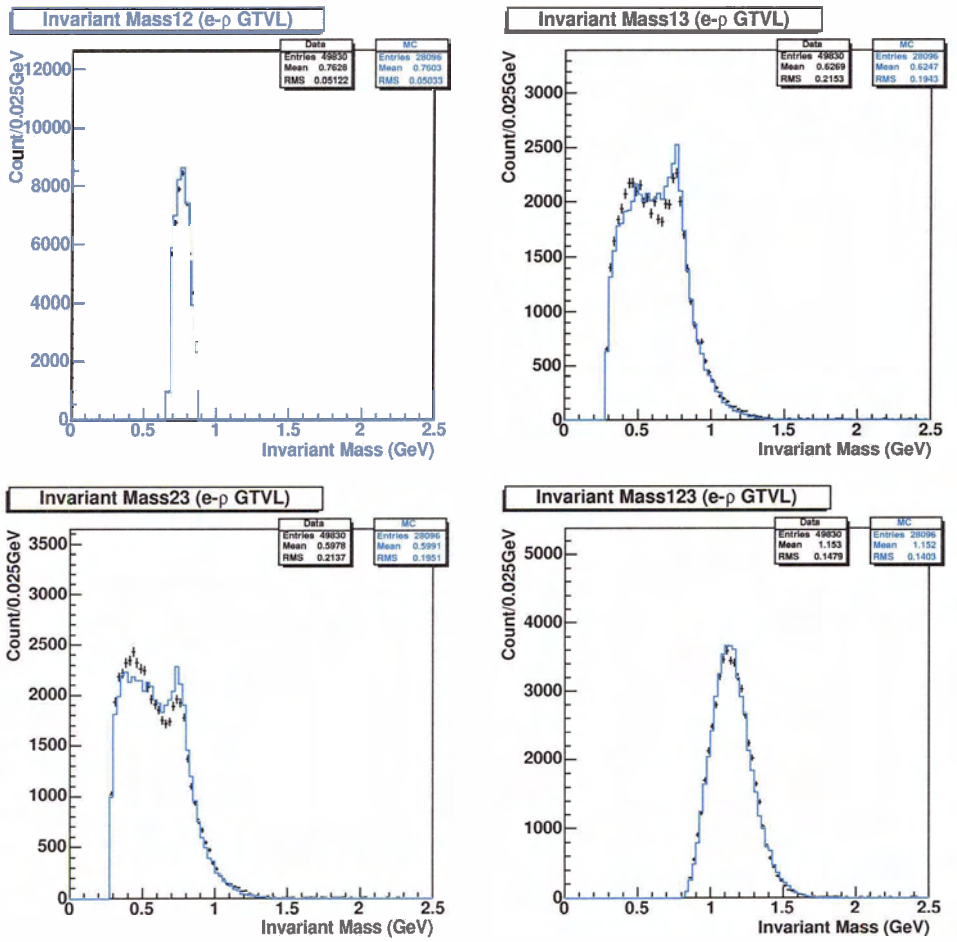

Figure 7.7: The Invariant Mass of the pions in the $e-\rho$ channel when all three pions are identified for the GTVL section criteria from 2002-2003 (1930V). The designation 1, 2 and 3 corresponds to the $\pi 1$, $\pi 2$ and the 4th track respectively. The MC types have a relative luminosity normalization that has been area normalized to the data. The data is represented by the points, while the MC is represented by the line.

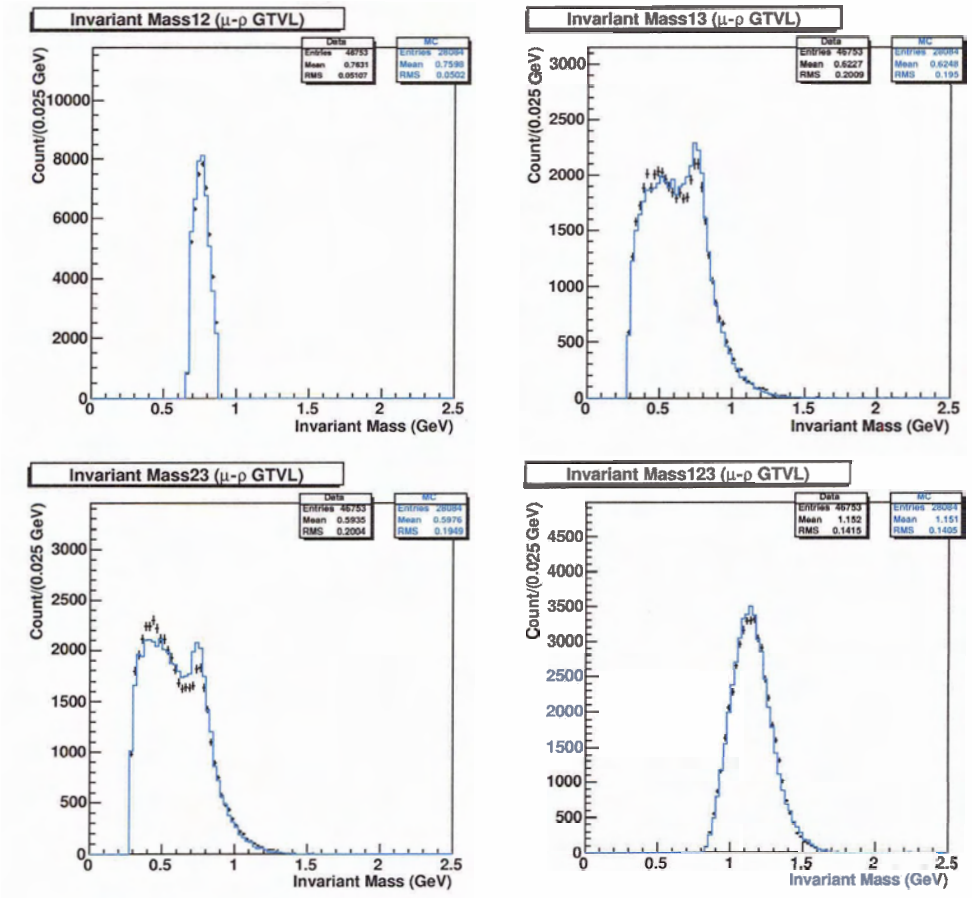

Figure 7.8: The Invariant Mass of the pions in the $\mu - \rho$ channel when all three pions are identified for the GTVL section criteria from 2002-2003 (1930V). The designation 1, 2 and 3 corresponds to the $\pi 1$, $\pi 2$ and the 4th track respectively. The MC types have a relative luminosity normalization that has been area normalized to the data. The data is represented by the points, while the MC is represented by the line.

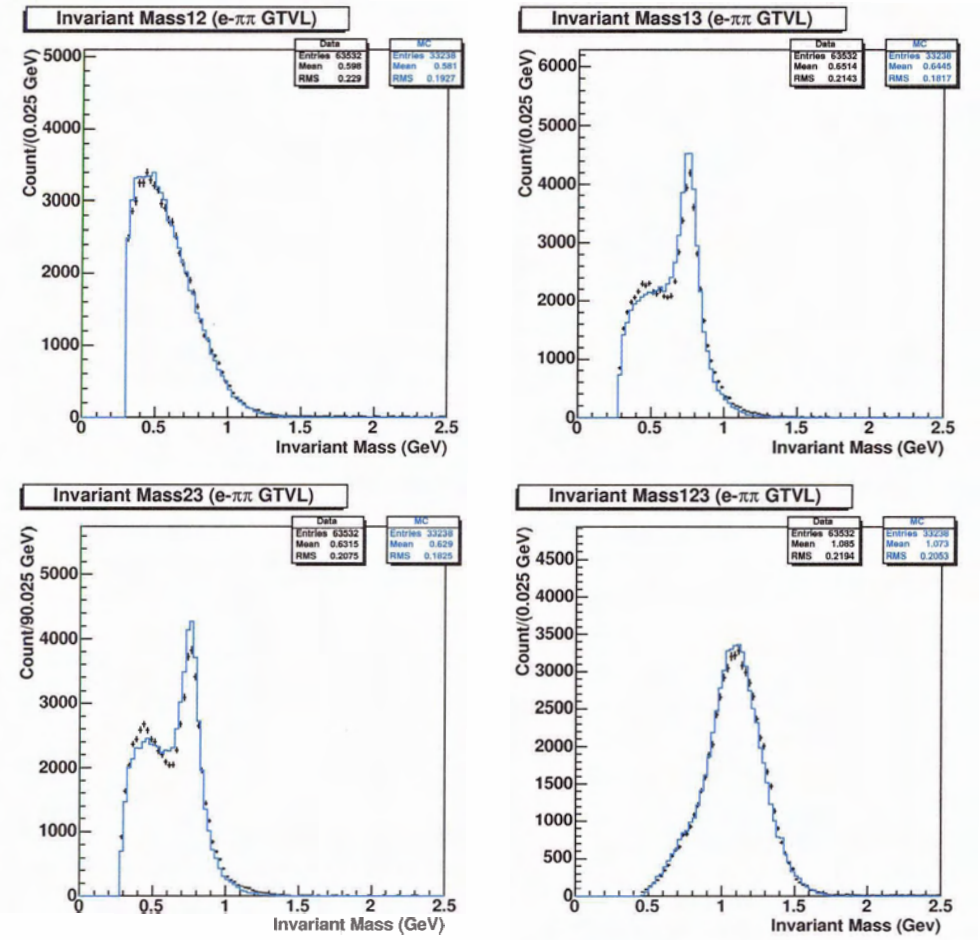

Figure 7.9: The Invariant Mass of the pions in the $e - \pi\pi$ channel when all three pions are identified for the GTVL section criteria from 2002-2003 (1930V) . The designation 1, 2 and 3 corresponds to the $\pi 1$, $\pi 2$ and the 4th track respectively. The MC types have a relative luminosity normalization that has been area normalized to the data. The data is represented by the points, while the MC is represented by the line.

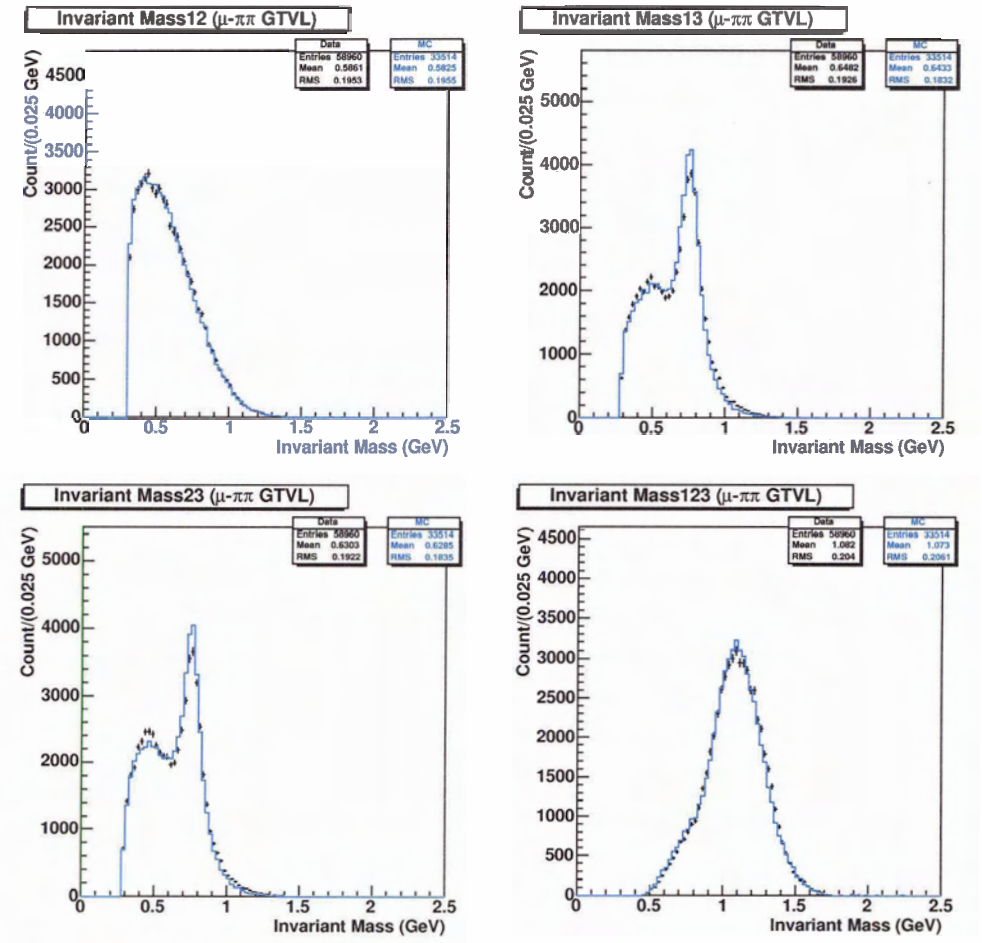

Figure 7.10: The Invariant Mass of the pions in the $\mu - \pi\pi$ channel when all three pions are identified for the GTVL section criteria from 2002-2003 (1930V) . The designation 1, 2 and 3 corresponds to the $\pi 1$, $\pi 2$ and the 4th track respectively. The MC types have a relative luminosity normalization that has been area normalized to the data. The data is represented by the points, while the MC is represented by the line.

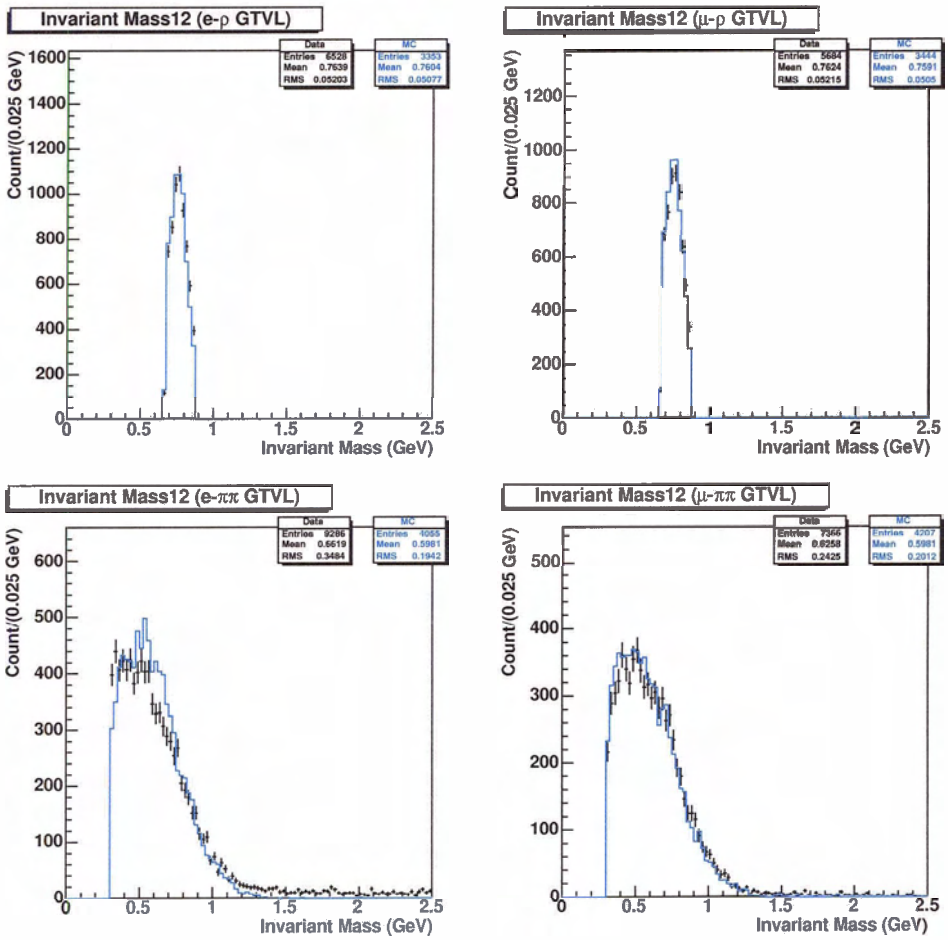

Figure 7.11: The Invariant Mass of the two identified pions for the four decay channels when the 4th track fails to be identified with the GTVL section criteria for the 2002-2003 (1930V) data set. The MC types have a relative luminosity normalization that has been area normalized to the data. The data is represented by the points, while the MC is represented by the line.

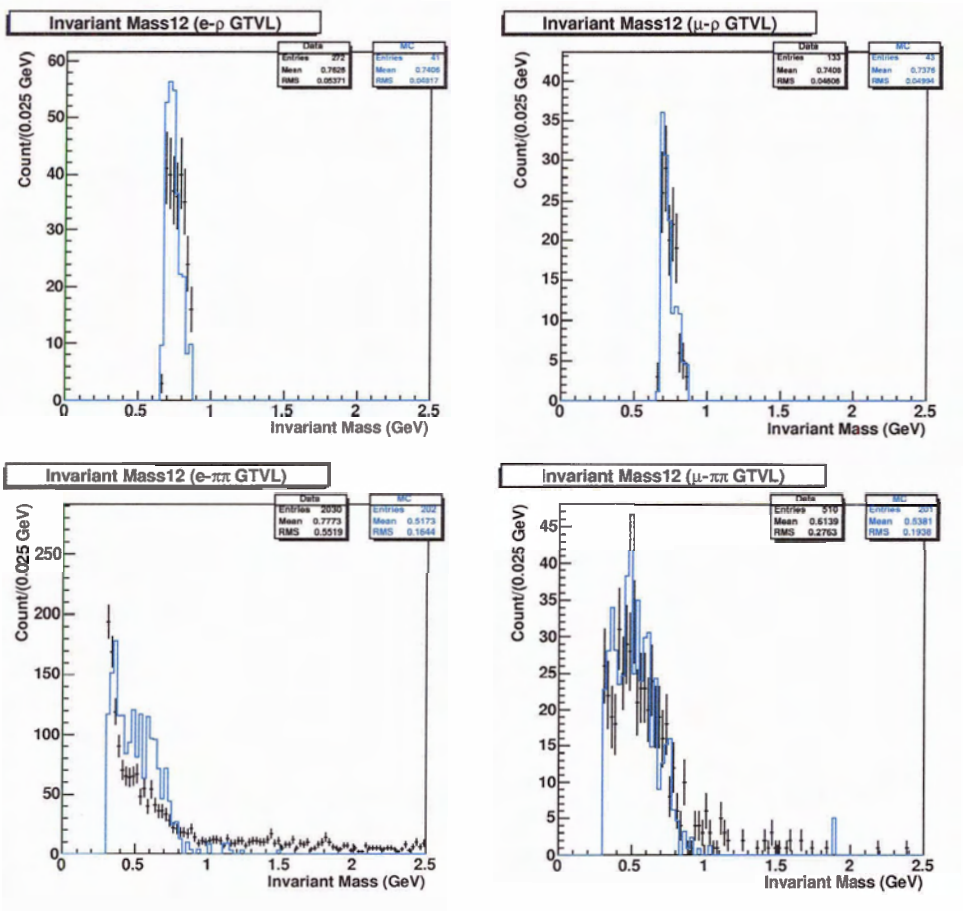

Figure 7.12: The Invariant Mass in the background region of the two identified pions for the four decay channel when the 4th track fails to be identified with the GTVL section criteria for the 2002-2003 (1930V) data set. The MC types have a relative luminosity normalization that has been area normalized to the data. The data is represented by the points, while the MC is represented by the line.

The efficiency and correction factor was then calculated with the background region rejected in the selection process to verify that the identified background was the source of the deviation between the electron and muon tag channels. Appendix D contains the efficiency and correction factor tables with the background rejected. This demonstrates that the identified background is the source of a significant amount of the deviation between the

electron and muon tagged channels.

An additional source of contamination was observed in the kinematically forbidden region, $P_t^{miss(lab)} < P_t^{(lab)}$, for the 4th track in the P_t distributions for the tracking efficiency as a function of P_t, θ and ϕ study. Figures, 7.13 and 7.14 show the discrepancy between the data and MC in the kinematically forbidden regions for the $e-\rho$ and $e-\pi\pi$ channels. The source of this un-modeled contamination in the $e-\rho$ and $e-\pi\pi$ channels is undetermined.

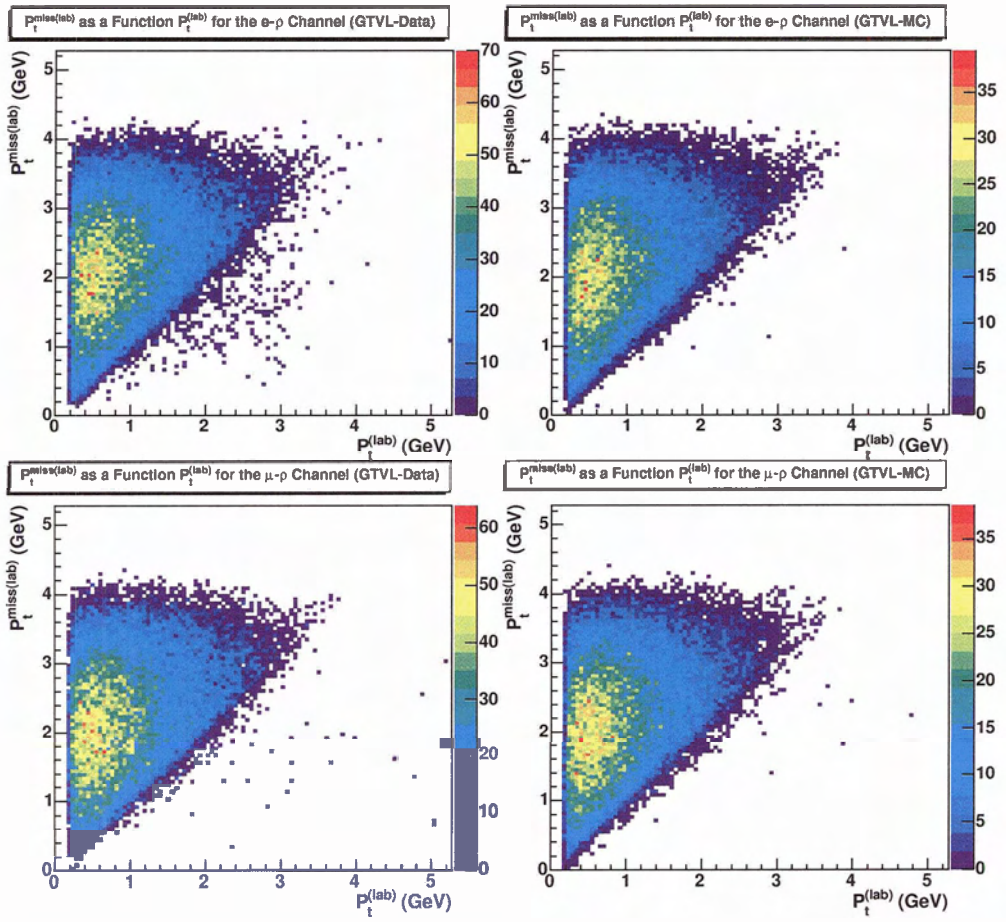

Figure 7.13: $P_t^{miss(lab)}$ as a function of $P_t^{(lab)}$ for the 4th track in the $e-\rho$ and $\mu-\rho$ channels with the GTVL section criteria for the 2002-2003 (1930V) data set. The $e-\rho$ channel contains an excess number of events which is neither present in the $\mu-\rho$ channels nor modeled by the MC. The MC types have a relative luminosity normalization.

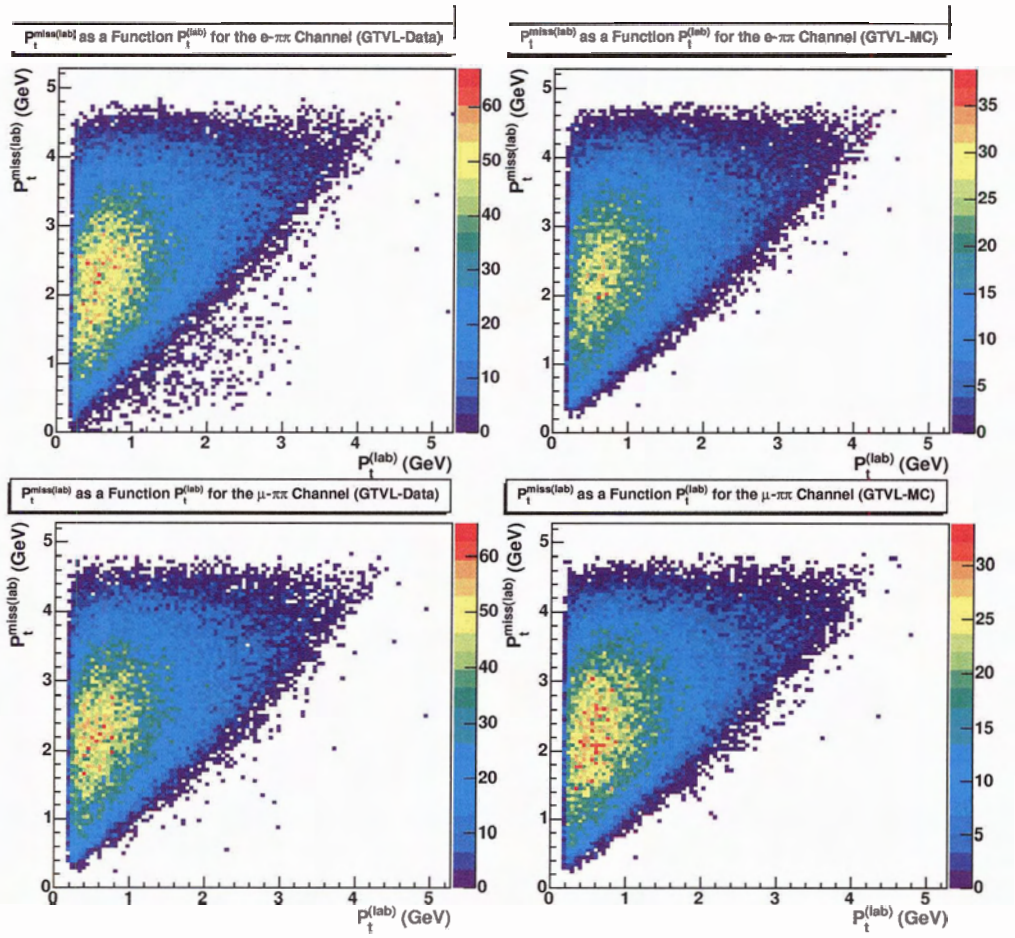

Figure 7.14: $P_t^{miss(lab)}$ as a function of $P_t^{(lab)}$ for the 4th track in the $e-\pi\pi$ and $\mu-\pi\pi$ channels with the GTVL section criteria for the 2002-2003 (1930V) data set. The $e-\pi\pi$ channel contains an excess number of events which is neither present in the $\mu-\pi\pi$ channels nor modeled by the MC. The MC types have a relative luminosity normalization.

Clearly, the $e-\rho$ and $e-\pi\pi$ channels have additional background contamination that is not modeled in the MC. This results in the shifting of the mean in the efficiency, the correction factor and the charge asymmetry for both the $e-\rho$ and $e-\pi\pi$ channels. As a result, the $e-\rho$ and $e-\pi\pi$ channels are removed from the average values. However, there is a slight bias between the $\mu-\rho$ and $\mu-\pi\pi$ channels in both the charge asymmetry and

correction factor. Thus a systematic uncertainty of half of the deviation between the $\mu - \rho$ and $\mu - \pi\pi$ channels is used.

7.2 Di-Muon Contamination

Just as the electron channels contains radiative Bhabha contamination that alters the mean values in the efficiency, correction factor and charge asymmetry in both the $e - \rho$ and $e - \pi\pi$, the corresponding di-muon, $e^+e^- \rightarrow \mu^+\mu^-(\gamma)$, interaction may contaminate the muon channels. Therefore, the di-muon contamination was estimated by repeating the Tau31 Study for the 1930V setting without the "e+e- → mu+mu-gamma (KK2F)" MC. Appendix E contains the correction factor and charge asymmetry tables for this study. Since the accuracy of the "e+e- → mu+mu-gamma (KK2F)" MC is significantly better than 10%, an upper limit of the systematic uncertainty may be very conservatively set as 10% of the difference between the correction factor and charge asymmetries with and without the "e+e- → mu+mu-gamma (KK2F)" MC. This represents a small contribution to the overall systematic error.

7.3 Ghost Tracks and Loopers

The absolute differences $|\Delta - \Delta'|$ and $|a_\pm - a_\pm'|$ quantifies the deviation caused by contamination due to Ghost Tracks, Loopers and events with more than 1 track missing in higher track multiplicity τ decay. The resulting systematic is half of the averaged absolute difference for the muon channels. Charge conservation, which is utilized in the selection of four track events, removes the dominant source of contamination due to Ghost Tracks, Loopers and more than one missing track from higher track multiplicity events. Therefore, only the 3 track events contain a significant source of contamination. As a result, analysis which employ techniques to remove the Ghost Tracks and Loopers may have a smaller systematic uncertainty.

7.4 Stability in P_t^{miss}, θ and ϕ

Since the results of this study will be applied to interactions with different kinematic conditions, in P_t, θ and ϕ a measurement of stability is required. The stability of the tracking efficiency correction factor and charge asymmetry were determined by measuring the average deviation between the tracking efficiency correction factor and charge asymmetry constructed in bins of P_t^{miss}, θ and ϕ. The bins utilized to determine the systematic uncertianty corresponding to these variations in P_t^{miss} , θ and ϕ are shown in tabular form below.

Var.	Cut 1	Cut 2	Cut 3
P_t^{miss}	$P_t^{miss} < 1.0$GeV	$1.0\text{GeV} < P_t^{miss} < 2.5$GeV	$2.5\text{GeV} < P_t^{miss}$
$cos(\theta)$	$cos(\theta_{avg}^{(lab)}) < 0.2$	$0.2 < cos(\theta_{avg}^{(lab)}) < 0.6$	$0.6 < cos(\theta_{avg}^{(lab)})$
ϕ	$\phi_{avg}^{(lab)} < -1.046$rad	$-1.046\text{rad} < \phi_{avg}^{(lab)} < 1.046$rad	$1.046\text{rad} < \phi_{avg}^{(lab)}$

Table 7.1: The cuts employed in determining the stability as a function of P_t^{miss}, θ and ϕ.

The systematic uncertainty quoted here is equal to half the maximum deviation between the bins. Correction factor and charge asymmetry tables for this study can be found in Appendix F. Appendix G contains the pseudo-efficiency for the P_t^{miss} cut in the central region of the detector where the geometric acceptance is 100%. The large decrease in efficiency between the CT and GTVL selection criteria is the result of the cut on the distance of closest approach to the interaction point. The systematic uncertainties related to stability in P_t^{miss}, θ and ϕ are required for analyses utilizing a topology significantly different from the one in the Tau31 Study and quoting a simple global efficiency correction.

7.5 Stability of the Detector in Time

The efficiency of the detector, and therefore the correction factor and charge asymmetry in the detector, may be altered over time as a result of radiation damage, damage from the Drift Chamber gas or due to upgrade of the detector. To verify that these differences

are negligible, the 1930V setting was separated into three blocks: the 2001 data set, the 2002 data set and the 2003 data set. The results of this study can be seen in table 7.2 and confirm that there is no significant time dependence.

Data Set	$\Delta(\%)$	$a_{\pm}(\%)$ (Data)	$a_{\pm}(\%)$ (MC)
Good Tracks Loose			
2001 (1930V)	$(1.6 \pm 1.8) \times 10^{-1}$	$(-3.1 \pm 1.8) \times 10^{-1}$	$(0.7 \pm 2.7) \times 10^{-1}$
2002 (1930V)	$(5.3 \pm 2.4) \times 10^{-1}$	$(-3.8 \pm 2.4) \times 10^{-1}$	$(-2.6 \pm 2.1) \times 10^{-1}$
2003 (1930V)	$(4.6 \pm 1.7) \times 10^{-1}$	$(-0.1 \pm 1.7) \times 10^{-1}$	$(-2.3 \pm 2.6) \times 10^{-1}$
Good Tracks Very Loose			
2001 (1930V)	$(-2.1 \pm 1.7) \times 10^{-1}$	$(-2.6 \pm 1.7) \times 10^{-1}$	$(0.4 \pm 2.6) \times 10^{-1}$
2002 (1930V)	$(0.8 \pm 2.3) \times 10^{-1}$	$(-2.7 \pm 2.3) \times 10^{-1}$	$(-3.0 \pm 2.0) \times 10^{-1}$
2003 (1930V)	$(-1.1 \pm 1.6) \times 10^{-1}$	$(0.3 \pm 1.6) \times 10^{-1}$	$(-2.1 \pm 2.5) \times 10^{-1}$
Charged Tracks			
2001 (1930V)	$(-3.9 \pm 1.1) \times 10^{-1}$	$(-0.6 \pm 1.1) \times 10^{-1}$	$(2.3 \pm 1.7) \times 10^{-1}$
2002 (1930V)	$(-2.7 \pm 1.5) \times 10^{-1}$	$(1.6 \pm 1.8) \times 10^{-1}$	$(1.6 \pm 1.8) \times 10^{-1}$
2003 (1930V)	$(-4.2 \pm 1.0) \times 10^{-1}$	$(-0.1 \pm 1.0) \times 10^{-1}$	$(-1.6 \pm 1.7) \times 10^{-1}$

Table 7.2: The variation of the detector's performance over time. The errors are statistical only.

A complete set of the results can be seen in Appendix H, I, and J. Table 7.2 illustrates that variances in the performance of the detector are statistical and therefore is neglected.

Chapter 8

Summary and Discussion

The results of the global tracking efficiency study and the systematic studies are combined to produce the MC correction factor and tracking efficiency charge asymmetry of the detector and the errors. Table 8.1 displays the tracking efficiency correction results for the various track definitions in the three voltage settings. The total error, which is calculated by adding the statistical and systematic errors in quadrature, is in all cases dominated by the systematic error. The individual components of the systematic errors are shown. These are added, in quadrature, to give the total systematic error. The systematic uncertainty related to the deviation between the $\mu - \pi\pi$ and $\mu - \rho$ channels is referred to as the "channel". The "Di-muon" background contamination study results in a systematic uncertainty that is negligible relative to the other uncertainties. The systematic uncertainty caused by spurious tracks (Ghost Tracks, Loopers, and contamination from higher multiplicity τ decays with more than one missing track) is also small compared to the total systematic uncertainty. The $cos(\theta^{(lab)})$ dependence is the dominating systematic error followed by the $P_t^{(lab)}$ dependence. Currently, there is no conclusive explanation for the large $cos(\theta^{(lab)})$ dependence. The efficiency was independent of $\phi^{(lab)}$, thus yielding a small systematic uncertainty on the global efficiency. The tracking efficiency correction factors displayed in table 8.1 are all consistent with zero.

Volt.	Δ(%)	Total Error (%)	Stat. Error (%)	Syst. Error (%)	Decomposition of the Systematic Error (%)					
					Channel	Di-muon	Ghost & Loopers	P_t^{miss}	θ	ϕ
Good Tracks Loose										
1900V	0.85	1.06	0.28	1.02	0.45	0.001	0.06	0.36	0.83	0.12
1930V	0.42	0.92	0.11	0.92	0.09	0.001	0.02	0.36	0.83	0.12
1960V	-0.32	0.99	0.38	0.92	0.05	0.001	0.09	0.36	0.83	0.12
Good Tracks Very Loose										
1900V	0.26	0.94	0.26	0.90	0.45	0.000	0.03	0.28	0.71	0.18
1930V	-0.06	0.79	0.10	0.79	0.02	0.000	0.07	0.28	0.71	0.18
1960V	-0.34	0.89	0.37	0.81	0.14	0.000	0.13	0.28	0.71	0.18
Charged Tracks										
1900V	-0.16	0.91	0.17	0.89	0.21	0.0003	0.05	0.49	0.70	0.14
1930V	-0.35	0.88	0.07	0.88	0.09	0.0003	0.14	0.49	0.70	0.14
1960V	-0.60	0.91	0.24	0.88	0.17	0.0003	0.01	0.49	0.70	0.14

Table 8.1: The correction factor with the corresponding uncertainties.

The tracking efficiency charge asymmetry of the detector with the combined error for the three track definition and associated voltage settings can be seen in table 8.2. In parallel to table 8.1, the total error is the quadrature sum of the statistical and systematic errors. The decomposition of the systematic error is also similar, however, the $cos(\theta^{(lab)})$ dependence is significantly reduced leaving the $P_t^{(lab)}$ dependence as the dominate systematic uncertainty. Further investigation is required to determine the source of this dependence. The charge asymmetry of both the MC and data are consistent with zero.

These results indicate that the detector simulation models the tracking efficiency of the BaBar Detector to an accuracy of approximately 1%. The absolute results from the τ Tracking Efficiency Study may be applied directly to events, such as τ decays, with similar topologies. To produce a tracking efficiency correction factor useful for events with more tracks and with alternate topologies, the τ Tracking Efficiency Study is combined with a relative tracking efficiency study that can examine events that contain more tracks. Figure 8.1 demonstrates the efficiency as a function of multiplicity, or track number per event, for the SVT Tracking Efficiency Study, which measures the GTL efficiency relative to the GTVL

Data										
Volt.	$a_{\pm}(\%)$	Total Error (%)	Stat. Error (%)	Syst. Error (%)	Decomposition of the Systematic Error (%)					
					Channel	Di-muon	Ghost & Loopers	P_t^{miss}	θ	ϕ
Good Tracks Loose										
1900V	-0.37	0.63	0.28	0.57	0.14	0.000	0.02	0.38	0.28	0.28
1930V	-0.20	0.64	0.11	0.63	0.31	0.000	0.02	0.38	0.28	0.28
1960V	-0.30	0.83	0.38	0.74	0.50	0.000	0.01	0.38	0.28	0.28
Good Tracks Very Loose										
1900V	-0.32	0.52	0.26	0.45	0.20	0.000	0.00	0.15	0.26	0.27
1930V	-0.14	0.49	0.10	0.48	0.25	0.000	0.02	0.15	0.26	0.27
1960V	-0.31	0.70	0.36	0.60	0.45	0.000	0.00	0.15	0.26	0.27
Charged Tracks										
1900V	-0.21	0.52	0.17	0.49	0.45	0.000	0.11	0.13	0.05	0.08
1930V	-0.06	0.28	0.065	0.27	0.21	0.000	0.05	0.13	0.05	0.08
1960V	-0.12	0.32	0.24	0.21	0.09	0.000	0.11	0.13	0.05	0.08

MC										
Volt.	$a_{\pm}(\%)$	Total Error (%)	Stat. Error (%)	Syst. Error (%)	Decomposition of the Systematic Error (%)					
					Channel	Di-muon	Ghost & Loopers	P_t^{miss}	θ	ϕ
Good Tracks Loose										
1900V	-0.14	0.67	0.27	0.62	0.02	0.000	0.01	0.48	0.34	0.19
1930V	-0.16	0.64	0.14	0.62	0.04	0.000	0.01	0.48	0.34	0.19
1960V	-0.04	0.82	0.50	0.65	0.21	0.000	0.03	0.48	0.34	0.19
Good Tracks Very Loose										
1900V	-0.17	0.71	0.25	0.66	0.07	0.001	0.03	0.54	0.36	0.12
1930V	-0.18	0.67	0.13	0.66	0.04	0.001	0.01	0.54	0.36	0.12
1960V	-0.11	0.84	0.48	0.69	0.21	0.001	0.05	0.54	0.36	0.12
Charged Tracks										
1900V	0.24	0.48	0.17	0.45	0.09	0.0002	0.12	0.39	0.15	0.07
1930V	-0.08	0.46	0.09	0.45	0.10	0.0002	0.13	0.39	0.15	0.07
1960V	0.14	0.62	0.33	0.53	0.23	0.0002	0.21	0.39	0.15	0.07

Table 8.2: The charge asymmetry with the corresponding uncertainties.

efficiency. Unfortunately, the SVT study assumes independent tracking reconstruction for the DCH and SVT, an assumption that is incorrect as outlined in Section 4.3.2. However, this is a high statistics study permitting examination of the relative GTL to GTVL efficiencies as a function of multiplicity, P_t, $cos(\theta)$ and ϕ. The difference between the two tracking

efficiency methods are evaluated by comparing the global τ tracking efficiency correction factor to a global SVT tracking correction factor that has been calculated from a global SVT tracking efficiency weighted by the $P_t^{(lab)}$ and $cos(\theta^{(lab)})$ τ distribution. This technique suffers from the additional assumption that there is no correction for the SVT efficiency for the GTVL tracks. This assumption is validated by the τ Study to $\pm 0.5\%$. Below is a table with a comparison of the tracking efficiency correction factors. In addition, the tracking efficiency charge asymmetry can be applied to CP violation studies that analyze events with similar topologies to that of the τ Tracking Efficiency Study.

Channel	$\Delta(\%)$
Global τ Tracking Efficiency Correction Factor (GTL)	
$\mu - \rho$	$(5.2 \pm 1.6) \times 10^{-1}$
$\mu - \pi\pi$	$(3.4 \pm 1.4) \times 10^{-1}$
Global SVT Tracking Efficiency Correction Factor	
$\mu - \rho$	$(2.9) \times 10^{-1}$
$\mu - \pi\pi$	$(3.1) \times 10^{-1}$

Table 8.3: A comparison between the global τ Tracking Efficiency correction factor and global SVT Tracking Efficiency correction factor for the 1930V setting. The errors for the Global τ Tracking Efficiency Correction Factor (GTL) are statistical.

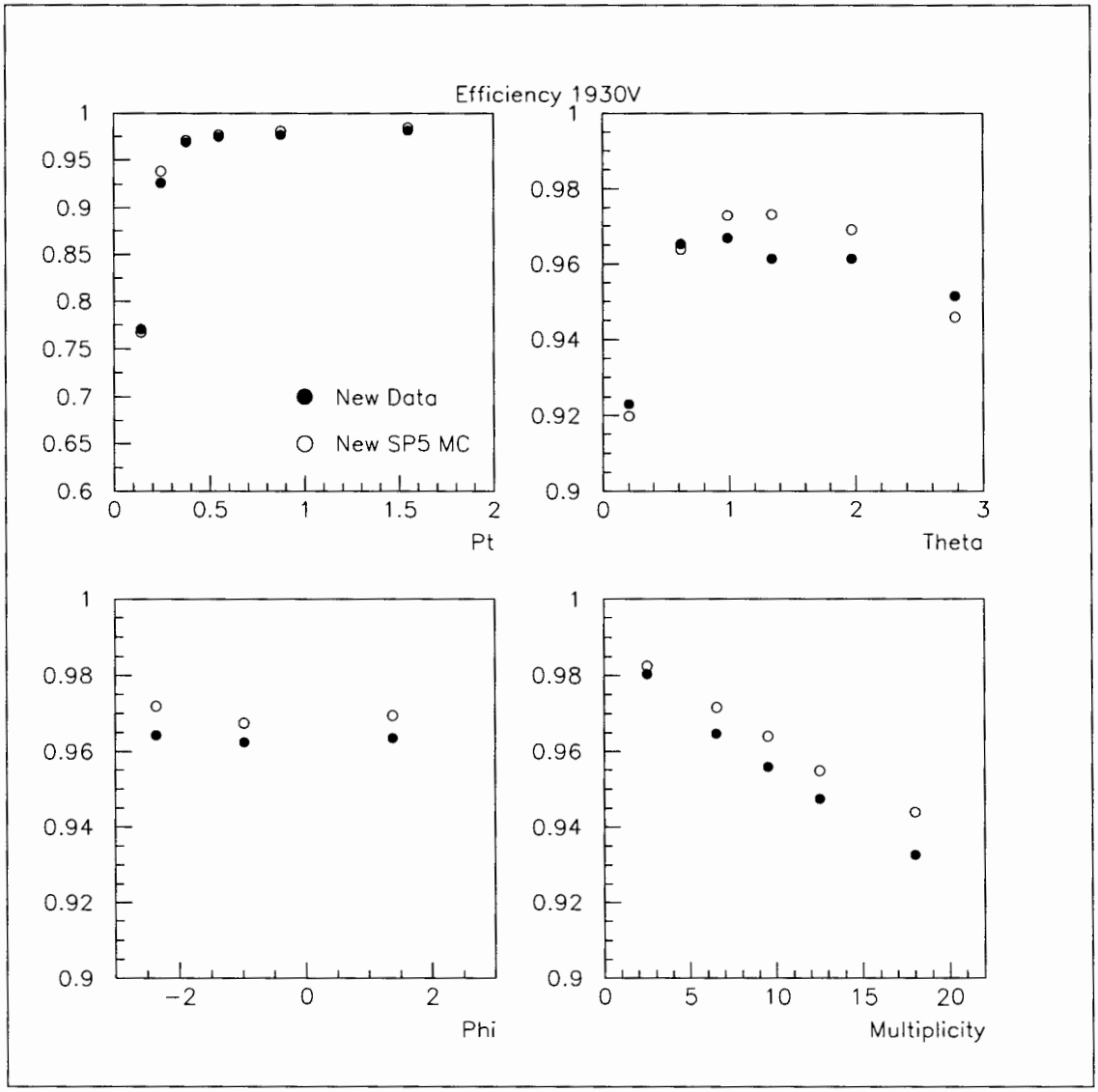

Figure 8.1: The relative tracking efficiency between the GTL and GTVL track criteria displayed in terms of transverse momentum in the laboratory frame, θ in the laboratory frame, ϕ in the laboratory frame, and the multiplicity of the event for the SVT Tracking Efficiency Study. [31, Efficiency Plots of New Study]

Chapter 9

Conclusion

The Tau31 Tracking Efficiency Study successfully determined the global MC correction factor and tracking efficiency charge asymmetry for BaBar data in low multiplicity events. The efficiency correction factors were determined to be consistent with zero. The charge asymmetries for the data and MC were determined to also be consistent with zero. The systematic studies indicated that the deviation between the τ decay channels identified by electrons and muons was caused by radiative Bhabha contamination in the electron channels and therefore only the muon channels were used. The variation in tracking efficiency was determined to be independent in time. These results, in addition to those from alternative tracking studies, have been employed to determine a net tracking efficiency correction factor and charge asymmetry for all physics events reconstructed with release 12 version of the reconstruction software. The results of this study can be applied directly to τ analysis that contain a similar topology. The $cos(\theta^{(lab)})$ dependent tracking efficiency study indicated the presence of a $cos(\theta^{(lab)})$ dependency in the tracking efficiency correction factor and the charge asymmetry. Further studies are required to determine if this is a result of correlations between the track momentum distribution and the polar angle, $cos(\theta^{(lab)})$. The tracking efficiency $\phi^{(lab)}$ dependency study indicated that the tracking efficiency, the tracking efficiency correction factor, and the charge asymmetry of the detector are independent of $\phi^{(lab)}$. It was successfully demonstrated, for the first time, that the efficiency can

be determined as a function of the transverse momentum in the laboratory frame, $P_t^{(lab)}$, by using a probability matrix method. However, this work was limited by the size of the data set employed in this study. In the future, the statistics for this study can be improved by an order of magnitude, therefore making it necessary to remove the bias caused by the zero efficiency region at low momenta. Moreover, the tracking efficiency $P_t^{(lab)}$ dependency, with the enhanced statistics, should be analyzed in separate $cos(\theta^{(lab)})$ bins in order to understand the $P_t^{(lab)}$-$cos(\theta^{(lab)})$ correlations.

Bibliography

[1] Erick J. Weinberg *et al.*, "Physical Review D Particle and Fields Part 1 Review of Particles Physics", Volume 66 Third Series, The American Physical Society, July 1, 2002.

[2] Peskun and Schrodier, "Introduction to Quantum Field Theory", Westview Press, USA, 1995.

[3] Francis Halzen, Alan D. Martin, "Quarks and Leptons: An Introduction to Modern Particle Physics" , John Wiley and Sons, Inc., USA, 1984.

[4] Michel Lefebvre, "PHYS506B: Particle Physics II" (Notes), Spring 2003.

[5] John F. Donoghue, Eugene Golowich, Barry R. Holstein, "Dynamics of the Standard Model", Cambridge University Press, USA, 1996.

[6] Donald H. Perkins, "Introduction to High Energy Physics 4th edition", Cambridge University Press, England, 2001.

[7] E. W. Varnes, "Measurement of the Tracking Efficiency Using 3+1 τ Events", BaBar Analysis Document #87 version 5, March 15, 2001.

[8] BaBar WebSite: http://www.slac.stanford.edu/BFROOT Last Accessed: August 30, 2004.

[9] P. F. Harrison, H. R. Quinn, "The BaBar Physics Book", SLAC-R-504, 1998.

[10] C. Boutigny *et al.*[BaBar Collaboration], "The BaBar Technical Design Report", SLAC-R-95-457(1993).

[11] R. Bartoldus, *et al*, "Trigger and Filter Document for Run1", BaBar Analysis Document #194, April 9, 2002.

[12] Louis Lyons, "Statistics for Nuclear and Particle Physicists", Cambridge University Press 1992.

[13] Jorg Stelzer, "A new IFR tracking algorithim utilizing the Kalman fit theory", BaBar Analysis Document #799, June 9, 2004.

[14] Paul Avery, "Applied Fitting Theory V Track Fitting Using the Kalman Filter", Internal CLEO Note CBX 92-39, August 20, 1992.

[15] BaBar workbook http://www.slac.stanford.edu/BFROOT/www/doc/workbook/ Last Accessed: August 30, 2004.

[16] Eric Charles [BaBar SVT Track Reconstruction Group], private communication.

[17] Wouter Hulsbergen [BaBar SVT Track Reconstruction Group], private communication.

[18] Gerald Lynch [BaBar SVT Track Reconstruction Group], private communication.

[19] John Walsh [BaBar SVT Track Reconstruction Group], private communication.

[20] David N. Brown, Erich A. Charles, Douglas A. Roberts, "The BaBar Track Fitting Algorithm", CHEP A328, 2000.

[21] Natalia Kuznetsova, Gerald Lynch, Gloria Vuagnin, "SVT Offline Software" BaBar Draft, October 10, 1999.

[22] F. A Kirsten *et al.*, "BaBar Level 1 Drift Chamber and Global Trigger Implimetation V4.2" Lawrence Berkeley National Laboratory and Stanford Linear Accelerator Center, September 29, 1998

[23] Brown, David N., "Current Tracking Sequence", Report to BaBar Tracking, May 16, 2001.

[24] Lynch, Gerald, "SvtTrackFinder", BaBar Internal Document, November 19, 1997.

[25] Owen Long, "An alternative algorithm for stand-alone SVT pattern recognition", Babar Note 499 Version 0.1, July 8, 1999.

[26] BaBar workbook http://www.slac.stanford.edu/BFROOT/www/doc/workbook/mini/mini.html Last Accessed: August 30, 2004.

[27] Francisco Yumiceva, "Search for CP Violation in D^+ Mesons Decays", May 5 2003.

[28] http://www.bctf.bc.ca/bcscta/Hebden%20Demos/Chemical%20In-ventory.pdf Last Accessed: July 15, 2004.

[29] Yosef Nir, "CP Violation: The CKM Matrix and New Physics", hep-ph/0208080 V2 August 19, 2002.

[30] Yosef Nir, "CP Violation - A new Era", hep-ph/0109090 V1, September 11, 2001.

[31] http://www.slac.stanford.edu/BFROOT/www/Physics/TrackEfficTaskForce/SvtEff/SVTEff.html Last Accessed: August 30, 2004.

[32] S. Agostelli, S., *et al.*, [Geant4 Collaboration]. Nucl. Instrum. Methods A506:250, 2003.

[33] B. F. Ward, S. Jadach, and Z. Was, "Precision calculation for e+ e- → 2f: The K K MC project", Nucl. Phys. Proc. Suppl. **116**, 73 (2003). [arXiv:hep-ph/0211132].

[34] [Electron Identification Analysis Working Group], "Cut based Electron Identification", BaBar Analysis Document #90 Version 5, May 9, 2001.

[35] [Muon Identification Analysis Working Group], "Muon Identification in the BaBar Experiment", BaBar Analysis Document #60 Version 1, June 21, 2000.

[36] T. Sjöstrand, Computer Physics Commun. 39 (1986) 347.

[37] T. Sjöstrand and M. Bengtsson, Computer Physics Commun. 43 (1987) 367.

[38] H.-U. Bengtsson and T. Sjöstrand, Computer Physics Commun. 46 (1987) 43.

[39] David J. Lange, "The EvtGen particle decay simulation package", Nuclear Instruments and Methods A462 (2001) 152-155.

[40] S. X. Liao, "Image Analysis by Moments" Ph.D. dissertation, The University of Manitoba, 1993.

[41] A. Drescher et al., Nuclear Instruments and Methods A237, 464 (1985).

[42] The BaBar Collaboration, "The BaBar Detector", Nuclear Instruments and Methods, A479 (2002) 1-116.

[43] J. D. Jackson, "Classical Electrodynamics" 3rd Ed., John Wiley & Sons, Inc. United States of America, 2001.

Appendix A: 1900V Tables

Good Tracks Loose		
Decay	$\epsilon \times A(\%)$	$\epsilon' \times A(\%)$
$e-\rho$ (Data)	$(8.655 \pm 0.037) \times 10^1$	$(8.637 \pm 0.038) \times 10^1$
$e-\rho$ (MC)	$(8.851 \pm 0.035) \times 10^1$	$(8.830 \pm 0.036) \times 10^1$
$\mu-\rho$ (Data)	$(8.715 \pm 0.037) \times 10^1$	$(8.699 \pm 0.037) \times 10^1$
$\mu-\rho$ (MC)	$(8.834 \pm 0.034) \times 10^1$	$(8.806 \pm 0.034) \times 10^1$
$e-\pi\pi$ (Data)	$(8.460 \pm 0.035) \times 10^1$	$(8.396 \pm 0.035) \times 10^1$
$e-\pi\pi$ (MC)	$(8.790 \pm 0.033) \times 10^1$	$(8.754 \pm 0.033) \times 10^1$
$\mu-\pi\pi$ (Data)	$(8.718 \pm 0.032) \times 10^1$	$(8.685 \pm 0.033) \times 10^1$
$\mu-\pi\pi$ (MC)	$(8.758 \pm 0.032) \times 10^1$	$(8.716 \pm 0.033) \times 10^1$
μ–Avg. (Data)	$(8.717 \pm 0.024) \times 10^1$	$(8.691 \pm 0.025) \times 10^1$
μ–Avg. (MC)	$(8.794 \pm 0.023) \times 10^1$	$(8.758 \pm 0.024) \times 10^1$
Good Tracks Very Loose		
Decay	$\epsilon \times A(\%)$	$\epsilon' \times A(\%)$
$e-\rho$ (Data)	$(8.855 \pm 0.035) \times 10^1$	$(8.807 \pm 0.035) \times 10^1$
$e-\rho$ (MC)	$(8.971 \pm 0.034) \times 10^1$	$(8.926 \pm 0.034) \times 10^1$
$\mu-\rho$ (Data)	$(8.879 \pm 0.035) \times 10^1$	$(8.836 \pm 0.035) \times 10^1$
$\mu-\rho$ (MC)	$(8.945 \pm 0.033) \times 10^1$	$(8.892 \pm 0.033) \times 10^1$
$e-\pi\pi$ (Data)	$(8.626 \pm 0.033) \times 10^1$	$(8.533 \pm 0.034) \times 10^1$
$e-\pi\pi$ (MC)	$(8.858 \pm 0.032) \times 10^1$	$(8.803 \pm 0.033) \times 10^1$
$\mu-\pi\pi$ (Data)	$(8.864 \pm 0.031) \times 10^1$	$(8.796 \pm 0.032) \times 10^1$
$\mu-\pi\pi$ (MC)	$(8.851 \pm 0.031) \times 10^1$	$(8.784 \pm 0.032) \times 10^1$
μ–Avg. (Data)	$(8.870 \pm 0.023) \times 10^1$	$(8.814 \pm 0.023) \times 10^1$
μ–Avg. (MC)	$(8.896 \pm 0.023) \times 10^1$	$(8.835 \pm 0.023) \times 10^1$
Charged Tracks		
Decay	$\epsilon \times A(\%)$	$\epsilon' \times A(\%)$
$e-\rho$ (Data)	$(9.450 \pm 0.025) \times 10^1$	$(9.082 \pm 0.032) \times 10^1$
$e-\rho$ (MC)	$(9.559 \pm 0.023) \times 10^1$	$(9.241 \pm 0.029) \times 10^1$
$\mu-\rho$ (Data)	$(9.562 \pm 0.023) \times 10^1$	$(9.244 \pm 0.029) \times 10^1$
$\mu-\rho$ (MC)	$(9.568 \pm 0.022) \times 10^1$	$(9.243 \pm 0.028) \times 10^1$
$e-\pi\pi$ (Data)	$(9.298 \pm 0.025) \times 10^1$	$(8.944 \pm 0.029) \times 10^1$
$e-\pi\pi$ (MC)	$(9.411 \pm 0.024) \times 10^1$	$(9.155 \pm 0.028) \times 10^1$
$\mu-\pi\pi$ (Data)	$(9.468 \pm 0.022) \times 10^1$	$(9.139 \pm 0.027) \times 10^1$
$\mu-\pi\pi$ (MC)	$(9.434 \pm 0.023) \times 10^1$	$(9.128 \pm 0.027) \times 10^1$
μ–Avg. (Data)	$(9.514 \pm 0.016) \times 10^1$	$(9.188 \pm 0.020) \times 10^1$
μ–Avg. (MC)	$(9.503 \pm 0.016) \times 10^1$	$(9.184 \pm 0.020) \times 10^1$

Table A.1: The tracking efficiency for the three different track definitions from the 1900V setting. The average values in this table are the weighted average of the $\mu-\rho$ and $\mu-\pi\pi$ channels as discussed in Chapter 7: Systematic Uncertainty Studies.

Good Tracks Loose		
Decay	$\Delta(\%)$	$\Delta'(\%)$
$e-\rho$	(2.22 ± 0.42)	(2.19 ± 0.42)
$\mu-\rho$	(1.35 ± 0.42)	(1.21 ± 0.42)
$e-\pi\pi$	(3.75 ± 0.39)	(4.09 ± 0.40)
$\mu-\pi\pi$	$(4.5 \pm 3.7) \times 10^{-1}$	$(3.6 \pm 3.8) \times 10^{-1}$
μ–Avg.	$(8.5 \pm 2.8) \times 10^{-1}$	$(7.4 \pm 2.8) \times 10^{-1}$
Good Tracks Very Loose		
Decay	$\Delta(\%)$	$\Delta'(\%)$
$e-\rho$	(1.29 ± 0.39)	(1.34 ± 0.40)
$\mu-\rho$	$(7.5 \pm 3.9) \times 10^{-1}$	$(6.3 \pm 4.0) \times 10^{-1}$
$e-\pi\pi$	(2.61 ± 0.37)	(3.07 ± 0.38)
$\mu-\pi\pi$	$(-1.4 \pm 3.5) \times 10^{-1}$	$(-1.4 \pm 3.6) \times 10^{-1}$
μ–Avg.	$(2.6 \pm 2.6) \times 10^{-1}$	$(2.1 \pm 2.7) \times 10^{-1}$
Charged Tracks		
Decay	$\Delta(\%)$	$\Delta'(\%)$
$e-\rho$	(1.14 ± 0.27)	(1.72 ± 0.34)
$\mu-\rho$	$(0.6 \pm 2.4) \times 10^{-1}$	$(-0.1 \pm 3.1) \times 10^{-1}$
$e-\pi\pi$	(1.20 ± 0.26)	(2.31 ± 0.32)
$\mu-\pi\pi$	$(-3.6 \pm 2.3) \times 10^{-1}$	$(-1.2 \pm 3.0) \times 10^{-1}$
μ–Avg.	$(-1.6 \pm 1.7) \times 10^{-1}$	$(-0.7 \pm 2.2) \times 10^{-1}$

Table A.2: The tracking efficiency correction factor for the three different track definitions from the 1900V setting. The average values in this table are the weighted average of the $\mu-\rho$ and $\mu-\pi\pi$ channels as discussed in Chapter 7: Systematic Uncertainty Studies.

Good Tracks Loose		
Decay	$a_{\pm}(\%)$	$a'_{\pm}(\%)$
$e-\rho$ (Data)	$(-5.7 \pm 4.3) \times 10^{-1}$	$(-6.3 \pm 4.3) \times 10^{-1}$
$e-\rho$ (MC)	$(3.2 \pm 4.0) \times 10^{-1}$	$(3.0 \pm 4.0) \times 10^{-1}$
$\mu-\rho$ (Data)	$(-2.2 \pm 4.2) \times 10^{-1}$	$(-2.6 \pm 4.2) \times 10^{-1}$
$\mu-\rho$ (MC)	$(-1.1 \pm 3.9) \times 10^{-1}$	$(-0.8 \pm 3.9) \times 10^{-1}$
$e-\pi\pi$ (Data)	(-1.39 ± 0.41)	(-1.45 ± 0.42)
$e-\pi\pi$ (MC)	$(-5.8 \pm 3.7) \times 10^{-1}$	$(-5.8 \pm 3.8) \times 10^{-1}$
$\mu-\pi\pi$ (Data)	$(-4.9 \pm 3.7) \times 10^{-1}$	$(-5.1 \pm 3.8) \times 10^{-1}$
$\mu-\pi\pi$ (MC)	$(-1.6 \pm 3.7) \times 10^{-1}$	$(-1.6 \pm 3.7) \times 10^{-1}$
μ–Avg. (Data)	$(-3.7 \pm 2.8) \times 10^{-1}$	$(-4.0 \pm 2.8) \times 10^{-1}$
μ–Avg. (MC)	$(-1.4 \pm 2.7) \times 10^{-1}$	$(-1.3 \pm 2.7) \times 10^{-1}$
Good Tracks Very Loose		
Decay	$a_{\pm}(\%)$	$a'_{\pm}(\%)$
$e-\rho$ (Data)	$(-3.5 \pm 3.9) \times 10^{-1}$	$(-4.4 \pm 4.0) \times 10^{-1}$
$e-\rho$ (MC)	$(2.5 \pm 3.8) \times 10^{-1}$	$(1.9 \pm 3.8) \times 10^{-1}$
$\mu-\rho$ (Data)	$(-1.0 \pm 3.9) \times 10^{-1}$	$(-0.6 \pm 4.0) \times 10^{-1}$
$\mu-\rho$ (MC)	$(-1.0 \pm 3.7) \times 10^{-1}$	$(-0.5 \pm 3.8) \times 10^{-1}$
$e-\pi\pi$ (Data)	(-1.37 ± 0.38)	(-1.49 ± 0.40)
$e-\pi\pi$ (MC)	$(-6.0 \pm 3.6) \times 10^{-1}$	$(-5.8 \pm 3.7) \times 10^{-1}$
$\mu-\pi\pi$ (Data)	$(-5.0 \pm 3.5) \times 10^{-1}$	$(-5.4 \pm 3.6) \times 10^{-1}$
$\mu-\pi\pi$ (MC)	$(-2.4 \pm 3.5) \times 10^{-1}$	$(-1.8 \pm 3.6) \times 10^{-1}$
μ–Avg. (Data)	$(-3.2 \pm 2.6) \times 10^{-1}$	$(-3.2 \pm 2.7) \times 10^{-1}$
μ–Avg. (MC)	$(-1.7 \pm 2.5) \times 10^{-1}$	$(-1.2 \pm 2.6) \times 10^{-1}$
Charged Tracks		
Decay	$a_{\pm}(\%)$	$a'_{\pm}(\%)$
$e-\rho$ (Data)	$(-1.5 \pm 2.7) \times 10^{-1}$	$(-4.2 \pm 3.5) \times 10^{-1}$
$e-\rho$ (MC)	$(1.6 \pm 2.4) \times 10^{-1}$	$(4.1 \pm 3.2) \times 10^{-1}$
$\mu-\rho$ (Data)	$(2.5 \pm 2.4) \times 10^{-1}$	$(6.1 \pm 3.1) \times 10^{-1}$
$\mu-\rho$ (MC)	$(-1.6 \pm 2.3) \times 10^{-1}$	$(-0.1 \pm 3.0) \times 10^{-1}$
$e-\pi\pi$ (Data)	$(-8.3 \pm 2.7) \times 10^{-1}$	$(-5.4 \pm 3.3) \times 10^{-1}$
$e-\pi\pi$ (MC)	$(-2.8 \pm 2.6) \times 10^{-1}$	$(0.9 \pm 3.1) \times 10^{-1}$
$\mu-\pi\pi$ (Data)	$(-6.5 \pm 2.3) \times 10^{-1}$	$(-5.4 \pm 3.0) \times 10^{-1}$
$\mu-\pi\pi$ (MC)	$(-3.3 \pm 2.4) \times 10^{-1}$	$(-0.2 \pm 3.0) \times 10^{-1}$
μ–Avg. (Data)	$(-2.1 \pm 1.7) \times 10^{-1}$	$(0 \pm 2.2) \times 10^{-1}$
μ–Avg. (MC)	$(-2.4 \pm 1.7) \times 10^{-1}$	$(-0.1 \pm 2.1) \times 10^{-1}$

Table A.3: The tracking efficiency charge asymmetry for the three different track definitions from the 1900V setting. The average values in this table are the weighted average of the $\mu-\rho$ and $\mu-\pi\pi$ channels as discussed in Chapter 7: Systematic Uncertainty Studies.

Appendix B: 1930V Tables

Good Tracks Loose		
Decay	$\epsilon \times A(\%)$	$\epsilon' \times A(\%)$
$e-\rho$ (Data)	$(8.690 \pm 0.014) \times 10^1$	$(8.669 \pm 0.014) \times 10^1$
$e-\rho$ (MC)	$(8.833 \pm 0.018) \times 10^1$	$(8.810 \pm 0.018) \times 10^1$
$\mu-\rho$ (Data)	$(8.759 \pm 0.014) \times 10^1$	$(8.732 \pm 0.014) \times 10^1$
$\mu-\rho$ (MC)	$(8.805 \pm 0.018) \times 10^1$	$(8.785 \pm 0.018) \times 10^1$
$e-\pi\pi$ (Data)	$(8.614 \pm 0.013) \times 10^1$	$(8.550 \pm 0.013) \times 10^1$
$e-\pi\pi$ (MC)	$(8.837 \pm 0.017) \times 10^1$	$(8.805 \pm 0.017) \times 10^1$
$\mu-\pi\pi$ (Data)	$(8.775 \pm 0.013) \times 10^1$	$(8.739 \pm 0.013) \times 10^1$
$\mu-\pi\pi$ (MC)	$(8.806 \pm 0.017) \times 10^1$	$(8.769 \pm 0.017) \times 10^1$
μ–Avg. (Data)	$(8.768 \pm 0.010) \times 10^1$	$(8.736 \pm 0.010) \times 10^1$
μ–Avg. (MC)	$(8.805 \pm 0.012) \times 10^1$	$(8.776 \pm 0.012) \times 10^1$
Good Tracks Very Loose		
Decay	$\epsilon \times A(\%)$	$\epsilon' \times A(\%)$
$e-\rho$ (Data)	$(8.842 \pm 0.013) \times 10^1$	$(8.792 \pm 0.014) \times 10^1$
$e-\rho$ (MC)	$(8.935 \pm 0.017) \times 10^1$	$(8.886 \pm 0.018) \times 10^1$
$\mu-\rho$ (Data)	$(8.916 \pm 0.014) \times 10^1$	$(8.854 \pm 0.014) \times 10^1$
$\mu-\rho$ (MC)	$(8.909 \pm 0.018) \times 10^1$	$(8.864 \pm 0.018) \times 10^1$
$e-\pi\pi$ (Data)	$(8.725 \pm 0.012) \times 10^1$	$(8.635 \pm 0.013) \times 10^1$
$e-\pi\pi$ (MC)	$(8.911 \pm 0.016) \times 10^1$	$(8.861 \pm 0.016) \times 10^1$
$\mu-\pi\pi$ (Data)	$(8.889 \pm 0.012) \times 10^1$	$(8.827 \pm 0.012) \times 10^1$
$\mu-\pi\pi$ (MC)	$(8.885 \pm 0.016) \times 10^1$	$(8.832 \pm 0.017) \times 10^1$
μ–Avg. (Data)	$(8.9013 \pm 0.0091) \times 10^1$	$(8.8390 \pm 0.0093) \times 10^1$
μ–Avg. (MC)	$(8.896 \pm 0.012) \times 10^1$	$(8.847 \pm 0.012) \times 10^1$
Charged Tracks		
Decay	$\epsilon \times A(\%)$	$\epsilon' \times A(\%)$
$e-\rho$ (Data)	$(9.4872 \pm 0.0094) \times 10^1$	$(9.146 \pm 0.012) \times 10^1$
$e-\rho$ (MC)	$(9.546 \pm 0.012) \times 10^1$	$(9.209 \pm 0.015) \times 10^1$
$\mu-\rho$ (Data)	$(9.5860 \pm 0.0088) \times 10^1$	$(9.218 \pm 0.012) \times 10^1$
$\mu-\rho$ (MC)	$(9.545 \pm 0.012) \times 10^1$	$(9.200 \pm 0.015) \times 10^1$
$e-\pi\pi$ (Data)	$(9.3554 \pm 0.0092) \times 10^1$	$(9.017 \pm 0.011) \times 10^1$
$e-\pi\pi$ (MC)	$(9.471 \pm 0.012) \times 10^1$	$(9.199 \pm 0.014) \times 10^1$
$\mu-\pi\pi$ (Data)	$(9.4746 \pm 0.0088) \times 10^1$	$(9.160 \pm 0.011) \times 10^1$
$\mu-\pi\pi$ (MC)	$(9.450 \pm 0.012) \times 10^1$	$(9.163 \pm 0.014) \times 10^1$
μ–Avg. (Data)	$(9.5299 \pm 0.0062) \times 10^1$	$(9.1864 \pm 0.0079) \times 10^1$
μ–Avg. (MC)	$(9.4971 \pm 0.0084) \times 10^1$	$(9.180 \pm 0.010) \times 10^1$

Table B.1: The tracking efficiency for the three different track definitions from the 1930V setting. The average values in this table are the weighted average of the $\mu-\rho$ and $\mu-\pi\pi$ channels as discussed in Chapter 7: Systematic Uncertainty Studies.

Good Tracks Loose		
Decay	$\Delta(\%)$	$\Delta'(\%)$
$e-\rho$	(1.62 ± 0.16)	(1.60 ± 0.16)
$\mu-\rho$	$(5.2 \pm 1.6) \times 10^{-1}$	$(6.1 \pm 1.6) \times 10^{-1}$
$e-\pi\pi$	(2.53 ± 0.14)	(2.90 ± 0.15)
$\mu-\pi\pi$	$(3.4 \pm 1.4) \times 10^{-1}$	$(3.4 \pm 1.5) \times 10^{-1}$
μ–Avg.	$(4.2 \pm 1.1) \times 10^{-1}$	$(4.6 \pm 1.1) \times 10^{-1}$
Good Tracks Very Loose		
Decay	$\Delta(\%)$	$\Delta'(\%)$
$e-\rho$	(1.05 ± 0.15)	(1.06 ± 0.15)
$\mu-\rho$	$(-0.8 \pm 1.5) \times 10^{-1}$	$(1.1 \pm 1.6) \times 10^{-1}$
$e-\pi\pi$	(2.10 ± 0.14)	(2.55 ± 0.14)
$\mu-\pi\pi$	$(-0.5 \pm 1.4) \times 10^{-1}$	$(0.5 \pm 1.4) \times 10^{-1}$
μ–Avg.	$(-0.6 \pm 1.0) \times 10^{-1}$	$(0.8 \pm 1.0) \times 10^{-1}$
Charged Tracks		
Decay	$\Delta(\%)$	$\Delta'(\%)$
$e-\rho$	$(6.2 \pm 1.0) \times 10^{-1}$	$(6.9 \pm 1.3) \times 10^{-1}$
$\mu-\rho$	$(-4.35 \pm 0.93) \times 10^{-1}$	$(-2.0 \pm 1.3) \times 10^{-1}$
$e-\pi\pi$	(1.23 ± 0.10)	(1.98 ± 0.12)
$\mu-\pi\pi$	$(-2.59 \pm 0.93) \times 10^{-1}$	$(0.4 \pm 1.2) \times 10^{-1}$
μ–Avg.	$(-3.47 \pm 0.66) \times 10^{-1}$	$(-7.2 \pm 8.6) \times 10^{-2}$

Table B.2: The tracking efficiency correction factor for the three different track definitions from the 1930V setting. The average values in this table are the weighted average of the $\mu-\rho$ and $\mu-\pi\pi$ channels as discussed in Chapter 7: Systematic Uncertainty Studies.

Good Tracks Loose		
Decay	$a_{\pm}(\%)$	$a'_{\pm}(\%)$
$e-\rho$ (Data)	$(-0.4 \pm 1.6) \times 10^{-1}$	$(-0.1 \pm 1.6) \times 10^{-1}$
$e-\rho$ (MC)	$(0.8 \pm 2.0) \times 10^{-1}$	$(1.2 \pm 2.1) \times 10^{-1}$
$\mu-\rho$ (Data)	$(1.6 \pm 1.6) \times 10^{-1}$	$(1.7 \pm 1.7) \times 10^{-1}$
$\mu-\rho$ (MC)	$(-1.2 \pm 2.1) \times 10^{-1}$	$(-1.3 \pm 2.1) \times 10^{-1}$
$e-\pi\pi$ (Data)	$(-9.7 \pm 1.5) \times 10^{-1}$	(-1.08 ± 0.15)
$e-\pi\pi$ (MC)	$(-1.5 \pm 1.9) \times 10^{-1}$	$(-1.3 \pm 1.9) \times 10^{-1}$
$\mu-\pi\pi$ (Data)	$(-4.7 \pm 1.4) \times 10^{-1}$	$(-4.3 \pm 1.5) \times 10^{-1}$
$\mu-\pi\pi$ (MC)	$(-1.9 \pm 1.9) \times 10^{-1}$	$(-2.0 \pm 1.9) \times 10^{-1}$
μ–Avg. (Data)	$(-2.0 \pm 1.1) \times 10^{-1}$	$(-1.7 \pm 1.1) \times 10^{-1}$
μ–Avg. (MC)	$(-1.6 \pm 1.4) \times 10^{-1}$	$(-1.7 \pm 1.4) \times 10^{-1}$
Good Tracks Very Loose		
Decay	$a_{\pm}(\%)$	$a'_{\pm}(\%)$
$e-\rho$ (Data)	$(-0.8 \pm 1.5) \times 10^{-1}$	$(-0.6 \pm 1.6) \times 10^{-1}$
$e-\rho$ (MC)	$(0.4 \pm 1.9) \times 10^{-1}$	$(0.9 \pm 2.0) \times 10^{-1}$
$\mu-\rho$ (Data)	$(1.4 \pm 1.5) \times 10^{-1}$	$(1.3 \pm 1.6) \times 10^{-1}$
$\mu-\rho$ (MC)	$(-1.4 \pm 2.0) \times 10^{-1}$	$(-1.6 \pm 2.0) \times 10^{-1}$
$e-\pi\pi$ (Data)	(-1.04 ± 0.14)	(-1.14 ± 0.15)
$e-\pi\pi$ (MC)	$(-1.6 \pm 1.8) \times 10^{-1}$	$(-1.3 \pm 1.9) \times 10^{-1}$
$\mu-\pi\pi$ (Data)	$(-3.6 \pm 1.4) \times 10^{-1}$	$(-3.1 \pm 1.4) \times 10^{-1}$
$\mu-\pi\pi$ (MC)	$(-2.2 \pm 1.8) \times 10^{-1}$	$(-2.2 \pm 1.9) \times 10^{-1}$
μ–Avg. (Data)	$(-1.4 \pm 1.0) \times 10^{-1}$	$(-1.1 \pm 1.0) \times 10^{-1}$
μ–Avg. (MC)	$(-1.8 \pm 1.3) \times 10^{-1}$	$(-1.9 \pm 1.4) \times 10^{-1}$
Charged Tracks		
Decay	$a_{\pm}(\%)$	$a'_{\pm}(\%)$
$e-\rho$ (Data)	$(1.0 \pm 1.0) \times 10^{-1}$	$(2.8 \pm 1.3) \times 10^{-1}$
$e-\rho$ (MC)	$(0.5 \pm 1.2) \times 10^{-1}$	$(3.0 \pm 1.6) \times 10^{-1}$
$\mu-\rho$ (Data)	$(1.50 \pm 0.92) \times 10^{-1}$	$(3.1 \pm 1.3) \times 10^{-1}$
$\mu-\rho$ (MC)	$(0.2 \pm 1.3) \times 10^{-1}$	$(2.7 \pm 1.7) \times 10^{-1}$
$e-\pi\pi$ (Data)	$(-8.7 \pm 1.0) \times 10^{-1}$	$(-7.5 \pm 1.2) \times 10^{-1}$
$e-\pi\pi$ (MC)	$(-0.8 \pm 1.2) \times 10^{-1}$	$(1.8 \pm 1.5) \times 10^{-1}$
$\mu-\pi\pi$ (Data)	$(-2.70 \pm 0.93) \times 10^{-1}$	$(-1.7 \pm 1.2) \times 10^{-1}$
$\mu-\pi\pi$ (MC)	$(-1.7 \pm 1.3) \times 10^{-1}$	$(1.0 \pm 1.6) \times 10^{-1}$
μ–Avg. (Data)	$(-5.9 \pm 6.5) \times 10^{-2}$	$(4.9 \pm 8.6) \times 10^{-2}$
μ–Avg. (MC)	$(-7.4 \pm 8.9) \times 10^{-2}$	$(1.8 \pm 1.1) \times 10^{-1}$

Table B.3: The tracking efficiency charge asymmetry for the three different track definitions from the 1930V setting. The average values in this table are the weighted average of the $\mu-\rho$ and $\mu-\pi\pi$ channels as discussed in Chapter 7: Systematic Uncertainty Studies.

Appendix C: 1960V Tables

Good Tracks Loose		
Decay	$\epsilon \times A(\%)$	$\epsilon' \times A(\%)$
$e-\rho$ (Data)	$(8.713 \pm 0.052) \times 10^1$	$(8.693 \pm 0.052) \times 10^1$
$e-\rho$ (MC)	$(8.866 \pm 0.065) \times 10^1$	$(8.829 \pm 0.066) \times 10^1$
$\mu-\rho$ (Data)	$(8.794 \pm 0.051) \times 10^1$	$(8.777 \pm 0.052) \times 10^1$
$\mu-\rho$ (MC)	$(8.771 \pm 0.066) \times 10^1$	$(8.747 \pm 0.066) \times 10^1$
$e-\pi\pi$ (Data)	$(8.744 \pm 0.046) \times 10^1$	$(8.675 \pm 0.047) \times 10^1$
$e-\pi\pi$ (MC)	$(8.808 \pm 0.061) \times 10^1$	$(8.772 \pm 0.062) \times 10^1$
$\mu-\pi\pi$ (Data)	$(8.846 \pm 0.045) \times 10^1$	$(8.826 \pm 0.045) \times 10^1$
$\mu-\pi\pi$ (MC)	$(8.814 \pm 0.059) \times 10^1$	$(8.765 \pm 0.060) \times 10^1$
μ–Avg. (Data)	$(8.824 \pm 0.034) \times 10^1$	$(8.805 \pm 0.034) \times 10^1$
μ–Avg. (MC)	$(8.795 \pm 0.044) \times 10^1$	$(8.757 \pm 0.044) \times 10^1$
Good Tracks Very Loose		
Decay	$\epsilon \times A(\%)$	$\epsilon' \times A(\%)$
$e-\rho$ (Data)	$(8.861 \pm 0.049) \times 10^1$	$(8.819 \pm 0.050) \times 10^1$
$e-\rho$ (MC)	$(8.964 \pm 0.063) \times 10^1$	$(8.901 \pm 0.064) \times 10^1$
$\mu-\rho$ (Data)	$(8.918 \pm 0.049) \times 10^1$	$(8.876 \pm 0.050) \times 10^1$
$\mu-\rho$ (MC)	$(8.873 \pm 0.064) \times 10^1$	$(8.811 \pm 0.065) \times 10^1$
$e-\pi\pi$ (Data)	$(8.834 \pm 0.044) \times 10^1$	$(8.737 \pm 0.046) \times 10^1$
$e-\pi\pi$ (MC)	$(8.864 \pm 0.060) \times 10^1$	$(8.816 \pm 0.061) \times 10^1$
$\mu-\pi\pi$ (Data)	$(8.919 \pm 0.043) \times 10^1$	$(8.882 \pm 0.044) \times 10^1$
$\mu-\pi\pi$ (MC)	$(8.899 \pm 0.057) \times 10^1$	$(8.839 \pm 0.058) \times 10^1$
μ–Avg. (Data)	$(8.918 \pm 0.032) \times 10^1$	$(8.879 \pm 0.033) \times 10^1$
μ–Avg. (MC)	$(8.887 \pm 0.042) \times 10^1$	$(8.827 \pm 0.043) \times 10^1$
Charged Tracks		
Decay	$\epsilon \times A(\%)$	$\epsilon' \times A(\%)$
$e-\rho$ (Data)	$(9.531 \pm 0.033) \times 10^1$	$(9.187 \pm 0.042) \times 10^1$
$e-\rho$ (MC)	$(9.577 \pm 0.042) \times 10^1$	$(9.228 \pm 0.055) \times 10^1$
$\mu-\rho$ (Data)	$(9.524 \pm 0.034) \times 10^1$	$(9.163 \pm 0.044) \times 10^1$
$\mu-\rho$ (MC)	$(9.484 \pm 0.045) \times 10^1$	$(9.136 \pm 0.056) \times 10^1$
$e-\pi\pi$ (Data)	$(9.426 \pm 0.033) \times 10^1$	$(9.086 \pm 0.040) \times 10^1$
$e-\pi\pi$ (MC)	$(9.437 \pm 0.044) \times 10^1$	$(9.192 \pm 0.051) \times 10^1$
$\mu-\pi\pi$ (Data)	$(9.484 \pm 0.031) \times 10^1$	$(9.220 \pm 0.037) \times 10^1$
$\mu-\pi\pi$ (MC)	$(9.414 \pm 0.043) \times 10^1$	$(9.141 \pm 0.051) \times 10^1$
μ–Avg. (Data)	$(9.502 \pm 0.023) \times 10^1$	$(9.196 \pm 0.028) \times 10^1$
μ–Avg. (MC)	$(9.447 \pm 0.031) \times 10^1$	$(9.139 \pm 0.038) \times 10^1$

Table C.1: The tracking efficiency for the three different track definitions from the 1960V setting. The average values in this table are the weighted average of the $\mu-\rho$ and $\mu-\pi\pi$ channels as discussed in Chapter 7: Systematic Uncertainty Studies.

Good Tracks Loose		
Decay	$\Delta(\%)$	$\Delta'(\%)$
$e-\rho$	(1.72 ± 0.58)	(1.55 ± 0.59)
$\mu-\rho$	$(-2.7 \pm 5.8) \times 10^{-1}$	$(-3.4 \pm 5.9) \times 10^{-1}$
$e-\pi\pi$	$(7.2 \pm 5.2) \times 10^{-1}$	(1.11 ± 0.53)
$\mu-\pi\pi$	$(-3.7 \pm 5.1) \times 10^{-1}$	$(-7.0 \pm 5.1) \times 10^{-1}$
μ–Avg.	$(-3.2 \pm 3.8) \times 10^{-1}$	$(-5.4 \pm 3.9) \times 10^{-1}$
Good Tracks Very Loose		
Decay	$\Delta(\%)$	$\Delta'(\%)$
$e-\rho$	(1.15 ± 0.55)	$(9.2 \pm 5.6) \times 10^{-1}$
$\mu-\rho$	$(-5.0 \pm 5.5) \times 10^{-1}$	$(-7.4 \pm 5.6) \times 10^{-1}$
$e-\pi\pi$	$(3.4 \pm 5.0) \times 10^{-1}$	$(8.9 \pm 5.2) \times 10^{-1}$
$\mu-\pi\pi$	$(-2.2 \pm 4.9) \times 10^{-1}$	$(-4.9 \pm 5.0) \times 10^{-1}$
μ–Avg.	$(-3.4 \pm 3.7) \times 10^{-1}$	$(-6.0 \pm 3.7) \times 10^{-1}$
Charged Tracks		
Decay	$\Delta(\%)$	$\Delta'(\%)$
$e-\rho$	$(4.7 \pm 3.5) \times 10^{-1}$	$(4.4 \pm 4.6) \times 10^{-1}$
$\mu-\rho$	$(-4.2 \pm 3.6) \times 10^{-1}$	$(-3.0 \pm 4.8) \times 10^{-1}$
$e-\pi\pi$	$(1.1 \pm 3.4) \times 10^{-1}$	(1.14 ± 0.43)
$\mu-\pi\pi$	$(-7.5 \pm 3.3) \times 10^{-1}$	$(-8.7 \pm 4.1) \times 10^{-1}$
μ–Avg.	$(-6.0 \pm 2.4) \times 10^{-1}$	$(-6.2 \pm 3.1) \times 10^{-1}$

Table C.2: The tracking efficiency correction for the three different track definitions from the 1960V setting. The average values in this table are the weighted average of the $\mu-\rho$ and $\mu-\pi\pi$ channels as discussed in Chapter 7: Systematic Uncertainty Studies.

Good Tracks Loose		
Decay	$a_{\pm}(\%)$	$a'_{\pm}(\%)$
$e-\rho$ (Data)	$(0.7 \pm 5.9) \times 10^{-1}$	$(0.2 \pm 6.0) \times 10^{-1}$
$e-\rho$ (MC)	$(-9.2 \pm 7.4) \times 10^{-1}$	(-1.11 ± 0.75)
$\mu-\rho$ (Data)	$(2.7 \pm 5.8) \times 10^{-1}$	$(3.7 \pm 5.9) \times 10^{-1}$
$\mu-\rho$ (MC)	$(1.9 \pm 7.5) \times 10^{-1}$	$(2.8 \pm 7.6) \times 10^{-1}$
$e-\pi\pi$ (Data)	(-1.83 ± 0.52)	(-1.96 ± 0.53)
$e-\pi\pi$ (MC)	$(1.6 \pm 6.9) \times 10^{-1}$	$(3.1 \pm 7.1) \times 10^{-1}$
$\mu-\pi\pi$ (Data)	$(-7.3 \pm 5.0) \times 10^{-1}$	$(-7.7 \pm 5.1) \times 10^{-1}$
$\mu-\pi\pi$ (MC)	$(-2.3 \pm 6.7) \times 10^{-1}$	$(-1.9 \pm 6.8) \times 10^{-1}$
μ–Avg. (Data)	$(-3.0 \pm 3.8) \times 10^{-1}$	$(-2.8 \pm 3.8) \times 10^{-1}$
μ–Avg. (MC)	$(-0.4 \pm 5.0) \times 10^{-1}$	$(0.2 \pm 5.1) \times 10^{-1}$
Good Tracks Very Loose		
Decay	$a_{\pm}(\%)$	$a'_{\pm}(\%)$
$e-\rho$ (Data)	$(-2.2 \pm 5.5) \times 10^{-1}$	$(-4.7 \pm 5.6) \times 10^{-1}$
$e-\rho$ (MC)	$(-9.0 \pm 7.0) \times 10^{-1}$	(-1.06 ± 0.72)
$\mu-\rho$ (Data)	$(1.9 \pm 5.5) \times 10^{-1}$	$(4.2 \pm 5.6) \times 10^{-1}$
$\mu-\rho$ (MC)	$(1.3 \pm 7.2) \times 10^{-1}$	$(2.5 \pm 7.4) \times 10^{-1}$
$e-\pi\pi$ (Data)	(-1.82 ± 0.50)	(-1.95 ± 0.52)
$e-\pi\pi$ (MC)	$(0.2 \pm 6.8) \times 10^{-1}$	$(2.8 \pm 6.9) \times 10^{-1}$
$\mu-\pi\pi$ (Data)	$(-7.0 \pm 4.9) \times 10^{-1}$	$(-8.7 \pm 4.9) \times 10^{-1}$
$\mu-\pi\pi$ (MC)	$(-2.9 \pm 6.4) \times 10^{-1}$	$(-2.1 \pm 6.6) \times 10^{-1}$
μ–Avg. (Data)	$(-3.1 \pm 3.6) \times 10^{-1}$	$(-3.1 \pm 3.7) \times 10^{-1}$
μ–Avg. (MC)	$(-1.1 \pm 4.8) \times 10^{-1}$	$(-0.1 \pm 4.9) \times 10^{-1}$
Charged Tracks		
Decay	$a_{\pm}(\%)$	$a'_{\pm}(\%)$
$e-\rho$ (Data)	$(1.5 \pm 3.5) \times 10^{-1}$	$(-0.8 \pm 4.6) \times 10^{-1}$
$e-\rho$ (MC)	$(-1.3 \pm 4.4) \times 10^{-1}$	$(-8.3 \pm 5.9) \times 10^{-1}$
$\mu-\rho$ (Data)	$(-0.2 \pm 3.6) \times 10^{-1}$	$(6.5 \pm 4.8) \times 10^{-1}$
$\mu-\rho$ (MC)	$(3.8 \pm 4.8) \times 10^{-1}$	(1.06 ± 0.61)
$e-\pi\pi$ (Data)	$(-1.2 \pm 3.5) \times 10^{-1}$	$(-2.4 \pm 4.4) \times 10^{-1}$
$e-\pi\pi$ (MC)	$(2.8 \pm 4.7) \times 10^{-1}$	(1.05 ± 0.56)
$\mu-\pi\pi$ (Data)	$(-2.0 \pm 3.3) \times 10^{-1}$	$(-3.2 \pm 4.1) \times 10^{-1}$
$\mu-\pi\pi$ (MC)	$(-0.8 \pm 4.6) \times 10^{-1}$	$(1.6 \pm 5.6) \times 10^{-1}$
μ–Avg. (Data)	$(-1.2 \pm 2.4) \times 10^{-1}$	$(0.9 \pm 3.1) \times 10^{-1}$
μ–Avg. (MC)	$(1.4 \pm 3.3) \times 10^{-1}$	$(5.6 \pm 4.1) \times 10^{-1}$

Table C.3: The tracking efficiency charge asymmetry for the three different track definitions from the 1960V setting. The average values in this table are the weighted average of the $\mu-\rho$ and $\mu-\pi\pi$ channels as discussed in Chapter 7: Systematic Uncertainty Studies.

Appendix D: Background Study Tables

Good Tracks Loose		
Decay	$\epsilon \times A(\%)$	$\epsilon' \times A(\%)$
$e-\rho$ (Data)	$(8.711 \pm 0.014) \times 10^1$	$(8.690 \pm 0.014) \times 10^1$
$e-\rho$ (MC)	$(8.838 \pm 0.018) \times 10^1$	$(8.815 \pm 0.018) \times 10^1$
$\mu-\rho$ (Data)	$(8.759 \pm 0.014) \times 10^1$	$(8.732 \pm 0.014) \times 10^1$
$\mu-\rho$ (MC)	$(8.805 \pm 0.018) \times 10^1$	$(8.785 \pm 0.018) \times 10^1$
$e-\pi\pi$ (Data)	$(8.711 \pm 0.014) \times 10^1$	$(8.690 \pm 0.014) \times 10^1$
$e-\pi\pi$ (MC)	$(8.838 \pm 0.018) \times 10^1$	$(8.815 \pm 0.018) \times 10^1$
$\mu-\pi\pi$ (Data)	$(8.775 \pm 0.013) \times 10^1$	$(8.739 \pm 0.013) \times 10^1$
$\mu-\pi\pi$ (MC)	$(8.806 \pm 0.017) \times 10^1$	$(8.769 \pm 0.017) \times 10^1$
μ–Avg. (Data)	$(8.768 \pm 0.010) \times 10^1$	$(8.736 \pm 0.010) \times 10^1$
μ–Avg. (MC)	$(8.805 \pm 0.012) \times 10^1$	$(8.776 \pm 0.012) \times 10^1$
Good Tracks Very Loose		
Decay	$\epsilon \times A(\%)$	$\epsilon' \times A(\%)$
$e-\rho$ (Data)	$(8.863 \pm 0.014) \times 10^1$	$(8.814 \pm 0.014) \times 10^1$
$e-\rho$ (MC)	$(8.941 \pm 0.017) \times 10^1$	$(8.891 \pm 0.018) \times 10^1$
$\mu-\rho$ (Data)	$(8.916 \pm 0.014) \times 10^1$	$(8.854 \pm 0.014) \times 10^1$
$\mu-\rho$ (MC)	$(8.909 \pm 0.018) \times 10^1$	$(8.864 \pm 0.018) \times 10^1$
$e-\pi\pi$ (Data)	$(8.895 \pm 0.012) \times 10^1$	$(8.805 \pm 0.013) \times 10^1$
$e-\pi\pi$ (MC)	$(8.922 \pm 0.016) \times 10^1$	$(8.872 \pm 0.017) \times 10^1$
$\mu-\pi\pi$ (Data)	$(8.889 \pm 0.012) \times 10^1$	$(8.827 \pm 0.012) \times 10^1$
$\mu-\pi\pi$ (MC)	$(8.885 \pm 0.016) \times 10^1$	$(8.832 \pm 0.017) \times 10^1$
μ–Avg. (Data)	$(8.9013 \pm 0.0091) \times 10^1$	$(8.8390 \pm 0.0093) \times 10^1$
μ–Avg. (MC)	$(8.896 \pm 0.012) \times 10^1$	$(8.847 \pm 0.012) \times 10^1$
Charged Tracks		
Decay	$\epsilon \times A(\%)$	$\epsilon' \times A(\%)$
$e-\rho$ (Data)	$(9.5077 \pm 0.0094) \times 10^1$	$(9.166 \pm 0.012) \times 10^1$
$e-\rho$ (MC)	$(9.551 \pm 0.012) \times 10^1$	$(9.214 \pm 0.015) \times 10^1$
$\mu-\rho$ (Data)	$(9.5860 \pm 0.0088) \times 10^1$	$(9.218 \pm 0.012) \times 10^1$
$\mu-\rho$ (MC)	$(9.545 \pm 0.012) \times 10^1$	$(9.200 \pm 0.015) \times 10^1$
$e-\pi\pi$ (Data)	$(9.4964 \pm 0.0086) \times 10^1$	$(9.148 \pm 0.011) \times 10^1$
$e-\pi\pi$ (MC)	$(9.478 \pm 0.012) \times 10^1$	$(9.204 \pm 0.014) \times 10^1$
$\mu-\pi\pi$ (Data)	$(9.4746 \pm 0.0088) \times 10^1$	$(9.160 \pm 0.011) \times 10^1$
$\mu-\pi\pi$ (MC)	$(9.450 \pm 0.012) \times 10^1$	$(9.163 \pm 0.014) \times 10^1$
μ–Avg. (Data)	$(9.5299 \pm 0.0062) \times 10^1$	$(9.1864 \pm 0.0079) \times 10^1$
μ–Avg. (MC)	$(9.4971 \pm 0.0084) \times 10^1$	$(9.180 \pm 0.010) \times 10^1$

Table D.1: The tracking efficiency for the three different track definitions from the 1930V setting (Background Study). The average values in this table are the weighted average of the $\mu-\rho$ and $\mu-\pi\pi$ channels as discussed in Chapter 7: Systematic Uncertainty Studies.

Good Tracks Loose		
Decay	$\Delta(\%)$	$\Delta'(\%)$
$e-\rho$	(1.44 ± 0.16)	(1.42 ± 0.16)
$\mu-\rho$	$(5.2 \pm 1.6) \times 10^{-1}$	$(6.1 \pm 1.6) \times 10^{-1}$
$e-\pi\pi$	(1.44 ± 0.16)	(1.42 ± 0.16)
$\mu-\pi\pi$	$(3.4 \pm 1.4) \times 10^{-1}$	$(3.4 \pm 1.5) \times 10^{-1}$
μ–Avg.	$(4.2 \pm 1.1) \times 10^{-1}$	$(4.6 \pm 1.1) \times 10^{-1}$
Good Tracks Very Loose		
Decay	$\Delta(\%)$	$\Delta'(\%)$
$e-\rho$	$(8.7 \pm 1.5) \times 10^{-1}$	$(8.7 \pm 1.5) \times 10^{-1}$
$\mu-\rho$	$(-0.8 \pm 1.5) \times 10^{-1}$	$(1.1 \pm 1.6) \times 10^{-1}$
$e-\pi\pi$	$(3.0 \pm 1.4) \times 10^{-1}$	$(7.5 \pm 1.4) \times 10^{-1}$
$\mu-\pi\pi$	$(-0.5 \pm 1.4) \times 10^{-1}$	$(0.5 \pm 1.4) \times 10^{-1}$
μ–Avg.	$(-0.6 \pm 1.0) \times 10^{-1}$	$(0.8 \pm 1.0) \times 10^{-1}$
Charged Tracks		
Decay	$\Delta(\%)$	$\Delta'(\%)$
$e-\rho$	$(4.6 \pm 1.0) \times 10^{-1}$	$(5.3 \pm 1.3) \times 10^{-1}$
$\mu-\rho$	$(-4.35 \pm 0.93) \times 10^{-1}$	$(-2.0 \pm 1.3) \times 10^{-1}$
$e-\pi\pi$	$(-1.92 \pm 0.91) \times 10^{-1}$	$(6.1 \pm 1.2) \times 10^{-1}$
$\mu-\pi\pi$	$(-2.59 \pm 0.93) \times 10^{-1}$	$(0.4 \pm 1.2) \times 10^{-1}$
μ–Avg.	$(-3.47 \pm 0.66) \times 10^{-1}$	$(-7.2 \pm 8.6) \times 10^{-2}$

Table D.2: The tracking efficiency correction factor for the three different track definitions from the 1930V setting (Background Study). The average values in this table are the weighted average of the $\mu-\rho$ and $\mu-\pi\pi$ channels as discussed in Chapter 7: Systematic Uncertainty Studies.

Appendix E: Di-muon Contamination Tables

Good Tracks Loose		
Decay	$\epsilon \times A(\%)$	$\epsilon' \times A(\%)$
$e-\rho$ (Data)	$(8.690 \pm 0.014) \times 10^1$	$(8.669 \pm 0.014) \times 10^1$
$e-\rho$ (MC)	$(8.834 \pm 0.018) \times 10^1$	$(8.811 \pm 0.018) \times 10^1$
$\mu-\rho$ (Data)	$(8.759 \pm 0.014) \times 10^1$	$(8.732 \pm 0.014) \times 10^1$
$\mu-\rho$ (MC)	$(8.805 \pm 0.018) \times 10^1$	$(8.785 \pm 0.018) \times 10^1$
$e-\pi\pi$ (Data)	$(8.614 \pm 0.013) \times 10^1$	$(8.550 \pm 0.013) \times 10^1$
$e-\pi\pi$ (MC)	$(8.837 \pm 0.017) \times 10^1$	$(8.805 \pm 0.017) \times 10^1$
$\mu-\pi\pi$ (Data)	$(8.775 \pm 0.013) \times 10^1$	$(8.739 \pm 0.013) \times 10^1$
$\mu-\pi\pi$ (MC)	$(8.806 \pm 0.017) \times 10^1$	$(8.770 \pm 0.017) \times 10^1$
μ–Avg. (Data)	$(8.768 \pm 0.010) \times 10^1$	$(8.736 \pm 0.010) \times 10^1$
μ–Avg. (MC)	$(8.805 \pm 0.012) \times 10^1$	$(8.777 \pm 0.012) \times 10^1$
Good Tracks Very Loose		
Decay	$\epsilon \times A(\%)$	$\epsilon' \times A(\%)$
$e-\rho$ (Data)	$(8.842 \pm 0.013) \times 10^1$	$(8.792 \pm 0.014) \times 10^1$
$e-\rho$ (MC)	$(8.936 \pm 0.017) \times 10^1$	$(8.887 \pm 0.018) \times 10^1$
$\mu-\rho$ (Data)	$(8.916 \pm 0.014) \times 10^1$	$(8.854 \pm 0.014) \times 10^1$
$\mu-\rho$ (MC)	$(8.909 \pm 0.018) \times 10^1$	$(8.864 \pm 0.018) \times 10^1$
$e-\pi\pi$ (Data)	$(8.725 \pm 0.012) \times 10^1$	$(8.635 \pm 0.013) \times 10^1$
$e-\pi\pi$ (MC)	$(8.911 \pm 0.016) \times 10^1$	$(8.861 \pm 0.016) \times 10^1$
$\mu-\pi\pi$ (Data)	$(8.889 \pm 0.012) \times 10^1$	$(8.827 \pm 0.012) \times 10^1$
$\mu-\pi\pi$ (MC)	$(8.886 \pm 0.016) \times 10^1$	$(8.832 \pm 0.017) \times 10^1$
μ–Avg. (Data)	$(8.9013 \pm 0.0091) \times 10^1$	$(8.8390 \pm 0.0093) \times 10^1$
μ–Avg. (MC)	$(8.896 \pm 0.012) \times 10^1$	$(8.847 \pm 0.012) \times 10^1$
Charged Tracks		
Decay	$\epsilon \times A(\%)$	$\epsilon' \times A(\%)$
$e-\rho$ (Data)	$(9.4872 \pm 0.0094) \times 10^1$	$(9.146 \pm 0.012) \times 10^1$
$e-\rho$ (MC)	$(9.547 \pm 0.012) \times 10^1$	$(9.210 \pm 0.015) \times 10^1$
$\mu-\rho$ (Data)	$(9.5860 \pm 0.0088) \times 10^1$	$(9.218 \pm 0.012) \times 10^1$
$\mu-\rho$ (MC)	$(9.545 \pm 0.012) \times 10^1$	$(9.200 \pm 0.015) \times 10^1$
$e-\pi\pi$ (Data)	$(9.3554 \pm 0.0092) \times 10^1$	$(9.017 \pm 0.011) \times 10^1$
$e-\pi\pi$ (MC)	$(9.471 \pm 0.012) \times 10^1$	$(9.199 \pm 0.014) \times 10^1$
$\mu-\pi\pi$ (Data)	$(9.4746 \pm 0.0088) \times 10^1$	$(9.160 \pm 0.011) \times 10^1$
$\mu-\pi\pi$ (MC)	$(9.451 \pm 0.012) \times 10^1$	$(9.164 \pm 0.014) \times 10^1$
μ–Avg. (Data)	$(9.5299 \pm 0.0062) \times 10^1$	$(9.1864 \pm 0.0079) \times 10^1$
μ–Avg. (MC)	$(9.4974 \pm 0.0084) \times 10^1$	$(9.181 \pm 0.010) \times 10^1$

Table E.1: The tracking efficiency for the three different track definitions from the 1930V setting (Di-muon Study). The average values in this table are the weighted average of the $\mu-\rho$ and $\mu-\pi\pi$ channels as discussed in Chapter 7: Systematic Uncertainty Studies.

Good Tracks Loose		
Decay	$\Delta(\%)$	$\Delta'(\%)$
$e-\rho$	(1.63 ± 0.16)	(1.62 ± 0.16)
$\mu-\rho$	$(5.2 \pm 1.6) \times 10^{-1}$	$(6.1 \pm 1.6) \times 10^{-1}$
$e-\pi\pi$	(2.53 ± 0.14)	(2.90 ± 0.15)
$\mu-\pi\pi$	$(3.5 \pm 1.4) \times 10^{-1}$	$(3.4 \pm 1.5) \times 10^{-1}$
μ–Avg.	$(4.3 \pm 1.1) \times 10^{-1}$	$(4.6 \pm 1.1) \times 10^{-1}$
Good Tracks Very Loose		
Decay	$\Delta(\%)$	$\Delta'(\%)$
$e-\rho$	(1.06 ± 0.15)	(1.07 ± 0.15)
$\mu-\rho$	$(-0.8 \pm 1.5) \times 10^{-1}$	$(1.1 \pm 1.6) \times 10^{-1}$
$e-\pi\pi$	(2.10 ± 0.14)	(2.55 ± 0.14)
$\mu-\pi\pi$	$(-0.4 \pm 1.4) \times 10^{-1}$	$(0.6 \pm 1.4) \times 10^{-1}$
μ–Avg.	$(-0.6 \pm 1.0) \times 10^{-1}$	$(0.8 \pm 1.0) \times 10^{-1}$
Charged Tracks		
Decay	$\Delta(\%)$	$\Delta'(\%)$
$e-\rho$	$(6.3 \pm 1.0) \times 10^{-1}$	$(7.0 \pm 1.3) \times 10^{-1}$
$\mu-\rho$	$(-4.35 \pm 0.93) \times 10^{-1}$	$(-2.0 \pm 1.3) \times 10^{-1}$
$e-\pi\pi$	(1.23 ± 0.10)	(1.98 ± 0.12)
$\mu-\pi\pi$	$(-2.53 \pm 0.93) \times 10^{-1}$	$(0.5 \pm 1.2) \times 10^{-1}$
μ–Avg.	$(-3.44 \pm 0.66) \times 10^{-1}$	$(-6.7 \pm 8.6) \times 10^{-2}$

Table E.2: The tracking efficiency correction factor for the three different track definitions from the 1930V setting (Di-muon Study). The average values in this table are the weighted average of the $\mu-\rho$ and $\mu-\pi\pi$ channels as discussed in Chapter 7: Systematic Uncertainty Studies.

Good Tracks Loose		
Decay	$a_{\pm}(\%)$	$a'_{\pm}(\%)$
$e-\rho$ (Data)	$(-0.4 \pm 1.6) \times 10^{-1}$	$(-0.1 \pm 1.6) \times 10^{-1}$
$e-\rho$ (MC)	$(0.8 \pm 2.0) \times 10^{-1}$	$(1.2 \pm 2.1) \times 10^{-1}$
$\mu-\rho$ (Data)	$(1.6 \pm 1.6) \times 10^{-1}$	$(1.7 \pm 1.7) \times 10^{-1}$
$\mu-\rho$ (MC)	$(-1.2 \pm 2.1) \times 10^{-1}$	$(-1.3 \pm 2.1) \times 10^{-1}$
$e-\pi\pi$ (Data)	$(-9.7 \pm 1.5) \times 10^{-1}$	(-1.08 ± 0.15)
$e-\pi\pi$ (MC)	$(-1.5 \pm 1.9) \times 10^{-1}$	$(-1.3 \pm 1.9) \times 10^{-1}$
$\mu-\pi\pi$ (Data)	$(-4.7 \pm 1.4) \times 10^{-1}$	$(-4.3 \pm 1.5) \times 10^{-1}$
$\mu-\pi\pi$ (MC)	$(-1.9 \pm 1.9) \times 10^{-1}$	$(-2.0 \pm 1.9) \times 10^{-1}$
μ–Avg. (Data)	$(-2.0 \pm 1.1) \times 10^{-1}$	$(-1.7 \pm 1.1) \times 10^{-1}$
μ–Avg. (MC)	$(-1.6 \pm 1.4) \times 10^{-1}$	$(-1.7 \pm 1.4) \times 10^{-1}$
Good Tracks Very Loose		
Decay	$a_{\pm}(\%)$	$a'_{\pm}(\%)$
$e-\rho$ (Data)	$(-0.8 \pm 1.5) \times 10^{-1}$	$(-0.6 \pm 1.6) \times 10^{-1}$
$e-\rho$ (MC)	$(0.4 \pm 1.9) \times 10^{-1}$	$(0.9 \pm 2.0) \times 10^{-1}$
$\mu-\rho$ (Data)	$(1.4 \pm 1.5) \times 10^{-1}$	$(1.3 \pm 1.6) \times 10^{-1}$
$\mu-\rho$ (MC)	$(-1.4 \pm 2.0) \times 10^{-1}$	$(-1.6 \pm 2.0) \times 10^{-1}$
$e-\pi\pi$ (Data)	(-1.04 ± 0.14)	(-1.14 ± 0.15)
$e-\pi\pi$ (MC)	$(-1.6 \pm 1.8) \times 10^{-1}$	$(-1.3 \pm 1.9) \times 10^{-1}$
$\mu-\pi\pi$ (Data)	$(-3.6 \pm 1.4) \times 10^{-1}$	$(-3.1 \pm 1.4) \times 10^{-1}$
$\mu-\pi\pi$ (MC)	$(-2.3 \pm 1.8) \times 10^{-1}$	$(-2.2 \pm 1.9) \times 10^{-1}$
μ–Avg. (Data)	$(-1.4 \pm 1.0) \times 10^{-1}$	$(-1.1 \pm 1.0) \times 10^{-1}$
μ–Avg. (MC)	$(-1.9 \pm 1.3) \times 10^{-1}$	$(-1.9 \pm 1.4) \times 10^{-1}$
Charged Tracks		
Decay	$a_{\pm}(\%)$	$a'_{\pm}(\%)$
$e-\rho$ (Data)	$(1.0 \pm 1.0) \times 10^{-1}$	$(2.8 \pm 1.3) \times 10^{-1}$
$e-\rho$ (MC)	$(0.5 \pm 1.2) \times 10^{-1}$	$(3.0 \pm 1.6) \times 10^{-1}$
$\mu-\rho$ (Data)	$(1.50 \pm 0.92) \times 10^{-1}$	$(3.1 \pm 1.3) \times 10^{-1}$
$\mu-\rho$ (MC)	$(0.2 \pm 1.3) \times 10^{-1}$	$(2.7 \pm 1.7) \times 10^{-1}$
$e-\pi\pi$ (Data)	$(-8.7 \pm 1.0) \times 10^{-1}$	$(-7.5 \pm 1.2) \times 10^{-1}$
$e-\pi\pi$ (MC)	$(-0.8 \pm 1.2) \times 10^{-1}$	$(1.8 \pm 1.5) \times 10^{-1}$
$\mu-\pi\pi$ (Data)	$(-2.70 \pm 0.93) \times 10^{-1}$	$(-1.7 \pm 1.2) \times 10^{-1}$
$\mu-\pi\pi$ (MC)	$(-1.8 \pm 1.3) \times 10^{-1}$	$(1.0 \pm 1.6) \times 10^{-1}$
μ–Avg. (Data)	$(-5.9 \pm 6.5) \times 10^{-2}$	$(4.9 \pm 8.6) \times 10^{-2}$
μ–Avg. (MC)	$(-7.6 \pm 8.9) \times 10^{-2}$	$(1.8 \pm 1.1) \times 10^{-1}$

Table E.3: The tracking efficiency charge asymmetry for the three different track definitions from the 1930V setting (Di-muon Study). The average values in this table are the weighted average of the $\mu-\rho$ and $\mu-\pi\pi$ channels as discussed in Chapter 7: Systematic Uncertainty Studies.

Appendix F: Stability in P_t^{miss}, θ and ϕ Tables

Good Tracks Loose		
Decay	$\epsilon \times A(\%)$	$\epsilon' \times A(\%)$
$e-\rho$ (Data)	$(7.184 \pm 0.071) \times 10^1$	$(7.174 \pm 0.071) \times 10^1$
$e-\rho$ (MC)	$(7.333 \pm 0.093) \times 10^1$	$(7.322 \pm 0.093) \times 10^1$
$\mu-\rho$ (Data)	$(7.174 \pm 0.075) \times 10^1$	$(7.156 \pm 0.075) \times 10^1$
$\mu-\rho$ (MC)	$(7.210 \pm 0.094) \times 10^1$	$(7.203 \pm 0.094) \times 10^1$
$e-\pi\pi$ (Data)	$(5.647 \pm 0.069) \times 10^1$	$(5.638 \pm 0.069) \times 10^1$
$e-\pi\pi$ (MC)	$(6.56 \pm 0.11) \times 10^1$	$(6.55 \pm 0.11) \times 10^1$
$\mu-\pi\pi$ (Data)	$(6.541 \pm 0.085) \times 10^1$	$(6.532 \pm 0.085) \times 10^1$
$\mu-\pi\pi$ (MC)	$(6.64 \pm 0.11) \times 10^1$	$(6.63 \pm 0.11) \times 10^1$
μ–Avg. (Data)	$(6.895 \pm 0.056) \times 10^1$	$(6.881 \pm 0.056) \times 10^1$
μ–Avg. (MC)	$(6.978 \pm 0.072) \times 10^1$	$(6.968 \pm 0.072) \times 10^1$
Good Tracks Very Loose		
Decay	$\epsilon \times A(\%)$	$\epsilon' \times A(\%)$
$e-\rho$ (Data)	$(7.327 \pm 0.070) \times 10^1$	$(7.303 \pm 0.070) \times 10^1$
$e-\rho$ (MC)	$(7.437 \pm 0.092) \times 10^1$	$(7.413 \pm 0.092) \times 10^1$
$\mu-\rho$ (Data)	$(7.330 \pm 0.074) \times 10^1$	$(7.301 \pm 0.074) \times 10^1$
$\mu-\rho$ (MC)	$(7.313 \pm 0.093) \times 10^1$	$(7.297 \pm 0.093) \times 10^1$
$e-\pi\pi$ (Data)	$(5.757 \pm 0.069) \times 10^1$	$(5.733 \pm 0.069) \times 10^1$
$e-\pi\pi$ (MC)	$(6.66 \pm 0.11) \times 10^1$	$(6.64 \pm 0.11) \times 10^1$
$\mu-\pi\pi$ (Data)	$(6.727 \pm 0.084) \times 10^1$	$(6.704 \pm 0.084) \times 10^1$
$\mu-\pi\pi$ (MC)	$(6.75 \pm 0.11) \times 10^1$	$(6.73 \pm 0.11) \times 10^1$
μ–Avg. (Data)	$(7.066 \pm 0.055) \times 10^1$	$(7.039 \pm 0.055) \times 10^1$
μ–Avg. (MC)	$(7.085 \pm 0.071) \times 10^1$	$(7.066 \pm 0.071) \times 10^1$
Charged Tracks		
Decay	$\epsilon \times A(\%)$	$\epsilon' \times A(\%)$
$e-\rho$ (Data)	$(8.832 \pm 0.052) \times 10^1$	$(8.461 \pm 0.057) \times 10^1$
$e-\rho$ (MC)	$(8.988 \pm 0.065) \times 10^1$	$(8.677 \pm 0.072) \times 10^1$
$\mu-\rho$ (Data)	$(9.061 \pm 0.050) \times 10^1$	$(8.751 \pm 0.055) \times 10^1$
$\mu-\rho$ (MC)	$(8.928 \pm 0.066) \times 10^1$	$(8.640 \pm 0.072) \times 10^1$
$e-\pi\pi$ (Data)	$(7.587 \pm 0.060) \times 10^1$	$(7.370 \pm 0.061) \times 10^1$
$e-\pi\pi$ (MC)	$(8.639 \pm 0.083) \times 10^1$	$(8.351 \pm 0.089) \times 10^1$
$\mu-\pi\pi$ (Data)	$(8.584 \pm 0.063) \times 10^1$	$(8.230 \pm 0.068) \times 10^1$
$\mu-\pi\pi$ (MC)	$(8.586 \pm 0.084) \times 10^1$	$(8.302 \pm 0.090) \times 10^1$
μ–Avg. (Data)	$(8.880 \pm 0.039) \times 10^1$	$(8.544 \pm 0.043) \times 10^1$
μ–Avg. (MC)	$(8.799 \pm 0.052) \times 10^1$	$(8.508 \pm 0.056) \times 10^1$

Table F.1: The tracking efficiency, $P_t^{miss} < 1.0$, for the three different track definitions from the 1930V setting (Stability Study). The average values in this table are the weighted average of the $\mu-\rho$ and $\mu-\pi\pi$ channels as discussed in Chapter 7: Systematic Uncertainty Studies.

Good Tracks Loose		
Decay	$\epsilon \times A(\%)$	$\epsilon' \times A(\%)$
$e-\rho$ (Data)	$(8.584 \pm 0.020) \times 10^1$	$(8.563 \pm 0.020) \times 10^1$
$e-\rho$ (MC)	$(8.729 \pm 0.025) \times 10^1$	$(8.710 \pm 0.025) \times 10^1$
$\mu-\rho$ (Data)	$(8.657 \pm 0.020) \times 10^1$	$(8.633 \pm 0.020) \times 10^1$
$\mu-\rho$ (MC)	$(8.689 \pm 0.026) \times 10^1$	$(8.671 \pm 0.026) \times 10^1$
$e-\pi\pi$ (Data)	$(8.395 \pm 0.021) \times 10^1$	$(8.348 \pm 0.021) \times 10^1$
$e-\pi\pi$ (MC)	$(8.542 \pm 0.028) \times 10^1$	$(8.520 \pm 0.028) \times 10^1$
$\mu-\pi\pi$ (Data)	$(8.484 \pm 0.021) \times 10^1$	$(8.457 \pm 0.021) \times 10^1$
$\mu-\pi\pi$ (MC)	$(8.486 \pm 0.028) \times 10^1$	$(8.460 \pm 0.029) \times 10^1$
μ–Avg. (Data)	$(8.575 \pm 0.015) \times 10^1$	$(8.549 \pm 0.015) \times 10^1$
μ–Avg. (MC)	$(8.597 \pm 0.019) \times 10^1$	$(8.576 \pm 0.019) \times 10^1$
Good Tracks Very Loose		
Decay	$\epsilon \times A(\%)$	$\epsilon' \times A(\%)$
$e-\rho$ (Data)	$(8.748 \pm 0.019) \times 10^1$	$(8.699 \pm 0.019) \times 10^1$
$e-\rho$ (MC)	$(8.833 \pm 0.024) \times 10^1$	$(8.788 \pm 0.025) \times 10^1$
$\mu-\rho$ (Data)	$(8.823 \pm 0.019) \times 10^1$	$(8.767 \pm 0.019) \times 10^1$
$\mu-\rho$ (MC)	$(8.801 \pm 0.025) \times 10^1$	$(8.755 \pm 0.025) \times 10^1$
$e-\pi\pi$ (Data)	$(8.523 \pm 0.020) \times 10^1$	$(8.455 \pm 0.020) \times 10^1$
$e-\pi\pi$ (MC)	$(8.624 \pm 0.027) \times 10^1$	$(8.586 \pm 0.028) \times 10^1$
$\mu-\pi\pi$ (Data)	$(8.613 \pm 0.020) \times 10^1$	$(8.561 \pm 0.021) \times 10^1$
$\mu-\pi\pi$ (MC)	$(8.574 \pm 0.028) \times 10^1$	$(8.535 \pm 0.028) \times 10^1$
μ–Avg. (Data)	$(8.726 \pm 0.014) \times 10^1$	$(8.671 \pm 0.014) \times 10^1$
μ–Avg. (MC)	$(8.700 \pm 0.018) \times 10^1$	$(8.657 \pm 0.019) \times 10^1$
Charged Tracks		
Decay	$\epsilon \times A(\%)$	$\epsilon' \times A(\%)$
$e-\rho$ (Data)	$(9.430 \pm 0.013) \times 10^1$	$(9.089 \pm 0.016) \times 10^1$
$e-\rho$ (MC)	$(9.467 \pm 0.017) \times 10^1$	$(9.125 \pm 0.021) \times 10^1$
$\mu-\rho$ (Data)	$(9.522 \pm 0.013) \times 10^1$	$(9.147 \pm 0.016) \times 10^1$
$\mu-\rho$ (MC)	$(9.465 \pm 0.017) \times 10^1$	$(9.098 \pm 0.022) \times 10^1$
$e-\pi\pi$ (Data)	$(9.254 \pm 0.015) \times 10^1$	$(8.917 \pm 0.017) \times 10^1$
$e-\pi\pi$ (MC)	$(9.289 \pm 0.021) \times 10^1$	$(9.005 \pm 0.024) \times 10^1$
$\mu-\pi\pi$ (Data)	$(9.332 \pm 0.015) \times 10^1$	$(9.017 \pm 0.018) \times 10^1$
$\mu-\pi\pi$ (MC)	$(9.262 \pm 0.021) \times 10^1$	$(8.972 \pm 0.024) \times 10^1$
μ–Avg. (Data)	$(9.442 \pm 0.010) \times 10^1$	$(9.086 \pm 0.012) \times 10^1$
μ–Avg. (MC)	$(9.383 \pm 0.013) \times 10^1$	$(9.041 \pm 0.016) \times 10^1$

Table F.2: The tracking efficiency, $1.0 < P_t^{miss} < 2.5$, for the three different track definitions from the 1930V setting (Stability Study). The average values in this table are the weighted average of the $\mu-\rho$ and $\mu-\pi\pi$ channels as discussed in Chapter 7: Systematic Uncertainty Studies.

Good Tracks Loose		
Decay	$\epsilon \times A(\%)$	$\epsilon' \times A(\%)$
$e-\rho$ (Data)	$(9.172 \pm 0.019) \times 10^1$	$(9.147 \pm 0.019) \times 10^1$
$e-\rho$ (MC)	$(9.279 \pm 0.024) \times 10^1$	$(9.248 \pm 0.024) \times 10^1$
$\mu-\rho$ (Data)	$(9.200 \pm 0.019) \times 10^1$	$(9.166 \pm 0.019) \times 10^1$
$\mu-\rho$ (MC)	$(9.292 \pm 0.023) \times 10^1$	$(9.266 \pm 0.024) \times 10^1$
$e-\pi\pi$ (Data)	$(9.226 \pm 0.014) \times 10^1$	$(9.136 \pm 0.015) \times 10^1$
$e-\pi\pi$ (MC)	$(9.271 \pm 0.018) \times 10^1$	$(9.228 \pm 0.019) \times 10^1$
$\mu-\pi\pi$ (Data)	$(9.218 \pm 0.014) \times 10^1$	$(9.172 \pm 0.015) \times 10^1$
$\mu-\pi\pi$ (MC)	$(9.251 \pm 0.019) \times 10^1$	$(9.203 \pm 0.019) \times 10^1$
μ–Avg. (Data)	$(9.212 \pm 0.012) \times 10^1$	$(9.170 \pm 0.012) \times 10^1$
μ–Avg. (MC)	$(9.267 \pm 0.015) \times 10^1$	$(9.228 \pm 0.015) \times 10^1$
Good Tracks Very Loose		
Decay	$\epsilon \times A(\%)$	$\epsilon' \times A(\%)$
$e-\rho$ (Data)	$(9.308 \pm 0.017) \times 10^1$	$(9.252 \pm 0.018) \times 10^1$
$e-\rho$ (MC)	$(9.379 \pm 0.022) \times 10^1$	$(9.316 \pm 0.023) \times 10^1$
$\mu-\rho$ (Data)	$(9.346 \pm 0.017) \times 10^1$	$(9.268 \pm 0.018) \times 10^1$
$\mu-\rho$ (MC)	$(9.385 \pm 0.022) \times 10^1$	$(9.334 \pm 0.023) \times 10^1$
$e-\pi\pi$ (Data)	$(9.322 \pm 0.013) \times 10^1$	$(9.201 \pm 0.014) \times 10^1$
$e-\pi\pi$ (MC)	$(9.337 \pm 0.018) \times 10^1$	$(9.273 \pm 0.018) \times 10^1$
$\mu-\pi\pi$ (Data)	$(9.314 \pm 0.014) \times 10^1$	$(9.239 \pm 0.014) \times 10^1$
$\mu-\pi\pi$ (MC)	$(9.322 \pm 0.018) \times 10^1$	$(9.253 \pm 0.019) \times 10^1$
μ–Avg. (Data)	$(9.326 \pm 0.011) \times 10^1$	$(9.250 \pm 0.011) \times 10^1$
μ–Avg. (MC)	$(9.347 \pm 0.014) \times 10^1$	$(9.285 \pm 0.014) \times 10^1$
Charged Tracks		
Decay	$\epsilon \times A(\%)$	$\epsilon' \times A(\%)$
$e-\rho$ (Data)	$(9.728 \pm 0.011) \times 10^1$	$(9.393 \pm 0.016) \times 10^1$
$e-\rho$ (MC)	$(9.770 \pm 0.014) \times 10^1$	$(9.436 \pm 0.021) \times 10^1$
$\mu-\rho$ (Data)	$(9.775 \pm 0.011) \times 10^1$	$(9.407 \pm 0.017) \times 10^1$
$\mu-\rho$ (MC)	$(9.780 \pm 0.014) \times 10^1$	$(9.458 \pm 0.021) \times 10^1$
$e-\pi\pi$ (Data)	$(9.6943 \pm 0.0092) \times 10^1$	$(9.336 \pm 0.013) \times 10^1$
$e-\pi\pi$ (MC)	$(9.687 \pm 0.012) \times 10^1$	$(9.427 \pm 0.016) \times 10^1$
$\mu-\pi\pi$ (Data)	$(9.672 \pm 0.010) \times 10^1$	$(9.361 \pm 0.013) \times 10^1$
$\mu-\pi\pi$ (MC)	$(9.675 \pm 0.013) \times 10^1$	$(9.391 \pm 0.017) \times 10^1$
μ–Avg. (Data)	$(9.7186 \pm 0.0072) \times 10^1$	$(9.379 \pm 0.010) \times 10^1$
μ–Avg. (MC)	$(9.7237 \pm 0.0093) \times 10^1$	$(9.418 \pm 0.013) \times 10^1$

Table F.3: The tracking efficiency, $2.5 < P_t^{miss}$, for the three different track definitions from the 1930V setting (Stability Study). The average values in this table are the weighted average of the $\mu-\rho$ and $\mu-\pi\pi$ channels as discussed in Chapter 7: Systematic Uncertainty Studies.

Good Tracks Loose		
Decay	$\epsilon \times A(\%)$	$\epsilon' \times A(\%)$
$e-\rho$ (Data)	$(8.580 \pm 0.027) \times 10^1$	$(8.562 \pm 0.027) \times 10^1$
$e-\rho$ (MC)	$(8.806 \pm 0.033) \times 10^1$	$(8.788 \pm 0.033) \times 10^1$
$\mu-\rho$ (Data)	$(8.579 \pm 0.027) \times 10^1$	$(8.556 \pm 0.027) \times 10^1$
$\mu-\rho$ (MC)	$(8.735 \pm 0.033) \times 10^1$	$(8.723 \pm 0.033) \times 10^1$
$e-\pi\pi$ (Data)	$(8.574 \pm 0.024) \times 10^1$	$(8.485 \pm 0.024) \times 10^1$
$e-\pi\pi$ (MC)	$(8.840 \pm 0.030) \times 10^1$	$(8.813 \pm 0.030) \times 10^1$
$\mu-\pi\pi$ (Data)	$(8.720 \pm 0.023) \times 10^1$	$(8.692 \pm 0.023) \times 10^1$
$\mu-\pi\pi$ (MC)	$(8.810 \pm 0.030) \times 10^1$	$(8.785 \pm 0.030) \times 10^1$
μ–Avg. (Data)	$(8.660 \pm 0.018) \times 10^1$	$(8.635 \pm 0.018) \times 10^1$
μ–Avg. (MC)	$(8.776 \pm 0.022) \times 10^1$	$(8.757 \pm 0.022) \times 10^1$
Good Tracks Very Loose		
Decay	$\epsilon \times A(\%)$	$\epsilon' \times A(\%)$
$e-\rho$ (Data)	$(8.730 \pm 0.026) \times 10^1$	$(8.682 \pm 0.026) \times 10^1$
$e-\rho$ (MC)	$(8.913 \pm 0.032) \times 10^1$	$(8.869 \pm 0.032) \times 10^1$
$\mu-\rho$ (Data)	$(8.759 \pm 0.026) \times 10^1$	$(8.705 \pm 0.026) \times 10^1$
$\mu-\rho$ (MC)	$(8.839 \pm 0.032) \times 10^1$	$(8.802 \pm 0.033) \times 10^1$
$e-\pi\pi$ (Data)	$(8.699 \pm 0.023) \times 10^1$	$(8.581 \pm 0.024) \times 10^1$
$e-\pi\pi$ (MC)	$(8.910 \pm 0.029) \times 10^1$	$(8.866 \pm 0.030) \times 10^1$
$\mu-\pi\pi$ (Data)	$(8.834 \pm 0.022) \times 10^1$	$(8.782 \pm 0.023) \times 10^1$
$\mu-\pi\pi$ (MC)	$(8.890 \pm 0.029) \times 10^1$	$(8.847 \pm 0.029) \times 10^1$
μ–Avg. (Data)	$(8.802 \pm 0.017) \times 10^1$	$(8.749 \pm 0.017) \times 10^1$
μ–Avg. (MC)	$(8.867 \pm 0.021) \times 10^1$	$(8.827 \pm 0.022) \times 10^1$
Charged Tracks		
Decay	$\epsilon \times A(\%)$	$\epsilon' \times A(\%)$
$e-\rho$ (Data)	$(9.467 \pm 0.018) \times 10^1$	$(9.091 \pm 0.022) \times 10^1$
$e-\rho$ (MC)	$(9.610 \pm 0.020) \times 10^1$	$(9.233 \pm 0.027) \times 10^1$
$\mu-\rho$ (Data)	$(9.563 \pm 0.016) \times 10^1$	$(9.150 \pm 0.022) \times 10^1$
$\mu-\rho$ (MC)	$(9.602 \pm 0.020) \times 10^1$	$(9.207 \pm 0.027) \times 10^1$
$e-\pi\pi$ (Data)	$(9.416 \pm 0.016) \times 10^1$	$(8.983 \pm 0.020) \times 10^1$
$e-\pi\pi$ (MC)	$(9.554 \pm 0.020) \times 10^1$	$(9.245 \pm 0.025) \times 10^1$
$\mu-\pi\pi$ (Data)	$(9.500 \pm 0.015) \times 10^1$	$(9.163 \pm 0.019) \times 10^1$
$\mu-\pi\pi$ (MC)	$(9.527 \pm 0.020) \times 10^1$	$(9.188 \pm 0.025) \times 10^1$
μ–Avg. (Data)	$(9.530 \pm 0.011) \times 10^1$	$(9.157 \pm 0.014) \times 10^1$
μ–Avg. (MC)	$(9.564 \pm 0.014) \times 10^1$	$(9.197 \pm 0.018) \times 10^1$

Table F.4: The tracking efficiency, $cos(\theta_{avg}^{(lab)}) < 0.2$, for the three different track definitions from the 1930V setting (Stability Study). The average values in this table are the weighted average of the $\mu-\rho$ and $\mu-\pi\pi$ channels as discussed in Chapter 7: Systematic Uncertainty Studies.

Good Tracks Loose		
Decay	$\epsilon \times A(\%)$	$\epsilon' \times A(\%)$
$e-\rho$ (Data)	$(9.020 \pm 0.023) \times 10^1$	$(9.000 \pm 0.023) \times 10^1$
$e-\rho$ (MC)	$(9.103 \pm 0.029) \times 10^1$	$(9.077 \pm 0.029) \times 10^1$
$\mu-\rho$ (Data)	$(9.095 \pm 0.023) \times 10^1$	$(9.067 \pm 0.023) \times 10^1$
$\mu-\rho$ (MC)	$(9.172 \pm 0.028) \times 10^1$	$(9.146 \pm 0.029) \times 10^1$
$e-\pi\pi$ (Data)	$(9.083 \pm 0.020) \times 10^1$	$(9.036 \pm 0.020) \times 10^1$
$e-\pi\pi$ (MC)	$(9.150 \pm 0.026) \times 10^1$	$(9.119 \pm 0.027) \times 10^1$
$\mu-\pi\pi$ (Data)	$(9.120 \pm 0.020) \times 10^1$	$(9.085 \pm 0.020) \times 10^1$
$\mu-\pi\pi$ (MC)	$(9.129 \pm 0.026) \times 10^1$	$(9.090 \pm 0.027) \times 10^1$
μ–Avg. (Data)	$(9.109 \pm 0.015) \times 10^1$	$(9.077 \pm 0.015) \times 10^1$
μ–Avg. (MC)	$(9.149 \pm 0.019) \times 10^1$	$(9.116 \pm 0.020) \times 10^1$
Good Tracks Very Loose		
Decay	$\epsilon \times A(\%)$	$\epsilon' \times A(\%)$
$e-\rho$ (Data)	$(9.189 \pm 0.021) \times 10^1$	$(9.138 \pm 0.021) \times 10^1$
$e-\rho$ (MC)	$(9.204 \pm 0.028) \times 10^1$	$(9.149 \pm 0.028) \times 10^1$
$\mu-\rho$ (Data)	$(9.259 \pm 0.021) \times 10^1$	$(9.185 \pm 0.021) \times 10^1$
$\mu-\rho$ (MC)	$(9.272 \pm 0.027) \times 10^1$	$(9.222 \pm 0.027) \times 10^1$
$e-\pi\pi$ (Data)	$(9.204 \pm 0.018) \times 10^1$	$(9.132 \pm 0.019) \times 10^1$
$e-\pi\pi$ (MC)	$(9.239 \pm 0.025) \times 10^1$	$(9.185 \pm 0.026) \times 10^1$
$\mu-\pi\pi$ (Data)	$(9.245 \pm 0.019) \times 10^1$	$(9.177 \pm 0.019) \times 10^1$
$\mu-\pi\pi$ (MC)	$(9.218 \pm 0.025) \times 10^1$	$(9.160 \pm 0.026) \times 10^1$
μ–Avg. (Data)	$(9.251 \pm 0.014) \times 10^1$	$(9.181 \pm 0.014) \times 10^1$
μ–Avg. (MC)	$(9.244 \pm 0.018) \times 10^1$	$(9.189 \pm 0.019) \times 10^1$
Charged Tracks		
Decay	$\epsilon \times A(\%)$	$\epsilon' \times A(\%)$
$e-\rho$ (Data)	$(9.751 \pm 0.012) \times 10^1$	$(9.382 \pm 0.018) \times 10^1$
$e-\rho$ (MC)	$(9.765 \pm 0.016) \times 10^1$	$(9.389 \pm 0.024) \times 10^1$
$\mu-\rho$ (Data)	$(9.822 \pm 0.011) \times 10^1$	$(9.433 \pm 0.018) \times 10^1$
$\mu-\rho$ (MC)	$(9.810 \pm 0.014) \times 10^1$	$(9.440 \pm 0.024) \times 10^1$
$e-\pi\pi$ (Data)	$(9.713 \pm 0.012) \times 10^1$	$(9.369 \pm 0.017) \times 10^1$
$e-\pi\pi$ (MC)	$(9.750 \pm 0.015) \times 10^1$	$(9.445 \pm 0.021) \times 10^1$
$\mu-\pi\pi$ (Data)	$(9.738 \pm 0.011) \times 10^1$	$(9.391 \pm 0.017) \times 10^1$
$\mu-\pi\pi$ (MC)	$(9.720 \pm 0.016) \times 10^1$	$(9.434 \pm 0.022) \times 10^1$
μ–Avg. (Data)	$(9.7827 \pm 0.0078) \times 10^1$	$(9.410 \pm 0.012) \times 10^1$
μ–Avg. (MC)	$(9.770 \pm 0.011) \times 10^1$	$(9.437 \pm 0.016) \times 10^1$

Table F.5: The tracking efficiency, $0.2 < cos(\theta_{avg}^{(lab)}) < 0.6$, for the three different track definitions from the 1930V setting (Stability Study). The average values in this table are the weighted average of the $\mu-\rho$ and $\mu-\pi\pi$ channels as discussed in Chapter 7: Systematic Uncertainty Studies.

Good Tracks Loose		
Decay	$\epsilon \times A(\%)$	$\epsilon' \times A(\%)$
$e-\rho$ (Data)	$(8.516 \pm 0.024) \times 10^1$	$(8.492 \pm 0.024) \times 10^1$
$e-\rho$ (MC)	$(8.645 \pm 0.031) \times 10^1$	$(8.621 \pm 0.031) \times 10^1$
$\mu-\rho$ (Data)	$(8.635 \pm 0.024) \times 10^1$	$(8.605 \pm 0.025) \times 10^1$
$\mu-\rho$ (MC)	$(8.575 \pm 0.032) \times 10^1$	$(8.552 \pm 0.032) \times 10^1$
$e-\pi\pi$ (Data)	$(8.304 \pm 0.022) \times 10^1$	$(8.248 \pm 0.022) \times 10^1$
$e-\pi\pi$ (MC)	$(8.594 \pm 0.029) \times 10^1$	$(8.558 \pm 0.029) \times 10^1$
$\mu-\pi\pi$ (Data)	$(8.547 \pm 0.022) \times 10^1$	$(8.503 \pm 0.022) \times 10^1$
$\mu-\pi\pi$ (MC)	$(8.549 \pm 0.029) \times 10^1$	$(8.505 \pm 0.030) \times 10^1$
μ–Avg. (Data)	$(8.587 \pm 0.016) \times 10^1$	$(8.549 \pm 0.017) \times 10^1$
μ–Avg. (MC)	$(8.561 \pm 0.022) \times 10^1$	$(8.527 \pm 0.022) \times 10^1$
Good Tracks Very Loose		
Decay	$\epsilon \times A(\%)$	$\epsilon' \times A(\%)$
$e-\rho$ (Data)	$(8.656 \pm 0.023) \times 10^1$	$(8.605 \pm 0.023) \times 10^1$
$e-\rho$ (MC)	$(8.745 \pm 0.030) \times 10^1$	$(8.695 \pm 0.030) \times 10^1$
$\mu-\rho$ (Data)	$(8.768 \pm 0.023) \times 10^1$	$(8.708 \pm 0.024) \times 10^1$
$\mu-\rho$ (MC)	$(8.681 \pm 0.031) \times 10^1$	$(8.634 \pm 0.031) \times 10^1$
$e-\pi\pi$ (Data)	$(8.397 \pm 0.021) \times 10^1$	$(8.317 \pm 0.022) \times 10^1$
$e-\pi\pi$ (MC)	$(8.660 \pm 0.028) \times 10^1$	$(8.608 \pm 0.028) \times 10^1$
$\mu-\pi\pi$ (Data)	$(8.652 \pm 0.021) \times 10^1$	$(8.586 \pm 0.022) \times 10^1$
$\mu-\pi\pi$ (MC)	$(8.620 \pm 0.029) \times 10^1$	$(8.562 \pm 0.029) \times 10^1$
μ–Avg. (Data)	$(8.705 \pm 0.016) \times 10^1$	$(8.642 \pm 0.016) \times 10^1$
μ–Avg. (MC)	$(8.648 \pm 0.021) \times 10^1$	$(8.595 \pm 0.021) \times 10^1$
Charged Tracks		
Decay	$\epsilon \times A(\%)$	$\epsilon' \times A(\%)$
$e-\rho$ (Data)	$(9.298 \pm 0.017) \times 10^1$	$(9.004 \pm 0.020) \times 10^1$
$e-\rho$ (MC)	$(9.330 \pm 0.023) \times 10^1$	$(9.052 \pm 0.026) \times 10^1$
$\mu-\rho$ (Data)	$(9.415 \pm 0.017) \times 10^1$	$(9.101 \pm 0.020) \times 10^1$
$\mu-\rho$ (MC)	$(9.291 \pm 0.024) \times 10^1$	$(9.005 \pm 0.027) \times 10^1$
$e-\pi\pi$ (Data)	$(9.055 \pm 0.017) \times 10^1$	$(8.789 \pm 0.019) \times 10^1$
$e-\pi\pi$ (MC)	$(9.197 \pm 0.023) \times 10^1$	$(8.976 \pm 0.025) \times 10^1$
$\mu-\pi\pi$ (Data)	$(9.246 \pm 0.017) \times 10^1$	$(8.972 \pm 0.019) \times 10^1$
$\mu-\pi\pi$ (MC)	$(9.176 \pm 0.023) \times 10^1$	$(8.930 \pm 0.026) \times 10^1$
μ–Avg. (Data)	$(9.330 \pm 0.012) \times 10^1$	$(9.033 \pm 0.014) \times 10^1$
μ–Avg. (MC)	$(9.232 \pm 0.017) \times 10^1$	$(8.965 \pm 0.019) \times 10^1$

Table F.6: The tracking efficiency, $0.6 < cos(\theta_{avg}^{(lab)})$, for the three different track definitions from the 1930V setting (Stability Study). The average values in this table are the weighted average of the $\mu-\rho$ and $\mu-\pi\pi$ channels as discussed in Chapter 7: Systematic Uncertainty Studies.

Good Tracks Loose		
Decay	$\epsilon \times A(\%)$	$\epsilon' \times A(\%)$
$e-\rho$ (Data)	$(8.737 \pm 0.024) \times 10^1$	$(8.715 \pm 0.024) \times 10^1$
$e-\rho$ (MC)	$(8.839 \pm 0.031) \times 10^1$	$(8.819 \pm 0.031) \times 10^1$
$\mu-\rho$ (Data)	$(8.766 \pm 0.025) \times 10^1$	$(8.746 \pm 0.025) \times 10^1$
$\mu-\rho$ (MC)	$(8.802 \pm 0.032) \times 10^1$	$(8.784 \pm 0.032) \times 10^1$
$e-\pi\pi$ (Data)	$(8.637 \pm 0.022) \times 10^1$	$(8.573 \pm 0.022) \times 10^1$
$e-\pi\pi$ (MC)	$(8.818 \pm 0.029) \times 10^1$	$(8.790 \pm 0.029) \times 10^1$
$\mu-\pi\pi$ (Data)	$(8.808 \pm 0.022) \times 10^1$	$(8.774 \pm 0.022) \times 10^1$
$\mu-\pi\pi$ (MC)	$(8.821 \pm 0.029) \times 10^1$	$(8.783 \pm 0.030) \times 10^1$
μ–Avg. (Data)	$(8.790 \pm 0.017) \times 10^1$	$(8.762 \pm 0.017) \times 10^1$
μ–Avg. (MC)	$(8.813 \pm 0.022) \times 10^1$	$(8.783 \pm 0.022) \times 10^1$
Good Tracks Very Loose		
Decay	$\epsilon \times A(\%)$	$\epsilon' \times A(\%)$
$e-\rho$ (Data)	$(8.875 \pm 0.023) \times 10^1$	$(8.825 \pm 0.023) \times 10^1$
$e-\rho$ (MC)	$(8.940 \pm 0.030) \times 10^1$	$(8.893 \pm 0.031) \times 10^1$
$\mu-\rho$ (Data)	$(8.927 \pm 0.024) \times 10^1$	$(8.872 \pm 0.024) \times 10^1$
$\mu-\rho$ (MC)	$(8.904 \pm 0.031) \times 10^1$	$(8.860 \pm 0.031) \times 10^1$
$e-\pi\pi$ (Data)	$(8.745 \pm 0.021) \times 10^1$	$(8.659 \pm 0.022) \times 10^1$
$e-\pi\pi$ (MC)	$(8.900 \pm 0.028) \times 10^1$	$(8.855 \pm 0.028) \times 10^1$
$\mu-\pi\pi$ (Data)	$(8.919 \pm 0.021) \times 10^1$	$(8.859 \pm 0.022) \times 10^1$
$\mu-\pi\pi$ (MC)	$(8.895 \pm 0.028) \times 10^1$	$(8.839 \pm 0.029) \times 10^1$
μ–Avg. (Data)	$(8.923 \pm 0.016) \times 10^1$	$(8.865 \pm 0.016) \times 10^1$
μ–Avg. (MC)	$(8.899 \pm 0.021) \times 10^1$	$(8.849 \pm 0.021) \times 10^1$
Charged Tracks		
Decay	$\epsilon \times A(\%)$	$\epsilon' \times A(\%)$
$e-\rho$ (Data)	$(9.518 \pm 0.016) \times 10^1$	$(9.203 \pm 0.020) \times 10^1$
$e-\rho$ (MC)	$(9.548 \pm 0.021) \times 10^1$	$(9.225 \pm 0.026) \times 10^1$
$\mu-\rho$ (Data)	$(9.588 \pm 0.015) \times 10^1$	$(9.230 \pm 0.020) \times 10^1$
$\mu-\rho$ (MC)	$(9.545 \pm 0.021) \times 10^1$	$(9.212 \pm 0.027) \times 10^1$
$e-\pi\pi$ (Data)	$(9.369 \pm 0.016) \times 10^1$	$(9.021 \pm 0.019) \times 10^1$
$e-\pi\pi$ (MC)	$(9.458 \pm 0.020) \times 10^1$	$(9.180 \pm 0.024) \times 10^1$
$\mu-\pi\pi$ (Data)	$(9.502 \pm 0.015) \times 10^1$	$(9.201 \pm 0.018) \times 10^1$
$\mu-\pi\pi$ (MC)	$(9.475 \pm 0.021) \times 10^1$	$(9.186 \pm 0.025) \times 10^1$
μ–Avg. (Data)	$(9.543 \pm 0.011) \times 10^1$	$(9.214 \pm 0.014) \times 10^1$
μ–Avg. (MC)	$(9.509 \pm 0.015) \times 10^1$	$(9.198 \pm 0.018) \times 10^1$

Table F.7: The tracking efficiency, $\phi_{avg}^{(lab)} < -1.046$, for the three different track definitions from the 1930V setting (Stability Study). The average values in this table are the weighted average of the $\mu-\rho$ and $\mu-\pi\pi$ channels as discussed in Chapter 7: Systematic Uncertainty Studies.

Good Tracks Loose		
Decay	$\epsilon \times A(\%)$	$\epsilon' \times A(\%)$
$e-\rho$ (Data)	$(8.626 \pm 0.025) \times 10^1$	$(8.603 \pm 0.025) \times 10^1$
$e-\rho$ (MC)	$(8.829 \pm 0.031) \times 10^1$	$(8.804 \pm 0.032) \times 10^1$
$\mu-\rho$ (Data)	$(8.714 \pm 0.025) \times 10^1$	$(8.679 \pm 0.025) \times 10^1$
$\mu-\rho$ (MC)	$(8.802 \pm 0.031) \times 10^1$	$(8.779 \pm 0.032) \times 10^1$
$e-\pi\pi$ (Data)	$(8.590 \pm 0.023) \times 10^1$	$(8.526 \pm 0.023) \times 10^1$
$e-\pi\pi$ (MC)	$(8.814 \pm 0.029) \times 10^1$	$(8.781 \pm 0.029) \times 10^1$
$\mu-\pi\pi$ (Data)	$(8.744 \pm 0.022) \times 10^1$	$(8.706 \pm 0.022) \times 10^1$
$\mu-\pi\pi$ (MC)	$(8.753 \pm 0.029) \times 10^1$	$(8.719 \pm 0.030) \times 10^1$
μ–Avg. (Data)	$(8.731 \pm 0.017) \times 10^1$	$(8.694 \pm 0.017) \times 10^1$
μ–Avg. (MC)	$(8.776 \pm 0.021) \times 10^1$	$(8.747 \pm 0.022) \times 10^1$
Good Tracks Very Loose		
Decay	$\epsilon \times A(\%)$	$\epsilon' \times A(\%)$
$e-\rho$ (Data)	$(8.789 \pm 0.024) \times 10^1$	$(8.732 \pm 0.024) \times 10^1$
$e-\rho$ (MC)	$(8.923 \pm 0.030) \times 10^1$	$(8.868 \pm 0.031) \times 10^1$
$\mu-\rho$ (Data)	$(8.871 \pm 0.024) \times 10^1$	$(8.797 \pm 0.024) \times 10^1$
$\mu-\rho$ (MC)	$(8.907 \pm 0.030) \times 10^1$	$(8.861 \pm 0.031) \times 10^1$
$e-\pi\pi$ (Data)	$(8.693 \pm 0.022) \times 10^1$	$(8.599 \pm 0.022) \times 10^1$
$e-\pi\pi$ (MC)	$(8.888 \pm 0.028) \times 10^1$	$(8.837 \pm 0.029) \times 10^1$
$\mu-\pi\pi$ (Data)	$(8.862 \pm 0.021) \times 10^1$	$(8.794 \pm 0.022) \times 10^1$
$\mu-\pi\pi$ (MC)	$(8.846 \pm 0.028) \times 10^1$	$(8.794 \pm 0.029) \times 10^1$
μ–Avg. (Data)	$(8.866 \pm 0.016) \times 10^1$	$(8.795 \pm 0.016) \times 10^1$
μ–Avg. (MC)	$(8.875 \pm 0.021) \times 10^1$	$(8.825 \pm 0.021) \times 10^1$
Charged Tracks		
Decay	$\epsilon \times A(\%)$	$\epsilon' \times A(\%)$
$e-\rho$ (Data)	$(9.455 \pm 0.017) \times 10^1$	$(9.073 \pm 0.021) \times 10^1$
$e-\rho$ (MC)	$(9.539 \pm 0.021) \times 10^1$	$(9.177 \pm 0.027) \times 10^1$
$\mu-\rho$ (Data)	$(9.580 \pm 0.015) \times 10^1$	$(9.195 \pm 0.020) \times 10^1$
$\mu-\rho$ (MC)	$(9.544 \pm 0.021) \times 10^1$	$(9.195 \pm 0.026) \times 10^1$
$e-\pi\pi$ (Data)	$(9.349 \pm 0.016) \times 10^1$	$(9.014 \pm 0.019) \times 10^1$
$e-\pi\pi$ (MC)	$(9.458 \pm 0.021) \times 10^1$	$(9.184 \pm 0.025) \times 10^1$
$\mu-\pi\pi$ (Data)	$(9.461 \pm 0.015) \times 10^1$	$(9.131 \pm 0.019) \times 10^1$
$\mu-\pi\pi$ (MC)	$(9.407 \pm 0.021) \times 10^1$	$(9.112 \pm 0.025) \times 10^1$
μ–Avg. (Data)	$(9.520 \pm 0.011) \times 10^1$	$(9.161 \pm 0.014) \times 10^1$
μ–Avg. (MC)	$(9.478 \pm 0.015) \times 10^1$	$(9.152 \pm 0.018) \times 10^1$

Table F.8: The tracking efficiency, $1.046 < \phi_{avg}^{(lab)} < 1.046$, for the three different track definitions from the 1930V setting (Stability Study). The average values in this table are the weighted average of the $\mu-\rho$ and $\mu-\pi\pi$ channels as discussed in Chapter 7: Systematic Uncertainty Studies.

Good Tracks Loose		
Decay	$\epsilon \times A(\%)$	$\epsilon' \times A(\%)$
$e-\rho$ (Data)	$(8.706 \pm 0.024) \times 10^1$	$(8.687 \pm 0.025) \times 10^1$
$e-\rho$ (MC)	$(8.833 \pm 0.031) \times 10^1$	$(8.808 \pm 0.032) \times 10^1$
$\mu-\rho$ (Data)	$(8.796 \pm 0.024) \times 10^1$	$(8.769 \pm 0.025) \times 10^1$
$\mu-\rho$ (MC)	$(8.811 \pm 0.031) \times 10^1$	$(8.791 \pm 0.031) \times 10^1$
$e-\pi\pi$ (Data)	$(8.614 \pm 0.022) \times 10^1$	$(8.550 \pm 0.022) \times 10^1$
$e-\pi\pi$ (MC)	$(8.880 \pm 0.028) \times 10^1$	$(8.845 \pm 0.029) \times 10^1$
$\mu-\pi\pi$ (Data)	$(8.774 \pm 0.022) \times 10^1$	$(8.740 \pm 0.022) \times 10^1$
$\mu-\pi\pi$ (MC)	$(8.843 \pm 0.028) \times 10^1$	$(8.806 \pm 0.029) \times 10^1$
μ–Avg. (Data)	$(8.784 \pm 0.016) \times 10^1$	$(8.753 \pm 0.016) \times 10^1$
μ–Avg. (MC)	$(8.828 \pm 0.021) \times 10^1$	$(8.799 \pm 0.021) \times 10^1$
Good Tracks Very Loose		
Decay	$\epsilon \times A(\%)$	$\epsilon' \times A(\%)$
$e-\rho$ (Data)	$(8.859 \pm 0.023) \times 10^1$	$(8.816 \pm 0.023) \times 10^1$
$e-\rho$ (MC)	$(8.943 \pm 0.030) \times 10^1$	$(8.895 \pm 0.031) \times 10^1$
$\mu-\rho$ (Data)	$(8.950 \pm 0.023) \times 10^1$	$(8.893 \pm 0.023) \times 10^1$
$\mu-\rho$ (MC)	$(8.916 \pm 0.030) \times 10^1$	$(8.871 \pm 0.031) \times 10^1$
$e-\pi\pi$ (Data)	$(8.735 \pm 0.021) \times 10^1$	$(8.647 \pm 0.022) \times 10^1$
$e-\pi\pi$ (MC)	$(8.946 \pm 0.028) \times 10^1$	$(8.892 \pm 0.028) \times 10^1$
$\mu-\pi\pi$ (Data)	$(8.888 \pm 0.021) \times 10^1$	$(8.829 \pm 0.021) \times 10^1$
$\mu-\pi\pi$ (MC)	$(8.915 \pm 0.027) \times 10^1$	$(8.862 \pm 0.028) \times 10^1$
μ–Avg. (Data)	$(8.916 \pm 0.015) \times 10^1$	$(8.858 \pm 0.016) \times 10^1$
μ–Avg. (MC)	$(8.915 \pm 0.020) \times 10^1$	$(8.866 \pm 0.021) \times 10^1$
Charged Tracks		
Decay	$\epsilon \times A(\%)$	$\epsilon' \times A(\%)$
$e-\rho$ (Data)	$(9.488 \pm 0.016) \times 10^1$	$(9.159 \pm 0.020) \times 10^1$
$e-\rho$ (MC)	$(9.552 \pm 0.020) \times 10^1$	$(9.225 \pm 0.026) \times 10^1$
$\mu-\rho$ (Data)	$(9.591 \pm 0.015) \times 10^1$	$(9.230 \pm 0.020) \times 10^1$
$\mu-\rho$ (MC)	$(9.545 \pm 0.020) \times 10^1$	$(9.193 \pm 0.026) \times 10^1$
$e-\pi\pi$ (Data)	$(9.348 \pm 0.016) \times 10^1$	$(9.018 \pm 0.019) \times 10^1$
$e-\pi\pi$ (MC)	$(9.498 \pm 0.020) \times 10^1$	$(9.234 \pm 0.024) \times 10^1$
$\mu-\pi\pi$ (Data)	$(9.462 \pm 0.015) \times 10^1$	$(9.147 \pm 0.019) \times 10^1$
$\mu-\pi\pi$ (MC)	$(9.469 \pm 0.020) \times 10^1$	$(9.191 \pm 0.024) \times 10^1$
μ–Avg. (Data)	$(9.527 \pm 0.011) \times 10^1$	$(9.186 \pm 0.014) \times 10^1$
μ–Avg. (MC)	$(9.506 \pm 0.014) \times 10^1$	$(9.192 \pm 0.018) \times 10^1$

Table F.9: The tracking efficiency, $1.046 < \phi_{avg}^{(lab)}$, for the three different track definitions from the 1930V setting (Stability Study). The average values in this table are the weighted average of the $\mu-\rho$ and $\mu-\pi\pi$ channels as discussed in Chapter 7: Systematic Uncertainty Studies.

Good Tracks Loose		
Decay	$\Delta(\%)$	$\Delta'(\%)$
$e-\rho$	(2.03 ± 0.97)	(2.03 ± 0.97)
$\mu-\rho$	(0.5 ± 1.0)	(0.6 ± 1.0)
$e-\pi\pi$	$(1.39 \pm 0.11) \times 10^{1}$	$(1.40 \pm 0.11) \times 10^{1}$
$\mu-\pi\pi$	(1.5 ± 1.3)	(1.5 ± 1.3)
μ–Avg.	$(9.2 \pm 8.1) \times 10^{-1}$	$(9.7 \pm 8.1) \times 10^{-1}$
Good Tracks Very Loose		
Decay	$\Delta(\%)$	$\Delta'(\%)$
$e-\rho$	(1.48 ± 0.94)	(1.49 ± 0.94)
$\mu-\rho$	(-0.2 ± 1.0)	$(- \pm 1.0)$
$e-\pi\pi$	$(1.35 \pm 0.11) \times 10^{1}$	$(1.37 \pm 0.11) \times 10^{1}$
$\mu-\pi\pi$	(0.4 ± 1.2)	(0.4 ± 1.2)
μ–Avg.	$(0.2 \pm 7.8) \times 10^{-1}$	$(1.3 \pm 7.9) \times 10^{-1}$
Charged Tracks		
Decay	$\Delta(\%)$	$\Delta'(\%)$
$e-\rho$	(1.73 ± 0.58)	(2.49 ± 0.66)
$\mu-\rho$	(-1.49 ± 0.55)	(-1.28 ± 0.64)
$e-\pi\pi$	$(1.217 \pm 0.071) \times 10^{1}$	$(1.176 \pm 0.074) \times 10^{1}$
$\mu-\pi\pi$	$(0.2 \pm 7.4) \times 10^{-1}$	$(8.7 \pm 8.2) \times 10^{-1}$
μ–Avg.	$(-9.4 \pm 4.4) \times 10^{-1}$	$(-4.7 \pm 5.0) \times 10^{-1}$

Table F.10: The tracking efficiency correction factor, $P_t^{miss} < 1.0$, for the three different track definitions from the 1930V setting (Stability Study). The average values in this table are the weighted average of the $\mu - \rho$ and $\mu - \pi\pi$ channels as discussed in Chapter 7: Systematic Uncertainty Studies.

Good Tracks Loose		
Decay	$\Delta(\%)$	$\Delta'(\%)$
$e-\rho$	(1.66 ± 0.23)	(1.68 ± 0.23)
$\mu-\rho$	$(3.6 \pm 2.3) \times 10^{-1}$	$(4.4 \pm 2.3) \times 10^{-1}$
$e-\pi\pi$	(1.72 ± 0.24)	(2.02 ± 0.25)
$\mu-\pi\pi$	$(0.1 \pm 2.5) \times 10^{-1}$	$(0.3 \pm 2.5) \times 10^{-1}$
μ–Avg.	$(2.0 \pm 1.7) \times 10^{-1}$	$(2.5 \pm 1.7) \times 10^{-1}$
Good Tracks Very Loose		
Decay	$\Delta(\%)$	$\Delta'(\%)$
$e-\rho$	$(9.6 \pm 2.1) \times 10^{-1}$	(1.02 ± 0.22)
$\mu-\rho$	$(-2.6 \pm 2.2) \times 10^{-1}$	$(-1.3 \pm 2.2) \times 10^{-1}$
$e-\pi\pi$	(1.18 ± 0.23)	(1.53 ± 0.24)
$\mu-\pi\pi$	$(-4.6 \pm 2.4) \times 10^{-1}$	$(-3.1 \pm 2.4) \times 10^{-1}$
μ–Avg.	$(-3.5 \pm 1.6) \times 10^{-1}$	$(-2.1 \pm 1.6) \times 10^{-1}$
Charged Tracks		
Decay	$\Delta(\%)$	$\Delta'(\%)$
$e-\rho$	$(3.8 \pm 1.4) \times 10^{-1}$	$(4.0 \pm 1.8) \times 10^{-1}$
$\mu-\rho$	$(-6.0 \pm 1.4) \times 10^{-1}$	$(-5.4 \pm 1.8) \times 10^{-1}$
$e-\pi\pi$	$(3.7 \pm 1.6) \times 10^{-1}$	$(9.8 \pm 1.9) \times 10^{-1}$
$\mu-\pi\pi$	$(-7.5 \pm 1.6) \times 10^{-1}$	$(-5.1 \pm 2.0) \times 10^{-1}$
μ–Avg.	$(-6.6 \pm 1.0) \times 10^{-1}$	$(-5.2 \pm 1.3) \times 10^{-1}$

Table F.11: The tracking efficiency correction factor, $1.0 < P_t^{miss} < 2.5$, for the three different track definitions from the 1930V setting (Stability Study). The average values in this table are the weighted average of the $\mu-\rho$ and $\mu-\pi\pi$ channels as discussed in Chapter 7: Systematic Uncertainty Studies.

Good Tracks Loose		
Decay	$\Delta(\%)$	$\Delta'(\%)$
$e-\rho$	(1.16 ± 0.20)	(1.08 ± 0.21)
$\mu-\rho$	$(9.8 \pm 2.1) \times 10^{-1}$	(1.07 ± 0.21)
$e-\pi\pi$	$(4.9 \pm 1.5) \times 10^{-1}$	$(9.9 \pm 1.6) \times 10^{-1}$
$\mu-\pi\pi$	$(3.5 \pm 1.6) \times 10^{-1}$	$(3.4 \pm 1.6) \times 10^{-1}$
μ–Avg.	$(5.8 \pm 1.2) \times 10^{-1}$	$(6.1 \pm 1.3) \times 10^{-1}$
Good Tracks Very Loose		
Decay	$\Delta(\%)$	$\Delta'(\%)$
$e-\rho$	$(7.5 \pm 1.8) \times 10^{-1}$	$(6.9 \pm 1.9) \times 10^{-1}$
$\mu-\rho$	$(4.1 \pm 1.9) \times 10^{-1}$	$(7.1 \pm 2.0) \times 10^{-1}$
$e-\pi\pi$	$(1.6 \pm 1.4) \times 10^{-1}$	$(7.7 \pm 1.5) \times 10^{-1}$
$\mu-\pi\pi$	$(0.8 \pm 1.5) \times 10^{-1}$	$(1.5 \pm 1.5) \times 10^{-1}$
μ–Avg.	$(2.1 \pm 1.1) \times 10^{-1}$	$(3.6 \pm 1.2) \times 10^{-1}$
Charged Tracks		
Decay	$\Delta(\%)$	$\Delta'(\%)$
$e-\rho$	$(4.4 \pm 1.2) \times 10^{-1}$	$(4.6 \pm 1.7) \times 10^{-1}$
$\mu-\rho$	$(0.6 \pm 1.1) \times 10^{-1}$	$(5.4 \pm 1.8) \times 10^{-1}$
$e-\pi\pi$	$(-7.2 \pm 9.4) \times 10^{-2}$	$(9.6 \pm 1.4) \times 10^{-1}$
$\mu-\pi\pi$	$(0.3 \pm 1.0) \times 10^{-1}$	$(3.2 \pm 1.4) \times 10^{-1}$
μ–Avg.	$(4.1 \pm 7.4) \times 10^{-2}$	$(4.0 \pm 1.1) \times 10^{-1}$

Table F.12: The tracking efficiency correction factor, $2.5 < P_t^{miss}$, for the three different track definitions from the 1930V setting (Stability Study). The average values in this table are the weighted average of the $\mu - \rho$ and $\mu - \pi\pi$ channels as discussed in Chapter 7: Systematic Uncertainty Studies.

Good Tracks Loose		
Decay	$\Delta(\%)$	$\Delta'(\%)$
$e-\rho$	(2.57 ± 0.30)	(2.57 ± 0.31)
$\mu-\rho$	(1.79 ± 0.31)	(1.91 ± 0.31)
$e-\pi\pi$	(3.01 ± 0.27)	(3.72 ± 0.27)
$\mu-\pi\pi$	(1.02 ± 0.26)	(1.05 ± 0.27)
μ–Avg.	(1.34 ± 0.20)	(1.41 ± 0.20)
Good Tracks Very Loose		
Decay	$\Delta(\%)$	$\Delta'(\%)$
$e-\rho$	(2.04 ± 0.29)	(2.10 ± 0.29)
$\mu-\rho$	$(9.0 \pm 2.9) \times 10^{-1}$	(1.10 ± 0.30)
$e-\pi\pi$	(2.37 ± 0.26)	(3.21 ± 0.27)
$\mu-\pi\pi$	$(6.4 \pm 2.5) \times 10^{-1}$	$(7.4 \pm 2.6) \times 10^{-1}$
μ–Avg.	$(7.5 \pm 1.9) \times 10^{-1}$	$(8.9 \pm 1.9) \times 10^{-1}$
Charged Tracks		
Decay	$\Delta(\%)$	$\Delta'(\%)$
$e-\rho$	(1.49 ± 0.18)	(1.54 ± 0.24)
$\mu-\rho$	$(4.0 \pm 1.7) \times 10^{-1}$	$(6.3 \pm 2.4) \times 10^{-1}$
$e-\pi\pi$	(1.44 ± 0.17)	(2.83 ± 0.22)
$\mu-\pi\pi$	$(2.9 \pm 1.6) \times 10^{-1}$	$(2.8 \pm 2.1) \times 10^{-1}$
μ–Avg.	$(3.4 \pm 1.2) \times 10^{-1}$	$(4.3 \pm 1.6) \times 10^{-1}$

Table F.13: The tracking efficiency correction factor, $cos(\theta_{avg}^{(lab)}) < 0.2$, for the three different track definitions from the 1930V setting (Stability Study). The average values in this table are the weighted average of the $\mu-\rho$ and $\mu-\pi\pi$ channels as discussed in Chapter 7: Systematic Uncertainty Studies.

Good Tracks Loose		
Decay	$\Delta(\%)$	$\Delta'(\%)$
$e-\rho$	$(9.1 \pm 2.5) \times 10^{-1}$	$(8.5 \pm 2.5) \times 10^{-1}$
$\mu-\rho$	$(8.3 \pm 2.5) \times 10^{-1}$	$(8.6 \pm 2.5) \times 10^{-1}$
$e-\pi\pi$	$(7.3 \pm 2.1) \times 10^{-1}$	$(9.1 \pm 2.2) \times 10^{-1}$
$\mu-\pi\pi$	$(1.0 \pm 2.2) \times 10^{-1}$	$(0.5 \pm 2.2) \times 10^{-1}$
μ–Avg.	$(4.2 \pm 1.6) \times 10^{-1}$	$(4.1 \pm 1.7) \times 10^{-1}$
Good Tracks Very Loose		
Decay	$\Delta(\%)$	$\Delta'(\%)$
$e-\rho$	$(1.6 \pm 2.3) \times 10^{-1}$	$(1.2 \pm 2.3) \times 10^{-1}$
$\mu-\rho$	$(1.4 \pm 2.2) \times 10^{-1}$	$(4.0 \pm 2.3) \times 10^{-1}$
$e-\pi\pi$	$(3.7 \pm 2.0) \times 10^{-1}$	$(5.8 \pm 2.1) \times 10^{-1}$
$\mu-\pi\pi$	$(-2.9 \pm 2.0) \times 10^{-1}$	$(-1.8 \pm 2.1) \times 10^{-1}$
μ–Avg.	$(-1.0 \pm 1.5) \times 10^{-1}$	$(0.8 \pm 1.6) \times 10^{-1}$
Charged Tracks		
Decay	$\Delta(\%)$	$\Delta'(\%)$
$e-\rho$	$(1.5 \pm 1.2) \times 10^{-1}$	$(0.7 \pm 1.9) \times 10^{-1}$
$\mu-\rho$	$(-1.1 \pm 1.1) \times 10^{-1}$	$(0.8 \pm 1.9) \times 10^{-1}$
$e-\pi\pi$	$(3.7 \pm 1.2) \times 10^{-1}$	$(8.1 \pm 1.8) \times 10^{-1}$
$\mu-\pi\pi$	$(-1.8 \pm 1.2) \times 10^{-1}$	$(4.6 \pm 1.8) \times 10^{-1}$
μ–Avg.	$(-1.46 \pm 0.80) \times 10^{-1}$	$(2.8 \pm 1.3) \times 10^{-1}$

Table F.14: The tracking efficiency correction factor, $0.2 < cos(\theta_{avg}^{(lab)}) < 0.6$, for the three different track definitions from the 1930V setting (Stability Study). The average values in this table are the weighted average of the $\mu-\rho$ and $\mu-\pi\pi$ channels as discussed in Chapter 7: Systematic Uncertainty Studies.

Good Tracks Loose		
Decay	$\Delta(\%)$	$\Delta'(\%)$
$e-\rho$	(1.49 ± 0.28)	(1.49 ± 0.28)
$\mu-\rho$	$(-7.1 \pm 2.8) \times 10^{-1}$	$(-6.2 \pm 2.9) \times 10^{-1}$
$e-\pi\pi$	(3.38 ± 0.25)	(3.63 ± 0.26)
$\mu-\pi\pi$	$(0.2 \pm 2.6) \times 10^{-1}$	$(0.3 \pm 2.6) \times 10^{-1}$
μ–Avg.	$(-3.1 \pm 1.9) \times 10^{-1}$	$(-2.7 \pm 1.9) \times 10^{-1}$
Good Tracks Very Loose		
Decay	$\Delta(\%)$	$\Delta'(\%)$
$e-\rho$	(1.02 ± 0.26)	(1.03 ± 0.27)
$\mu-\rho$	(-1.00 ± 0.27)	$(-8.6 \pm 2.7) \times 10^{-1}$
$e-\pi\pi$	(3.05 ± 0.25)	(3.38 ± 0.25)
$\mu-\pi\pi$	$(-3.7 \pm 2.5) \times 10^{-1}$	$(-2.8 \pm 2.5) \times 10^{-1}$
μ–Avg.	$(-6.6 \pm 1.8) \times 10^{-1}$	$(-5.5 \pm 1.9) \times 10^{-1}$
Charged Tracks		
Decay	$\Delta(\%)$	$\Delta'(\%)$
$e-\rho$	$(3.5 \pm 1.9) \times 10^{-1}$	$(5.3 \pm 2.2) \times 10^{-1}$
$\mu-\rho$	(-1.34 ± 0.18)	(-1.07 ± 0.22)
$e-\pi\pi$	(1.54 ± 0.19)	(2.08 ± 0.21)
$\mu-\pi\pi$	$(-7.6 \pm 1.8) \times 10^{-1}$	$(-4.8 \pm 2.1) \times 10^{-1}$
μ–Avg.	(-1.05 ± 0.13)	$(-7.6 \pm 1.5) \times 10^{-1}$

Table F.15: The tracking efficiency correction factor, $0.6 < cos(\theta_{avg}^{(lab)})$, for the three different track definitions from the 1930V setting (Stability Study). The average values in this table are the weighted average of the $\mu - \rho$ and $\mu - \pi\pi$ channels as discussed in Chapter 7: Systematic Uncertainty Studies.

Good Tracks Loose		
Decay	$\Delta(\%)$	$\Delta'(\%)$
$e-\rho$	(1.15 ± 0.27)	(1.18 ± 0.27)
$\mu-\rho$	$(4.1 \pm 2.9) \times 10^{-1}$	$(4.3 \pm 2.9) \times 10^{-1}$
$e-\pi\pi$	(2.06 ± 0.25)	(2.47 ± 0.25)
$\mu-\pi\pi$	$(1.5 \pm 2.5) \times 10^{-1}$	$(1.0 \pm 2.5) \times 10^{-1}$
μ–Avg.	$(2.6 \pm 1.9) \times 10^{-1}$	$(2.5 \pm 1.9) \times 10^{-1}$
Good Tracks Very Loose		
Decay	$\Delta(\%)$	$\Delta'(\%)$
$e-\rho$	$(7.3 \pm 2.6) \times 10^{-1}$	$(7.7 \pm 2.6) \times 10^{-1}$
$\mu-\rho$	$(-2.6 \pm 2.7) \times 10^{-1}$	$(-1.4 \pm 2.7) \times 10^{-1}$
$e-\pi\pi$	(1.74 ± 0.24)	(2.22 ± 0.24)
$\mu-\pi\pi$	$(-2.7 \pm 2.4) \times 10^{-1}$	$(-2.2 \pm 2.4) \times 10^{-1}$
μ–Avg.	$(-2.7 \pm 1.8) \times 10^{-1}$	$(-1.9 \pm 1.8) \times 10^{-1}$
Charged Tracks		
Decay	$\Delta(\%)$	$\Delta'(\%)$
$e-\rho$	$(3.1 \pm 1.6) \times 10^{-1}$	$(2.4 \pm 2.1) \times 10^{-1}$
$\mu-\rho$	$(-4.5 \pm 1.6) \times 10^{-1}$	$(-2.0 \pm 2.2) \times 10^{-1}$
$e-\pi\pi$	$(9.4 \pm 1.7) \times 10^{-1}$	(1.74 ± 0.21)
$\mu-\pi\pi$	$(-2.9 \pm 1.6) \times 10^{-1}$	$(-1.6 \pm 2.0) \times 10^{-1}$
μ–Avg.	$(-3.7 \pm 1.1) \times 10^{-1}$	$(-1.8 \pm 1.5) \times 10^{-1}$

Table F.16: The tracking efficiency correction factor, $\phi_{avg}^{(lab)} < -1.046$, for the three different track definitions from the 1930V setting (Stability Study). The average values in this table are the weighted average of the $\mu - \rho$ and $\mu - \pi\pi$ channels as discussed in Chapter 7: Systematic Uncertainty Studies.

Good Tracks Loose		
Decay	$\Delta(\%)$	$\Delta'(\%)$
$e-\rho$	(2.30 ± 0.29)	(2.28 ± 0.29)
$\mu-\rho$	$(9.9 \pm 2.9) \times 10^{-1}$	(1.14 ± 0.29)
$e-\pi\pi$	(2.54 ± 0.26)	(2.90 ± 0.26)
$\mu-\pi\pi$	$(1.0 \pm 2.5) \times 10^{-1}$	$(1.5 \pm 2.6) \times 10^{-1}$
μ–Avg.	$(4.9 \pm 1.9) \times 10^{-1}$	$(5.9 \pm 1.9) \times 10^{-1}$
Good Tracks Very Loose		
Decay	$\Delta(\%)$	$\Delta'(\%)$
$e-\rho$	(1.50 ± 0.27)	(1.53 ± 0.28)
$\mu-\rho$	$(4.1 \pm 2.7) \times 10^{-1}$	$(7.2 \pm 2.8) \times 10^{-1}$
$e-\pi\pi$	(2.20 ± 0.25)	(2.69 ± 0.25)
$\mu-\pi\pi$	$(-1.8 \pm 2.4) \times 10^{-1}$	$(-0.1 \pm 2.5) \times 10^{-1}$
μ–Avg.	$(0.9 \pm 1.8) \times 10^{-1}$	$(3.2 \pm 1.8) \times 10^{-1}$
Charged Tracks		
Decay	$\Delta(\%)$	$\Delta'(\%)$
$e-\rho$	$(8.8 \pm 1.8) \times 10^{-1}$	(1.14 ± 0.23)
$\mu-\rho$	$(-3.8 \pm 1.6) \times 10^{-1}$	$(-0 \pm 2.2) \times 10^{-1}$
$e-\pi\pi$	(1.16 ± 0.17)	(1.86 ± 0.21)
$\mu-\pi\pi$	$(-5.8 \pm 1.6) \times 10^{-1}$	$(-2.1 \pm 2.1) \times 10^{-1}$
μ–Avg.	$(-4.7 \pm 1.1) \times 10^{-1}$	$(-1.1 \pm 1.5) \times 10^{-1}$

Table F.17: The tracking efficiency correction factor, $1.046 < \phi_{avg}^{(lab)} < 1.046$, for the three different track definitions from the 1930V setting (Stability Study). The average values in this table are the weighted average of the $\mu-\rho$ and $\mu-\pi\pi$ channels as discussed in Chapter 7: Systematic Uncertainty Studies.

Good Tracks Loose		
Decay	$\Delta(\%)$	$\Delta'(\%)$
$e-\rho$	(1.44 ± 0.28)	(1.37 ± 0.28)
$\mu-\rho$	$(1.7 \pm 2.8) \times 10^{-1}$	$(2.5 \pm 2.8) \times 10^{-1}$
$e-\pi\pi$	(3.00 ± 0.25)	(3.33 ± 0.25)
$\mu-\pi\pi$	$(7.7 \pm 2.5) \times 10^{-1}$	$(7.6 \pm 2.5) \times 10^{-1}$
μ–Avg.	$(5.0 \pm 1.8) \times 10^{-1}$	$(5.3 \pm 1.9) \times 10^{-1}$
Good Tracks Very Loose		
Decay	$\Delta(\%)$	$\Delta'(\%)$
$e-\rho$	$(9.3 \pm 2.6) \times 10^{-1}$	$(8.9 \pm 2.6) \times 10^{-1}$
$\mu-\rho$	$(-3.9 \pm 2.6) \times 10^{-1}$	$(-2.5 \pm 2.6) \times 10^{-1}$
$e-\pi\pi$	(2.36 ± 0.24)	(2.75 ± 0.24)
$\mu-\pi\pi$	$(3.0 \pm 2.3) \times 10^{-1}$	$(3.8 \pm 2.4) \times 10^{-1}$
μ–Avg.	$(-0.1 \pm 1.7) \times 10^{-1}$	$(1.0 \pm 1.8) \times 10^{-1}$
Charged Tracks		
Decay	$\Delta(\%)$	$\Delta'(\%)$
$e-\rho$	$(6.7 \pm 1.7) \times 10^{-1}$	$(7.1 \pm 2.2) \times 10^{-1}$
$\mu-\rho$	$(-4.8 \pm 1.6) \times 10^{-1}$	$(-4.0 \pm 2.2) \times 10^{-1}$
$e-\pi\pi$	(1.58 ± 0.17)	(2.34 ± 0.20)
$\mu-\pi\pi$	$(0.8 \pm 1.6) \times 10^{-1}$	$(4.8 \pm 2.0) \times 10^{-1}$
μ–Avg.	$(-2.0 \pm 1.1) \times 10^{-1}$	$(0.7 \pm 1.5) \times 10^{-1}$

Table F.18: The tracking efficiency correction factor, $1.046 < \phi_{avg}^{(lab)}$, for the three different track definitions from the 1930V setting (Stability Study). The average values in this table are the weighted average of the $\mu-\rho$ and $\mu-\pi\pi$ channels as discussed in Chapter 7: Systematic Uncertainty Studies.

Good Tracks Loose		
Decay	$a_{\pm}(\%)$	$a'_{\pm}(\%)$
$e-\rho$ (Data)	$(7.8 \pm 9.9) \times 10^{-1}$	$(9.3 \pm 9.9) \times 10^{-1}$
$e-\rho$ (MC)	(0.6 ± 1.3)	(0.7 ± 1.3)
$\mu-\rho$ (Data)	(-0.2 ± 1.0)	(-0.3 ± 1.1)
$\mu-\rho$ (MC)	(1.3 ± 1.3)	(1.4 ± 1.3)
$e-\pi\pi$ (Data)	(-4.0 ± 1.2)	(-4.0 ± 1.2)
$e-\pi\pi$ (MC)	(± 1.7)	(0 ± 1.7)
$\mu-\pi\pi$ (Data)	(-1.8 ± 1.3)	(-1.9 ± 1.3)
$\mu-\pi\pi$ (MC)	(-0.3 ± 1.7)	(-0.3 ± 1.7)
μ–Avg. (Data)	$(-8.2 \pm 8.2) \times 10^{-1}$	$(-9.5 \pm 8.2) \times 10^{-1}$
μ–Avg. (MC)	(0.7 ± 1.0)	$0(0.8 \pm 1.0)$
Good Tracks Very Loose		
Decay	$a_{\pm}(\%)$	$a'_{\pm}(\%)$
$e-\rho$ (Data)	$(8.1 \pm 9.5) \times 10^{-1}$	$(8.8 \pm 9.6) \times 10^{-1}$
$e-\rho$ (MC)	(0.6 ± 1.2)	(0.8 ± 1.2)
$\mu-\rho$ (Data)	$(- \pm 1.0)$	$(- \pm 1.0)$
$\mu-\rho$ (MC)	(1.3 ± 1.3)	(1.4 ± 1.3)
$e-\pi\pi$ (Data)	(-4.6 ± 1.2)	(-4.6 ± 1.2)
$e-\pi\pi$ (MC)	(-0 ± 1.7)	$(- \pm 1.7)$
$\mu-\pi\pi$ (Data)	(-0.8 ± 1.2)	(-0.8 ± 1.2)
$\mu-\pi\pi$ (MC)	(-0.2 ± 1.7)	(-0.3 ± 1.7)
μ–Avg. (Data)	$(-3.3 \pm 7.8) \times 10^{-1}$	$(-3.5 \pm 7.9) \times 10^{-1}$
μ–Avg. (MC)	(0.8 ± 1.0)	(0.8 ± 1.0)
Charged Tracks		
Decay	$a_{\pm}(\%)$	$a'_{\pm}(\%)$
$e-\rho$ (Data)	(1.32 ± 0.59)	(2.14 ± 0.67)
$e-\rho$ (MC)	$(5.8 \pm 7.2) \times 10^{-1}$	$(8.1 \pm 8.2) \times 10^{-1}$
$\mu-\rho$ (Data)	$(1.9 \pm 5.5) \times 10^{-1}$	$(4.5 \pm 6.3) \times 10^{-1}$
$\mu-\rho$ (MC)	(1.11 ± 0.74)	$(7.7 \pm 8.3) \times 10^{-1}$
$e-\pi\pi$ (Data)	(-5.25 ± 0.79)	(-4.92 ± 0.82)
$e-\pi\pi$ (MC)	$(-5.8 \pm 9.7) \times 10^{-1}$	(-0.4 ± 1.1)
$\mu-\pi\pi$ (Data)	(-1.07 ± 0.74)	(-1.64 ± 0.83)
$\mu-\pi\pi$ (MC)	$(-0.5 \pm 9.8) \times 10^{-1}$	$(- \pm 1.1)$
μ–Avg. (Data)	$(-2.5 \pm 4.4) \times 10^{-1}$	$(-3.2 \pm 5.0) \times 10^{-1}$
μ–Avg. (MC)	$(7.0 \pm 5.9) \times 10^{-1}$	$(4.8 \pm 6.6) \times 10^{-1}$

Table F.19: The tracking efficiency charge asymmetry, $P_t^{miss} < 1.0$, for the three different track definitions from the 1930V setting (Stability Study). The average values in this table are the weighted average of the $\mu - \rho$ and $\mu - \pi\pi$ channels as discussed in Chapter 7: Systematic Uncertainty Studies.

Good Tracks Loose		
Decay	$a_{\pm}(\%)$	$a'_{\pm}(\%)$
$e-\rho$ (Data)	$(-0.4 \pm 2.3) \times 10^{-1}$	$(0.2 \pm 2.3) \times 10^{-1}$
$e-\rho$ (MC)	$(-0.6 \pm 2.9) \times 10^{-1}$	$(-0.4 \pm 2.9) \times 10^{-1}$
$\mu-\rho$ (Data)	$(4.4 \pm 2.3) \times 10^{-1}$	$(4.2 \pm 2.4) \times 10^{-1}$
$\mu-\rho$ (MC)	$(-0.8 \pm 3.0) \times 10^{-1}$	$(-0.9 \pm 3.0) \times 10^{-1}$
$e-\pi\pi$ (Data)	(-1.45 ± 0.26)	(-1.55 ± 0.26)
$e-\pi\pi$ (MC)	$(-1.8 \pm 3.4) \times 10^{-1}$	$(-1.8 \pm 3.4) \times 10^{-1}$
$\mu-\pi\pi$ (Data)	$(-6.4 \pm 2.5) \times 10^{-1}$	$(-6.1 \pm 2.6) \times 10^{-1}$
$\mu-\pi\pi$ (MC)	$(0.9 \pm 3.4) \times 10^{-1}$	$(1.4 \pm 3.4) \times 10^{-1}$
μ–Avg. (Data)	$(-0.6 \pm 1.7) \times 10^{-1}$	$(-0.6 \pm 1.7) \times 10^{-1}$
μ–Avg. (MC)	$(-0.1 \pm 2.2) \times 10^{-1}$	$(0.1 \pm 2.3) \times 10^{-1}$
Good Tracks Very Loose		
Decay	$a_{\pm}(\%)$	$a'_{\pm}(\%)$
$e-\rho$ (Data)	$(-0.1 \pm 2.2) \times 10^{-1}$	$(-0 \pm 2.2) \times 10^{-1}$
$e-\rho$ (MC)	$(-1.3 \pm 2.8) \times 10^{-1}$	$(-1.0 \pm 2.8) \times 10^{-1}$
$\mu-\rho$ (Data)	$(3.5 \pm 2.2) \times 10^{-1}$	$(3.3 \pm 2.2) \times 10^{-1}$
$\mu-\rho$ (MC)	$(-0.7 \pm 2.9) \times 10^{-1}$	$(-1.0 \pm 2.9) \times 10^{-1}$
$e-\pi\pi$ (Data)	(-1.58 ± 0.25)	(-1.67 ± 0.25)
$e-\pi\pi$ (MC)	$(-2.3 \pm 3.3) \times 10^{-1}$	$(-2.1 \pm 3.3) \times 10^{-1}$
$\mu-\pi\pi$ (Data)	$(-5.0 \pm 2.4) \times 10^{-1}$	$(-4.4 \pm 2.5) \times 10^{-1}$
$\mu-\pi\pi$ (MC)	$(0.1 \pm 3.3) \times 10^{-1}$	$(0.9 \pm 3.3) \times 10^{-1}$
μ–Avg. (Data)	$(-0.3 \pm 1.6) \times 10^{-1}$	$(-0.2 \pm 1.7) \times 10^{-1}$
μ–Avg. (MC)	$(-0.4 \pm 2.2) \times 10^{-1}$	$(-0.2 \pm 2.2) \times 10^{-1}$
Charged Tracks		
Decay	$a_{\pm}(\%)$	$a'_{\pm}(\%)$
$e-\rho$ (Data)	$(1.4 \pm 1.4) \times 10^{-1}$	$(3.0 \pm 1.8) \times 10^{-1}$
$e-\rho$ (MC)	$(0.2 \pm 1.8) \times 10^{-1}$	$(1.8 \pm 2.3) \times 10^{-1}$
$\mu-\rho$ (Data)	$(2.6 \pm 1.3) \times 10^{-1}$	$(4.0 \pm 1.7) \times 10^{-1}$
$\mu-\rho$ (MC)	$(0.2 \pm 1.8) \times 10^{-1}$	$(2.4 \pm 2.3) \times 10^{-1}$
$e-\pi\pi$ (Data)	(-1.52 ± 0.17)	(-1.34 ± 0.20)
$e-\pi\pi$ (MC)	$(-0.8 \pm 2.2) \times 10^{-1}$	$(1.6 \pm 2.6) \times 10^{-1}$
$\mu-\pi\pi$ (Data)	$(-3.7 \pm 1.6) \times 10^{-1}$	$(-2.6 \pm 1.9) \times 10^{-1}$
$\mu-\pi\pi$ (MC)	$(-1.4 \pm 2.3) \times 10^{-1}$	$(2.4 \pm 2.6) \times 10^{-1}$
μ–Avg. (Data)	$(0 \pm 1.0) \times 10^{-1}$	$(1.0 \pm 1.3) \times 10^{-1}$
μ–Avg. (MC)	$(-0.4 \pm 1.4) \times 10^{-1}$	$(2.4 \pm 1.7) \times 10^{-1}$

Table F.20: The tracking efficiency charge asymmetry, $1.0 < P_t^{miss} < 2.5$, for the three different track definitions from the 1930V setting (Stability Study). The average values in this table are the weighted average of the $\mu-\rho$ and $\mu-\pi\pi$ channels as discussed in Chapter 7: Systematic Uncertainty Studies.

Good Tracks Loose		
Decay	$a_{\pm}(\%)$	$a'_{\pm}(\%)$
$e-\rho$ (Data)	$(0.7 \pm 2.1) \times 10^{-1}$	$(0.8 \pm 2.1) \times 10^{-1}$
$e-\rho$ (MC)	$(2.9 \pm 2.5) \times 10^{-1}$	$(3.5 \pm 2.6) \times 10^{-1}$
$\mu-\rho$ (Data)	$(-2.7 \pm 2.1) \times 10^{-1}$	$(-2.1 \pm 2.1) \times 10^{-1}$
$\mu-\rho$ (MC)	$(-1.1 \pm 2.5) \times 10^{-1}$	$(-1.1 \pm 2.6) \times 10^{-1}$
$e-\pi\pi$ (Data)	$(-3.9 \pm 1.5) \times 10^{-1}$	$(-5.4 \pm 1.6) \times 10^{-1}$
$e-\pi\pi$ (MC)	$(-1.4 \pm 2.0) \times 10^{-1}$	$(-1.0 \pm 2.0) \times 10^{-1}$
$\mu-\pi\pi$ (Data)	$(-4.1 \pm 1.6) \times 10^{-1}$	$(-3.6 \pm 1.6) \times 10^{-1}$
$\mu-\pi\pi$ (MC)	$(-3.6 \pm 2.0) \times 10^{-1}$	$(-4.3 \pm 2.1) \times 10^{-1}$
μ–Avg. (Data)	$(-3.6 \pm 1.2) \times 10^{-1}$	$(-3.1 \pm 1.3) \times 10^{-1}$
μ–Avg. (MC)	$(-2.6 \pm 1.6) \times 10^{-1}$	$(-3.0 \pm 1.6) \times 10^{-1}$
Good Tracks Very Loose		
Decay	$a_{\pm}(\%)$	$a'_{\pm}(\%)$
$e-\rho$ (Data)	$(-0.5 \pm 1.9) \times 10^{-1}$	$(-0.2 \pm 1.9) \times 10^{-1}$
$e-\rho$ (MC)	$(3.0 \pm 2.4) \times 10^{-1}$	$(3.8 \pm 2.5) \times 10^{-1}$
$\mu-\rho$ (Data)	$(-1.9 \pm 1.9) \times 10^{-1}$	$(-1.7 \pm 2.0) \times 10^{-1}$
$\mu-\rho$ (MC)	$(-1.6 \pm 2.3) \times 10^{-1}$	$(-1.7 \pm 2.4) \times 10^{-1}$
$e-\pi\pi$ (Data)	$(-4.2 \pm 1.4) \times 10^{-1}$	$(-5.3 \pm 1.5) \times 10^{-1}$
$e-\pi\pi$ (MC)	$(-1.2 \pm 1.9) \times 10^{-1}$	$(-0.8 \pm 2.0) \times 10^{-1}$
$\mu-\pi\pi$ (Data)	$(-3.1 \pm 1.5) \times 10^{-1}$	$(-2.7 \pm 1.5) \times 10^{-1}$
$\mu-\pi\pi$ (MC)	$(-3.6 \pm 1.9) \times 10^{-1}$	$(-4.2 \pm 2.0) \times 10^{-1}$
μ–Avg. (Data)	$(-2.7 \pm 1.1) \times 10^{-1}$	$(-2.3 \pm 1.2) \times 10^{-1}$
μ–Avg. (MC)	$(-2.8 \pm 1.5) \times 10^{-1}$	$(-3.2 \pm 1.5) \times 10^{-1}$
Charged Tracks		
Decay	$a_{\pm}(\%)$	$a'_{\pm}(\%)$
$e-\rho$ (Data)	$(1.0 \pm 1.2) \times 10^{-1}$	$(3.2 \pm 1.7) \times 10^{-1}$
$e-\rho$ (MC)	$(0.9 \pm 1.4) \times 10^{-1}$	$(5.0 \pm 2.2) \times 10^{-1}$
$\mu-\rho$ (Data)	$(-0.4 \pm 1.1) \times 10^{-1}$	$(1.6 \pm 1.8) \times 10^{-1}$
$\mu-\rho$ (MC)	$(0.5 \pm 1.4) \times 10^{-1}$	$(3.4 \pm 2.2) \times 10^{-1}$
$e-\pi\pi$ (Data)	$(-1.82 \pm 0.94) \times 10^{-1}$	$(-1.3 \pm 1.4) \times 10^{-1}$
$e-\pi\pi$ (MC)	$(-0.8 \pm 1.3) \times 10^{-1}$	$(1.8 \pm 1.7) \times 10^{-1}$
$\mu-\pi\pi$ (Data)	$(-2.1 \pm 1.0) \times 10^{-1}$	$(-1.3 \pm 1.4) \times 10^{-1}$
$\mu-\pi\pi$ (MC)	$(-1.7 \pm 1.3) \times 10^{-1}$	$(0 \pm 1.8) \times 10^{-1}$
μ–Avg. (Data)	$(-1.31 \pm 0.74) \times 10^{-1}$	$(-0.2 \pm 1.1) \times 10^{-1}$
μ–Avg. (MC)	$(-0.7 \pm 1.0) \times 10^{-1}$	$(1.4 \pm 1.4) \times 10^{-1}$

Table F.21: The tracking efficiency charge asymmetry, $2.5 < P_t^{miss}$, for the three different track definitions from the 1930V setting (Stability Study). The average values in this table are the weighted average of the $\mu-\rho$ and $\mu-\pi\pi$ channels as discussed in Chapter 7: Systematic Uncertainty Studies.

Good Tracks Loose		
Decay	$a_{\pm}(\%)$	$a'_{\pm}(\%)$
$e-\rho$ (Data)	$(-3.3 \pm 3.1) \times 10^{-1}$	$(-2.5 \pm 3.1) \times 10^{-1}$
$e-\rho$ (MC)	$(2.1 \pm 3.8) \times 10^{-1}$	$(2.0 \pm 3.8) \times 10^{-1}$
$\mu-\rho$ (Data)	$(0.3 \pm 3.2) \times 10^{-1}$	$(0.6 \pm 3.2) \times 10^{-1}$
$\mu-\rho$ (MC)	$(0.4 \pm 3.8) \times 10^{-1}$	$(-0.2 \pm 3.8) \times 10^{-1}$
$e-\pi\pi$ (Data)	(1.40 ± 0.28)	$(8.9 \pm 2.8) \times 10^{-1}$
$e-\pi\pi$ (MC)	$(2.8 \pm 3.4) \times 10^{-1}$	$(2.6 \pm 3.5) \times 10^{-1}$
$\mu-\pi\pi$ (Data)	$(2.1 \pm 2.7) \times 10^{-1}$	$(2.5 \pm 2.7) \times 10^{-1}$
$\mu-\pi\pi$ (MC)	$(2.0 \pm 3.4) \times 10^{-1}$	$(2.4 \pm 3.4) \times 10^{-1}$
μ–Avg. (Data)	$(1.4 \pm 2.0) \times 10^{-1}$	$(1.7 \pm 2.1) \times 10^{-1}$
μ–Avg. (MC)	$(1.3 \pm 2.5) \times 10^{-1}$	$(1.2 \pm 2.5) \times 10^{-1}$
Good Tracks Very Loose		
Decay	$a_{\pm}(\%)$	$a'_{\pm}(\%)$
$e-\rho$ (Data)	$(-2.9 \pm 2.9) \times 10^{-1}$	$(-3.0 \pm 3.0) \times 10^{-1}$
$e-\rho$ (MC)	$(2.3 \pm 3.6) \times 10^{-1}$	$(2.3 \pm 3.7) \times 10^{-1}$
$\mu-\rho$ (Data)	$(-1.1 \pm 2.9) \times 10^{-1}$	$(-0.7 \pm 3.0) \times 10^{-1}$
$\mu-\rho$ (MC)	$(0.7 \pm 3.6) \times 10^{-1}$	$(0.2 \pm 3.7) \times 10^{-1}$
$e-\pi\pi$ (Data)	(1.37 ± 0.26)	$(8.9 \pm 2.7) \times 10^{-1}$
$e-\pi\pi$ (MC)	$(2.4 \pm 3.3) \times 10^{-1}$	$(2.2 \pm 3.4) \times 10^{-1}$
$\mu-\pi\pi$ (Data)	$(3.2 \pm 2.5) \times 10^{-1}$	$(4.2 \pm 2.6) \times 10^{-1}$
$\mu-\pi\pi$ (MC)	$(1.5 \pm 3.2) \times 10^{-1}$	$(1.8 \pm 3.3) \times 10^{-1}$
μ–Avg. (Data)	$(1.4 \pm 1.9) \times 10^{-1}$	$(2.1 \pm 2.0) \times 10^{-1}$
μ–Avg. (MC)	$(1.1 \pm 2.4) \times 10^{-1}$	$(1.1 \pm 2.5) \times 10^{-1}$
Charged Tracks		
Decay	$a_{\pm}(\%)$	$a'_{\pm}(\%)$
$e-\rho$ (Data)	$(-2.1 \pm 1.9) \times 10^{-1}$	$(-1.0 \pm 2.4) \times 10^{-1}$
$e-\rho$ (MC)	$(0.6 \pm 2.1) \times 10^{-1}$	$(3.5 \pm 3.0) \times 10^{-1}$
$\mu-\rho$ (Data)	$(-1.5 \pm 1.7) \times 10^{-1}$	$(1.1 \pm 2.4) \times 10^{-1}$
$\mu-\rho$ (MC)	$(0.1 \pm 2.1) \times 10^{-1}$	$(1.3 \pm 2.9) \times 10^{-1}$
$e-\pi\pi$ (Data)	(1.03 ± 0.17)	$(5.3 \pm 2.3) \times 10^{-1}$
$e-\pi\pi$ (MC)	$(2.6 \pm 2.1) \times 10^{-1}$	$(2.8 \pm 2.7) \times 10^{-1}$
$\mu-\pi\pi$ (Data)	$(1.6 \pm 1.6) \times 10^{-1}$	$(4.1 \pm 2.1) \times 10^{-1}$
$\mu-\pi\pi$ (MC)	$(0.9 \pm 2.1) \times 10^{-1}$	$(2.9 \pm 2.7) \times 10^{-1}$
μ–Avg. (Data)	$(0.1 \pm 1.2) \times 10^{-1}$	$(2.8 \pm 1.6) \times 10^{-1}$
μ–Avg. (MC)	$(0.5 \pm 1.5) \times 10^{-1}$	$(2.2 \pm 2.0) \times 10^{-1}$

Table F.22: The tracking efficiency charge asymmetry, $cos(\theta_{avg}^{(lab)}) < 0.2$, for the three different track definitions from the 1930V setting (Stability Study). The average values in this table are the weighted average of the $\mu-\rho$ and $\mu-\pi\pi$ channels as discussed in Chapter 7: Systematic Uncertainty Studies.

Good Tracks Loose		
Decay	$a_{\pm}(\%)$	$a'_{\pm}(\%)$
$e-\rho$ (Data)	$(-0.4 \pm 2.5) \times 10^{-1}$	$(-0.2 \pm 2.5) \times 10^{-1}$
$e-\rho$ (MC)	$(-0.2 \pm 3.2) \times 10^{-1}$	$(0.2 \pm 3.2) \times 10^{-1}$
$\mu-\rho$ (Data)	$(-0.7 \pm 2.5) \times 10^{-1}$	$(-0.3 \pm 2.5) \times 10^{-1}$
$\mu-\rho$ (MC)	$(1.5 \pm 3.1) \times 10^{-1}$	$(2.0 \pm 3.1) \times 10^{-1}$
$e-\pi\pi$ (Data)	$(-0.7 \pm 2.2) \times 10^{-1}$	$(-0.9 \pm 2.2) \times 10^{-1}$
$e-\pi\pi$ (MC)	$(-2.7 \pm 2.9) \times 10^{-1}$	$(-2.1 \pm 2.9) \times 10^{-1}$
$\mu-\pi\pi$ (Data)	$(-2.6 \pm 2.2) \times 10^{-1}$	$(-1.9 \pm 2.2) \times 10^{-1}$
$\mu-\pi\pi$ (MC)	$(-0.4 \pm 2.9) \times 10^{-1}$	$(-1.3 \pm 3.0) \times 10^{-1}$
μ–Avg. (Data)	$(-1.8 \pm 1.6) \times 10^{-1}$	$(-1.2 \pm 1.7) \times 10^{-1}$
μ–Avg. (MC)	$(0.5 \pm 2.1) \times 10^{-1}$	$(0.2 \pm 2.2) \times 10^{-1}$
Good Tracks Very Loose		
Decay	$a_{\pm}(\%)$	$a'_{\pm}(\%)$
$e-\rho$ (Data)	$(-1.9 \pm 2.3) \times 10^{-1}$	$(-2.0 \pm 2.3) \times 10^{-1}$
$e-\rho$ (MC)	$(-0 \pm 3.0) \times 10^{-1}$	$(0.6 \pm 3.1) \times 10^{-1}$
$\mu-\rho$ (Data)	$(-0.3 \pm 2.2) \times 10^{-1}$	$(-0.4 \pm 2.3) \times 10^{-1}$
$\mu-\rho$ (MC)	$(2.0 \pm 2.9) \times 10^{-1}$	$(1.4 \pm 3.0) \times 10^{-1}$
$e-\pi\pi$ (Data)	$(-1.3 \pm 2.0) \times 10^{-1}$	$(-1.1 \pm 2.1) \times 10^{-1}$
$e-\pi\pi$ (MC)	$(-2.2 \pm 2.7) \times 10^{-1}$	$(-1.2 \pm 2.8) \times 10^{-1}$
$\mu-\pi\pi$ (Data)	$(-0.7 \pm 2.0) \times 10^{-1}$	$(0.2 \pm 2.1) \times 10^{-1}$
$\mu-\pi\pi$ (MC)	$(-0.3 \pm 2.7) \times 10^{-1}$	$(-1.4 \pm 2.8) \times 10^{-1}$
μ–Avg. (Data)	$(-0.5 \pm 1.5) \times 10^{-1}$	$(-0.1 \pm 1.6) \times 10^{-1}$
μ–Avg. (MC)	$(0.8 \pm 2.0) \times 10^{-1}$	$(-0.1 \pm 2.1) \times 10^{-1}$
Charged Tracks		
Decay	$a_{\pm}(\%)$	$a'_{\pm}(\%)$
$e-\rho$ (Data)	$(-0.6 \pm 1.2) \times 10^{-1}$	$(3.4 \pm 1.9) \times 10^{-1}$
$e-\rho$ (MC)	$(-0.8 \pm 1.6) \times 10^{-1}$	$(1.9 \pm 2.6) \times 10^{-1}$
$\mu-\rho$ (Data)	$(-0.5 \pm 1.1) \times 10^{-1}$	$(1.4 \pm 1.9) \times 10^{-1}$
$\mu-\rho$ (MC)	$(0.3 \pm 1.5) \times 10^{-1}$	$(4.3 \pm 2.5) \times 10^{-1}$
$e-\pi\pi$ (Data)	$(-1.5 \pm 1.2) \times 10^{-1}$	$(2.6 \pm 1.8) \times 10^{-1}$
$e-\pi\pi$ (MC)	$(-1.5 \pm 1.5) \times 10^{-1}$	$(3.1 \pm 2.3) \times 10^{-1}$
$\mu-\pi\pi$ (Data)	$(-0.8 \pm 1.2) \times 10^{-1}$	$(1.0 \pm 1.8) \times 10^{-1}$
$\mu-\pi\pi$ (MC)	$(0 \pm 1.6) \times 10^{-1}$	$(1.1 \pm 2.3) \times 10^{-1}$
μ–Avg. (Data)	$(-6.3 \pm 7.9) \times 10^{-2}$	$(1.2 \pm 1.3) \times 10^{-1}$
μ–Avg. (MC)	$(0.2 \pm 1.1) \times 10^{-1}$	$(2.6 \pm 1.7) \times 10^{-1}$

Table F.23: The tracking efficiency charge asymmetry, $0.2 < cos(\theta_{avg}^{(lab)}) < 0.6$, for the three different track definitions from the 1930V setting (Stability Study). The average values in this table are the weighted average of the $\mu-\rho$ and $\mu-\pi\pi$ channels as discussed in Chapter 7: Systematic Uncertainty Studies.

Good Tracks Loose		
Decay	$a_{\pm}(\%)$	$a'_{\pm}(\%)$
$e-\rho$ (Data)	$(1.3 \pm 2.8) \times 10^{-1}$	$(1.4 \pm 2.8) \times 10^{-1}$
$e-\rho$ (MC)	$(-0.1 \pm 3.6) \times 10^{-1}$	$(0.4 \pm 3.6) \times 10^{-1}$
$\mu-\rho$ (Data)	$(4.2 \pm 2.8) \times 10^{-1}$	$(3.8 \pm 2.8) \times 10^{-1}$
$\mu-\rho$ (MC)	$(-5.8 \pm 3.7) \times 10^{-1}$	$(-5.9 \pm 3.7) \times 10^{-1}$
$e-\pi\pi$ (Data)	(-3.18 ± 0.26)	(-3.10 ± 0.26)
$e-\pi\pi$ (MC)	$(-2.7 \pm 3.3) \times 10^{-1}$	$(-2.5 \pm 3.4) \times 10^{-1}$
$\mu-\pi\pi$ (Data)	(-1.12 ± 0.26)	(-1.10 ± 0.26)
$\mu-\pi\pi$ (MC)	$(-5.0 \pm 3.4) \times 10^{-1}$	$(-4.7 \pm 3.5) \times 10^{-1}$
μ–Avg. (Data)	$(-4.2 \pm 1.9) \times 10^{-1}$	$(-4.2 \pm 1.9) \times 10^{-1}$
μ–Avg. (MC)	$(-5.4 \pm 2.5) \times 10^{-1}$	$(-5.3 \pm 2.5) \times 10^{-1}$
Good Tracks Very Loose		
Decay	$a_{\pm}(\%)$	$a'_{\pm}(\%)$
$e-\rho$ (Data)	$(1.4 \pm 2.7) \times 10^{-1}$	$(1.9 \pm 2.7) \times 10^{-1}$
$e-\rho$ (MC)	$(-1.5 \pm 3.4) \times 10^{-1}$	$(-0.7 \pm 3.5) \times 10^{-1}$
$\mu-\rho$ (Data)	$(4.4 \pm 2.7) \times 10^{-1}$	$(4.0 \pm 2.7) \times 10^{-1}$
$\mu-\rho$ (MC)	$(-6.8 \pm 3.6) \times 10^{-1}$	$(-6.5 \pm 3.6) \times 10^{-1}$
$e-\pi\pi$ (Data)	(-3.29 ± 0.25)	(-3.20 ± 0.26)
$e-\pi\pi$ (MC)	$(-3.1 \pm 3.2) \times 10^{-1}$	$(-2.8 \pm 3.3) \times 10^{-1}$
$\mu-\pi\pi$ (Data)	(-1.06 ± 0.25)	(-1.09 ± 0.25)
$\mu-\pi\pi$ (MC)	$(-5.5 \pm 3.3) \times 10^{-1}$	$(-4.7 \pm 3.4) \times 10^{-1}$
μ–Avg. (Data)	$(-3.7 \pm 1.8) \times 10^{-1}$	$(-4.0 \pm 1.9) \times 10^{-1}$
μ–Avg. (MC)	$(-6.1 \pm 2.4) \times 10^{-1}$	$(-5.6 \pm 2.5) \times 10^{-1}$
Charged Tracks		
Decay	$a_{\pm}(\%)$	$a'_{\pm}(\%)$
$e-\rho$ (Data)	$(3.8 \pm 1.9) \times 10^{-1}$	$(4.9 \pm 2.2) \times 10^{-1}$
$e-\rho$ (MC)	$(0.1 \pm 2.4) \times 10^{-1}$	$(2.7 \pm 2.9) \times 10^{-1}$
$\mu-\rho$ (Data)	$(5.0 \pm 1.8) \times 10^{-1}$	$(5.7 \pm 2.2) \times 10^{-1}$
$\mu-\rho$ (MC)	$(-1.2 \pm 2.6) \times 10^{-1}$	$(1.7 \pm 3.0) \times 10^{-1}$
$e-\pi\pi$ (Data)	(-2.55 ± 0.19)	(-2.30 ± 0.21)
$e-\pi\pi$ (MC)	$(-1.3 \pm 2.5) \times 10^{-1}$	$(1.1 \pm 2.8) \times 10^{-1}$
$\mu-\pi\pi$ (Data)	$(-6.7 \pm 1.8) \times 10^{-1}$	$(-7.9 \pm 2.1) \times 10^{-1}$
$\mu-\pi\pi$ (MC)	$(-3.7 \pm 2.5) \times 10^{-1}$	$(0.5 \pm 2.9) \times 10^{-1}$
μ–Avg. (Data)	$(-0.8 \pm 1.3) \times 10^{-1}$	$(-1.4 \pm 1.5) \times 10^{-1}$
μ–Avg. (MC)	$(-2.4 \pm 1.8) \times 10^{-1}$	$(1.1 \pm 2.1) \times 10^{-1}$

Table F.24: The tracking efficiency charge asymmetry, $0.6 < cos(\theta_{avg}^{(lab)})$, for the three different track definitions from the 1930V setting (Stability Study). The average values in this table are the weighted average of the $\mu-\rho$ and $\mu-\pi\pi$ channels as discussed in Chapter 7: Systematic Uncertainty Studies.

Good Tracks Loose		
Decay	$a_{\pm}(\%)$	$a'_{\pm}(\%)$
$e-\rho$ (Data)	$(-2.1 \pm 2.7) \times 10^{-1}$	$(-1.8 \pm 2.8) \times 10^{-1}$
$e-\rho$ (MC)	$(-1.1 \pm 3.5) \times 10^{-1}$	$(-1.2 \pm 3.6) \times 10^{-1}$
$\mu-\rho$ (Data)	$(-3.5 \pm 2.9) \times 10^{-1}$	$(-3.7 \pm 2.9) \times 10^{-1}$
$\mu-\rho$ (MC)	$(-1.6 \pm 3.7) \times 10^{-1}$	$(-2.5 \pm 3.7) \times 10^{-1}$
$e-\pi\pi$ (Data)	$(-9.2 \pm 2.5) \times 10^{-1}$	(-1.02 ± 0.26)
$e-\pi\pi$ (MC)	$(2.4 \pm 3.3) \times 10^{-1}$	$(2.5 \pm 3.3) \times 10^{-1}$
$\mu-\pi\pi$ (Data)	$(-2.3 \pm 2.5) \times 10^{-1}$	$(-1.9 \pm 2.5) \times 10^{-1}$
$\mu-\pi\pi$ (MC)	$(0.3 \pm 3.3) \times 10^{-1}$	$(0.7 \pm 3.4) \times 10^{-1}$
μ–Avg. (Data)	$(-2.8 \pm 1.9) \times 10^{-1}$	$(-2.7 \pm 1.9) \times 10^{-1}$
μ–Avg. (MC)	$(-0.5 \pm 2.5) \times 10^{-1}$	$(-0.8 \pm 2.5) \times 10^{-1}$
Good Tracks Very Loose		
Decay	$a_{\pm}(\%)$	$a'_{\pm}(\%)$
$e-\rho$ (Data)	$(-2.0 \pm 2.6) \times 10^{-1}$	$(-1.7 \pm 2.6) \times 10^{-1}$
$e-\rho$ (MC)	$(-2.0 \pm 3.4) \times 10^{-1}$	$(-1.7 \pm 3.4) \times 10^{-1}$
$\mu-\rho$ (Data)	$(-2.6 \pm 2.7) \times 10^{-1}$	$(-2.6 \pm 2.7) \times 10^{-1}$
$\mu-\rho$ (MC)	$(-1.8 \pm 3.5) \times 10^{-1}$	$(-3.1 \pm 3.5) \times 10^{-1}$
$e-\pi\pi$ (Data)	$(-9.6 \pm 2.4) \times 10^{-1}$	(-1.02 ± 0.25)
$e-\pi\pi$ (MC)	$(1.9 \pm 3.1) \times 10^{-1}$	$(1.8 \pm 3.2) \times 10^{-1}$
$\mu-\pi\pi$ (Data)	$(-0.7 \pm 2.4) \times 10^{-1}$	$(0 \pm 2.4) \times 10^{-1}$
$\mu-\pi\pi$ (MC)	$(-0.4 \pm 3.2) \times 10^{-1}$	$(-0.1 \pm 3.3) \times 10^{-1}$
μ–Avg. (Data)	$(-1.5 \pm 1.8) \times 10^{-1}$	$(-1.1 \pm 1.8) \times 10^{-1}$
μ–Avg. (MC)	$(-1.1 \pm 2.4) \times 10^{-1}$	$(-1.4 \pm 2.4) \times 10^{-1}$
Charged Tracks		
Decay	$a_{\pm}(\%)$	$a'_{\pm}(\%)$
$e-\rho$ (Data)	$(-0.8 \pm 1.7) \times 10^{-1}$	$(-0.1 \pm 2.1) \times 10^{-1}$
$e-\rho$ (MC)	$(1.1 \pm 2.2) \times 10^{-1}$	$(1.2 \pm 2.8) \times 10^{-1}$
$\mu-\rho$ (Data)	$(-0.5 \pm 1.6) \times 10^{-1}$	$(0.8 \pm 2.2) \times 10^{-1}$
$\mu-\rho$ (MC)	$(-0.2 \pm 2.2) \times 10^{-1}$	$(2.2 \pm 2.9) \times 10^{-1}$
$e-\pi\pi$ (Data)	$(-8.0 \pm 1.7) \times 10^{-1}$	$(-5.5 \pm 2.1) \times 10^{-1}$
$e-\pi\pi$ (MC)	$(0.8 \pm 2.2) \times 10^{-1}$	$(3.6 \pm 2.7) \times 10^{-1}$
$\mu-\pi\pi$ (Data)	$(-1.6 \pm 1.6) \times 10^{-1}$	$(-0.9 \pm 2.0) \times 10^{-1}$
$\mu-\pi\pi$ (MC)	$(0.2 \pm 2.2) \times 10^{-1}$	$(3.9 \pm 2.7) \times 10^{-1}$
μ–Avg. (Data)	$(-1.1 \pm 1.1) \times 10^{-1}$	$(-0.1 \pm 1.5) \times 10^{-1}$
μ–Avg. (MC)	$(0 \pm 1.5) \times 10^{-1}$	$(3.1 \pm 2.0) \times 10^{-1}$

Table F.25: The tracking efficiency charge asymmetry, $\phi_{avg}^{(lab)} < -1.046$, for the three different track definitions from the 1930V setting (Stability Study). The average values in this table are the weighted average of the $\mu-\rho$ and $\mu-\pi\pi$ channels as discussed in Chapter 7: Systematic Uncertainty Studies.

Good Tracks Loose		
Decay	$a_{\pm}(\%)$	$a'_{\pm}(\%)$
$e-\rho$ (Data)	$(-1.1 \pm 2.9) \times 10^{-1}$	$(-0.2 \pm 3.0) \times 10^{-1}$
$e-\rho$ (MC)	$(0 \pm 3.6) \times 10^{-1}$	$(0.4 \pm 3.6) \times 10^{-1}$
$\mu-\rho$ (Data)	$(6.6 \pm 2.9) \times 10^{-1}$	$(6.1 \pm 2.9) \times 10^{-1}$
$\mu-\rho$ (MC)	$(4.0 \pm 3.6) \times 10^{-1}$	$(4.5 \pm 3.6) \times 10^{-1}$
$e-\pi\pi$ (Data)	$(-8.6 \pm 2.6) \times 10^{-1}$	(-1.05 ± 0.27)
$e-\pi\pi$ (MC)	$(-2.9 \pm 3.3) \times 10^{-1}$	$(-3.0 \pm 3.3) \times 10^{-1}$
$\mu-\pi\pi$ (Data)	$(-2.8 \pm 2.5) \times 10^{-1}$	$(-2.5 \pm 2.6) \times 10^{-1}$
$\mu-\pi\pi$ (MC)	$(-3.8 \pm 3.4) \times 10^{-1}$	$(-3.8 \pm 3.4) \times 10^{-1}$
μ–Avg. (Data)	$(1.3 \pm 1.9) \times 10^{-1}$	$(1.3 \pm 1.9) \times 10^{-1}$
μ–Avg. (MC)	$(-0.2 \pm 2.4) \times 10^{-1}$	$(0.1 \pm 2.5) \times 10^{-1}$
Good Tracks Very Loose		
Decay	$a_{\pm}(\%)$	$a'_{\pm}(\%)$
$e-\rho$ (Data)	$(-2.2 \pm 2.7) \times 10^{-1}$	$(-1.6 \pm 2.8) \times 10^{-1}$
$e-\rho$ (MC)	$(0.3 \pm 3.4) \times 10^{-1}$	$(0.6 \pm 3.5) \times 10^{-1}$
$\mu-\rho$ (Data)	$(6.4 \pm 2.7) \times 10^{-1}$	$(6.2 \pm 2.8) \times 10^{-1}$
$\mu-\rho$ (MC)	$(2.8 \pm 3.4) \times 10^{-1}$	$(3.2 \pm 3.5) \times 10^{-1}$
$e-\pi\pi$ (Data)	$(-9.6 \pm 2.5) \times 10^{-1}$	(-1.16 ± 0.26)
$e-\pi\pi$ (MC)	$(-2.9 \pm 3.2) \times 10^{-1}$	$(-2.3 \pm 3.3) \times 10^{-1}$
$\mu-\pi\pi$ (Data)	$(-2.6 \pm 2.4) \times 10^{-1}$	$(-2.3 \pm 2.5) \times 10^{-1}$
$\mu-\pi\pi$ (MC)	$(-4.4 \pm 3.2) \times 10^{-1}$	$(-3.9 \pm 3.3) \times 10^{-1}$
μ–Avg. (Data)	$(1.4 \pm 1.8) \times 10^{-1}$	$(1.5 \pm 1.8) \times 10^{-1}$
μ–Avg. (MC)	$(-1.0 \pm 2.3) \times 10^{-1}$	$(-0.5 \pm 2.4) \times 10^{-1}$
Charged Tracks		
Decay	$a_{\pm}(\%)$	$a'_{\pm}(\%)$
$e-\rho$ (Data)	$(0.4 \pm 1.8) \times 10^{-1}$	$(5.0 \pm 2.3) \times 10^{-1}$
$e-\rho$ (MC)	$(0.1 \pm 2.2) \times 10^{-1}$	$(3.6 \pm 2.9) \times 10^{-1}$
$\mu-\rho$ (Data)	$(3.6 \pm 1.6) \times 10^{-1}$	$(4.9 \pm 2.2) \times 10^{-1}$
$\mu-\rho$ (MC)	$(2.3 \pm 2.2) \times 10^{-1}$	$(6.3 \pm 2.9) \times 10^{-1}$
$e-\pi\pi$ (Data)	$(-7.8 \pm 1.7) \times 10^{-1}$	$(-8.6 \pm 2.1) \times 10^{-1}$
$e-\pi\pi$ (MC)	$(-2.7 \pm 2.2) \times 10^{-1}$	$(-0.1 \pm 2.7) \times 10^{-1}$
$\mu-\pi\pi$ (Data)	$(-3.0 \pm 1.6) \times 10^{-1}$	$(-2.0 \pm 2.1) \times 10^{-1}$
$\mu-\pi\pi$ (MC)	$(-4.0 \pm 2.3) \times 10^{-1}$	$(-0.7 \pm 2.8) \times 10^{-1}$
μ–Avg. (Data)	$(0.3 \pm 1.1) \times 10^{-1}$	$(1.2 \pm 1.5) \times 10^{-1}$
μ–Avg. (MC)	$(-0.7 \pm 1.6) \times 10^{-1}$	$(2.7 \pm 2.0) \times 10^{-1}$

Table F.26: The tracking efficiency charge asymmetry, $1.046\phi_{avg}^{(lab)} < 1.046$, for the three different track definitions from the 1930V setting (Stability Study). The average values in this table are the weighted average of the $\mu-\rho$ and $\mu-\pi\pi$ channels as discussed in Chapter 7: Systematic Uncertainty Studies.

Good Tracks Loose		
Decay	$a_{\pm}(\%)$	$a'_{\pm}(\%)$
$e-\rho$ (Data)	$(1.8 \pm 2.8) \times 10^{-1}$	$(1.7 \pm 2.8) \times 10^{-1}$
$e-\rho$ (MC)	$(3.5 \pm 3.5) \times 10^{-1}$	$(4.3 \pm 3.6) \times 10^{-1}$
$\mu-\rho$ (Data)	$(1.6 \pm 2.8) \times 10^{-1}$	$(2.4 \pm 2.8) \times 10^{-1}$
$\mu-\rho$ (MC)	$(-6.1 \pm 3.5) \times 10^{-1}$	$(-5.9 \pm 3.6) \times 10^{-1}$
$e-\pi\pi$ (Data)	(-1.11 ± 0.25)	(-1.18 ± 0.26)
$e-\pi\pi$ (MC)	$(-4.0 \pm 3.2) \times 10^{-1}$	$(-3.5 \pm 3.2) \times 10^{-1}$
$\mu-\pi\pi$ (Data)	$(-9.0 \pm 2.5) \times 10^{-1}$	$(-8.5 \pm 2.5) \times 10^{-1}$
$\mu-\pi\pi$ (MC)	$(-2.1 \pm 3.2) \times 10^{-1}$	$(-2.8 \pm 3.2) \times 10^{-1}$
μ–Avg. (Data)	$(-4.3 \pm 1.8) \times 10^{-1}$	$(-3.6 \pm 1.9) \times 10^{-1}$
μ–Avg. (MC)	$(-3.9 \pm 2.4) \times 10^{-1}$	$(-4.2 \pm 2.4) \times 10^{-1}$
Good Tracks Very Loose		
Decay	$a_{\pm}(\%)$	$a'_{\pm}(\%)$
$e-\rho$ (Data)	$(2.0 \pm 2.6) \times 10^{-1}$	$(1.4 \pm 2.7) \times 10^{-1}$
$e-\rho$ (MC)	$(2.9 \pm 3.4) \times 10^{-1}$	$(3.9 \pm 3.4) \times 10^{-1}$
$\mu-\rho$ (Data)	$(0.2 \pm 2.6) \times 10^{-1}$	$(0.2 \pm 2.6) \times 10^{-1}$
$\mu-\rho$ (MC)	$(-5.2 \pm 3.4) \times 10^{-1}$	$(-5.0 \pm 3.4) \times 10^{-1}$
$e-\pi\pi$ (Data)	(-1.20 ± 0.24)	(-1.22 ± 0.25)
$e-\pi\pi$ (MC)	$(-3.9 \pm 3.1) \times 10^{-1}$	$(-3.5 \pm 3.2) \times 10^{-1}$
$\mu-\pi\pi$ (Data)	$(-7.4 \pm 2.4) \times 10^{-1}$	$(-6.9 \pm 2.4) \times 10^{-1}$
$\mu-\pi\pi$ (MC)	$(-1.8 \pm 3.1) \times 10^{-1}$	$(-2.5 \pm 3.2) \times 10^{-1}$
μ–Avg. (Data)	$(-3.9 \pm 1.7) \times 10^{-1}$	$(-3.6 \pm 1.8) \times 10^{-1}$
μ–Avg. (MC)	$(-3.4 \pm 2.3) \times 10^{-1}$	$(-3.6 \pm 2.3) \times 10^{-1}$
Charged Tracks		
Decay	$a_{\pm}(\%)$	$a'_{\pm}(\%)$
$e-\rho$ (Data)	$(3.4 \pm 1.7) \times 10^{-1}$	$(3.7 \pm 2.2) \times 10^{-1}$
$e-\rho$ (MC)	$(0.2 \pm 2.1) \times 10^{-1}$	$(4.2 \pm 2.8) \times 10^{-1}$
$\mu-\rho$ (Data)	$(1.4 \pm 1.6) \times 10^{-1}$	$(3.4 \pm 2.2) \times 10^{-1}$
$\mu-\rho$ (MC)	$(-1.5 \pm 2.1) \times 10^{-1}$	$(-0.3 \pm 2.9) \times 10^{-1}$
$e-\pi\pi$ (Data)	(-1.03 ± 0.17)	$(-8.5 \pm 2.1) \times 10^{-1}$
$e-\pi\pi$ (MC)	$(-0.4 \pm 2.1) \times 10^{-1}$	$(1.9 \pm 2.6) \times 10^{-1}$
$\mu-\pi\pi$ (Data)	$(-3.5 \pm 1.6) \times 10^{-1}$	$(-2.3 \pm 2.0) \times 10^{-1}$
$\mu-\pi\pi$ (MC)	$(-1.3 \pm 2.1) \times 10^{-1}$	$(-0.2 \pm 2.6) \times 10^{-1}$
μ–Avg. (Data)	$(-1.0 \pm 1.1) \times 10^{-1}$	$(0.4 \pm 1.5) \times 10^{-1}$
μ–Avg. (MC)	$(-1.4 \pm 1.5) \times 10^{-1}$	$(-0.3 \pm 1.9) \times 10^{-1}$

Table F.27: The tracking efficiency charge asymmetry, $1.046 < \phi_{avg}^{(lab)}$, for the three different track definitions from the 1930V setting (Stability Study). The average values in this table are the weighted average of the $\mu-\rho$ and $\mu-\pi\pi$ channels as discussed in Chapter 7: Systematic Uncertainty Studies.

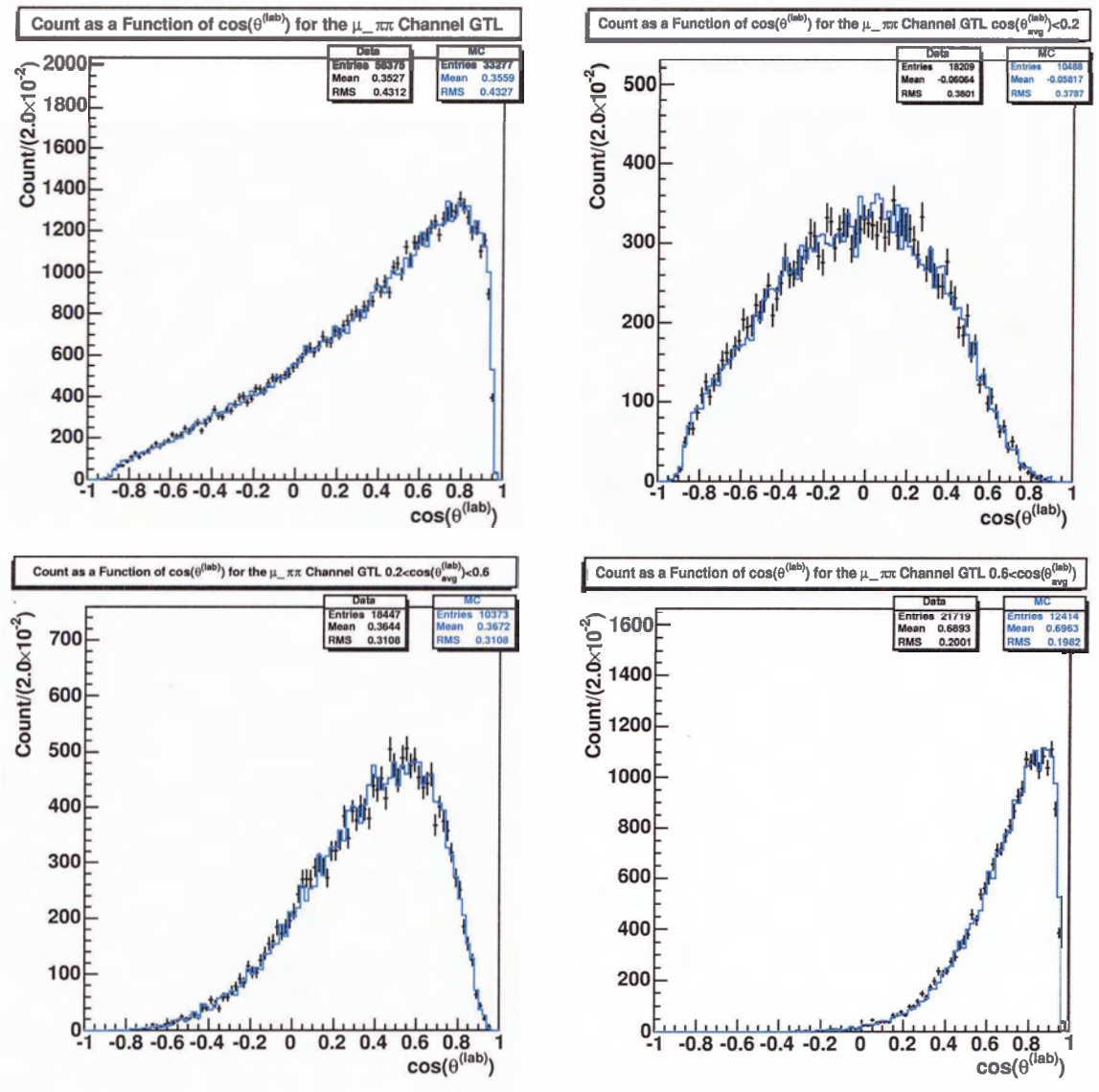

Figure F.1: Plots of $\theta^{(lab)}$ of the 4th track in the GTL $\mu - \pi\pi$ channel for the entire distribution and three bin in $\theta_{avg}^{(lab)}$: $\theta_{avg}^{(lab)} < 0.2$, $0.2 < \theta_{avg}^{(lab)} < 0.6$ and $0.6 < \theta_{avg}^{(lab)}$.

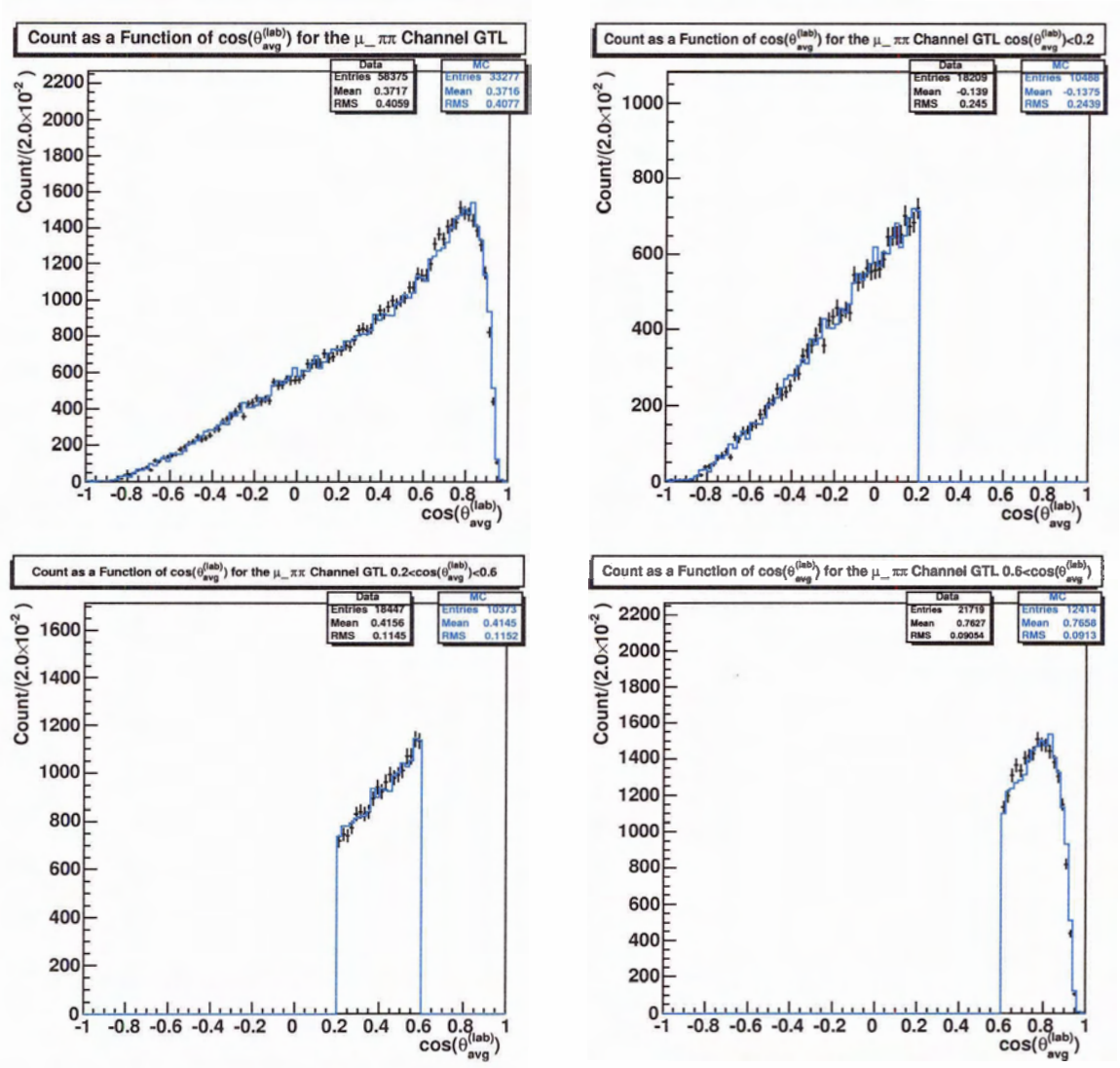

Figure F.2: Plots of $\theta_{avg}^{(lab)}$ of the 4th track in the GTL $\mu - \pi\pi$ channel for the entire distribution and three bin in $\theta_{avg}^{(lab)}$: $\theta_{avg}^{(lab)} < 0.2$, $0.2 < \theta_{avg}^{(lab)} < 0.6$ and $0.6 < \theta_{avg}^{(lab)}$.

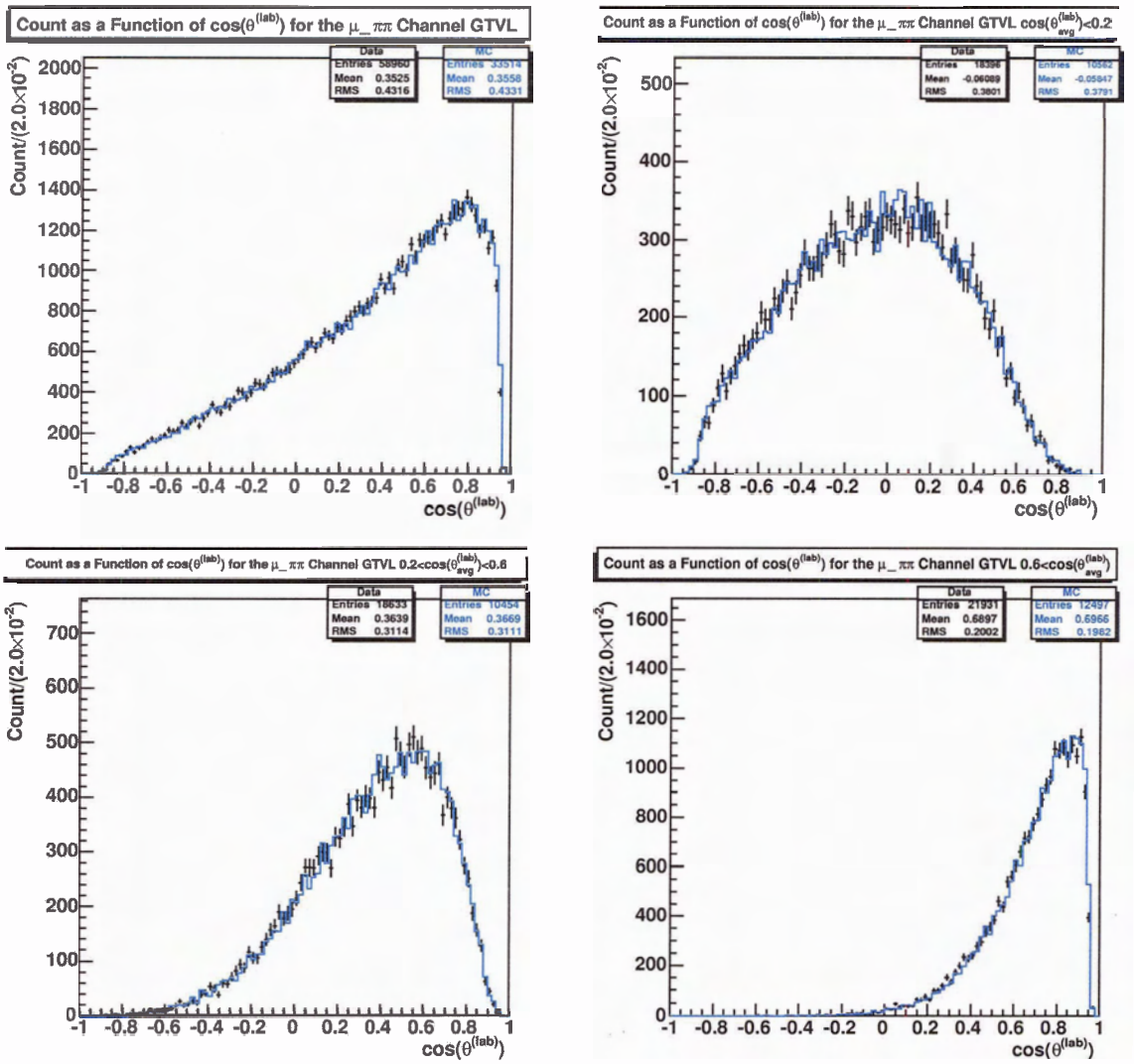

Figure F.3: Plots of $\theta^{(lab)}$ of the 4th track in the GTVL $\mu - \pi\pi$ channel for the entire distribution and three bin in $\theta_{avg}^{(lab)}$: $\theta_{avg}^{(lab)} < 0.2$, $0.2 < \theta_{avg}^{(lab)} < 0.6$ and $0.6 < \theta_{avg}^{(lab)}$.

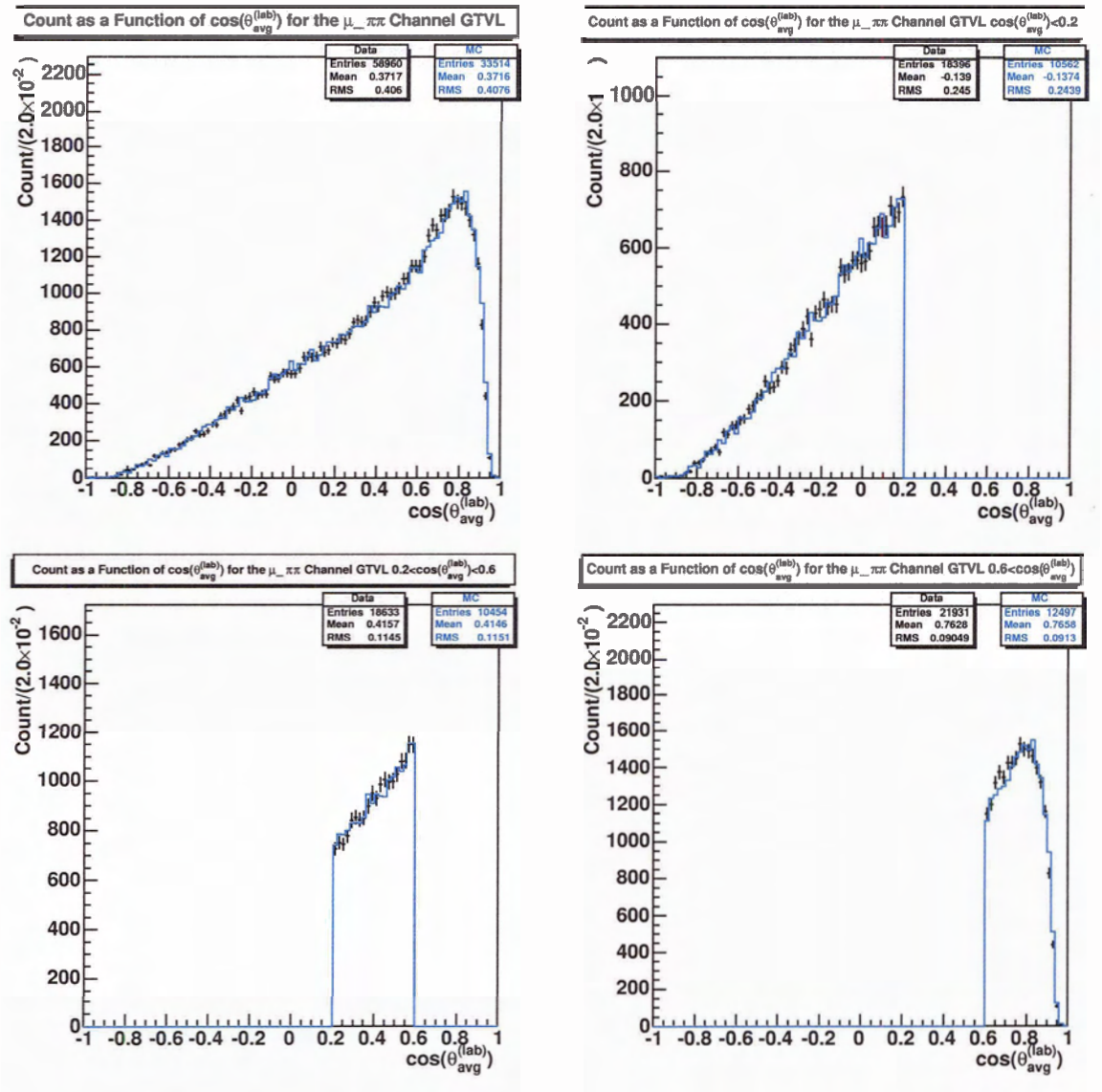

Figure F.4: Plots of $\theta_{avg}^{(lab)}$ of the 4th track in the GTVL $\mu - \pi\pi$ channel for the entire distribution and three bin in $\theta_{avg}^{(lab)}$: $\theta_{avg}^{(lab)} < 0.2$, $0.2 < \theta_{avg}^{(lab)} < 0.6$ and $0.6 < \theta_{avg}^{(lab)}$.

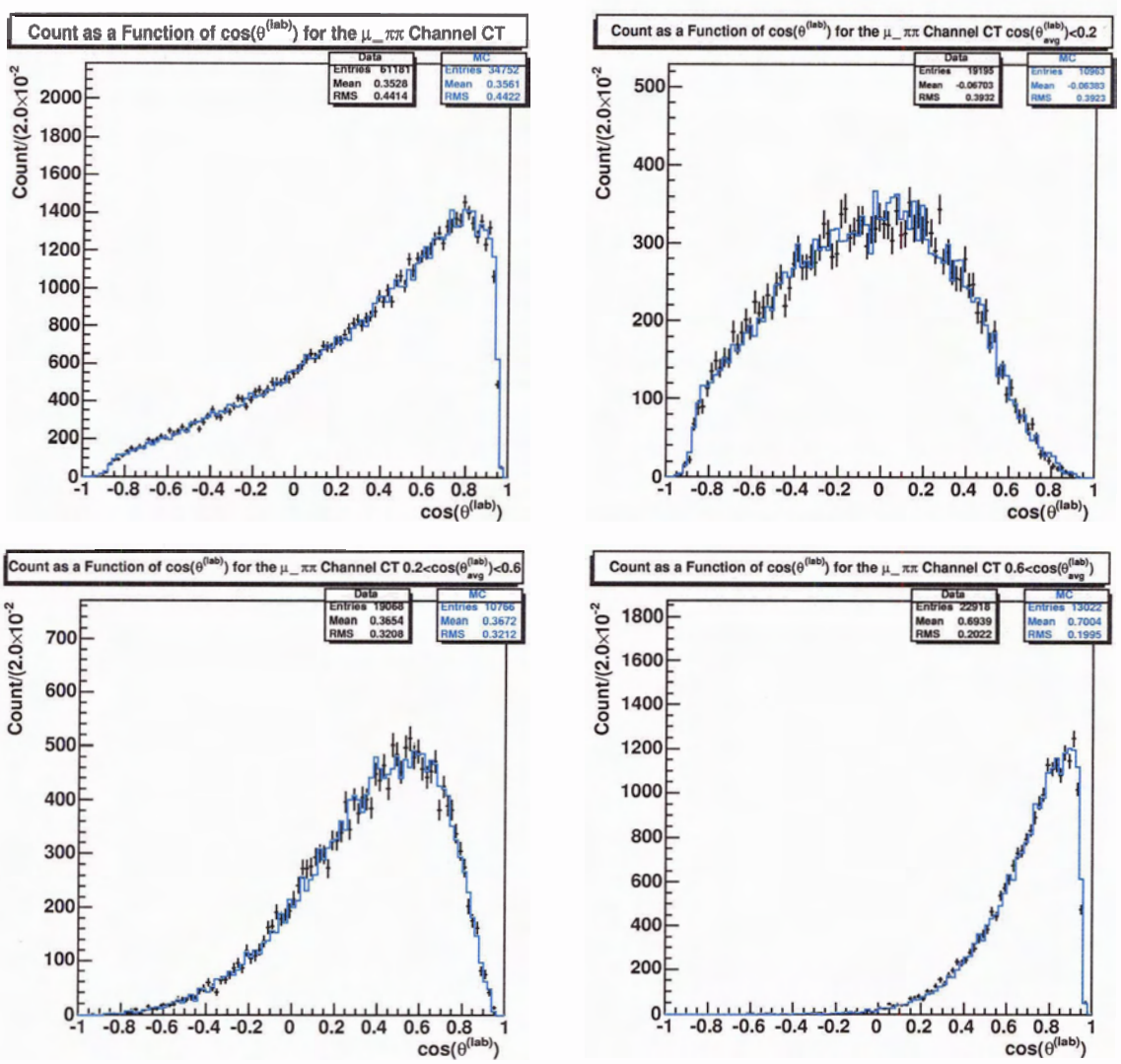

Figure F.5: Plots of $\theta^{(lab)}$ of the 4th track in the CT $\mu-\pi\pi$ channel for the entire distribution and three bin in $\theta_{avg}^{(lab)}$: $\theta_{avg}^{(lab)} < 0.2$, $0.2 < \theta_{avg}^{(lab)} < 0.6$ and $0.6 < \theta_{avg}^{(lab)}$.

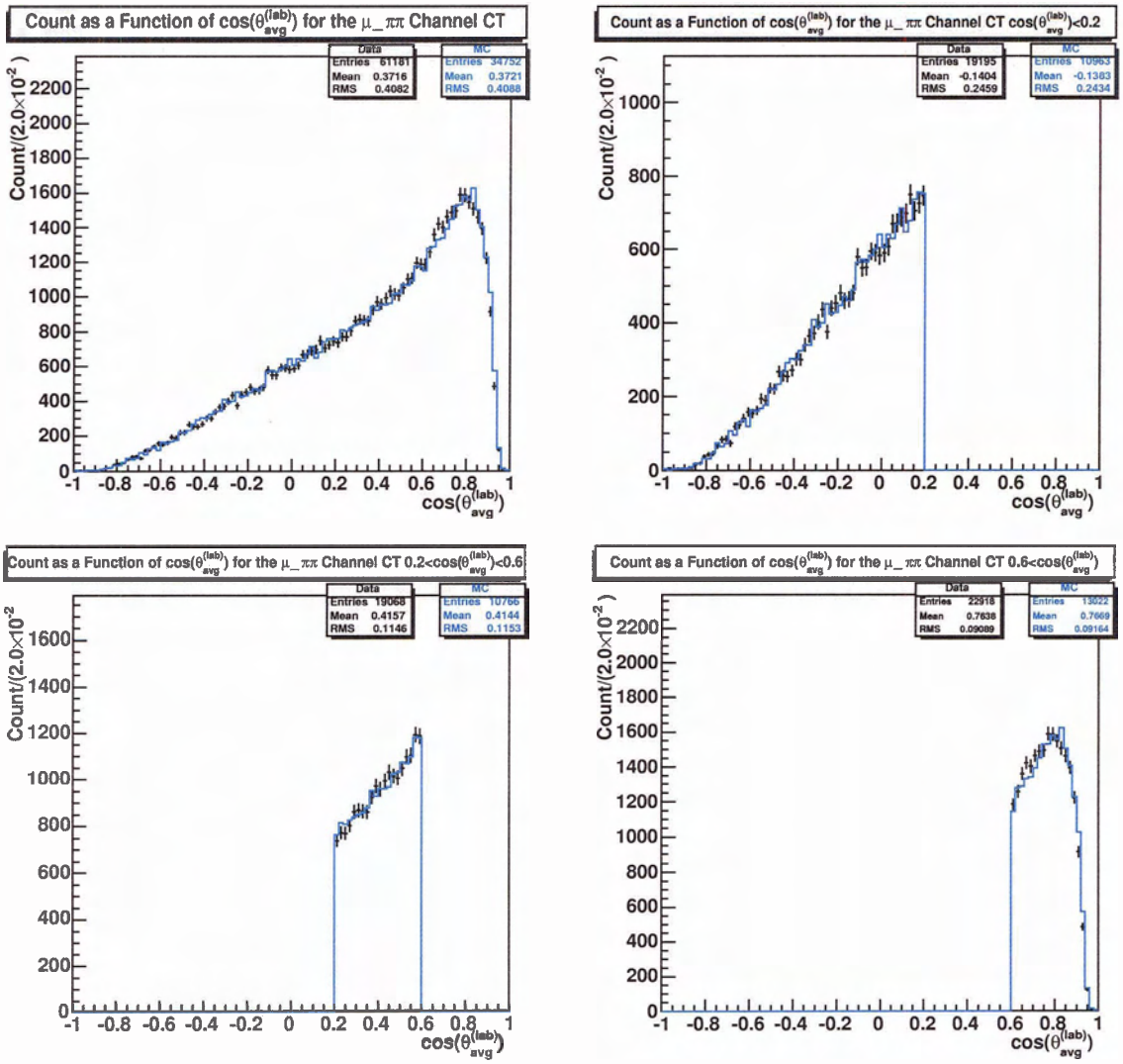

Figure F.6: Plots of $\theta_{avg}^{(lab)}$ of the 4th track in the CT $\mu-\pi\pi$ channel for the entire distribution and three bin in $\theta_{avg}^{(lab)}$: $\theta_{avg}^{(lab)} < 0.2$, $0.2 < \theta_{avg}^{(lab)} < 0.6$ and $0.6 < \theta_{avg}^{(lab)}$.

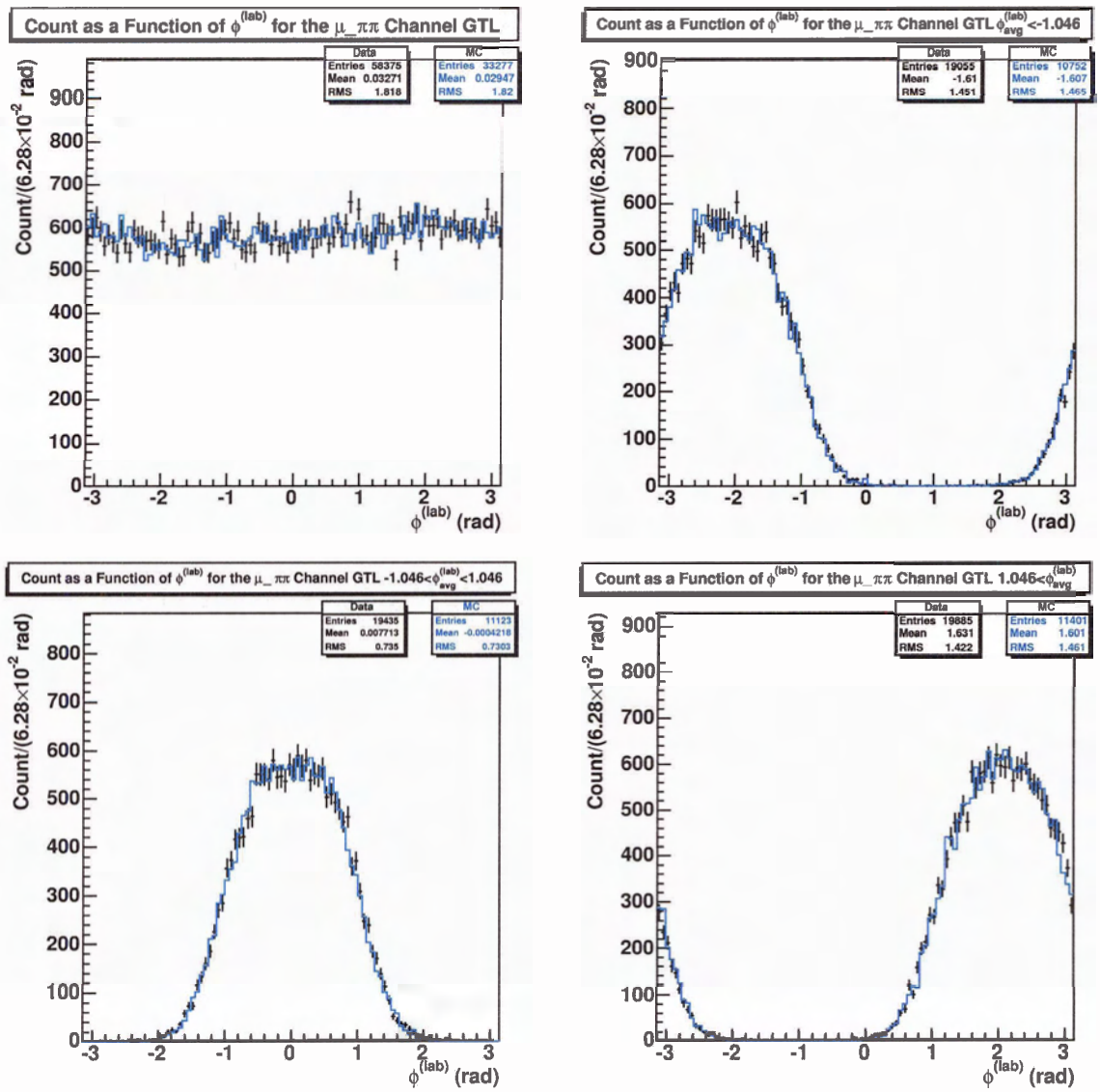

Figure F.7: Plots of $\phi^{(lab)}$ of the 4th track in the GTL $\mu - \pi\pi$ channel for the entire distribution and three bin in $\phi^{(lab)}_{avg}$: $\phi^{(lab)}_{avg} < -1.046$rad, $-1.046\text{rad} < \phi^{(lab)}_{avg} < 1.046$rad and $1.046\text{rad} < \phi^{(lab)}_{avg}$.

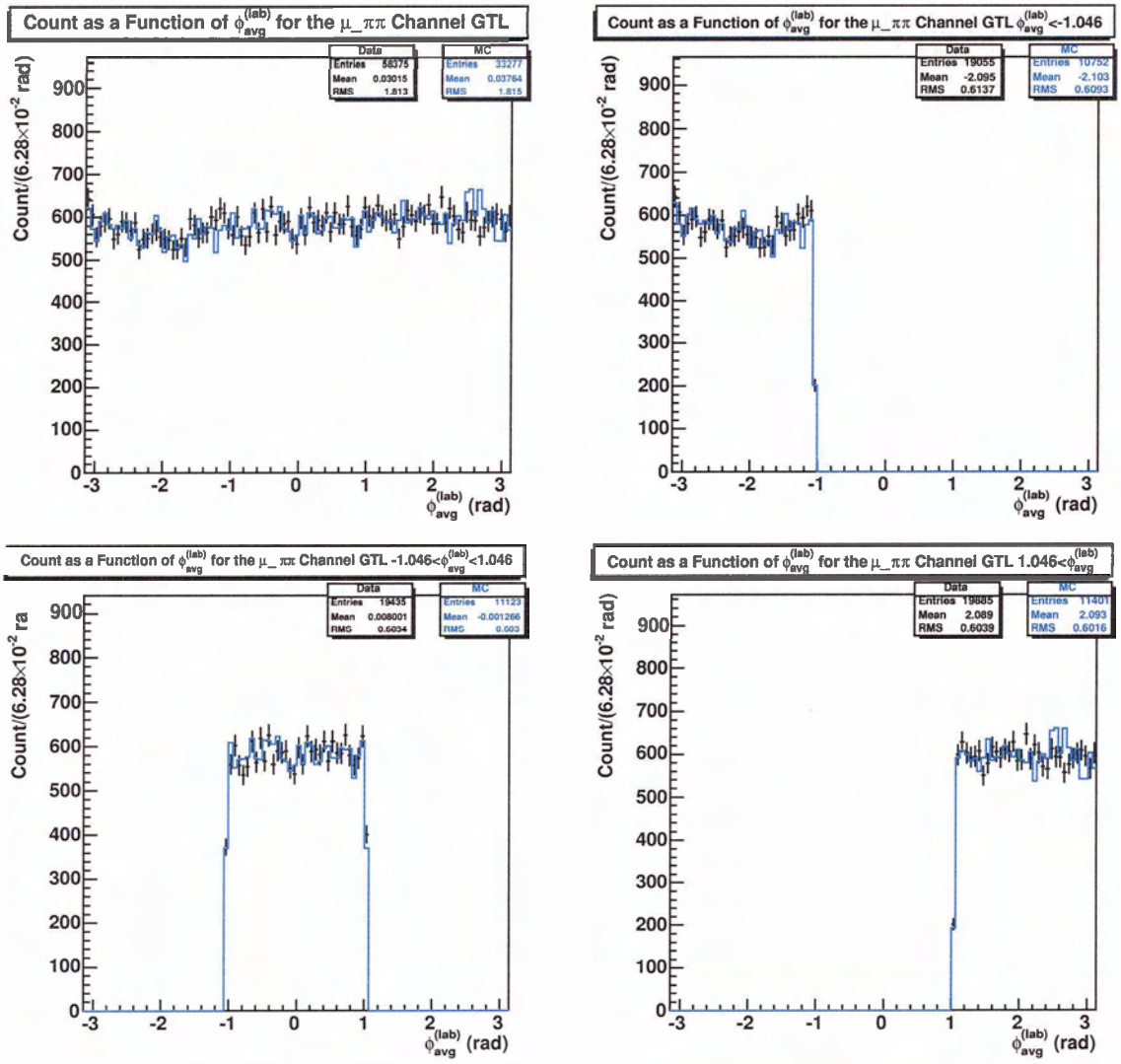

Figure F.8: Plots of $\phi_{avg}^{(lab)}$ of the 4th track in the GTL $\mu - \pi\pi$ channel for the entire distribution and three bin in $\phi_{avg}^{(lab)}$: $\phi_{avg}^{(lab)} < -1.046$rad, $-1.046\text{rad} < \phi_{avg}^{(lab)} < 1.046$rad and $1.046\text{rad} < \phi_{avg}^{(lab)}$.

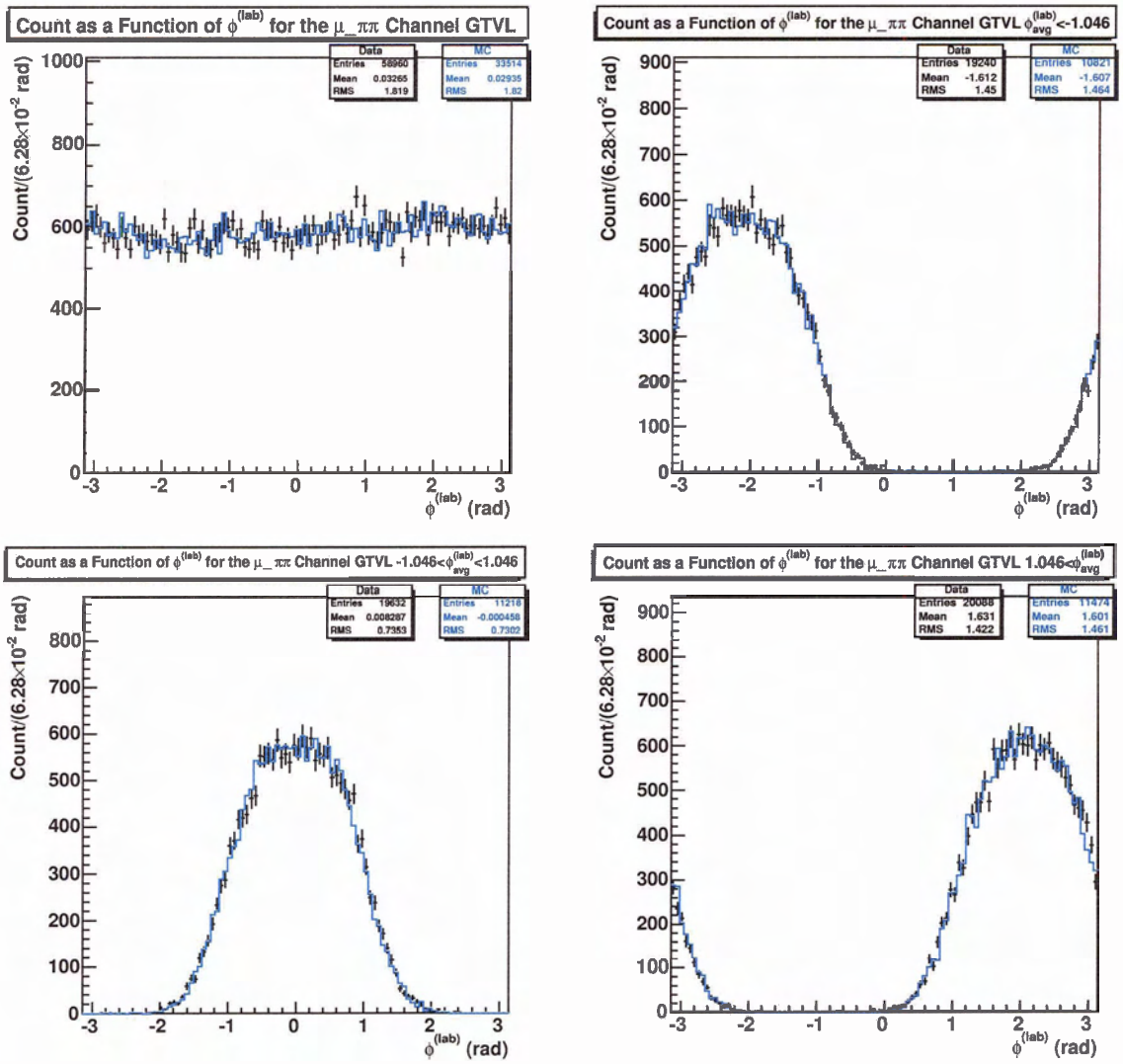

Figure F.9: Plots of $\phi^{(lab)}$ of the 4th track in the GTVL $\mu - \pi\pi$ channel for the entire distribution and three bin in $\phi^{(lab)}_{avg}$: $\phi^{(lab)}_{avg} < -1.046$rad, $-1.046\text{rad} < \phi^{(lab)}_{avg} < 1.046$rad and $1.046\text{rad} < \phi^{(lab)}_{avg}$.

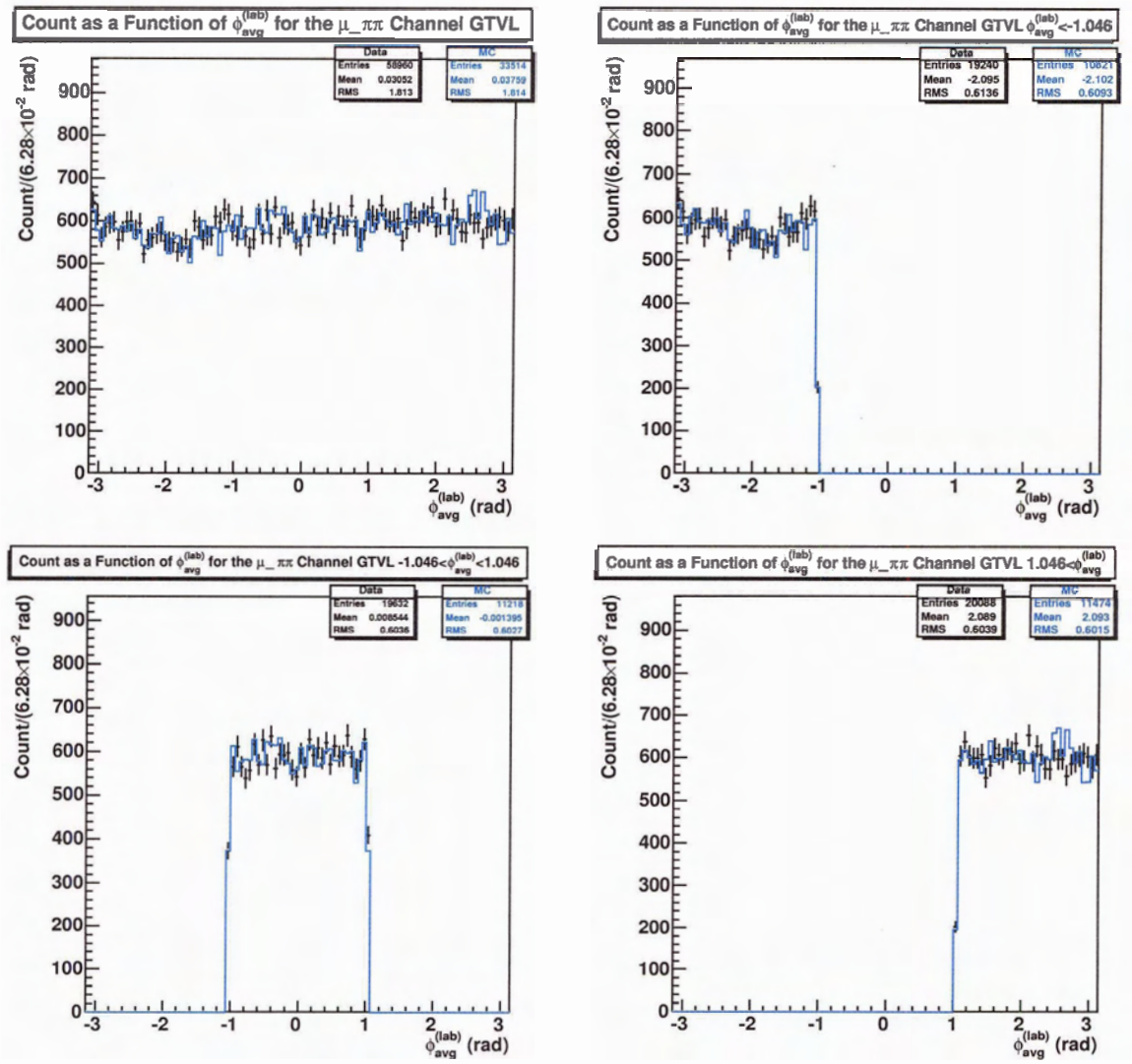

Figure F.10: Plots of $\phi_{avg}^{(lab)}$ of the 4th track in the GTVL $\mu - \pi\pi$ channel for the entire distribution and three bin in $\phi_{avg}^{(lab)}$: $\phi_{avg}^{(lab)} < -1.046$rad, $-1.046\text{rad} < \phi_{avg}^{(lab)} < 1.046$rad and $1.046\text{rad} < \phi_{avg}^{(lab)}$.

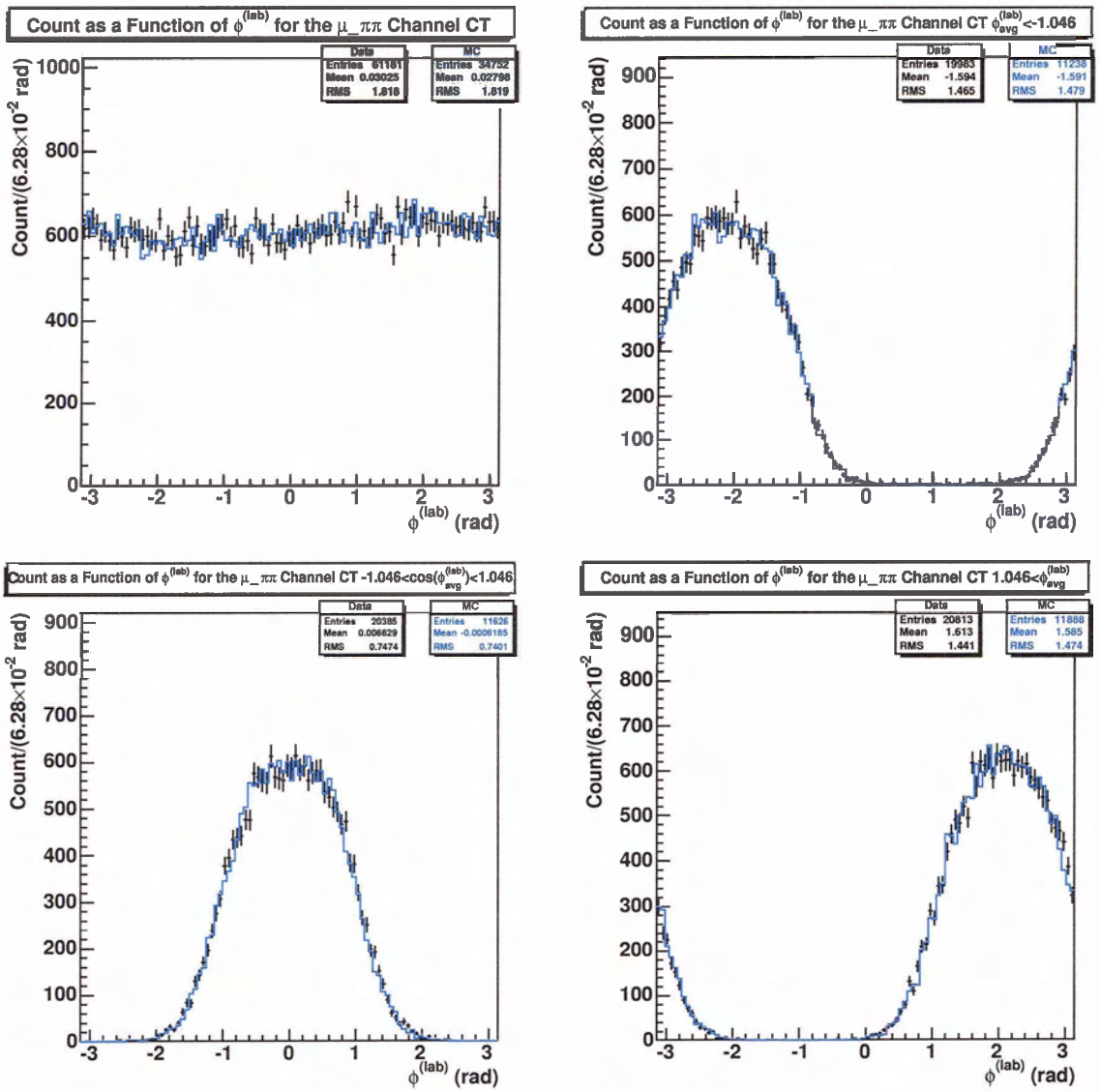

Figure F.11: Plots of $\phi^{(lab)}$ of the 4th track in the CT $\mu - \pi\pi$ channel for the entire distribution and three bin in $\phi^{(lab)}_{avg}$: $\phi^{(lab)}_{avg} < -1.046$rad, $-1.046\text{rad} < \phi^{(lab)}_{avg} < 1.046$rad and $1.046\text{rad} < \phi^{(lab)}_{avg}$.

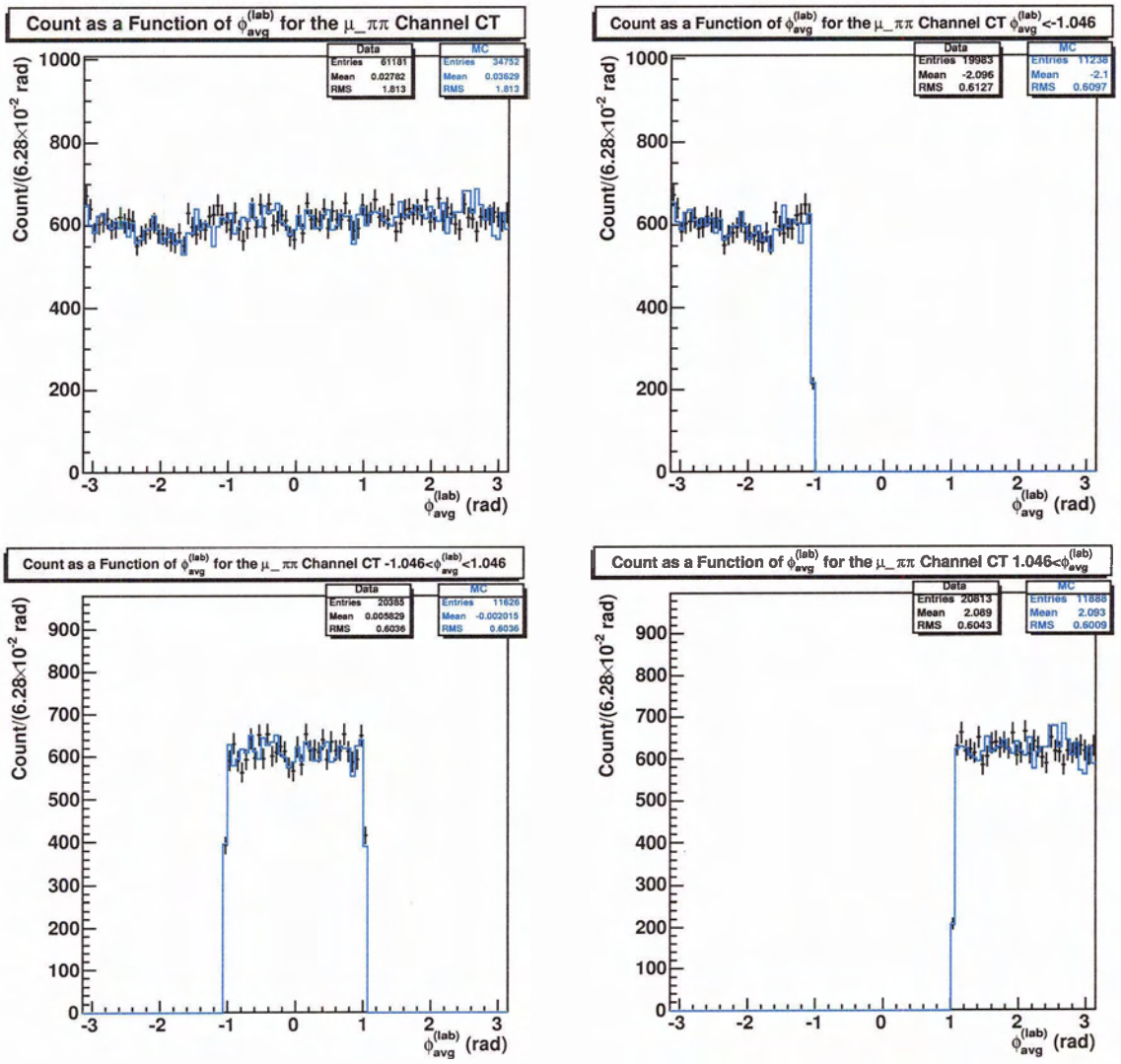

Figure F.12: Plots of $\phi_{avg}^{(lab)}$ of the 4th track in the CT $\mu - \pi\pi$ channel for the entire distribution and three bin in $\phi_{avg}^{(lab)}$: $\phi_{avg}^{(lab)} < -1.046$rad, $-1.046\text{rad} < \phi_{avg}^{(lab)} < 1.046$rad and $1.046\text{rad} < \phi_{avg}^{(lab)}$.

Appendix G: Efficiency in Central Detector Region

Good Tracks Loose		
Decay	$\epsilon \times A(\%)$	$\epsilon' \times A(\%)$
$e-\rho$ (Data)	$(7.71 \pm 0.15) \times 10^1$	$(7.70 \pm 0.15) \times 10^1$
$e-\rho$ (MC)	$(7.76 \pm 0.20) \times 10^1$	$(7.74 \pm 0.20) \times 10^1$
$\mu-\rho$ (Data)	$(7.53 \pm 0.16) \times 10^1$	$(7.50 \pm 0.16) \times 10^1$
$\mu-\rho$ (MC)	$(8.03 \pm 0.19) \times 10^1$	$(8.03 \pm 0.19) \times 10^1$
$e-\pi\pi$ (Data)	$(6.61 \pm 0.17) \times 10^1$	$(6.59 \pm 0.17) \times 10^1$
$e-\pi\pi$ (MC)	$(6.78 \pm 0.26) \times 10^1$	$(6.77 \pm 0.26) \times 10^1$
$\mu-\pi\pi$ (Data)	$(7.14 \pm 0.19) \times 10^1$	$(7.13 \pm 0.19) \times 10^1$
$\mu-\pi\pi$ (MC)	$(6.88 \pm 0.25) \times 10^1$	$(6.87 \pm 0.25) \times 10^1$
μ–Avg. (Data)	$(7.37 \pm 0.12) \times 10^1$	$(7.35 \pm 0.12) \times 10^1$
μ–Avg. (MC)	$(7.61 \pm 0.15) \times 10^1$	$(7.60 \pm 0.15) \times 10^1$
Good Tracks Very Loose		
Decay	$\epsilon \times A(\%)$	$\epsilon' \times A(\%)$
$e-\rho$ (Data)	$(7.92 \pm 0.15) \times 10^1$	$(7.90 \pm 0.15) \times 10^1$
$e-\rho$ (MC)	$(7.85 \pm 0.19) \times 10^1$	$(7.83 \pm 0.19) \times 10^1$
$\mu-\rho$ (Data)	$(7.70 \pm 0.16) \times 10^1$	$(7.64 \pm 0.16) \times 10^1$
$\mu-\rho$ (MC)	$(8.19 \pm 0.19) \times 10^1$	$(8.18 \pm 0.19) \times 10^1$
$e-\pi\pi$ (Data)	$(6.77 \pm 0.17) \times 10^1$	$(6.72 \pm 0.17) \times 10^1$
$e-\pi\pi$ (MC)	$(6.92 \pm 0.26) \times 10^1$	$(6.90 \pm 0.26) \times 10^1$
$\mu-\pi\pi$ (Data)	$(7.34 \pm 0.18) \times 10^1$	$(7.30 \pm 0.19) \times 10^1$
$\mu-\pi\pi$ (MC)	$(7.09 \pm 0.25) \times 10^1$	$(7.07 \pm 0.25) \times 10^1$
μ–Avg. (Data)	$(7.55 \pm 0.12) \times 10^1$	$(7.50 \pm 0.12) \times 10^1$
μ–Avg. (MC)	$(7.79 \pm 0.15) \times 10^1$	$(7.78 \pm 0.15) \times 10^1$
Charged Tracks		
Decay	$\epsilon \times A(\%)$	$\epsilon' \times A(\%)$
$e-\rho$ (Data)	$(9.534 \pm 0.079) \times 10^1$	$(8.98 \pm 0.11) \times 10^1$
$e-\rho$ (MC)	$(9.567 \pm 0.096) \times 10^1$	$(9.30 \pm 0.12) \times 10^1$
$\mu-\rho$ (Data)	$(9.617 \pm 0.072) \times 10^1$	$(9.20 \pm 0.10) \times 10^1$
$\mu-\rho$ (MC)	$(9.682 \pm 0.086) \times 10^1$	$(9.27 \pm 0.12) \times 10^1$
$e-\pi\pi$ (Data)	$(8.79 \pm 0.12) \times 10^1$	$(8.46 \pm 0.13) \times 10^1$
$e-\pi\pi$ (MC)	$(9.31 \pm 0.14) \times 10^1$	$(8.96 \pm 0.17) \times 10^1$
$\mu-\pi\pi$ (Data)	$(9.34 \pm 0.11) \times 10^1$	$(8.85 \pm 0.13) \times 10^1$
$\mu-\pi\pi$ (MC)	$(9.14 \pm 0.16) \times 10^1$	$(8.70 \pm 0.18) \times 10^1$
μ–Avg. (Data)	$(9.529 \pm 0.060) \times 10^1$	$(9.074 \pm 0.080) \times 10^1$
μ–Avg. (MC)	$(9.555 \pm 0.076) \times 10^1$	$(9.09 \pm 0.10) \times 10^1$

Table G.1: The tracking efficiency, $P_t^{miss} < 1.0$ and $0.2 < cos(\theta_{avg}^{(lab)}) < 0.6$, for the three different track definitions from the 1930V setting (Stability Study). The average values in this table are the weighted average of the $\mu-\rho$ and $\mu-\pi\pi$ channels as discussed in Chapter 7: Systematic Uncertainty Studies.

Good Tracks Loose		
Decay	$\epsilon \times A(\%)$	$\epsilon' \times A(\%)$
$e-\rho$ (Data)	$(8.900 \pm 0.036) \times 10^1$	$(8.883 \pm 0.036) \times 10^1$
$e-\rho$ (MC)	$(8.970 \pm 0.048) \times 10^1$	$(8.949 \pm 0.048) \times 10^1$
$\mu-\rho$ (Data)	$(9.027 \pm 0.036) \times 10^1$	$(9.004 \pm 0.036) \times 10^1$
$\mu-\rho$ (MC)	$(9.048 \pm 0.046) \times 10^1$	$(9.026 \pm 0.046) \times 10^1$
$e-\pi\pi$ (Data)	$(8.801 \pm 0.040) \times 10^1$	$(8.779 \pm 0.040) \times 10^1$
$e-\pi\pi$ (MC)	$(8.889 \pm 0.054) \times 10^1$	$(8.870 \pm 0.054) \times 10^1$
$\mu-\pi\pi$ (Data)	$(8.855 \pm 0.040) \times 10^1$	$(8.836 \pm 0.040) \times 10^1$
$\mu-\pi\pi$ (MC)	$(8.859 \pm 0.054) \times 10^1$	$(8.830 \pm 0.055) \times 10^1$
μ–Avg. (Data)	$(8.950 \pm 0.027) \times 10^1$	$(8.929 \pm 0.027) \times 10^1$
μ–Avg. (MC)	$(8.969 \pm 0.035) \times 10^1$	$(8.944 \pm 0.035) \times 10^1$
Good Tracks Very Loose		
Decay	$\epsilon \times A(\%)$	$\epsilon' \times A(\%)$
$e-\rho$ (Data)	$(9.095 \pm 0.033) \times 10^1$	$(9.043 \pm 0.034) \times 10^1$
$e-\rho$ (MC)	$(9.077 \pm 0.045) \times 10^1$	$(9.029 \pm 0.046) \times 10^1$
$\mu-\rho$ (Data)	$(9.188 \pm 0.033) \times 10^1$	$(9.126 \pm 0.034) \times 10^1$
$\mu-\rho$ (MC)	$(9.159 \pm 0.043) \times 10^1$	$(9.110 \pm 0.044) \times 10^1$
$e-\pi\pi$ (Data)	$(8.947 \pm 0.037) \times 10^1$	$(8.902 \pm 0.038) \times 10^1$
$e-\pi\pi$ (MC)	$(8.999 \pm 0.052) \times 10^1$	$(8.953 \pm 0.052) \times 10^1$
$\mu-\pi\pi$ (Data)	$(9.006 \pm 0.037) \times 10^1$	$(8.951 \pm 0.038) \times 10^1$
$\mu-\pi\pi$ (MC)	$(8.951 \pm 0.052) \times 10^1$	$(8.910 \pm 0.053) \times 10^1$
μ–Avg. (Data)	$(9.109 \pm 0.025) \times 10^1$	$(9.049 \pm 0.025) \times 10^1$
μ–Avg. (MC)	$(9.074 \pm 0.033) \times 10^1$	$(9.027 \pm 0.034) \times 10^1$
Charged Tracks		
Decay	$\epsilon \times A(\%)$	$\epsilon' \times A(\%)$
$e-\rho$ (Data)	$(9.724 \pm 0.019) \times 10^1$	$(9.348 \pm 0.029) \times 10^1$
$e-\rho$ (MC)	$(9.730 \pm 0.026) \times 10^1$	$(9.323 \pm 0.039) \times 10^1$
$\mu-\rho$ (Data)	$(9.789 \pm 0.018) \times 10^1$	$(9.402 \pm 0.029) \times 10^1$
$\mu-\rho$ (MC)	$(9.786 \pm 0.023) \times 10^1$	$(9.399 \pm 0.037) \times 10^1$
$e-\pi\pi$ (Data)	$(9.640 \pm 0.023) \times 10^1$	$(9.284 \pm 0.031) \times 10^1$
$e-\pi\pi$ (MC)	$(9.707 \pm 0.029) \times 10^1$	$(9.340 \pm 0.043) \times 10^1$
$\mu-\pi\pi$ (Data)	$(9.730 \pm 0.021) \times 10^1$	$(9.384 \pm 0.030) \times 10^1$
$\mu-\pi\pi$ (MC)	$(9.660 \pm 0.031) \times 10^1$	$(9.379 \pm 0.041) \times 10^1$
μ–Avg. (Data)	$(9.764 \pm 0.013) \times 10^1$	$(9.393 \pm 0.021) \times 10^1$
μ–Avg. (MC)	$(9.742 \pm 0.019) \times 10^1$	$(9.390 \pm 0.027) \times 10^1$

Table G.2: The tracking efficiency, $1.0 < P_t^{miss} < 2.5$ and $0.2 < cos(\theta_{avg}^{(lab)}) < 0.6$, for the three different track definitions from the 1930V setting (Stability Study). The average values in this table are the weighted average of the $\mu-\rho$ and $\mu-\pi\pi$ channels as discussed in Chapter 7: Systematic Uncertainty Studies.

Good Tracks Loose		
Decay	$\epsilon \times A(\%)$	$\epsilon' \times A(\%)$
$e-\rho$ (Data)	$(9.242 \pm 0.028) \times 10^1$	$(9.218 \pm 0.028) \times 10^1$
$e-\rho$ (MC)	$(9.345 \pm 0.035) \times 10^1$	$(9.313 \pm 0.035) \times 10^1$
$\mu-\rho$ (Data)	$(9.297 \pm 0.028) \times 10^1$	$(9.264 \pm 0.028) \times 10^1$
$\mu-\rho$ (MC)	$(9.381 \pm 0.034) \times 10^1$	$(9.350 \pm 0.035) \times 10^1$
$e-\pi\pi$ (Data)	$(9.355 \pm 0.021) \times 10^1$	$(9.293 \pm 0.022) \times 10^1$
$e-\pi\pi$ (MC)	$(9.367 \pm 0.028) \times 10^1$	$(9.329 \pm 0.029) \times 10^1$
$\mu-\pi\pi$ (Data)	$(9.333 \pm 0.022) \times 10^1$	$(9.290 \pm 0.022) \times 10^1$
$\mu-\pi\pi$ (MC)	$(9.353 \pm 0.028) \times 10^1$	$(9.308 \pm 0.029) \times 10^1$
μ–Avg. (Data)	$(9.319 \pm 0.017) \times 10^1$	$(9.280 \pm 0.017) \times 10^1$
μ–Avg. (MC)	$(9.365 \pm 0.022) \times 10^1$	$(9.325 \pm 0.022) \times 10^1$
Good Tracks Very Loose		
Decay	$\epsilon \times A(\%)$	$\epsilon' \times A(\%)$
$e-\rho$ (Data)	$(9.385 \pm 0.025) \times 10^1$	$(9.333 \pm 0.026) \times 10^1$
$e-\rho$ (MC)	$(9.442 \pm 0.032) \times 10^1$	$(9.378 \pm 0.034) \times 10^1$
$\mu-\rho$ (Data)	$(9.463 \pm 0.024) \times 10^1$	$(9.377 \pm 0.026) \times 10^1$
$\mu-\rho$ (MC)	$(9.469 \pm 0.032) \times 10^1$	$(9.412 \pm 0.033) \times 10^1$
$e-\pi\pi$ (Data)	$(9.462 \pm 0.019) \times 10^1$	$(9.375 \pm 0.020) \times 10^1$
$e-\pi\pi$ (MC)	$(9.444 \pm 0.026) \times 10^1$	$(9.385 \pm 0.027) \times 10^1$
$\mu-\pi\pi$ (Data)	$(9.443 \pm 0.020) \times 10^1$	$(9.366 \pm 0.021) \times 10^1$
$\mu-\pi\pi$ (MC)	$(9.437 \pm 0.027) \times 10^1$	$(9.368 \pm 0.028) \times 10^1$
μ–Avg. (Data)	$(9.451 \pm 0.015) \times 10^1$	$(9.371 \pm 0.016) \times 10^1$
μ–Avg. (MC)	$(9.450 \pm 0.020) \times 10^1$	$(9.386 \pm 0.021) \times 10^1$
Charged Tracks		
Decay	$\epsilon \times A(\%)$	$\epsilon' \times A(\%)$
$e-\rho$ (Data)	$(9.800 \pm 0.015) \times 10^1$	$(9.452 \pm 0.024) \times 10^1$
$e-\rho$ (MC)	$(9.817 \pm 0.019) \times 10^1$	$(9.454 \pm 0.032) \times 10^1$
$\mu-\rho$ (Data)	$(9.869 \pm 0.013) \times 10^1$	$(9.481 \pm 0.024) \times 10^1$
$\mu-\rho$ (MC)	$(9.844 \pm 0.018) \times 10^1$	$(9.491 \pm 0.031) \times 10^1$
$e-\pi\pi$ (Data)	$(9.799 \pm 0.012) \times 10^1$	$(9.460 \pm 0.019) \times 10^1$
$e-\pi\pi$ (MC)	$(9.787 \pm 0.017) \times 10^1$	$(9.513 \pm 0.025) \times 10^1$
$\mu-\pi\pi$ (Data)	$(9.758 \pm 0.014) \times 10^1$	$(9.418 \pm 0.020) \times 10^1$
$\mu-\pi\pi$ (MC)	$(9.772 \pm 0.017) \times 10^1$	$(9.492 \pm 0.025) \times 10^1$
μ–Avg. (Data)	$(9.8176 \pm 0.0092) \times 10^1$	$(9.445 \pm 0.015) \times 10^1$
μ–Avg. (MC)	$(9.807 \pm 0.012) \times 10^1$	$(9.492 \pm 0.020) \times 10^1$

Table G.3: The tracking efficiency, $2.5 < P_t^{miss}$ and $0.2 < cos(\theta_{avg}^{(lab)}) < 0.6$, for the three different track definitions from the 1930V setting (Stability Study). The average values in this table are the weighted average of the $\mu-\rho$ and $\mu-\pi\pi$ channels as discussed in Chapter 7: Systematic Uncertainty Studies.

Appendix H: 2001 (1930V) Tables

Good Tracks Loose		
Decay	$\epsilon \times A(\%)$	$\epsilon' \times A(\%)$
$e-\rho$ (Data)	$(8.697 \pm 0.024) \times 10^1$	$(8.677 \pm 0.024) \times 10^1$
$e-\rho$ (MC)	$(8.826 \pm 0.036) \times 10^1$	$(8.813 \pm 0.036) \times 10^1$
$\mu-\rho$ (Data)	$(8.750 \pm 0.024) \times 10^1$	$(8.718 \pm 0.024) \times 10^1$
$\mu-\rho$ (MC)	$(8.790 \pm 0.035) \times 10^1$	$(8.767 \pm 0.036) \times 10^1$
$e-\pi\pi$ (Data)	$(8.622 \pm 0.021) \times 10^1$	$(8.559 \pm 0.022) \times 10^1$
$e-\pi\pi$ (MC)	$(8.830 \pm 0.033) \times 10^1$	$(8.794 \pm 0.033) \times 10^1$
$\mu-\pi\pi$ (Data)	$(8.784 \pm 0.021) \times 10^1$	$(8.744 \pm 0.021) \times 10^1$
$\mu-\pi\pi$ (MC)	$(8.777 \pm 0.033) \times 10^1$	$(8.740 \pm 0.033) \times 10^1$
μ–Avg. (Data)	$(8.769 \pm 0.016) \times 10^1$	$(8.733 \pm 0.016) \times 10^1$
μ–Avg. (MC)	$(8.783 \pm 0.024) \times 10^1$	$(8.752 \pm 0.024) \times 10^1$
Good Tracks Very Loose		
Decay	$\epsilon \times A(\%)$	$\epsilon' \times A(\%)$
$e-\rho$ (Data)	$(8.839 \pm 0.023) \times 10^1$	$(8.788 \pm 0.023) \times 10^1$
$e-\rho$ (MC)	$(8.925 \pm 0.034) \times 10^1$	$(8.886 \pm 0.035) \times 10^1$
$\mu-\rho$ (Data)	$(8.908 \pm 0.022) \times 10^1$	$(8.847 \pm 0.023) \times 10^1$
$\mu-\rho$ (MC)	$(8.893 \pm 0.034) \times 10^1$	$(8.845 \pm 0.035) \times 10^1$
$e-\pi\pi$ (Data)	$(8.729 \pm 0.021) \times 10^1$	$(8.643 \pm 0.021) \times 10^1$
$e-\pi\pi$ (MC)	$(8.903 \pm 0.032) \times 10^1$	$(8.845 \pm 0.033) \times 10^1$
$\mu-\pi\pi$ (Data)	$(8.890 \pm 0.020) \times 10^1$	$(8.827 \pm 0.020) \times 10^1$
$\mu-\pi\pi$ (MC)	$(8.868 \pm 0.032) \times 10^1$	$(8.814 \pm 0.032) \times 10^1$
μ–Avg. (Data)	$(8.898 \pm 0.015) \times 10^1$	$(8.836 \pm 0.015) \times 10^1$
μ–Avg. (MC)	$(8.879 \pm 0.023) \times 10^1$	$(8.828 \pm 0.024) \times 10^1$
Charged Tracks		
Decay	$\epsilon \times A(\%)$	$\epsilon' \times A(\%)$
$e-\rho$ (Data)	$(9.496 \pm 0.016) \times 10^1$	$(9.152 \pm 0.020) \times 10^1$
$e-\rho$ (MC)	$(9.546 \pm 0.023) \times 10^1$	$(9.220 \pm 0.030) \times 10^1$
$\mu-\rho$ (Data)	$(9.600 \pm 0.014) \times 10^1$	$(9.245 \pm 0.019) \times 10^1$
$\mu-\rho$ (MC)	$(9.529 \pm 0.023) \times 10^1$	$(9.196 \pm 0.030) \times 10^1$
$e-\pi\pi$ (Data)	$(9.361 \pm 0.015) \times 10^1$	$(9.036 \pm 0.018) \times 10^1$
$e-\pi\pi$ (MC)	$(9.468 \pm 0.023) \times 10^1$	$(9.183 \pm 0.028) \times 10^1$
$\mu-\pi\pi$ (Data)	$(9.450 \pm 0.015) \times 10^1$	$(9.131 \pm 0.018) \times 10^1$
$\mu-\pi\pi$ (MC)	$(9.450 \pm 0.023) \times 10^1$	$(9.154 \pm 0.028) \times 10^1$
μ–Avg. (Data)	$(9.527 \pm 0.010) \times 10^1$	$(9.185 \pm 0.013) \times 10^1$
μ–Avg. (MC)	$(9.489 \pm 0.016) \times 10^1$	$(9.173 \pm 0.020) \times 10^1$

Table H.1: The tracking efficiency for the 1930V setting (2001). The average values in this table are the weighted average of the $\mu-\rho$ and $\mu-\pi\pi$ channels as discussed in Chapter 7: Systematic Uncertainty Studies.

Good Tracks Loose		
Decay	$\Delta(\%)$	$\Delta'(\%)$
$e-\rho$	(1.46 ± 0.27)	(1.54 ± 0.27)
$\mu-\rho$	$(4.5 \pm 2.7) \times 10^{-1}$	$(5.6 \pm 2.7) \times 10^{-1}$
$e-\pi\pi$	(2.36 ± 0.24)	(2.68 ± 0.25)
$\mu-\pi\pi$	$(-0.7 \pm 2.4) \times 10^{-1}$	$(-0.5 \pm 2.4) \times 10^{-1}$
μ–Avg.	$(1.6 \pm 1.8) \times 10^{-1}$	$(2.2 \pm 1.8) \times 10^{-1}$
Good Tracks Very Loose		
Decay	$\Delta(\%)$	$\Delta'(\%)$
$e-\rho$	$(9.7 \pm 2.5) \times 10^{-1}$	(1.11 ± 0.26)
$\mu-\rho$	$(-1.7 \pm 2.5) \times 10^{-1}$	$(-0.2 \pm 2.6) \times 10^{-1}$
$e-\pi\pi$	(1.96 ± 0.23)	(2.29 ± 0.24)
$\mu-\pi\pi$	$(-2.5 \pm 2.3) \times 10^{-1}$	$(-1.4 \pm 2.3) \times 10^{-1}$
μ–Avg.	$(-2.1 \pm 1.7) \times 10^{-1}$	$(-0.9 \pm 1.7) \times 10^{-1}$
Charged Tracks		
Decay	$\Delta(\%)$	$\Delta'(\%)$
$e-\rho$	$(5.2 \pm 1.6) \times 10^{-1}$	$(7.4 \pm 2.1) \times 10^{-1}$
$\mu-\rho$	$(-7.5 \pm 1.5) \times 10^{-1}$	$(-5.4 \pm 2.1) \times 10^{-1}$
$e-\pi\pi$	(1.13 ± 0.16)	(1.60 ± 0.20)
$\mu-\pi\pi$	$(0.1 \pm 1.6) \times 10^{-1}$	$(2.5 \pm 2.0) \times 10^{-1}$
μ–Avg.	$(-3.9 \pm 1.1) \times 10^{-1}$	$(-1.2 \pm 1.4) \times 10^{-1}$

Table H.2: The tracking efficiency correction factor for the 1930V setting (2001). The average values in this table are the weighted average of the $\mu-\rho$ and $\mu-\pi\pi$ channels as discussed in Chapter 7: Systematic Uncertainty Studies.

Good Tracks Loose		
Decay	$a_{\pm}(\%)$	$a'_{\pm}(\%)$
$e-\rho$ (Data)	$(1.9 \pm 2.7) \times 10^{-1}$	$(2.2 \pm 2.7) \times 10^{-1}$
$e-\rho$ (MC)	$(2.1 \pm 4.0) \times 10^{-1}$	$(2.4 \pm 4.1) \times 10^{-1}$
$\mu-\rho$ (Data)	$(0.5 \pm 2.7) \times 10^{-1}$	$(0.5 \pm 2.7) \times 10^{-1}$
$\mu-\rho$ (MC)	$(0.8 \pm 4.0) \times 10^{-1}$	$(0.4 \pm 4.1) \times 10^{-1}$
$e-\pi\pi$ (Data)	$(-8.6 \pm 2.5) \times 10^{-1}$	$(-9.7 \pm 2.5) \times 10^{-1}$
$e-\pi\pi$ (MC)	$(-1.4 \pm 3.7) \times 10^{-1}$	$(-2.3 \pm 3.8) \times 10^{-1}$
$\mu-\pi\pi$ (Data)	$(-5.8 \pm 2.4) \times 10^{-1}$	$(-5.3 \pm 2.4) \times 10^{-1}$
$\mu-\pi\pi$ (MC)	$(0.7 \pm 3.7) \times 10^{-1}$	$(0 \pm 3.8) \times 10^{-1}$
μ–Avg. (Data)	$(-3.1 \pm 1.8) \times 10^{-1}$	$(-2.8 \pm 1.8) \times 10^{-1}$
μ–Avg. (MC)	$(0.7 \pm 2.7) \times 10^{-1}$	$(0.2 \pm 2.8) \times 10^{-1}$
Good Tracks Very Loose		
Decay	$a_{\pm}(\%)$	$a'_{\pm}(\%)$
$e-\rho$ (Data)	$(0 \pm 2.6) \times 10^{-1}$	$(-0.4 \pm 2.6) \times 10^{-1}$
$e-\rho$ (MC)	$(0.2 \pm 3.8) \times 10^{-1}$	$(0.7 \pm 3.9) \times 10^{-1}$
$\mu-\rho$ (Data)	$(0.6 \pm 2.5) \times 10^{-1}$	$(1.1 \pm 2.6) \times 10^{-1}$
$\mu-\rho$ (MC)	$(1.0 \pm 3.8) \times 10^{-1}$	$(0.2 \pm 3.9) \times 10^{-1}$
$e-\pi\pi$ (Data)	$(-8.7 \pm 2.4) \times 10^{-1}$	$(-9.7 \pm 2.4) \times 10^{-1}$
$e-\pi\pi$ (MC)	$(-0.7 \pm 3.6) \times 10^{-1}$	$(-1.5 \pm 3.7) \times 10^{-1}$
$\mu-\pi\pi$ (Data)	$(-5.1 \pm 2.3) \times 10^{-1}$	$(-4.3 \pm 2.3) \times 10^{-1}$
$\mu-\pi\pi$ (MC)	$(-0.1 \pm 3.6) \times 10^{-1}$	$(-0.5 \pm 3.6) \times 10^{-1}$
μ–Avg. (Data)	$(-2.6 \pm 1.7) \times 10^{-1}$	$(-1.9 \pm 1.7) \times 10^{-1}$
μ–Avg. (MC)	$(0.4 \pm 2.6) \times 10^{-1}$	$(-0.2 \pm 2.7) \times 10^{-1}$
Charged Tracks		
Decay	$a_{\pm}(\%)$	$a'_{\pm}(\%)$
$e-\rho$ (Data)	$(2.7 \pm 1.6) \times 10^{-1}$	$(4.2 \pm 2.1) \times 10^{-1}$
$e-\rho$ (MC)	$(-0 \pm 2.5) \times 10^{-1}$	$(1.6 \pm 3.2) \times 10^{-1}$
$\mu-\rho$ (Data)	$(1.9 \pm 1.5) \times 10^{-1}$	$(3.6 \pm 2.0) \times 10^{-1}$
$\mu-\rho$ (MC)	$(3.2 \pm 2.5) \times 10^{-1}$	$(5.2 \pm 3.2) \times 10^{-1}$
$e-\pi\pi$ (Data)	$(-6.8 \pm 1.6) \times 10^{-1}$	$(-7.2 \pm 2.0) \times 10^{-1}$
$e-\pi\pi$ (MC)	$(-1.3 \pm 2.5) \times 10^{-1}$	$(0.5 \pm 3.0) \times 10^{-1}$
$\mu-\pi\pi$ (Data)	$(-3.4 \pm 1.6) \times 10^{-1}$	$(-1.1 \pm 2.0) \times 10^{-1}$
$\mu-\pi\pi$ (MC)	$(1.4 \pm 2.4) \times 10^{-1}$	$(3.9 \pm 3.0) \times 10^{-1}$
μ–Avg. (Data)	$(-0.6 \pm 1.1) \times 10^{-1}$	$(1.2 \pm 1.4) \times 10^{-1}$
μ–Avg. (MC)	$(2.3 \pm 1.7) \times 10^{-1}$	$(4.5 \pm 2.2) \times 10^{-1}$

Table H.3: The tracking efficiency charge asymmetry for the 1930V setting (2001). The average values in this table are the weighted average of the $\mu-\rho$ and $\mu-\pi\pi$ channels as discussed in Chapter 7: Systematic Uncertainty Studies.

Appendix I: 2002 (1930V) Tables

Good Tracks Loose		
Decay	$\epsilon \times A(\%)$	$\epsilon' \times A(\%)$
$e-\rho$ (Data)	$(8.679 \pm 0.030) \times 10^1$	$(8.659 \pm 0.031) \times 10^1$
$e-\rho$ (MC)	$(8.833 \pm 0.027) \times 10^1$	$(8.806 \pm 0.027) \times 10^1$
$\mu-\rho$ (Data)	$(8.781 \pm 0.032) \times 10^1$	$(8.759 \pm 0.032) \times 10^1$
$\mu-\rho$ (MC)	$(8.814 \pm 0.027) \times 10^1$	$(8.794 \pm 0.027) \times 10^1$
$e-\pi\pi$ (Data)	$(8.629 \pm 0.027) \times 10^1$	$(8.567 \pm 0.028) \times 10^1$
$e-\pi\pi$ (MC)	$(8.848 \pm 0.025) \times 10^1$	$(8.820 \pm 0.025) \times 10^1$
$\mu-\pi\pi$ (Data)	$(8.768 \pm 0.028) \times 10^1$	$(8.731 \pm 0.029) \times 10^1$
$\mu-\pi\pi$ (MC)	$(8.822 \pm 0.025) \times 10^1$	$(8.787 \pm 0.025) \times 10^1$
μ–Avg. (Data)	$(8.774 \pm 0.021) \times 10^1$	$(8.744 \pm 0.021) \times 10^1$
μ–Avg. (MC)	$(8.819 \pm 0.018) \times 10^1$	$(8.790 \pm 0.018) \times 10^1$
Good Tracks Very Loose		
Decay	$\epsilon \times A(\%)$	$\epsilon' \times A(\%)$
$e-\rho$ (Data)	$(8.824 \pm 0.029) \times 10^1$	$(8.787 \pm 0.029) \times 10^1$
$e-\rho$ (MC)	$(8.940 \pm 0.026) \times 10^1$	$(8.887 \pm 0.027) \times 10^1$
$\mu-\rho$ (Data)	$(8.921 \pm 0.030) \times 10^1$	$(8.861 \pm 0.031) \times 10^1$
$\mu-\rho$ (MC)	$(8.917 \pm 0.026) \times 10^1$	$(8.874 \pm 0.027) \times 10^1$
$e-\pi\pi$ (Data)	$(8.737 \pm 0.026) \times 10^1$	$(8.653 \pm 0.027) \times 10^1$
$e-\pi\pi$ (MC)	$(8.917 \pm 0.024) \times 10^1$	$(8.871 \pm 0.025) \times 10^1$
$\mu-\pi\pi$ (Data)	$(8.883 \pm 0.027) \times 10^1$	$(8.819 \pm 0.028) \times 10^1$
$\mu-\pi\pi$ (MC)	$(8.898 \pm 0.024) \times 10^1$	$(8.845 \pm 0.025) \times 10^1$
μ–Avg. (Data)	$(8.900 \pm 0.020) \times 10^1$	$(8.838 \pm 0.021) \times 10^1$
μ–Avg. (MC)	$(8.907 \pm 0.018) \times 10^1$	$(8.858 \pm 0.018) \times 10^1$
Charged Tracks		
Decay	$\epsilon \times A(\%)$	$\epsilon' \times A(\%)$
$e-\rho$ (Data)	$(9.468 \pm 0.021) \times 10^1$	$(9.143 \pm 0.025) \times 10^1$
$e-\rho$ (MC)	$(9.541 \pm 0.018) \times 10^1$	$(9.188 \pm 0.023) \times 10^1$
$\mu-\rho$ (Data)	$(9.584 \pm 0.020) \times 10^1$	$(9.232 \pm 0.026) \times 10^1$
$\mu-\rho$ (MC)	$(9.548 \pm 0.018) \times 10^1$	$(9.200 \pm 0.023) \times 10^1$
$e-\pi\pi$ (Data)	$(9.350 \pm 0.020) \times 10^1$	$(9.015 \pm 0.024) \times 10^1$
$e-\pi\pi$ (MC)	$(9.480 \pm 0.017) \times 10^1$	$(9.223 \pm 0.021) \times 10^1$
$\mu-\pi\pi$ (Data)	$(9.472 \pm 0.020) \times 10^1$	$(9.155 \pm 0.024) \times 10^1$
$\mu-\pi\pi$ (MC)	$(9.457 \pm 0.018) \times 10^1$	$(9.178 \pm 0.021) \times 10^1$
μ–Avg. (Data)	$(9.528 \pm 0.014) \times 10^1$	$(9.191 \pm 0.017) \times 10^1$
μ–Avg. (MC)	$(9.502 \pm 0.013) \times 10^1$	$(9.188 \pm 0.015) \times 10^1$

Table I.1: The tracking efficiency for the three different track definitions from the 1930V setting (2002). The average values in this table are the weighted average of the $\mu-\rho$ and $\mu-\pi\pi$ channels as discussed in Chapter 7: Systematic Uncertainty Studies.

Good Tracks Loose		
Decay	$\Delta(\%)$	$\Delta'(\%)$
$e-\rho$	(1.75 ± 0.34)	(1.67 ± 0.35)
$\mu-\rho$	$(3.7 \pm 3.6) \times 10^{-1}$	$(3.9 \pm 3.6) \times 10^{-1}$
$e-\pi\pi$	(2.48 ± 0.31)	(2.86 ± 0.31)
$\mu-\pi\pi$	$(6.1 \pm 3.2) \times 10^{-1}$	$(6.3 \pm 3.3) \times 10^{-1}$
μ–Avg.	$(5.1 \pm 2.4) \times 10^{-1}$	$(5.2 \pm 2.4) \times 10^{-1}$
Good Tracks Very Loose		
Decay	$\Delta(\%)$	$\Delta'(\%)$
$e-\rho$	(1.31 ± 0.32)	(1.13 ± 0.33)
$\mu-\rho$	$(-0.4 \pm 3.4) \times 10^{-1}$	$(1.4 \pm 3.4) \times 10^{-1}$
$e-\pi\pi$	(2.02 ± 0.30)	(2.45 ± 0.30)
$\mu-\pi\pi$	$(1.7 \pm 3.1) \times 10^{-1}$	$(2.9 \pm 3.1) \times 10^{-1}$
μ–Avg.	$(0.8 \pm 2.3) \times 10^{-1}$	$(2.2 \pm 2.3) \times 10^{-1}$
Charged Tracks		
Decay	$\Delta(\%)$	$\Delta'(\%)$
$e-\rho$	$(7.6 \pm 2.2) \times 10^{-1}$	$(4.9 \pm 2.7) \times 10^{-1}$
$\mu-\rho$	$(-3.8 \pm 2.1) \times 10^{-1}$	$(-3.5 \pm 2.8) \times 10^{-1}$
$e-\pi\pi$	(1.37 ± 0.21)	(2.26 ± 0.26)
$\mu-\pi\pi$	$(-1.6 \pm 2.1) \times 10^{-1}$	$(2.4 \pm 2.6) \times 10^{-1}$
μ–Avg.	$(-2.7 \pm 1.5) \times 10^{-1}$	$(-0.3 \pm 1.9) \times 10^{-1}$

Table I.2: The tracking efficiency correction factor for the three different track definitions from the 1930V setting (2002). The average values in this table are the weighted average of the $\mu-\rho$ and $\mu-\pi\pi$ channels as discussed in Chapter 7: Systematic Uncertainty Studies.

Good Tracks Loose		
Decay	$a_{\pm}(\%)$	$a'_{\pm}(\%)$
$e-\rho$ (Data)	$(-5.1 \pm 3.5) \times 10^{-1}$	$(-4.9 \pm 3.5) \times 10^{-1}$
$e-\rho$ (MC)	$(-0.3 \pm 3.1) \times 10^{-1}$	$(0.2 \pm 3.1) \times 10^{-1}$
$\mu-\rho$ (Data)	$(0.5 \pm 3.6) \times 10^{-1}$	$(0.8 \pm 3.6) \times 10^{-1}$
$\mu-\rho$ (MC)	$(-4.0 \pm 3.1) \times 10^{-1}$	$(-3.6 \pm 3.1) \times 10^{-1}$
$e-\pi\pi$ (Data)	$(-8.8 \pm 3.2) \times 10^{-1}$	$(-9.5 \pm 3.2) \times 10^{-1}$
$e-\pi\pi$ (MC)	$(-1.7 \pm 2.8) \times 10^{-1}$	$(-1.2 \pm 2.8) \times 10^{-1}$
$\mu-\pi\pi$ (Data)	$(-7.3 \pm 3.2) \times 10^{-1}$	$(-7.3 \pm 3.3) \times 10^{-1}$
$\mu-\pi\pi$ (MC)	$(-1.4 \pm 2.8) \times 10^{-1}$	$(-1.5 \pm 2.9) \times 10^{-1}$
μ–Avg. (Data)	$(-3.8 \pm 2.4) \times 10^{-1}$	$(-3.7 \pm 2.4) \times 10^{-1}$
μ–Avg. (MC)	$(-2.6 \pm 2.1) \times 10^{-1}$	$(-2.5 \pm 2.1) \times 10^{-1}$
Good Tracks Very Loose		
Decay	$a_{\pm}(\%)$	$a'_{\pm}(\%)$
$e-\rho$ (Data)	$(-4.7 \pm 3.3) \times 10^{-1}$	$(-4.2 \pm 3.3) \times 10^{-1}$
$e-\rho$ (MC)	$(-0.2 \pm 2.9) \times 10^{-1}$	$(0.4 \pm 3.0) \times 10^{-1}$
$\mu-\rho$ (Data)	$(1.6 \pm 3.4) \times 10^{-1}$	$(1.5 \pm 3.5) \times 10^{-1}$
$\mu-\rho$ (MC)	$(-4.5 \pm 2.9) \times 10^{-1}$	$(-3.8 \pm 3.0) \times 10^{-1}$
$e-\pi\pi$ (Data)	(-1.09 ± 0.30)	(-1.15 ± 0.31)
$e-\pi\pi$ (MC)	$(-2.6 \pm 2.7) \times 10^{-1}$	$(-1.9 \pm 2.8) \times 10^{-1}$
$\mu-\pi\pi$ (Data)	$(-6.2 \pm 3.1) \times 10^{-1}$	$(-5.8 \pm 3.1) \times 10^{-1}$
$\mu-\pi\pi$ (MC)	$(-1.7 \pm 2.7) \times 10^{-1}$	$(-2.1 \pm 2.8) \times 10^{-1}$
μ–Avg. (Data)	$(-2.7 \pm 2.3) \times 10^{-1}$	$(-2.4 \pm 2.3) \times 10^{-1}$
μ–Avg. (MC)	$(-3.0 \pm 2.0) \times 10^{-1}$	$(-2.9 \pm 2.0) \times 10^{-1}$
Charged Tracks		
Decay	$a_{\pm}(\%)$	$a'_{\pm}(\%)$
$e-\rho$ (Data)	$(-2.7 \pm 2.2) \times 10^{-1}$	$(-0.4 \pm 2.8) \times 10^{-1}$
$e-\rho$ (MC)	$(0.6 \pm 1.9) \times 10^{-1}$	$(3.7 \pm 2.5) \times 10^{-1}$
$\mu-\rho$ (Data)	$(0.4 \pm 2.0) \times 10^{-1}$	$(2.6 \pm 2.8) \times 10^{-1}$
$\mu-\rho$ (MC)	$(-1.3 \pm 1.9) \times 10^{-1}$	$(2.5 \pm 2.5) \times 10^{-1}$
$e-\pi\pi$ (Data)	(-1.34 ± 0.21)	(-1.02 ± 0.26)
$e-\pi\pi$ (MC)	$(-0.9 \pm 1.8) \times 10^{-1}$	$(1.7 \pm 2.2) \times 10^{-1}$
$\mu-\pi\pi$ (Data)	$(-3.4 \pm 2.1) \times 10^{-1}$	$(-1.8 \pm 2.6) \times 10^{-1}$
$\mu-\pi\pi$ (MC)	$(-2.8 \pm 1.9) \times 10^{-1}$	$(-1.6 \pm 2.3) \times 10^{-1}$
μ–Avg. (Data)	$(-1.5 \pm 1.5) \times 10^{-1}$	$(0.3 \pm 1.9) \times 10^{-1}$
μ–Avg. (MC)	$(-2.0 \pm 1.3) \times 10^{-1}$	$(0.3 \pm 1.7) \times 10^{-1}$

Table I.3: The tracking efficiency charge asymmetry for the three different track definitions from the 1930V setting (2002). The average values in this table are the weighted average of the $\mu-\rho$ and $\mu-\pi\pi$ channels as discussed in Chapter 7: Systematic Uncertainty Studies.

Appendix J: 2003 (1930V) Tables

Good Tracks Loose		
Decay	$\epsilon \times A(\%)$	$\epsilon' \times A(\%)$
$e-\rho$ (Data)	$(8.690 \pm 0.022) \times 10^1$	$(8.667 \pm 0.022) \times 10^1$
$e-\rho$ (MC)	$(8.840 \pm 0.033) \times 10^1$	$(8.814 \pm 0.033) \times 10^1$
$\mu-\rho$ (Data)	$(8.756 \pm 0.022) \times 10^1$	$(8.730 \pm 0.022) \times 10^1$
$\mu-\rho$ (MC)	$(8.805 \pm 0.034) \times 10^1$	$(8.788 \pm 0.034) \times 10^1$
$e-\pi\pi$ (Data)	$(8.599 \pm 0.020) \times 10^1$	$(8.534 \pm 0.020) \times 10^1$
$e-\pi\pi$ (MC)	$(8.827 \pm 0.031) \times 10^1$	$(8.794 \pm 0.031) \times 10^1$
$\mu-\pi\pi$ (Data)	$(8.771 \pm 0.019) \times 10^1$	$(8.739 \pm 0.020) \times 10^1$
$\mu-\pi\pi$ (MC)	$(8.806 \pm 0.031) \times 10^1$	$(8.769 \pm 0.032) \times 10^1$
μ–Avg. (Data)	$(8.764 \pm 0.015) \times 10^1$	$(8.735 \pm 0.015) \times 10^1$
μ–Avg. (MC)	$(8.805 \pm 0.023) \times 10^1$	$(8.778 \pm 0.023) \times 10^1$
Good Tracks Very Loose		
Decay	$\epsilon \times A(\%)$	$\epsilon' \times A(\%)$
$e-\rho$ (Data)	$(8.854 \pm 0.021) \times 10^1$	$(8.798 \pm 0.021) \times 10^1$
$e-\rho$ (MC)	$(8.936 \pm 0.032) \times 10^1$	$(8.883 \pm 0.032) \times 10^1$
$\mu-\rho$ (Data)	$(8.920 \pm 0.021) \times 10^1$	$(8.856 \pm 0.021) \times 10^1$
$\mu-\rho$ (MC)	$(8.911 \pm 0.033) \times 10^1$	$(8.866 \pm 0.033) \times 10^1$
$e-\pi\pi$ (Data)	$(8.715 \pm 0.019) \times 10^1$	$(8.620 \pm 0.020) \times 10^1$
$e-\pi\pi$ (MC)	$(8.910 \pm 0.030) \times 10^1$	$(8.860 \pm 0.030) \times 10^1$
$\mu-\pi\pi$ (Data)	$(8.892 \pm 0.019) \times 10^1$	$(8.831 \pm 0.019) \times 10^1$
$\mu-\pi\pi$ (MC)	$(8.882 \pm 0.030) \times 10^1$	$(8.828 \pm 0.031) \times 10^1$
μ–Avg. (Data)	$(8.905 \pm 0.014) \times 10^1$	$(8.842 \pm 0.014) \times 10^1$
μ–Avg. (MC)	$(8.895 \pm 0.022) \times 10^1$	$(8.846 \pm 0.023) \times 10^1$
Charged Tracks		
Decay	$\epsilon \times A(\%)$	$\epsilon' \times A(\%)$
$e-\rho$ (Data)	$(9.489 \pm 0.014) \times 10^1$	$(9.143 \pm 0.018) \times 10^1$
$e-\rho$ (MC)	$(9.555 \pm 0.022) \times 10^1$	$(9.232 \pm 0.027) \times 10^1$
$\mu-\rho$ (Data)	$(9.575 \pm 0.014) \times 10^1$	$(9.188 \pm 0.018) \times 10^1$
$\mu-\rho$ (MC)	$(9.555 \pm 0.022) \times 10^1$	$(9.203 \pm 0.029) \times 10^1$
$e-\pi\pi$ (Data)	$(9.353 \pm 0.014) \times 10^1$	$(9.003 \pm 0.017) \times 10^1$
$e-\pi\pi$ (MC)	$(9.462 \pm 0.022) \times 10^1$	$(9.178 \pm 0.026) \times 10^1$
$\mu-\pi\pi$ (Data)	$(9.497 \pm 0.013) \times 10^1$	$(9.187 \pm 0.016) \times 10^1$
$\mu-\pi\pi$ (MC)	$(9.440 \pm 0.022) \times 10^1$	$(9.149 \pm 0.027) \times 10^1$
μ–Avg. (Data)	$(9.534 \pm 0.010) \times 10^1$	$(9.187 \pm 0.012) \times 10^1$
μ–Avg. (MC)	$(9.498 \pm 0.016) \times 10^1$	$(9.174 \pm 0.020) \times 10^1$

Table J.1: The tracking efficiency for the three different track definitions from the 1930V setting (2003). The average values in this table are the weighted average of the $\mu-\rho$ and $\mu-\pi\pi$ channels as discussed in Chapter 7: Systematic Uncertainty Studies.

Good Tracks Loose		
Decay	$\Delta(\%)$	$\Delta'(\%)$
$e-\rho$	(1.70 ± 0.25)	(1.67 ± 0.25)
$\mu-\rho$	$(5.6 \pm 2.5) \times 10^{-1}$	$(6.6 \pm 2.5) \times 10^{-1}$
$e-\pi\pi$	(2.58 ± 0.22)	(2.95 ± 0.23)
$\mu-\pi\pi$	$(3.9 \pm 2.2) \times 10^{-1}$	$(3.4 \pm 2.2) \times 10^{-1}$
μ–Avg.	$(4.6 \pm 1.7) \times 10^{-1}$	$(4.8 \pm 1.7) \times 10^{-1}$
Good Tracks Very Loose		
Decay	$\Delta(\%)$	$\Delta'(\%)$
$e-\rho$	$(9.2 \pm 2.3) \times 10^{-1}$	$(9.6 \pm 2.4) \times 10^{-1}$
$\mu-\rho$	$(-1.1 \pm 2.3) \times 10^{-1}$	$(1.1 \pm 2.4) \times 10^{-1}$
$e-\pi\pi$	(2.19 ± 0.21)	(2.71 ± 0.22)
$\mu-\pi\pi$	$(-1.2 \pm 2.1) \times 10^{-1}$	$(-0.3 \pm 2.2) \times 10^{-1}$
μ–Avg.	$(-1.1 \pm 1.6) \times 10^{-1}$	$(0.3 \pm 1.6) \times 10^{-1}$
Charged Tracks		
Decay	$\Delta(\%)$	$\Delta'(\%)$
$e-\rho$	$(6.8 \pm 1.5) \times 10^{-1}$	$(9.7 \pm 2.0) \times 10^{-1}$
$\mu-\rho$	$(-2.1 \pm 1.4) \times 10^{-1}$	$(1.6 \pm 2.0) \times 10^{-1}$
$e-\pi\pi$	(1.15 ± 0.15)	(1.91 ± 0.19)
$\mu-\pi\pi$	$(-6.1 \pm 1.4) \times 10^{-1}$	$(-4.1 \pm 1.8) \times 10^{-1}$
μ–Avg.	$(-4.2 \pm 1.0) \times 10^{-1}$	$(-1.6 \pm 1.3) \times 10^{-1}$

Table J.2: The tracking efficiency correction factor for the three different track definitions from the 1930V setting (2003). The average values in this table are the weighted average of the $\mu-\rho$ and $\mu-\pi\pi$ channels as discussed in Chapter 7: Systematic Uncertainty Studies.

Good Tracks Loose		
Decay	$a_{\pm}(\%)$	$a'_{\pm}(\%)$
$e-\rho$ (Data)	$(-0.1 \pm 2.5) \times 10^{-1}$	$(0.5 \pm 2.5) \times 10^{-1}$
$e-\rho$ (MC)	$(1.3 \pm 3.7) \times 10^{-1}$	$(1.4 \pm 3.8) \times 10^{-1}$
$\mu-\rho$ (Data)	$(3.0 \pm 2.5) \times 10^{-1}$	$(3.1 \pm 2.5) \times 10^{-1}$
$\mu-\rho$ (MC)	$(1.1 \pm 3.9) \times 10^{-1}$	$(0.7 \pm 3.9) \times 10^{-1}$
$e-\pi\pi$ (Data)	(-1.10 ± 0.23)	(-1.25 ± 0.23)
$e-\pi\pi$ (MC)	$(-1.4 \pm 3.5) \times 10^{-1}$	$(-0.7 \pm 3.5) \times 10^{-1}$
$\mu-\pi\pi$ (Data)	$(-2.6 \pm 2.2) \times 10^{-1}$	$(-2.1 \pm 2.3) \times 10^{-1}$
$\mu-\pi\pi$ (MC)	$(-5.1 \pm 3.5) \times 10^{-1}$	$(-4.6 \pm 3.6) \times 10^{-1}$
μ–Avg. (Data)	$(-0.1 \pm 1.7) \times 10^{-1}$	$(0.2 \pm 1.7) \times 10^{-1}$
μ–Avg. (MC)	$(-2.3 \pm 2.6) \times 10^{-1}$	$(-2.2 \pm 2.6) \times 10^{-1}$
Good Tracks Very Loose		
Decay	$a_{\pm}(\%)$	$a'_{\pm}(\%)$
$e-\rho$ (Data)	$(0.7 \pm 2.3) \times 10^{-1}$	$(1.1 \pm 2.4) \times 10^{-1}$
$e-\rho$ (MC)	$(1.5 \pm 3.6) \times 10^{-1}$	$(2.0 \pm 3.7) \times 10^{-1}$
$\mu-\rho$ (Data)	$(1.9 \pm 2.3) \times 10^{-1}$	$(1.4 \pm 2.4) \times 10^{-1}$
$\mu-\rho$ (MC)	$(1.2 \pm 3.7) \times 10^{-1}$	$(0.2 \pm 3.8) \times 10^{-1}$
$e-\pi\pi$ (Data)	(-1.16 ± 0.22)	(-1.27 ± 0.23)
$e-\pi\pi$ (MC)	$(-0.9 \pm 3.3) \times 10^{-1}$	$(-0.3 \pm 3.4) \times 10^{-1}$
$\mu-\pi\pi$ (Data)	$(-1.0 \pm 2.1) \times 10^{-1}$	$(-0.8 \pm 2.2) \times 10^{-1}$
$\mu-\pi\pi$ (MC)	$(-5.0 \pm 3.4) \times 10^{-1}$	$(-3.8 \pm 3.5) \times 10^{-1}$
μ–Avg. (Data)	$(0.3 \pm 1.6) \times 10^{-1}$	$(0.2 \pm 1.6) \times 10^{-1}$
μ–Avg. (MC)	$(-2.1 \pm 2.5) \times 10^{-1}$	$(-2.0 \pm 2.6) \times 10^{-1}$
Charged Tracks		
Decay	$a_{\pm}(\%)$	$a'_{\pm}(\%)$
$e-\rho$ (Data)	$(1.5 \pm 1.5) \times 10^{-1}$	$(3.4 \pm 2.0) \times 10^{-1}$
$e-\rho$ (MC)	$(0.7 \pm 2.3) \times 10^{-1}$	$(3.2 \pm 3.0) \times 10^{-1}$
$\mu-\rho$ (Data)	$(1.7 \pm 1.4) \times 10^{-1}$	$(2.9 \pm 2.0) \times 10^{-1}$
$\mu-\rho$ (MC)	$(-0.2 \pm 2.3) \times 10^{-1}$	$(0.8 \pm 3.1) \times 10^{-1}$
$e-\pi\pi$ (Data)	$(-8.0 \pm 1.5) \times 10^{-1}$	$(-6.4 \pm 1.9) \times 10^{-1}$
$e-\pi\pi$ (MC)	$(-0.2 \pm 2.3) \times 10^{-1}$	$(2.9 \pm 2.8) \times 10^{-1}$
$\mu-\pi\pi$ (Data)	$(-1.8 \pm 1.4) \times 10^{-1}$	$(-2.2 \pm 1.8) \times 10^{-1}$
$\mu-\pi\pi$ (MC)	$(-3.0 \pm 2.4) \times 10^{-1}$	$(2.2 \pm 2.9) \times 10^{-1}$
μ–Avg. (Data)	$(-0.1 \pm 1.0) \times 10^{-1}$	$(0.1 \pm 1.3) \times 10^{-1}$
μ–Avg. (MC)	$(-1.6 \pm 1.7) \times 10^{-1}$	$(1.6 \pm 2.1) \times 10^{-1}$

Table J.3: The tracking efficiency charge asymmetry for the three different track definitions from the 1930V setting (2003). The average values in this table are the weighted average of the $\mu-\rho$ and $\mu-\pi\pi$ channels as discussed in Chapter 7: Systematic Uncertainty Studies.

Appendix K: P_t Distribution Tables

In order to measure the efficiency in bins of $\mathrm{P}_t^{(lab)}$, the number of events with three tracks, n3, the number of events with four tracks, n4, and the number of events with five tracks, n5, in each bin of $\mathrm{P}_t^{(lab)}$ is required. The number of events in bins of $\mathrm{P}_t^{(lab)}$ of the 4th track, the track used to measure the efficiency, was measured directly for events with four and five tracks. However, the challenge is to determine n3 because it requires knowledge of the $\mathrm{P}_t^{(lab)}$ for the track that has not been reconstructed. The kinematics of the τ decay enables $\mathrm{P}_t^{(lab)}$ of the missing track to be estimated by using information from the reconstructed tracks in the event, contained in the measured quantity $\mathrm{P}_t^{miss(lab)}$. The number of events with three tracks in bins of $\mathrm{P}_t^{(lab)}$ was estimated from the number of three track events in bins of $\mathrm{P}_t^{miss(lab)}$ through the utilization of a probability matrix, M^{prob}. M^{prob} gives the transformation from bins of $\mathrm{P}_t^{(lab)}$ to bins of $\mathrm{P}_t^{miss(lab)}$. Defining $\mathbf{N}_3$ to be the vector of n3 values in each $\mathrm{P}_t^{(lab)}$ bin and $\mathbf{N}_3^{miss}$ to be the vector of the measured number of three track events in bins of $\mathrm{P}_t^{miss(lab)}$, yields

$$\mathbf{N}_3^{miss} = M^{prob}\mathbf{N}_3. \tag{K.1}$$

It follows that

$$(M^{prob})^{-1}\mathbf{N}_3^{miss} = \mathbf{N}_3, \tag{K.2}$$

thus estimating the number of events with three tracks in bins of $\mathrm{P}_t^{(lab)}$. The efficiencies defined in equations 5.1 and 5.4 are then calculated from n3, n4, and n5 in each $\mathrm{P}_t^{(lab)}$ bin.

The probability matrix was determined in events with four tracks.

$$M_{ij}^{prob} = \frac{M_{ij}^{count}}{\sum_l M_{lj}^{count}} \tag{K.3}$$

where M^{count}, the count matrix, contains the number of events with four tracks in bins of $\mathrm{P}_t^{miss(lab)}$ vs $\mathrm{P}_t^{(lab)}$. Note that M^{prob} is applied to the three track event under the assumption that the variation of the efficiency within each $\mathrm{P}_t^{(lab)}$ bin can be approximated by a constant.

The measured variables for the $\mu - \pi\pi$ Data GTL.

$$
\begin{aligned}
M^{count} &= \begin{pmatrix} (3.202 \pm 0.057) \times 10^3 & (2.823 \pm 0.017) \times 10^4 & (6.270 \pm 0.079) \times 10^3 \\ (2.218 \pm 0.047) \times 10^3 & (1.125 \pm 0.011) \times 10^4 & (1.89 \pm 0.14) \times 10^2 \\ (2.111 \pm 0.046) \times 10^3 & (4.879 \pm 0.070) \times 10^3 & (4.0 \pm 2.0) \end{pmatrix} \\
M^{Prob} &= \begin{pmatrix} (4.252 \pm 0.057) \times 10^{-1} & (6.364 \pm 0.023) \times 10^{-1} & (9.701 \pm 0.021) \times 10^{-1} \\ (2.945 \pm 0.053) \times 10^{-1} & (2.536 \pm 0.021) \times 10^{-1} & (2.92 \pm 0.21) \times 10^{-2} \\ (2.803 \pm 0.052) \times 10^{-1} & (1.100 \pm 0.015) \times 10^{-1} & (6.2 \pm 3.1) \times 10^{-4} \end{pmatrix} \\
\mathbf{N}_3^{miss} &= \begin{pmatrix} (3.452 \pm 0.059) \times 10^3 \\ (2.358 \pm 0.049) \times 10^3 \\ (2.220 \pm 0.047) \times 10^3 \end{pmatrix} \\
\mathbf{N}_3 &= \begin{pmatrix} (7.85 \pm 0.50) \times 10^3 \\ (1.9 \pm 7.8) \times 10^2 \\ (-0.0 \pm 3.3) \times 10^2 \end{pmatrix}
\end{aligned}
$$

The measured variables for the $\mu - \pi\pi$ MC GTL.

$$
\begin{aligned}
M^{count} &= \begin{pmatrix} (1.875 \pm 0.043) \times 10^3 & (1.617 \pm 0.013) \times 10^4 & (3.650 \pm 0.060) \times 10^3 \\ (1.152 \pm 0.034) \times 10^3 & (6.434 \pm 0.080) \times 10^3 & (9.61 \pm 0.98) \times 10^1 \\ (1.221 \pm 0.035) \times 10^3 & (2.655 \pm 0.052) \times 10^3 & (2.1 \pm 1.4) \end{pmatrix} \\
M^{Prob} &= \begin{pmatrix} (4.413 \pm 0.076) \times 10^{-1} & (6.401 \pm 0.030) \times 10^{-1} & (9.738 \pm 0.026) \times 10^{-1} \\ (2.712 \pm 0.068) \times 10^{-1} & (2.548 \pm 0.027) \times 10^{-1} & (2.56 \pm 0.26) \times 10^{-2} \\ (2.875 \pm 0.069) \times 10^{-1} & (1.051 \pm 0.019) \times 10^{-1} & (5.5 \pm 3.8) \times 10^{-4} \end{pmatrix} \\
\mathbf{N}_3^{miss} &= \begin{pmatrix} (1.903 \pm 0.044) \times 10^3 \\ (1.281 \pm 0.036) \times 10^3 \\ (1.269 \pm 0.036) \times 10^3 \end{pmatrix} \\
\mathbf{N}_3 &= \begin{pmatrix} (4.20 \pm 0.31) \times 10^3 \\ (5.9 \pm 4.7) \times 10^2 \\ (-3.4 \pm 2.0) \times 10^2 \end{pmatrix}
\end{aligned}
$$

The measured variables for the $\mu - \pi\pi$ Data GTVL.

$$
\begin{aligned}
M^{count} &= \begin{pmatrix} (3.279 \pm 0.057) \times 10^3 & (2.842 \pm 0.017) \times 10^4 & (6.293 \pm 0.079) \times 10^3 \\ (2.266 \pm 0.048) \times 10^3 & (1.137 \pm 0.011) \times 10^4 & (1.91 \pm 0.14) \times 10^2 \\ (2.170 \pm 0.047) \times 10^3 & (4.935 \pm 0.070) \times 10^3 & (4.0 \pm 2.0) \end{pmatrix} \\
M^{Prob} &= \begin{pmatrix} (4.250 \pm 0.056) \times 10^{-1} & (6.354 \pm 0.023) \times 10^{-1} & (9.699 \pm 0.021) \times 10^{-1} \\ (2.937 \pm 0.052) \times 10^{-1} & (2.542 \pm 0.021) \times 10^{-1} & (2.94 \pm 0.21) \times 10^{-2} \\ (2.813 \pm 0.051) \times 10^{-1} & (1.103 \pm 0.015) \times 10^{-1} & (6.2 \pm 3.1) \times 10^{-4} \end{pmatrix} \\
\mathbf{N}_3^{miss} &= \begin{pmatrix} (3.023 \pm 0.055) \times 10^3 \\ (2.143 \pm 0.046) \times 10^3 \\ (2.084 \pm 0.046) \times 10^3 \end{pmatrix} \\
\mathbf{N}_3 &= \begin{pmatrix} (7.50 \pm 0.47) \times 10^3 \\ (-2.4 \pm 7.4) \times 10^2 \\ (-0.2 \pm 3.1) \times 10^2 \end{pmatrix}
\end{aligned}
$$

The measured variables for the $\mu - \pi\pi$ MC GTVL.

$$
\begin{aligned}
M^{count} &= \begin{pmatrix} (1.910 \pm 0.044) \times 10^3 & (1.625 \pm 0.013) \times 10^4 & (3.659 \pm 0.060) \times 10^3 \\ (1.174 \pm 0.034) \times 10^3 & (6.479 \pm 0.080) \times 10^3 & (9.64 \pm 0.98) \times 10^1 \\ (1.245 \pm 0.035) \times 10^3 & (2.673 \pm 0.052) \times 10^3 & (2.4 \pm 1.6) \end{pmatrix} \\
M^{Prob} &= \begin{pmatrix} (4.411 \pm 0.075) \times 10^{-1} & (6.397 \pm 0.030) \times 10^{-1} & (9.737 \pm 0.026) \times 10^{-1} \\ (2.712 \pm 0.68) \times 10^{-1} & (2.550 \pm 0.027) \times 10^{-1} & (2.56 \pm 0.26) \times 10^{-2} \\ (2.877 \pm 0.69) \times 10^{-1} & (1.052 \pm 0.019) \times 10^{-1} & (6.4 \pm 4.1) \times 10^{-4} \end{pmatrix} \\
\mathbf{N}_3^{miss} &= \begin{pmatrix} (1.728 \pm 0.042) \times 10^3 \\ (1.196 \pm 0.035) \times 10^3 \\ (1.220 \pm 0.035) \times 10^3 \end{pmatrix} \\
\mathbf{N}_3 &= \begin{pmatrix} (4.11 \pm 0.30) \times 10^3 \\ (3.5 \pm 4.5) \times 10^2 \\ (-3.2 \pm 1.9) \times 10^2 \end{pmatrix}
\end{aligned}
$$

The measured variables for the $\mu - \pi\pi$ Data CT.

$$M^{count} = \begin{pmatrix} (4.364 \pm 0.066) \times 10^3 & (2.803 \pm 0.017) \times 10^4 & (6.173 \pm 0.079) \times 10^3 \\ (3.108 \pm 0.056) \times 10^3 & (1.123 \pm 0.011) \times 10^4 & (1.91 \pm 0.14) \times 10^2 \\ (3.096 \pm 0.056) \times 10^3 & (4.903 \pm 0.070) \times 10^3 & (5.0 \pm 2.2) \end{pmatrix}$$

$$M^{Prob} = \begin{pmatrix} (4.129 \pm 0.048) \times 10^{-1} & (6.347 \pm 0.023) \times 10^{-1} & (9.692 \pm 0.022) \times 10^{-1} \\ (2.941 \pm 0.044) \times 10^{-1} & (2.542 \pm 0.021) \times 10^{-1} & (3.00 \pm 0.21) \times 10^{-2} \\ (2.930 \pm 0.044) \times 10^{-1} & (1.110 \pm 0.015) \times 10^{-1} & (7.8 \pm 3.5) \times 10^{-4} \end{pmatrix}$$

$$\mathbf{N}_3^{miss} = \begin{pmatrix} (1.434 \pm 0.038) \times 10^3 \\ (9.99 \pm 0.32) \times 10^2 \\ (9.02 \pm 0.30) \times 10^2 \end{pmatrix}$$

$$\mathbf{N}_3 = \begin{pmatrix} (2.82 \pm 0.23) \times 10^3 \\ (6.9 \pm 3.7) \times 10^2 \\ (-1.7 \pm 1.6) \times 10^2 \end{pmatrix}$$

The measured variables for the $\mu - \pi\pi$ MC CT.

$$M^{count} = \begin{pmatrix} (2.546 \pm 0.050) \times 10^3 & (1.605 \pm 0.013) \times 10^4 & (3.595 \pm 0.060) \times 10^3 \\ (1.598 \pm 0.040) \times 10^3 & (6.394 \pm 0.080) \times 10^3 & (9.38 \pm 0.97) \times 10^1 \\ (1.771 \pm 0.042) \times 10^3 & (2.635 \pm 0.051) \times 10^3 & (2.4 \pm 1.6) \end{pmatrix}$$

$$M^{Prob} = \begin{pmatrix} (4.304 \pm 0.064) \times 10^{-1} & (6.400 \pm 0.030) \times 10^{-1} & (9.739 \pm 0.026) \times 10^{-1} \\ (2.702 \pm 0.058) \times 10^{-1} & (2.550 \pm 0.028) \times 10^{-1} & (2.54 \pm 0.26) \times 10^{-2} \\ (2.994 \pm 0.060) \times 10^{-1} & (1.051 \pm 0.019) \times 10^{-1} & (6.5 \pm 4.2) \times 10^{-4} \end{pmatrix}$$

$$\mathbf{N}_3^{miss} = \begin{pmatrix} (8.26 \pm 0.29) \times 10^2 \\ (6.20 \pm 0.25) \times 10^2 \\ (5.62 \pm 0.24) \times 10^2 \end{pmatrix}$$

$$\mathbf{N}_3 = \begin{pmatrix} (1.61 \pm 0.16) \times 10^3 \\ (7.6 \pm 2.4) \times 10^2 \\ (-3.6 \pm 1.1) \times 10^2 \end{pmatrix}$$

$\mu - \pi\pi$ (Good Track Loose)			
Range (GeV)	n3	n4	n5
$0.0 < Pt < 0.4$ (Data)	$(7.85 \pm 0.50) \times 10^3$	$(7.531 \pm 0.087) \times 10^3$	$(4.90 \pm 0.70) \times 10^1$
$0.0 < Pt < 0.4$ (MC)	$(4.20 \pm 0.31) \times 10^3$	$(4.248 \pm 0.065) \times 10^3$	$(2.32 \pm 0.48) \times 10^1$
$0.4 < Pt < 2.0$ (Data)	$(1.9 \pm 7.8) \times 10^2$	$(4.435 \pm 0.021) \times 10^4$	$(2.16 \pm 0.15) \times 10^2$
$0.4 < Pt < 2.0$ (MC)	$(5.9 \pm 4.7) \times 10^2$	$(2.526 \pm 0.016) \times 10^4$	$(1.29 \pm 0.11) \times 10^2$
$2.0 < Pt <$5.28 (Data)	$(-0.0 \pm 3.3) \times 10^2$	$(6.463 \pm 0.080) \times 10^3$	(7.0 ± 2.6)
$2.0 < Pt <$5.28 (MC)	$(-3.4 \pm 2.0) \times 10^2$	$(3.749 \pm 0.061) \times 10^3$	(5.3 ± 2.3)
$\mu - \pi\pi$ (Good Track Very Loose)			
Range (GeV)	n3	n4	n5
$0.0 < Pt < 0.4$ (Data)	$(7.50 \pm 0.47) \times 10^3$	$(7.715 \pm 0.088) \times 10^3$	$(7.10 \pm 0.84) \times 10^1$
$0.0 < Pt < 0.4$ (MC)	$(4.11 \pm 0.30) \times 10^3$	$(4.330 \pm 0.066) \times 10^3$	$(3.10 \pm 0.56) \times 10^1$
$0.4 < Pt < 2.0$ (Data)	$(-2.4 \pm 7.4) \times 10^2$	$(4.473 \pm 0.021) \times 10^4$	$(3.44 \pm 0.19) \times 10^2$
$0.4 < Pt < 2.0$ (MC)	$(3.5 \pm 4.5) \times 10^2$	$(2.540 \pm 0.016) \times 10^4$	$(1.75 \pm 0.13) \times 10^2$
$2.0 < Pt <$5.28 (Data)	$(-0.2 \pm 3.1) \times 10^2$	$(6.488 \pm 0.081) \times 10^3$	$(5.00 \pm 0.71) \times 10^1$
$2.0 < Pt <$5.28 (MC)	$(-3.2 \pm 1.9) \times 10^2$	$(3.758 \pm 0.061) \times 10^3$	$(2.29 \pm 0.48) \times 10^1$
$\mu - \pi\pi$ (Charge Track)			
Range (GeV)	n3	n4	n5
$0.0 < Pt < 0.4$ (Data)	$(2.82 \pm 0.23) \times 10^3$	$(1.057 \pm 0.010) \times 10^4$	$(5.47 \pm 0.23) \times 10^2$
$0.0 < Pt < 0.4$ (MC)	$(1.61 \pm 0.16) \times 10^3$	$(5.915 \pm 0.077) \times 10^3$	$(3.08 \pm 0.18) \times 10^2$
$0.4 < Pt < 2.0$ (Data)	$(6.9 \pm 3.7) \times 10^2$	$(4.416 \pm 0.021) \times 10^4$	$(1.423 \pm 0.038) \times 10^3$
$0.4 < Pt < 2.0$ (MC)	$(7.6 \pm 2.4) \times 10^2$	$(2.508 \pm 0.016) \times 10^4$	$(7.32 \pm 0.27) \times 10^2$
$2.0 < Pt <$5.28 (Data)	$(-1.7 \pm 1.6) \times 10^2$	$(6.369 \pm 0.080) \times 10^3$	$(2.19 \pm 0.15) \times 10^2$
$2.0 < Pt <$5.28 (MC)	$(-3.6 \pm 1.1) \times 10^2$	$(3.691 \pm 0.061) \times 10^3$	$(1.11 \pm 0.11) \times 10^2$

Table K.1: The number of events as a function of P_t for the $\mu - \pi\pi$ channel in the three different track definitions from the 1930V setting.

$\mu - \pi\pi$ (Good Track Loose)		
Range (GeV)	$\epsilon \times A(\%)$	$\epsilon' \times A(\%)$
$0.0 < Pt < 0.4$ (Data)	$(4.90 \pm 0.16) \times 10^1$	$(4.88 \pm 0.16) \times 10^1$
$0.0 < Pt < 0.4$ (MC)	$(5.03 \pm 0.19) \times 10^1$	$(5.01 \pm 0.19) \times 10^1$
$0.4 < Pt < 2.0$ (Data)	$(9.96 \pm 0.18) \times 10^1$	$(9.91 \pm 0.17) \times 10^1$
$0.4 < Pt < 2.0$ (MC)	$(9.77 \pm 0.18) \times 10^1$	$(9.72 \pm 0.18) \times 10^1$
$2.0 < Pt <$5.28 (Data)	$(1.000 \pm 0.051) \times 10^2$	$(9.99 \pm 0.51) \times 10^1$
$2.0 < Pt <$5.28 (MC)	$(1.099 \pm 0.064) \times 10^2$	$(1.097 \pm 0.064) \times 10^2$
$\mu - \pi\pi$ (Good Track Very Loose)		
Range (GeV)	$\epsilon \times A(\%)$	$\epsilon' \times A(\%)$
$0.0 < Pt < 0.4$ (Data)	$(5.07 \pm 0.16) \times 10^1$	$(5.05 \pm 0.16) \times 10^1$
$0.0 < Pt < 0.4$ (MC)	$(5.13 \pm 0.19) \times 10^1$	$(5.11 \pm 0.18) \times 10^1$
$0.4 < Pt < 2.0$ (Data)	$(1.005 \pm 0.017) \times 10^2$	$(9.98 \pm 0.17) \times 10^1$
$0.4 < Pt < 2.0$ (MC)	$(9.86 \pm 0.17) \times 10^1$	$(9.80 \pm 0.17) \times 10^1$
$2.0 < Pt <$5.28 (Data)	$(1.003 \pm 0.048) \times 10^2$	$(9.95 \pm 0.47) \times 10^1$
$2.0 < Pt <$5.28 (MC)	$(1.093 \pm 0.061) \times 10^2$	$(1.085 \pm 0.060) \times 10^2$
$\mu - \pi\pi$ (Charge Track)		
Range (GeV)	$\epsilon \times A(\%)$	$\epsilon' \times A(\%)$
$0.0 < Pt < 0.4$ (Data)	$(7.89 \pm 0.14) \times 10^1$	$(7.58 \pm 0.13) \times 10^1$
$0.0 < Pt < 0.4$ (MC)	$(7.86 \pm 0.16) \times 10^1$	$(7.55 \pm 0.15) \times 10^1$
$0.4 < Pt < 2.0$ (Data)	$(9.846 \pm 0.082) \times 10^1$	$(9.543 \pm 0.077) \times 10^1$
$0.4 < Pt < 2.0$ (MC)	$(9.707 \pm 0.091) \times 10^1$	$(9.439 \pm 0.087) \times 10^1$
$2.0 < Pt <$5.28 (Data)	$(1.028 \pm 0.027) \times 10^2$	$(9.93 \pm 0.25) \times 10^1$
$2.0 < Pt <$5.28 (MC)	$(1.109 \pm 0.036) \times 10^2$	$(1.073 \pm 0.034) \times 10^2$

Table K.2: The tracking efficiency as a function of P_t for the $\mu - \pi\pi$ channel in the three different track definitions from the 1930V setting.

$\mu - \pi\pi$ (Good Track Loose)		
Range (GeV)	$\Delta(\%)$	$\Delta'(\%)$
$0.0 < Pt < 0.4$ (Data)	(2.6 ± 3.2)	(2.7 ± 3.2)
$0.0 < Pt < 0.4$ (MC)	(2.6 ± 3.2)	(2.7 ± 3.2)
$0.4 < Pt < 2.0$ (Data)	(-1.9 ± 1.8)	(-1.9 ± 1.8)
$0.4 < Pt < 2.0$ (MC)	(-1.9 ± 1.8)	(-1.9 ± 1.8)
$2.0 < Pt <$5.28 (Data)	(9.0 ± 4.7)	(8.9 ± 4.7)
$2.0 < Pt <$5.28 (MC)	(9.0 ± 4.7)	(8.9 ± 4.7)
$\mu - \pi\pi$ (Good Track Very Loose)		
Range (GeV)	$\Delta(\%)$	$\Delta'(\%)$
$0.0 < Pt < 0.4$ (Data)	(1.1 ± 3.1)	(1.2 ± 3.1)
$0.0 < Pt < 0.4$ (MC)	(1.1 ± 3.1)	(1.2 ± 3.1)
$0.4 < Pt < 2.0$ (Data)	(-1.9 ± 1.7)	(-1.8 ± 1.7)
$0.4 < Pt < 2.0$ (MC)	(-1.9 ± 1.7)	(-1.8 ± 1.7)
$2.0 < Pt <$5.28 (Data)	(8.2 ± 4.4)	(8.3 ± 4.4)
$2.0 < Pt <$5.28 (MC)	(8.2 ± 4.4)	(8.3 ± 4.4)
$\mu - \pi\pi$ (Charge Track)		
Range (GeV)	$\Delta(\%)$	$\Delta'(\%)$
$0.0 < Pt < 0.4$ (Data)	(-0.5 ± 1.8)	(-0.5 ± 1.7)
$0.0 < Pt < 0.4$ (MC)	(-0.5 ± 1.8)	(-0.5 ± 1.7)
$0.4 < Pt < 2.0$ (Data)	(-1.44 ± 0.84)	(-1.10 ± 0.82)
$0.4 < Pt < 2.0$ (MC)	(-1.44 ± 0.84)	(-1.10 ± 0.82)
$2.0 < Pt <$5.28 (Data)	(7.3 ± 2.4)	(7.5 ± 2.4)
$2.0 < Pt <$5.28 (MC)	(7.3 ± 2.4)	(7.5 ± 2.4)

Table K.3: The tracking efficiency correction factor as a function of P_t for the $\mu - \pi\pi$ channel in the three different track definitions from the 1930V setting.

Appendix L: Particle Identification

In particle physics, subatomic particle are identified through their interactions with the detector. The detector parameters utilized in this work to select electrons and muons are displayed in table L.1.

Variable	Description
Tracking Detectors Variables (SVT and DCH)	
$\frac{dE}{dx}$	The mean energy loss per unit length
P	The momentum of a track (GeV/c)
P_t	The momentum of a track in the plane perpendicular to the beam axis (GeV/c)
q	The charge of the track
DIRC Variables	
$N_{\gamma\ \mathrm{DIRC}}$	The number of DIRC photons
θ_c	The Cherenkov angle (rad)
θ_c^x	The Cherenkov angle for the x particle hypothesis (rad)
EMC Variables	
E_{raw}	The energy deposited in the EMC (GeV)
ϕ_{EMC}	The ϕ coordinate of the extrapolated track position in the EMC (rad)
$\phi_{cluster}$	The ϕ coordinate of the position of a cluster in the EMC (rad)
$N_{crystal}$	The number of EMC crystals associated with a track
Lat	The Lateral moment in the EMC [41]
A_{42}	The 42nd Zernike moment in the EMC [40]
IFR Variables	
N_L	The number of IFR layers that registered a hit
λ	The number of interaction lengths[1] transversed by the track
λ_{exp}	The number of interaction lengths expected to be transversed if the track is a muon
χ^2_{fit}	The χ^2/ndof[2] for the fit applied to the IFR cluster
χ^2_{trk}	The χ^2/ndof between the extrapolated track and the clusters in the IFR
T_c	The continuity of a track in the IFR
$\bar{m}$	The mean number of IFR strips hit per layer
σ_m	The standard deviation on the mean number of IFR strips hit per layer

Table L.1: The definition of the variable used for particle identification.

[1] An interaction length is the mean distance between inelastic collisions.

[2] The number of degrees of freedom for a χ^2 fit is the number of point minus the number of parameters in the fit.

In BaBar, there are multiple particle identification criteria employed for each of the pseudo-stable particles that can be identified in the detector. The Tau31 Study used two of the standard BaBar electron identification criteria: the Very Loose Electron selection criteria, defined in table L.2, and the Very Tight Electron selection criteria, defined in table L.3. The $\Delta\phi = q(\phi_{EMC} - \phi_{cluster})$ cut referred to in table L.3 is a geometric cut in the $\Delta\phi$ vs P_t plane that separates electrons and pions at P_t. An illustration of this cut on both electron and pion distributions can be seen in figure L.1.

Selection Cuts
$500 < \frac{dE}{dx} < 1000$
$0.5 < \frac{E_{raw}}{P} < 5.0$
$3 < N_{crystal}$
$0 < Lat < 10$
$-10 < A_{42} < 10$

Table L.2: The Very Loose Electron selection criteria [34].

Selection Cuts
$540 < \frac{dE}{dx} < 860$
$0.89 < \frac{E_{raw}}{P} < 1.2$
$3 < N_{crystal}$
$0 < Lat < 0.6$
$-10 < A_{42} < 0.11$
$10 < N_{\gamma\ \mathrm{DIRC}}$
$\lvert\theta_c - \theta_c^e\rvert < 3\sigma_{\theta_c}$
$\Delta\phi = q(\phi_{EMC} - \phi_{cluster})$ cut

Table L.3: The Very Tight Electron selection criteria [34].

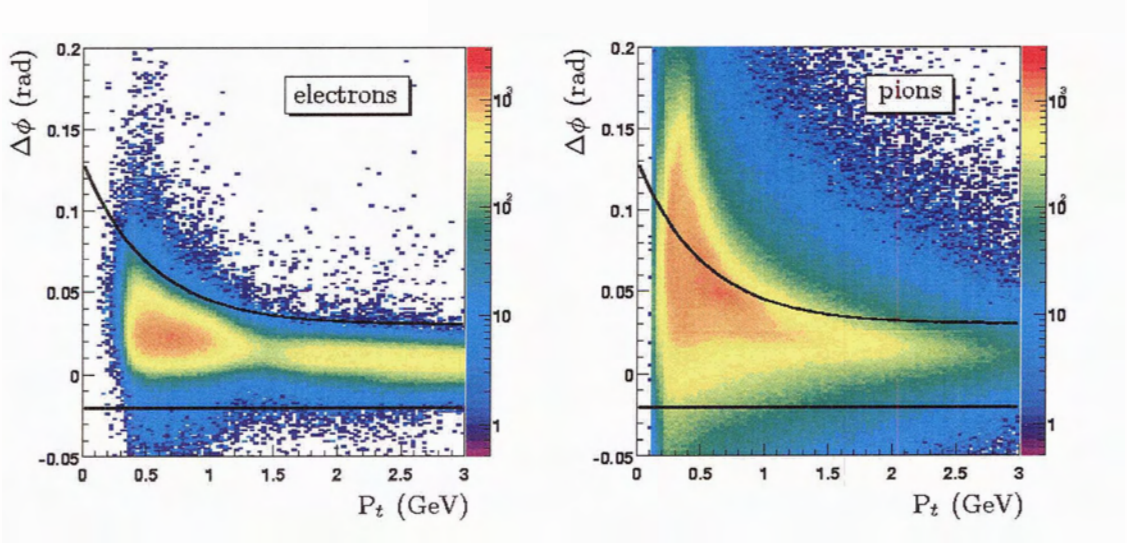

Figure L.1: $\Delta\phi = q(\phi_{EMC} - \phi_{cluster})$ as a function of P_t with the $\Delta\phi$ cut employed in the Very Tight Electron selection criteria superimposed for both electron (left plot) and pion (right Plot) MC [34, Figure 17].

The muon identification criteria used in the Tau31 Study, the Loose Muon selection criteria, can be seen in table L.4.

Selection Cuts
$E_{raw} < 0.5$(GeV)
$2 \leq N_L$
$2 \leq \lambda$
$\lvert\lambda - \lambda_{exp}\rvert \leq 2$
$\chi^2_{fit} \leq 4$
$\chi^2_{trk} \leq 7$
$0.2 < T_c$ for 0.3rad $< \theta <$ 1.0rad
$\bar{m} < 10$
$\sigma_m < 6$

Table L.4: The Loose Muon selection criteria [35].